



HAL
open science

**Biological role and structure/function characterization
of enzymes related to halogen metabolism during
alga-bacteria interactions: studies in the marine model
bacterium, *Zobellia galactanivorans***

Eugénie Grigorian

► **To cite this version:**

Eugénie Grigorian. Biological role and structure/function characterization of enzymes related to halogen metabolism during alga-bacteria interactions: studies in the marine model bacterium, *Zobellia galactanivorans*. Symbiosis. Sorbonne Université, 2021. English. NNT: 2021SORUS012 . tel-03621133

HAL Id: tel-03621133

<https://theses.hal.science/tel-03621133>

Submitted on 28 Mar 2022

HAL is a multi-disciplinary open access archive for the deposit and dissemination of scientific research documents, whether they are published or not. The documents may come from teaching and research institutions in France or abroad, or from public or private research centers.

L'archive ouverte pluridisciplinaire **HAL**, est destinée au dépôt et à la diffusion de documents scientifiques de niveau recherche, publiés ou non, émanant des établissements d'enseignement et de recherche français ou étrangers, des laboratoires publics ou privés.

Sorbonne Université

Ecole doctorale 227 - Sciences de la Nature et de l'Homme : Ecologie et Evolution

Laboratoire de Biologie Intégrative des Modèles Marins UMR8227

Equipe Biologie des algues et interactions avec l'environnement

Biological role and structure/function characterization of enzymes related to halogen metabolism during alga-bacteria interactions: studies in the marine model bacterium, *Zobellia galactanivorans*

Par Eugénie Grigorian

Thèse de doctorat en Microbiologie Marine

Dirigée par Catherine Leblanc et Ludovic Delage

Présentée et soutenue publiquement le 26 mars 2021

Devant un jury composé de :

Dr. Chantal Iobbi-Nivol	IMM-CNRS, Marseille	Rapportrice
Pr. Stéphane Vuilleumier	Université de Strasbourg	Rapporteur
Pr. Seigo Amachi	Université de Chiba, Japon	Examineur
Dr. Mirjam Czjzek	Station Biologique de Roscoff	Examinatrice
Dr. Angélique Gobet	IFREMER, Sète	Examinatrice
Dr. Catherine Leblanc	Station Biologique de Roscoff	Directrice de thèse
Dr. Ludovic Delage	Station Biologique de Roscoff	Co-encadrant de thèse

« Je suis de ceux qui pensent que la science est d'une grande beauté. Un scientifique dans son laboratoire est non seulement un technicien : il est aussi un enfant placé devant des phénomènes naturels qui l'impressionnent comme des contes de fées »

Marie Curie

Acknowledgments

Tout d'abord, je tiens à remercier mes encadrants Catherine Leblanc et Ludovic Delage qui m'ont donnée l'opportunité travailler sur ce sujet de thèse. Merci pour tous vos conseils, votre patience et votre aide au cours de ces 4 années. Merci de m'avoir fait confiance et de m'avoir soutenue quand j'en avais besoin. Sans vous je n'aurais pas pu y arriver.

Je remercie également la directrice de la Station Biologique Catherine Boyen de m'avoir accueillie, ainsi que tous les membres de l'équipe ABIE.

Merci à tous les membres de mon comité de thèse, Liz Ficko-Blean, Eric Duchaud, Christophe Destombes et François Thomas pour leurs recommandations et leur aide sur mon avancée dans la thèse, en particulier Liz et François qui m'ont énormément aidé et conseillé chaque fois que je les sollicitais.

I want to thank all of the jury members for agreeing to review my thesis. I wish you to enjoy reading my manuscript!

Arigatô gozaimasu Amachi-Sensei for welcoming me in your team and teaching me your work. I want to thank particularly Haruka Nakazawa, without who the fourth chapter of my thesis wouldn't exist. Thanks a lot for all your help and the conversations we had in the coldest building in Japan, and for showing me all the good spots in Kamakura.

Je remercie grandement l'école doctorale 227 pour tout leur soutien et pour m'avoir accordé la bourse qui m'a permis d'aller 7 semaines au Japon.

Je remercie la plateforme de cristallographie de Roscoff, notamment Mirjam Czjzek qui m'a formée en cristallographie et qui a beaucoup contribué au chapitre 2 de ma thèse, ainsi que Thomas Roret qui m'a énormément aidée à résoudre la structure de ZgHAD.

Un grand merci à Murielle Jam sans qui le labo ne tournerait pas aussi bien. Tu m'as énormément aidée à réussir les purifs sur l'Akta et tu es toujours disponible et à l'écoute.

Je remercie également Pauline Malardé qui a fait un excellent travail au cours de ses 6 semaines de stage. Je te souhaite beaucoup de réussite pour la suite.

I would like to thank Miriam Bernard, Lydia White and Miguel Méndez Sandín for reading and correcting my manuscript. Thank you for your valuable inputs.

A special thanks for Qikun who shared the office with me and helped me during difficult times. I really enjoyed being your office mate and I will miss our conversations and tea breaks.

I want to thank my friends at the station: Marieke, Mariarita, Lucile, Jasna, Elham, Maéva, Marie, Cédric, David, Joost, Giannis, Vaso, Yao, Hetty and Miriam for encouraging me until the end and for all the amazing moments I shared with you.

Je remercie chaleureusement Sarah, Elodie, Sham, Sofiane, Marine et Hugues, les rescapés de l'UPMC. Vous êtes les meilleurs amis du monde et je ne serais pas là aujourd'hui sans vous tous. Marine et Hugues vous m'accueilliez chez vous tous les ans et vous avez été présents à

mes côtés pour m'aider à surmonter toutes les difficultés au cours de ces 4 dernières années. Je vous en suis infiniment reconnaissante (même si vous n'avez pas relié ma thèse :p).

Enfin je remercie ma famille qui m'a toujours soutenu et poussé à faire des études. Avoir l'opportunité de faire ce doctorat c'est aussi énormément grâce à vous. շնորհակալությունսսմեն ինչի համար.

Merci à tous ! Thank you!

Table of contents

List of figures.....	7
List of tables.....	9
Abbreviations.....	10
General introduction.....	11
1. Biogeochemical cycle of halogens.....	11
1.1. Definition of halogens	11
1.2. Inorganic halogenated compounds.....	11
1.3. Organic halogenated compounds.....	12
1.4. Biogeochemical cycle of halogens.....	13
2. Biological importance of halogen metabolism in marine organisms.....	15
2.1. Biotic stress responses and halogenated compounds.....	15
2.2. Oxidative stress responses and iodine metabolism.....	16
2.3. Halogen-related metabolism in bacteria.....	17
3. Enzymatic mechanisms involved in halogenation and dehalogenation.....	17
3.1. Halogenating enzymes.....	18
3.2. Dehalogenating enzymes.....	22
4. Vanadium-dependent haloperoxidases (VHPO)	25
4.1. Biochemical and structural characterization of VHPOs.....	25
4.2. Occurrence, evolution and putative biological roles of VHPOs.....	27
5. Haloacid dehalogenases (HAD)	30
5.1. Classification of the HADs	30
5.2. Structural features and enzymatic properties of the L-2-HADs.....	32
5.3. Occurrence and putative biological roles of L-2-HADs.....	34
6. <i>Zobellia galactanivorans</i>, a model marine bacterium for studying specific metabolic pathways.....	35
7. Thesis project and outline.....	37
Chapter 1: Functional characterization of a L-2-haloacid dehalogenase from <i>Zobellia galactanivorans</i> suggests a role in haloacetic acid catabolism and a wide distribution in marine environment	41
Chapter 2: Purification, crystallization and structural analyses of ZgHAD, a L-2-haloacid dehalogenase from the marine Flavobacteria <i>Zobellia galactanivorans</i>.....	101
Chapter 3: Biochemical and structural characterization of Zg-VHPO3.....	127
I. Introduction.....	128
II. Material and methods.....	129
II. 1. <i>Zobellia_2250</i> gene cloning, overexpression and purification.....	129

II.2. Native gel and spectrophotometric haloperoxidase activity measurements.....	130
II.3. Protein stability and activity analysis	131
II.4. Crystallogenesis.....	132
II.5. Structure modelling.....	134
III. Results and discussion.....	134
III.1. Purification of the third vanadium-dependent haloperoxidase from <i>Z. galactanivorans</i>	134
III.2. Substrate specificity of Zg-VHPO ₃ and determination of steady-state kinetic parameters....	137
III.3. Effect of temperature on the folding of Zg-VIPO ₃	139
III.4. 3D structural studies of Zg-VIPO ₃	140
IV. Conclusions	143
Chapter 4: Studies on VIPO localization and biological roles in <i>Zobellia galactanivorans</i>.....	145
I. Introduction.....	146
II. Materials and methods.....	147
II.1. Chemicals and antibodies.....	147
II.2. Bacterial strains and culture conditions.....	147
II.3. <i>In silico</i> prediction of protein subcellular localization.....	147
II.4. Protein subcellular fractionation	148
II.5. Western blot analysis	148
II.6. Deletion of the Zg-VIPO ₁ -encoding gene.....	149
II.7. Iodine accumulation assays.....	150
II.8. Mass spectrometry analysis of the iodine-enriched protein fractions.....	151
II.9. Structure modelling.....	151
III. Results and discussion.....	152
III.1. Subcellular localization prediction of Zg-VIPOs.....	152
III.2. Effects of an iodide increase on the wild-type and the $\Delta IPO1$ KO mutant bacterial growth ..	157
III.3. Comparison of iodine accumulation and uptake in wild-type and $\Delta IPO1$ knock-out mutant strains.....	159
III.4. Localization and LC-MS/MS analysis of iodine-enriched protein fractions.....	161
IV. Conclusions.....	167
V. Supporting information.....	169
Conclusion and Perspectives.....	173
References.....	179
Abstract.....	200
Résumé.....	200

List of Figures

Figure 0-1: Schematic overview of the global halogen biogeochemical cycle.....	14
Figure 0-2: Key steps of the catalytic mechanisms of flavin-dependent halogenases. (A) Formation of FADHOOH, which oxidizes X ⁻ to HOX. (B) Proposed formation of a lysine N-haloamine intermediate. (C) Electrophilic aromatic substitution of the tryptophan substrate. (D) Nucleophilic halogenases catalyze the attack of halide anions (X ⁻) as nucleophiles on SAM. The fluorinase FIA and the chlorinase SaLL produce halogenated adenosines, whereas halide methyl-transferases produce halomethanes. (Source: Senn, 2014).....	20
Figure 0-3: (A) Catalytic mechanisms of the non-heme iron halogenases (Source: Timmins & de Visser, 2018). (B) Key steps of the heme-dependent haloperoxidase mechanism (Source: Senn, 2014).....	21
Figure 0-4: Deiodination catalyzed by (A) iodotyrosine deiodinase (IYD) and (B) iodothyronine deiodinase (ID) (source: Fournier, 2014).....	22
Figure 0-5: (A) reductive dehalogenation, (B) oxidative dehalogenation and, (C) hydrolytic dehalogenation (source: Sayyed & Patel, 2011).....	24
Figure 0-6: Reactions of the VHPO/H ₂ O ₂ system. X: Br, Cl, I. R-H: organic compound. (Fournier and Leblanc, 2014)	25
Figure 0-7: Phylogenetic analysis of VHPO proteins. A protein maximum likelihood (PML) tree was constructed using the multiple alignment of characterized and putative VHPO from 124 eukaryotic and selected bacterial species, and of five Bacterial Acid Phosphatases. When characterized at the biochemical level, the VHPO specificity towards halides is mentioned and refers to the legend code, i.e. iodo- (VIPO), bromo- (VBPO) or chloroperoxidase (VCPO) activity. The available 3D structures of VHPO are indicated by a star (from Fournier et al. 2014).....	28
Figure 0-8: Hypothetic mechanisms of iodine uptake in <i>L. digitata</i> (from Verhaeghe et al. 2008b)	29
Figure 0-9: Mechanisms for hydrolytic dehalogenation of 2-haloacetic acids. (A) Reaction mechanism involving nucleophilic attack of an active site carboxylate group on the substrate leading to the formation of an ester intermediate. The reaction of L-2-haloacid dehalogenase (L-2-HAD) proceeds by this mechanism. (B) Reaction mechanism involving direct nucleophilic attack of water on the substrate. The reactions of D-2-haloacid dehalogenase (D-2-HAD) and DL-2-haloacid dehalogenase (DL-2-HAD) proceed by this mechanism. L-2-Haloalkanoic acid is shown as the substrate here, but D-2-haloalkanoic acid can also serve as a substrate for this DL-2-HAD (Source: Kurihara & Esaki, 2008).	31
Figure 0-10: (A) Picture of <i>Z. galactanivorans</i> colonies on agar plate. (B) Phase contrast microscopy image of a <i>Z. galactanivorans</i> liquid culture (scale bar 6 μm).	36
Figure 0-11: Hypothetical model of iodine metabolism within <i>Z. galactanivorans</i> and its interaction with the brown alga <i>L. digitata</i> (adapted from Fournier, 2014).	38
Figure 3-1: Phase diagram of the conditions needed for crystallization by vapor diffusion. In the undersaturation area: the drop remained clear. The goal was to find the right ratio and the good protein/precipitant reagent concentrations in order to reach the nucleation area and promote crystal growth.	132
Figure 3-2: Crystallization technics (A) sitting drop vapor diffusion and (B) hanging drop vapor diffusion (François Thomas, 2011)	133
Figure 3-3: (A) Chromatogram and SDS-PAGE analyses of Zg-VHPO3 purification fractions by size exclusion chromatography. Elution buffer: 20 mM Tris/HCl, pH 8.0 and 150 mM NaCl. The polyacrylamide gel was stained with Coomassie Brilliant Blue R-250, revealing the presence of the recombinant protein in eluted fractions of the A280 peak (lanes 43 to 50 and 52 to 59). M = Precision Plus Protein™ Standards marker (Bio-Rad Laboratories) and molecular masses were indicated on the left of the lane. (B) Chromatogram analysis of the first peak from the previous size exclusion chromatography. Elution buffer: 20 mM Tris/HCl, pH 8.0 and 150 mM NaCl. Black dotted rectangle surrounded the 2 nd peak of the size exclusion chromatograph in A, corresponding to the dimeric form.	135
Figure 3-4: Chromatogram and SDS-PAGE analyses of Zg-VHPO3 purification by size exclusion chromatography. Elution buffer: 20 mM Tris/HCl, pH 8.0 and 50 mM NaCl. The polyacrylamide gel was stained with Coomassie Brilliant Blue R-250, revealing the presence of the recombinant protein in eluted fractions of the A280 peak (lanes D10 to E4 and E8 to F2). M = Precision Plus Protein™ Standards marker (Bio-Rad Laboratories) and molecular masses were indicated on the left of the lane.	136

Figure 3-5: <i>O</i> -dianisidine assay on native polyacrylamide electrophoresis gel of the recombinant protein Zg-VHPO3, purified as monomer (M) and dimer (D) batches. The assay was performed in presence of potassium chloride, bromide or iodide.	137
Figure 3-6: Thymol blue colorimetric assay of the recombinant protein Zg-VHPO3, purified as monomer and dimer batches. The assay was performed at room temperature for 1 h in clear flat-bottomed microplate wells, in presence of potassium iodide or potassium bromide. The negative control was performed without enzyme.	138
Figure 3-7: Thermal denaturation analysis using Nanotemper NT48 of recombinant protein Zg-VIPO3, purified as (A) Dimer batch, or (B) Monomer batch. Each peak represented denaturing protein step.....	139
Figure 3-8: SDS-PAGE gel revealing the iodoperoxidase activities of recombinant protein in dimeric or monomeric batches, after heating treatment at 10°C to 90°C for 30 minutes. The native polyacrylamide electrophoresis gel was stained with thymol blue. M = Precision Plus Protein™ Standards marker (Bio-Rad Laboratories) and molecular masses were indicated on the left of the lane.	140
Figure 3-9: Ribbon-type representation of Zg-VIPO3 3D model as monomer (A) based on Zg-VIPO1 (PDB accession number 4CIT) and as dimer (B) based on NapH1 (VCPO, PDB accession number 3W35). One monomer was colored in cyan and the other one in green. Red dotted circles showed the localization of the active sites. Corresponding surface representations of the monomer (C) and of the dimer (D) in side view with the vanadate molecule, represented in red.	142
Figure 4-1: Western blot analysis of the three recombinant Zg-VIPO proteins with antibodies recognizing the N-terminal 6xHis tag sequence (left panel) and the entire protein Zg-IPO1 (right panel). The same quantities (10 µg) of purified proteins were loaded into the wells of the SDS-PAGE before electro transfer onto nitrocellulose blotting membranes. (M) protein size marker; (1) Zg-VIPO1; (2) Zg-VIPO2; (3) Zg-VIPO3.....	155
Figure 4-2: Anti-Zg-VIPO1 western blot analysis of the fractionated cellular compartments of <i>Z. galactanivorans</i> . 10 µg of protein samples were loaded in each well. Legend: periplasmic (P1, P2), cytoplasmic (C1, C2) and membrane (M1, M2) duplicates. Precision Plus Protein™ Dual Color Standard Marker (PM).....	156
Figure 4-3: Growth curves of <i>Z. galactanivorans</i> wild-type (A) and $\Delta IPO1$ mutant (B) cultures with increasing concentrations of KI for 7 days. Values are mean \pm s.e.m.	158
Figure 4-4: Time course of iodide accumulation by <i>Arenibacter</i> sp. C-21 (black squares), <i>Zobellia galactanivorans</i> Dsij ^T WT (red squares), <i>Zobellia galactanivorans</i> $\Delta IPO1$ (blue triangles) and <i>Cellulophaga fucicola</i> (grey diamond-shape) strains grown in artificial ZoBell medium containing iodide ¹²⁵ I. The results are expressed as the means \pm standard deviations of triplicate analyses. (A) Relative iodide content in the culture medium. (B) Measure of the radioactive iodide concentration in culture pellets during 3 days of culture.	160
Figure 4-5: Picture of the SDS-PAGE polyacrylamide gel, stained by Coomassie Blue and loaded with 20 µL of <i>Z. galactanivorans</i> membrane fractions (5 deposits). In the corresponding gel charged with radioactive fractions, the bands #1, #2 and #3 showed the most intense signal and then cut in the non-radioactive gel. The ¹²⁵ I radioactivity values correspond to the mean and standard deviation of five independent measurements for each.	163
Figure 4-6: 3D model representation of <i>zobellia_1580</i> OmpA-like protein based on CgOmpA (PDB accession: 5WTL). The overall structure is colored in turquoise and shown as ribbons. The Tyr425 is colored in red and shown as sticks.	165
Figure S4-1: ¹²⁵ I radioactivity measured on the mutant strain membrane fraction, migrated on a SDS-PAGE gel and placed on miniGita.	171
Figure S4-2: ¹²⁵ I radioactivity measured on the wild-type strain membrane fraction, migrated on a SDS-PAGE gel and placed on miniGita.	171
Figure 5-1: Hypothetical model of halogen-related metabolism within <i>Z. galactanivorans</i> (adapted from Fournier, 2014).....	176

List of Tables

<u>Table 0-1:</u> Abundance of halogen elements in the Earth's crust and the oceans (Greenwood & Earnshaw, 1997; Guillory, 2009).....	12
<u>Table 0-2:</u> Some examples of biochemically and structurally characterized halogenating enzymes.....	18
<u>Table 0-3:</u> Structural characterization of vanadium-dependent haloperoxidases (adapted from Leblanc et al 2015).	27
<u>Table 0-4:</u> Biochemically and structurally characterized L-2-HADs enzymes from bacteria.....	33-34
<u>Table 3-1:</u> Kinetic parameters of Zg-VIPO1, and Zg-VIPO2 (Fournier et al., 2014).	128
<u>Table 3-2:</u> Kinetic parameters of Zg-VIPO1, VIPO2 and VIPO3 (Fournier et al., 2014)	138
<u>Table 3-3:</u> Protein-Protein interface analysis performed using PDBePISA online tool for the structure of Zg-VIPO3 dimeric model, VCPO of <i>Streptomyces</i> sp. CNQ-525 (NapH1, PDB accession number 3w35) and VBPOI of <i>Ascophyllum nodosum</i> (An-VBPOI, PDB accession number AQI9).	143
<u>Table 4-1:</u> Predictions of Zg-VIPOs subcellular protein localization using 7 different generalist tools developed to discriminate the sorting between 4 or 5 compartments (membranes are not dissociated for ProtComb whereas outer and inner membranes are separated in others). More detailed results are provided in Table S4-1.....	152
<u>Table 4-2:</u> Predictions of the presence/absence of signal peptides (SP) and the type of these signals in Zg-VIPOs protein sequences using 10 different specialized tools. The best predictions are summarized in the total predictions column. Legend: type I signal peptide (SPI), type II signal peptide (SPII). More detailed results are given in table S4-2.	153
<u>Table 4-3:</u> Total iodine content of lyophilized bacterial pellets analyzed by ICP-MS for the <i>Z. galactanivorans</i> WT and <i>ΔIPO1</i> mutant, and <i>C. fucicola</i> strains after 2-days cultured in artificial ZoBell medium. Values are mean ± std deviation.	159
<u>Table 4-4:</u> Radioactive iodide detected in periplasm, cytoplasm and membranes fractions of <i>Z. galactanivorans</i> and <i>ΔIPO1</i> mutant. Values are mean ± std deviation.	162
<u>Table S4-1:</u> Predictions of Zg-VIPOs subcellular protein localization using 7 different generalist tools developed to discriminate the sorting between 4 or 5 compartments (membranes are not dissociated for ProtComb whereas outer and inner membranes are separated in others). Resulting localization or probability scores are reported in the table. The best prediction of Zg-VIPOs are mentioned in bold in each line and in bold and underlined in the total predictions column. Potential secondary compartments are shown in bold in this latter column. Legend: not determined (nd).	169
<u>Table S4-2:</u> Predictions of the presence/absence of signal peptides (SP) and the type of these signals in Zg-IPOs protein sequences using 12 different specialized tools. Results are reported with the score probability, the location of cleavage site when found and the length of the signal peptide in amino acids. The best predictions are in bold in each line and are summarized in the total predictions column. Legend: type I signal peptide (SPI), type II signal peptide (SPII), not determined (nd).	170

Abbreviations

BAA: bromoacetic acid
CAA: chloroacetic acid
DLS: Dynamic light scattering
DMSO: dimethyl sulfoxide
EDTA: Ethylenediaminetetraacetic acid
FAD: flavin adenine dinucleotide
FMN: flavin mononucleotide
HAD: haloacid dehalogenase
HDH: hydrolytic dehalogenase
HEPES: 4-(2-hydroxyethyl)-1-piperazineethanesulfonic acid
HOC: halogenated organic compounds
HOX: hypohalogenous acid
HPO: haloperoxidase
HRP: horseradish peroxidase
IAA: iodoacetic acid
ICP-MS: Inductively coupled plasma mass spectrometry
ID: iodothyronine deiodinase
IgG: immunoglobulin G
IPTG: Isopropyl β -D-1-thiogalactopyranoside
IYD: iodotyrosine deiodinase
Km: Michaelis constant of the enzyme
Kcat: number of molecules of product formed per one molecule of enzyme and time unit
LC-MS: Liquid chromatography–mass spectrometry
MCD: monochlorodimedone
MID: mono-iodotyrosine
MIT: di-iodotyrosine
OD: optical density
PCR: Polymerase chain reaction
RDH: reductive dehalogenase
ROS: reactive oxygen species
SAH: S-adenosylhomocysteine
SAM: S-adenosyl-L-methionine
SDS-PAGE: sodium dodecyl sulfate polyacrylamide gel electrophoresis
TB: thymol blue
TBS-T: Tris-buffered saline –tween 20
TEMED: N,N,N',N'-tetramethyl- 1,2-diaminoethane
VBPO: vanadium bromoperoxidase
VCPO: vanadium chloroperoxidase
VHOC: volatile halogenated organic compounds
VHPO: vanadium haloperoxidase
VIPO: vanadium iodoperoxidase
Vmax: enzyme maximum reaction rate

General introduction

1. Biogeochemical cycle of halogens

1.1. Definition of halogens

Fluorine (F), chlorine (Cl), bromine (Br) and iodine (I) belong to the group of halogens, located on the 17th column of the periodic table. Astatine (At) is at the intersection between halogen and metalloid elements, highly unstable, and not considered as being part of the halogen group. The word “halogen” means “salt-producing”. These chemical elements produce salts by reacting with metals, for example: calcium fluoride (CaF₂), sodium chloride (NaCl), silver bromide (AgBr) or potassium iodide (KI) (Greenwood & Earnshaw, 1997).

Halogens are natural chemical elements that are heterogeneously distributed between different Earth system reservoirs. Because of their reactivity, halogens do not occur in free elemental state, but are more often found in ionic forms (e.g., X⁻, where X is either Cl, Br or I). They can also be found as diatomic molecules (F₂, Cl₂, Br₂, I₂) and these gaseous forms can be highly reactive, oxidizing and toxic to organisms at high concentrations (Greenwood & Earnshaw, 1997). Chlorine, bromine and iodine are indeed often used as disinfectants; their toxicity depends on their speciation and concentration levels. Halogens can also form bonds with carbon, producing organic halogenated compounds. Those are widely diverse and come from biogenic sources as well as anthropogenic.

1.2. Inorganic halogenated compounds

The inorganic halogenated compounds are divided between gaseous halogen molecules (F₂, Cl₂, Br₂ and I₂), ionic forms, and halogen salts, and their total concentrations vary by several order of magnitude, depending of halogen type and natural sources (**Table 1**). Globally, fluorine- and iodine-containing products are the least abundant found on Earth, even though fluorine is the richest halogen found in the Earth’s crust (O’Hagan & Harper, 1999; Gribble, 2003). The least abundant halogen in the Earth’s crust and in oceans is iodine, whereas chlorine is the most abundant in oceans (**Table 1**).

	Earth's crust	Ocean water
Fluorine	544 ppm 13 th most abundant	1.2 ppm 14 th most abundant
Chlorine	126 ppm 20 th most abundant	19 500 ppm 3 rd most abundant
Bromine	2.5 ppm 46 th most abundant	65 ppm 9 th most abundant
Iodine	0.46 ppm 60 th most abundant	0.05 ppm 20 th most abundant

Table 0-1: Abundance of halogen elements in the Earth's crust and the oceans (Greenwood & Earnshaw, 1997; Guillory, 2009).

The most widespread chemical species of chlorine on the Earth's crust is the inorganic halide mineral, sodium chloride (NaCl). Similarly, NaCl is the most abundant inorganic halogen found in oceans, salt lakes, brines, and chloride ions represent half of the ocean total salinity (Greenwood & Earnshaw, 1997; Atashgahi et al., 2018). The bromine inorganic species are less abundant than the chlorine and fluorine ones in crustal rocks, however they are more abundant in ocean waters (Table 0-1). Regarding iodine, it is very rare on Earth but it is mostly found in oceans as inorganic trace species ($\sim 0.5 \mu\text{M}$) (Wong et al., 2003). In the ocean, dissolved inorganic iodine exists as iodate (IO_3^-) (< 0.1 to $0.45 \mu\text{M}$) and as iodide (I^-) (< 0.01 to $0.3 \mu\text{M}$) depending on the pH and the temperature of waters. The iodide is concentrated in surface waters, whereas the iodate dominates in deeper waters (Wong et al., 2003; Schwehr & Santschi, 2003).

1.3. Organic halogenated compounds

Halogens can form covalent bonds with carbon, C-F being the strongest and least chemically reactive. The bond strength weakens and the reactivity increases moving down the halogen column of the periodic table, meaning that iodinated organic compounds are the most instable among natural halogenated compounds (Greenwood & Earnshaw, 1997). The organic halogenated compounds can derive from human activities, geochemical processes or biogenic sources. They can also be volatile and emitted in the atmosphere.

Over 5000 halogenated organic compounds (HOCs) have been identified until now, and they constitute one of the largest groups of natural chemical products (for review, Gribble, 2015). These halogenated organic compounds are structurally and chemically very diverse. For

example, polyvinyl chloride (PVC), a widely used polymer in plastic production, represents the largest single end-use of chlorine. Other industrial halogenated compounds (such as chlorinated hydrocarbons), can be used as solvents, biocides, flame retardants, fumigants, degreasers and chemical intermediates. Since the 1960s, it is publicly known that the dissemination of those compounds in the environment results in terrestrial, aquatic and atmospheric contaminations which strongly impact the functioning and the health of ecosystems (for review, [Hägglom & Bossert, 2005](#)).

The HOCs are also naturally produced by a wide diversity of living organisms such as bacteria, plants, fungi, algae, lichens, insects and mammals ([Siuda & DeBerbardi, 1973](#); [van Pée, 1996](#); [Gribble, 1998](#); [1999](#)); as well as during abiotic natural processes like volcanic emissions, forest fire and other pyrogenic processes ([Jordan et al., 2000](#); [Gribble, 2003](#)). Soil, sediments, groundwater, salt lakes and oceans have been found to be the major source of volatile halogenated organic compounds (VHOCs) emission ([Asplund et al., 1989](#); [Keppler et al., 2000](#); [Weissflog et al., 2005](#); [Ruecker et al., 2014](#)). Most chlorinated and fluorinated organic compounds come from terrestrial anthropogenic sources, whereas most iodinated and brominated organic compounds derived from marine biogenic sources ([Gribble, 2003](#); [Ballschmiter, 2003](#)). In terrestrial environments, the forest soils are known as a main source of volatile organochlorine compounds including chloromethane, chloroform and other alkylchlorides ([Keppler et al., 2000](#)). The ocean is a major source of VHOCs such as methyl halides (CH_3X where X is either Cl, Br or I), and a large majority of these biogenic compounds are produced by a diversity of marine organisms ([Brownell et al., 2010](#); [Paul & Pohnert, 2011](#); [Sato et al., 2019](#)). It is essential to consider all those diverse biotic and abiotic sources in the global halogen biogeochemical cycle.

1.4. Biogeochemical cycle of halogens

Both land- and marine-emitted volatile organic and inorganic halogenated compounds participate to a complex biogeochemical cycle (**Figure 0-1**) leading to the formation of highly reactive halogen radicals in the atmosphere ([O'Dowd et al., 2002](#)). Those are responsible of destroying tropospheric ozone (O_3), a greenhouse gas that is very toxic to humans, animals and plants when present in the low atmosphere layers ([Lazrus et al., 1975](#); [Carpenter, 2003](#)). The iodinated volatile compounds such as methyl iodide (CH_3I) and diiodomethane (CH_2I_2) could contribute significantly to ozone depletion in the marine boundary layer ([Carpenter et al., 2014](#)). Inorganic iodine compounds like hypiodous acid (HIO) and I_2 are also an important source of

atmospheric iodine and participate to tropospheric ozone destruction (Carpenter et al., 2013). After reacting with ozone, they can form iodine oxide species (OIO and IO) that result to new aerosols particles, which are precursors to cloud condensation nuclei (O'Dowd et al., 2002; Saiz-Lopez et al., 2007; Küpper et al., 2008). During rainfall, halogenated compounds reach soils where they can accumulate and/or be metabolized by living organisms. They can also return to oceans through runoff waters and underground rivers.

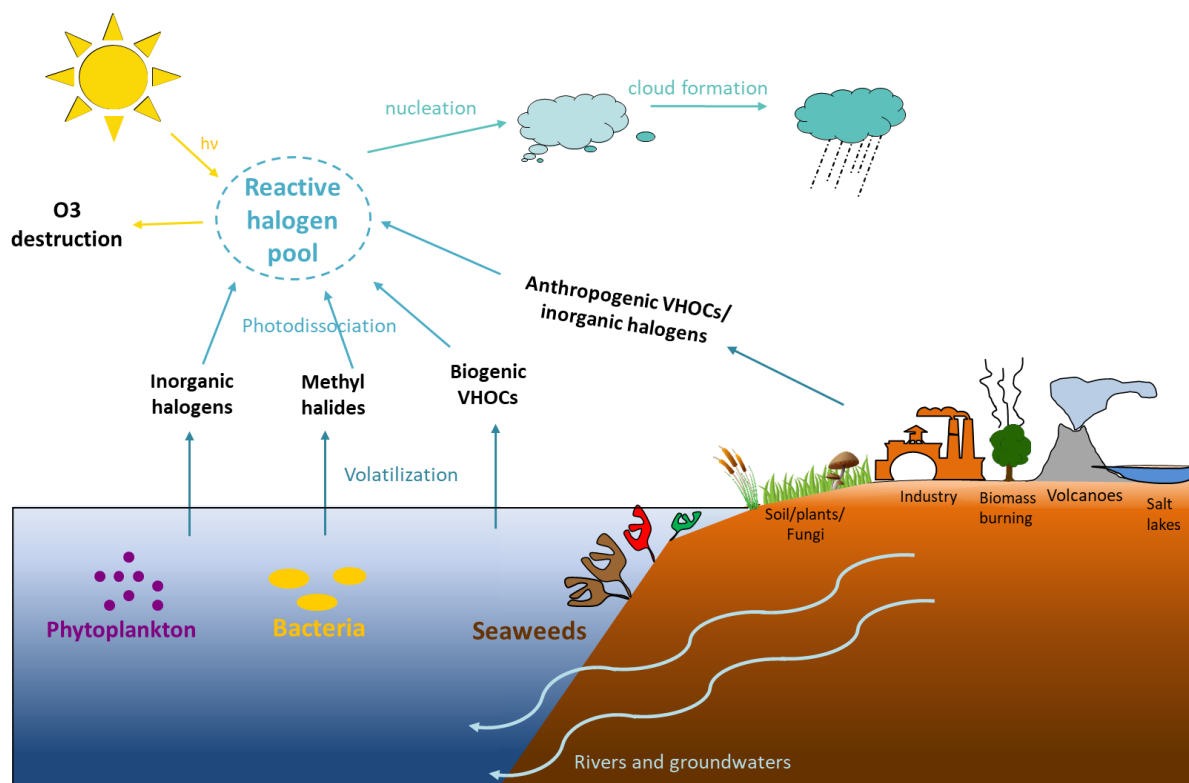


Figure 0-1: Schematic overview of the global halogen biogeochemical cycle (adapted from Fournier & Leblanc, 2014)

The marine macroalgae contribute approximately to 70% of the total atmospheric bromoform (CHBr_3) (Carpenter & Liss, 2000). The annual global production of methyl iodide (CH_3I) is estimated $1\text{--}4 \times 10^{11}$ g/year (Moore & Groszko, 1999), but the macroalgal contribution is less than 0.2% (Laternus, 2004). The marine phytoplankton and the cyanobacteria are the primary contributors of CH_3I emissions in the atmosphere with 1.2 to 38×10^9 g/year produced, followed by the bacterial production with 1.6×10^9 g/year (Moore & Groszko, 1999; Amachi et al., 2008; Brownell et al., 2010).

The marine macroalgae are also known to be strong accumulators of iodine in the case of brown algae, and especially *Laminariales* (Küpper et al., 1998) and, in a lesser extent, of bromine in the case of red algae (Latham, 2008). The red and brown macroalgae are therefore important

biogenic producers of halogenated compounds in the coastal marine areas (Carpenter et al., 2000; Laturnus, 2001). For example, red algal species of *Asparagopsis* or *Laurencia* genera are the source of more than 100 organohalogens (for review, Gribble, 2015). Moreover, *Fucus vesiculosus* and *Ascophyllum nodosum*, two brown algal species belonging to Fucales, have been found to be strong emitters of molecular iodine (Huang et al., 2013). The *Laminaria* genus is known to be producer of organic (methyl iodide, diiodomethane) but mainly inorganic iodinated compounds above seaweed beds (Carpenter, 2003; Leblanc et al., 2006). For these kelps, inorganic compound emissions, essentially I₂, actually dominate over the organic species by at least five orders of magnitude (Küpper et al., 2008).

2. Biological importance of halogen metabolism in marine organisms

2.1. Biotic stress responses and halogenated compounds

The marine organisms are exposed to biotic stresses from herbivores, bacteria, fungi, virus, during their life cycle. Naturally produced halogenated compounds are suggested to be involved in chemical defense, even though biological or ecological roles have been established for few of them. For example, the red alga *Asparagopsis taxiformis* released brominated compounds, mahorone and 5-bromomahorone, which were found to be highly toxic to the marine bacterium *Vibrio fisheri* (Greff et al., 2014). The bromoform and dibromoacetic acid, both natural products produced by the red alga *Asparagopsis armata*, were shown to be efficient antibacterial compounds (Paul et al., 2006). The halophenols and haloterpens are other secondary metabolites produced by red algae, and potential herbivore deterrents (Hay & Fenical, 1988). Fewer brominated metabolites have been identified in brown algae, but some members of this group, such as *Laminariales*, also featured iodinated compounds (for review, La Barre et al., 2010). *Laminaria digitata* can accumulate iodine at an average of 30,000-fold the seawater concentration. The cyanobacteria *Leptolyngbya crossbyana* produces an organic chlorinated compound that inhibits quorum sensing against *Vibrio harveyi* (Choi et al., 2012). The brominated compounds, synthesized by the green alga *Ulveella lens*, inhibit the growth of sea urchins (Agatsuma et al., 2008). Many of those marine halogenated compounds showing strong biological activities using laboratory bioassays have been investigated in the research field of natural product chemistry, to develop drugs against a wide range of bacterial and fungal pathogens but also for anti-tumoral or anti-inflammation applications (for review, Gribble, 2015).

2.2. Oxidative stress responses and iodine metabolism

As said above, molecular iodine emissions by kelps have been shown to be also related to environmental oxidant stress such as changes in temperature, salinity, nutrient depletion, UV radiation, especially during low tide and desiccation (Laternus, 2004; Mata et al., 2012; Leedham et al., 2013). Releases of iodide have also been observed in *L. digitata*, *Fucus serratus* and *Kallymenia antarctica* upon stress (Gall et al., 2004; Truesdale, 2008; Chance et al., 2009). The release of halogenated compounds by the red alga *Gymnogongrus antarcticus* was highly affected after its exposure to different environmental conditions (Laternus et al., 2000).

Endogenous defense elicitors such as oligogulonates, applied to the kelp *L. digitata*, induce an oxidative burst, i.e. a strong production of reactive oxygen species (ROS), such as hydrogen peroxide (H₂O₂), hypothesized to be part of antibacterial defense mechanisms (Küpper et al., 2001). In addition, *Laminariales* seem to feature a unique capability to use accumulated iodine as antioxidant following biotic or abiotic stresses (for review, La Barre et al., 2010). The massive release of iodine, mainly I₂, was proposed to have defense and antioxidant roles in brown algae during low tides (Palmer et al., 2005; Küpper et al., 2008; Ball et al., 2010). In *L. digitata*, the iodide (I⁻) is accumulated in the cell wall of peripheral algal tissues (Verhaeghe et al. 2008b) and could act as an efficient antioxidant protection by detoxifying the excess of hydrogen peroxide and other ROS on kelp surfaces, producing oxidized iodine species, such as I₂. Moreover, the defense elicitation seemed to specifically activate an iodine-related metabolism in the brown alga *L. digitata*, as observed by transcriptomic regulations of vanadium haloperoxidase enzymes (VHPO, cf. part 4) (Cosse et al., 2009). According to Strittmatter et al., 2016, when the brown alga *Ectocarpus siliculosus* is infected by *Eurychasma dicksonii*, the halogen metabolism is also upregulated in response to the pathogen attack. A bromoperoxidase was excreted after production of H₂O₂, and was the strongest upregulated protein during the infection. Similarly, the study of iodine-related metabolism in the marine microalga *Tisochrysis lutea* showed that a putative haloperoxidase might be involved in detoxifying ROS during an oxidative stress (Javier et al., 2018). All these examples suggest a putative key role of halogen-related metabolism during protection against biotic and abiotic stresses in marine algae, with particular defense mechanisms in *Laminariales*, related to iodine metabolism.

2.3. Halogen-related metabolism in bacteria

A wide diversity of bacteria lives on the surfaces of macroalgae as part of their associated microbiome. The influence of the iodinated exudates of the kelp *L. digitata* on bacterial adhesion and biofilm formation was investigated by [Salaün et al., 2012](#). Even though all the bacteria used for the experiments were isolated directly from this species, the impacts of those exudates were different depending on bacterial strains and chemical nature of tested compounds. In some cases, the biofilm growth decreased (*Pseudomonas* sp. LD6), or on the contrary it was induced (*Zobellia galactanivorans*). Some bacteria strains appeared to possess adaptive traits to survive on those particular algal surfaces: for instance, *Z. galactanivorans* could use mannitol, a potential anti-fouler, as carbon source ([Salaün et al., 2012](#)).

It was previously assessed that methyl halide production by marine bacteria was of main importance as they were the second major producers ([Amachi et al., 2008](#)). For instance, marine *Proteobacteria* such as *Erythrobacter* and *Pseudomonas* were detected as sources of methyl halides in the open ocean ([Fujimori et al., 2012](#)), and the emission rates were impacted by the water temperature ([Hirata et al., 2017](#)). Unfortunately, it is still not fully understood which bacteria and which enzymatic pathways are contributing to those emissions. Few studies have been dedicated to explore bacterial iodine metabolism. Some *Proteobacteria*, such as *Pseudomonas* sp. strain SCT, participate to the cycle of iodine by reducing IO_3^- into I^- ([Councill et al., 1997](#); [Amachi et al., 2007](#)), while some α -*Proteobacteria*, such as *Iodidimonas* sp. Q-1, are able to oxidize I^- into I_2 ([Amachi et al., 2005](#); [Suzuki et al., 2012](#)). Furthermore, two strains of *Roseovarius* spp. have been described to emit methyl iodide (CH_3I) and diiodomethane (CH_2I_2) thanks to GC-MS analysis ([Fuse et al., 2003](#)). Both iodine-reducing and iodine-oxidizing bacteria seem to be major contributors to the iodine cycle, but their exact global implication is yet to be discovered (for review, [Yeager et al., 2017](#)).

3. Enzymatic mechanisms involved in halogenation and dehalogenation

The biological uses of halogens are not widespread in the tree of life, but some emblematic examples of this particular metabolism have been described in specific lineages. For instance, the mammalian thyroid system is known to efficiently concentrate iodine through specific iodide symporters and is the place of biosynthesis of iodinated thyroid hormones, involved in essential physiological regulations (for review, [Rousset et al., 2015](#)). During the biosynthesis of halogenated organic compounds (HOCs), the halogenation step corresponds to a chemical reaction binding halogen and carbon atoms and requires specific enzymatic mechanisms, which

are diverse and have emerged independently in different lineages, such as those of animals, fungi, red and brown algae, and bacteria (for review, [Agarwal et al., 2017](#)). Another specialized enzymatic process is the dehalogenation which cleaves the carbon-halogen bond and leads to the recycling of halogens and/or the detoxification of HOCs. The enzyme-based microbial degradations of organohalogenes have been reviewed in a large number of papers since the last 30 years. It has been established for instance that some terrestrial bacteria can use organohalogenes for growth as a carbon source ([Fetzner, 1998](#); [Goodwin et al., 1998](#)), or as terminal electron acceptor for respiration ([McCarthy, 1997](#); [Atashgahi et al., 2018](#)). Organohalogenes degradation by dehalogenases was also investigated for potential bioremediation applications (for review, [Kurihara & Esaki 2008](#); [Jugder et al., 2015](#)). Both halogenation and dehalogenation enzymatic mechanisms are presented in the following paragraphs.

3.1. Halogenating enzymes

Six groups of halogenating enzymes have been described based on their enzymatic mechanisms and cofactor specificity (for review, [Xu & Wang, 2016](#)). Some examples are listed in **Table 0-2**.

Name	Species	Activity/Cofactor	PDB accession	References
Flavin-dependent halogenases	<i>Pseudomonas fluorescens</i>	Chloro/FADH ₂ , O ₂	2AQJ	Dong et al., 2005
Non-heme iron-dependent halogenases	<i>Pseudomonas syringae</i>	Chloro/Fe ²⁺ , O ₂ , α-KG	2FCT	Blasiak et al., 2006
	<i>Pseudomonas syringae</i>	Bromo/Fe ²⁺ , O ₂ , α-KG	2FCV	Blasiak et al., 2006
Heme iron-dependent haloperoxidases	<i>Caldariomyces fulmago</i>	Chloro/Heme	1CPO	Sundaramoorthy et al., 1995
SAM-dependent halogenases	<i>Streptomyces cattleya</i>	Fluoro/FDAS, SAM	1RQR	Dong et al., 2004
	<i>Salinispora tropica</i>	Chloro/SaIL, SAM	2Q6K	Eustaquio et al., 2008
Cofactor-free haloperoxidases	<i>Streptomyces aureofaciens</i>	Bromo	1BRO	Hofmann et al., 1998
	<i>Streptomyces aureofaciens</i>	Chloro	1A7U	Hofmann et al., 1998
Vanadium-dependent haloperoxidase	<i>Curvularia inaequalis</i>	Chloro/vanadate	1VNC	Messerschmidt & Wever, 1996
	<i>Ascophyllum nodosum</i>	Bromo/vanadate	1QI9	Weyand et al., 1999
	<i>Zobellia galactanivorans</i>	Iodo/vanadate	4CIT	Fournier et al., 2014

Table 0-2: Some examples of biochemically and structurally characterized halogenating enzymes

The first group is represented by the flavin adenine dinucleotide (FAD)-dependent halogenases. They are divided in two groups: those acting on free halide (usually chloride) and those acting on substrates tethered to a carrier protein (Ludewig et al., 2020). They were mostly isolated from several bacteria, but recently two putative fungal FAD-dependent halogenases have been reported to be involved in biosynthesis of halogenated metabolites (Ferrara et al., 2016; Han et al., 2019). In addition, the first viral FAD-dependent halogenase has been described recently from a marine virus (Gkotsi et al., 2019). Despite having a wide diversity of substrates like indoles, pyrroles, phenols or aliphatic compounds (Phintha et al., 2020), the catalytic mechanism is highly conserved and involves two separated and distant binding sites for FAD cofactor and substrate. The catalytic reaction is dependent of the FAD cofactor that needs to be firstly reduced in FADH₂ by a flavin-reductase, then undergoes a reaction with a water molecule to form a flavin-C(4a)-hydroperoxide intermediate (Yeh et al., 2006). A chloride anion then reacts with FADH₂ to form the corresponding hypochlorous acid (HOCl). This reactive HOCl species then moves through a tunnel from the FAD-binding site to the active site, where it interacts with a catalytic lysine residue to form a chloramine intermediate, followed by a regiospecific delivery to aromatic (tryptophan) residue (**Figure 0-2A-C**) (Ludewig et al., 2020).

The second group corresponds to the S-adenosyl-L-methionine (SAM)-dependent halogenases, which use a nucleophilic attack mechanism. These enzymes do not need to activate the halide by oxidation, but use SAM as a cofactor. Two classes of those enzymes are known: the 5'-halo-5'-deoxyadenosine synthases (5'-FDAS) and the halide methyl-transferases. The 5'-FDAS from *Streptomyces cattleya* is the only known fluorinating enzyme, which participates in the formation of fluoroacetate and fluorothreonine. It catalyzes the formation of C-F bond using a nucleophilic substitution on the C-5' carbon of the SAM co-substrate (Dong et al., 2004; Zhu et al., 2007). The halide methyl-transferases catalyze a nucleophilic substitution reaction between SAM and halide ions to form methyl halides and S-adenosylhomocysteine (SAH) (**Figure 0-2D**).

The third group comprises the non-heme iron-dependent halogenases, a class of highly homologous enzymes that halogenate an inactivated aliphatic carbon center, using non-heme iron (Fe²⁺), O₂ and α -ketoglutarate as cofactors. It is the only group of haloperoxidases that catalyzes reactions of radical halogenation (Ludewig et al., 2020). Those enzymes have been demonstrated to specifically catalyze the chlorination and bromination of organic compounds, and their resulting products are currently known to be amino acids and indole alkaloids derivatives (**Figure 0-3A**) (Vaillancourt et al., 2005; Voss et al., 2020). For instance, in

Pseudomonas syringae, this enzyme is involved in the chlorination of threonine during the biosynthesis of syringomycin E, a phytotoxic molecule (Vaillancourt et al., 2005). All these enzymes require substrates bound to a separate protein except for WelO5 from *Hapalosiphon welwitschii*, which acts on free substrates (Hillwig & Liu, 2014).

The fourth group is composed of the heme iron-dependent haloperoxidases, firstly characterized in the terrestrial fungus *Caldariomyces fumago* (Geigert et al., 1986). Those enzymes oxidize halides with H_2O_2 (Figure 0-3B) to produce free hypohalogenous acid (HOX), highly reactive (Kühnel et al, 2006). Consequently, they can halogenate a large panel of organic compounds and particularly aromatic, electron-rich substrates (Hofrichter & Ullrich, 2006). They are divided into two superfamilies regrouping on one hand the bacterial, fungal and plant enzymes and on the other hand the animal peroxidases like mammalian myeloperoxidase, lactoperoxidase, eosinophil peroxidase, and thyroid peroxidase. A broad range of halogen specificity is encountered in these latter enzymes where myeloperoxidases can oxidize Cl^- , Br^- and I^- , eosinophil peroxidases can catalyze bromination and iodination, and lactoperoxidases are specific to I^- oxidation. Thyroid peroxidases are responsible of the thyroid hormone thyroxine biosynthesis (for review, Blasiak et al., 2009).

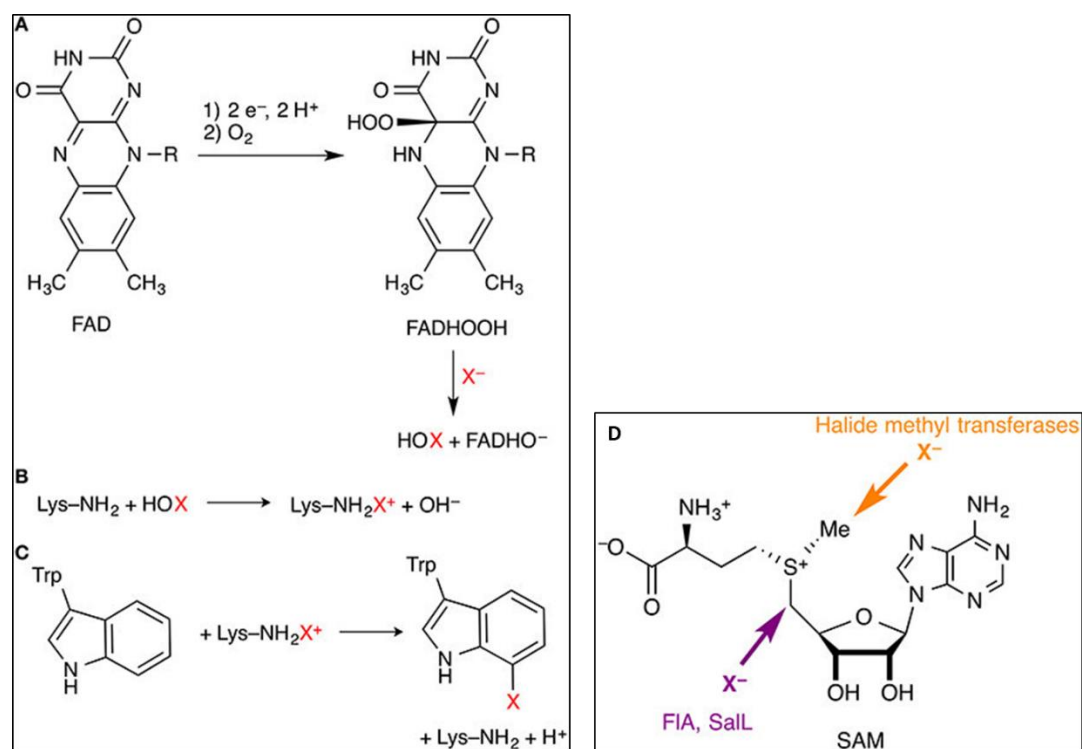


Figure 0-2: Key steps of the catalytic mechanisms of flavin-dependent halogenases. (A) Formation of FADHOOH, which oxidizes X^- to HOX. (B) Proposed formation of a lysine N-haloamine intermediate. (C) Electrophilic aromatic substitution of the tryptophan substrate. (D) Nucleophilic halogenases catalyze the attack

of halide anions (X^-) as nucleophiles on SAM. The fluorinase FIA and the chlorinase SaL produce halogenated adenosines, whereas halide methyl-transferases produce halomethanes. (Source: Senn, 2014).

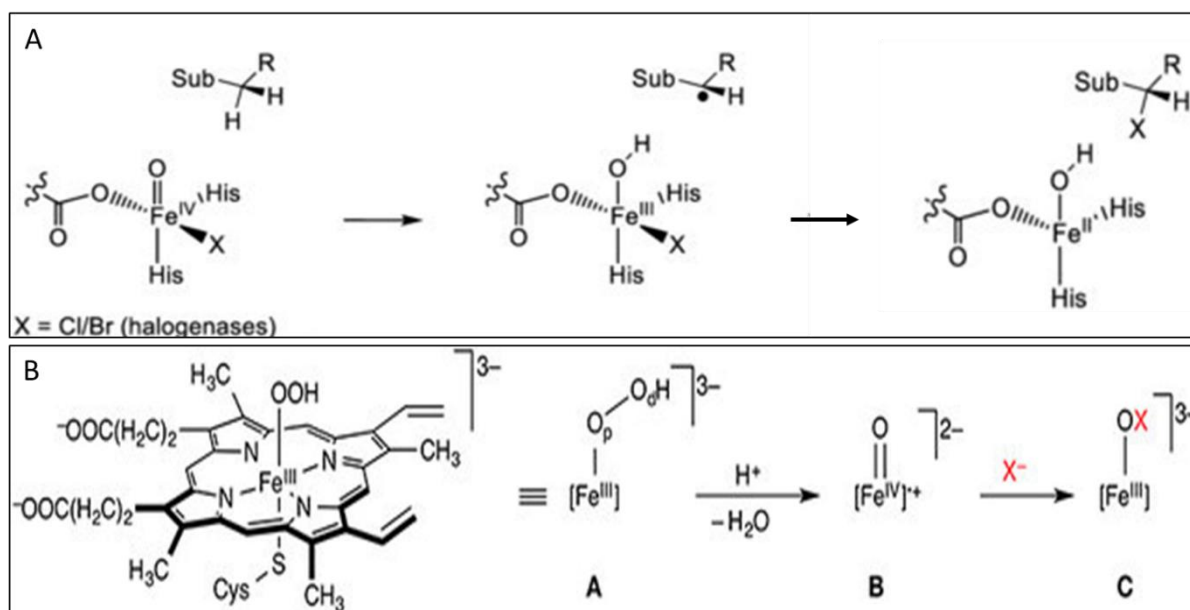


Figure 0-3: (A) Catalytic mechanisms of the non-heme iron halogenases (Source: Timmins & de Visser, 2018). (B) Key steps of the heme-dependent haloperoxidase mechanism (Source: Senn, 2014).

The fifth group is represented by the cofactor-free haloperoxidases (HPOs), for which a catalytic mechanism of halide oxidation using hydrogen peroxide (H_2O_2) has been proposed to produce peroxyacid and hypohalogenous acid (HOX) intermediates (Hofmann et al., 1998). The HPOs have an active site pocket as well as a conserved substrate-binding site that may be involved in the halogenation of hydrophobic compounds (for review, Xu and Wang, 2016). The cofactor-free haloperoxidases probably need to function with organic acids like benzoate or propionate as co-substrates. Eight structures of these enzymes, all belonging to bacteria, have been solved and released in the PDB database. Evolutionary relationship and similar overall topology have been found between HPOs and enzymes of the α/β hydrolase group, such as esterases and lipases (for review, Xu & Wang, 2016). Among HPOs, the bromoperoxidase from *Streptomyces aureofaciens* (Krenn et al., 1988) and the chloroperoxidase from *Pseudomonas pyrocinia* (Wolfframm et al., 1993) appear to be involved in the biosynthesis of pyrrolnitrin and chlortetracycline antibiotics.

The last group refers to vanadium-dependent haloperoxidases (VHPOs). Like the previous group, they catalyze the oxidation of halides using H_2O_2 , except that they feature vanadium as a cofactor. The biochemistry and characteristics of this group of halogenating enzymes are fully described later, in **paragraph 4**.

3.2. Dehalogenating enzymes

There are four types of dehalogenating enzymes described up to now based on their enzymatic mechanisms and substrate specificities (for review, [Agarwal et al., 2017](#)):

The first type belongs to the deiodinases from the thyroid hormone system of mammals. They are the only known dehalogenases from mammals. They play an essential role in human health as they control the thyroid hormone biosynthesis. Iodotyrosine deiodinases (IYD) are transmembrane proteins and they use flavin mononucleotide (FMN) as a cofactor. They scavenge iodide in the thyroid gland by catalyzing the Tyr-I bond of mono- and di-iodotyrosine (MIT and DIT), the byproducts of thyroid hormones T3 and T4. The scavenged iodide is then used to synthesize thyroid hormones again, creating an iodide cycle within the thyroid gland (**Figure 0-4A**) ([Thomas et al., 2009](#)). Iodothyronine deiodinases (ID) are responsible for dehalogenating thyroxine (T4) into triiodothyronine (T3) hormone. These enzymes have the particularity to contain a selenocysteine in the active site (**Figure 0-4B**) (for review: [Bianco & Kim, 2006](#); [Gereben et al., 2008](#)). In addition, the mammalian deiodinases can display in vitro debrominase and dechlorinase activities on halogenated tyrosines ([McTamney & Rokita, 2009](#)). The last studies tend to demonstrate that IYDs are more widely spread in the nature than primarily thought as marine invertebrate and insect protein orthologues have been heterologously expressed and recently characterized at the biochemical and structural level ([Sun & Rokita, 2018](#)). Homologous IYD proteins are also found in bacteria without the N-terminal transmembrane segment. The recombinant IYD of *Haliscomenobacter hydrossis* exhibited a substrate specificity for halotyrosines ([Ingavat et al., 2017](#)), even though the nature of the biological substrates and metabolic roles of these bacterial IYDs have not yet been solved.

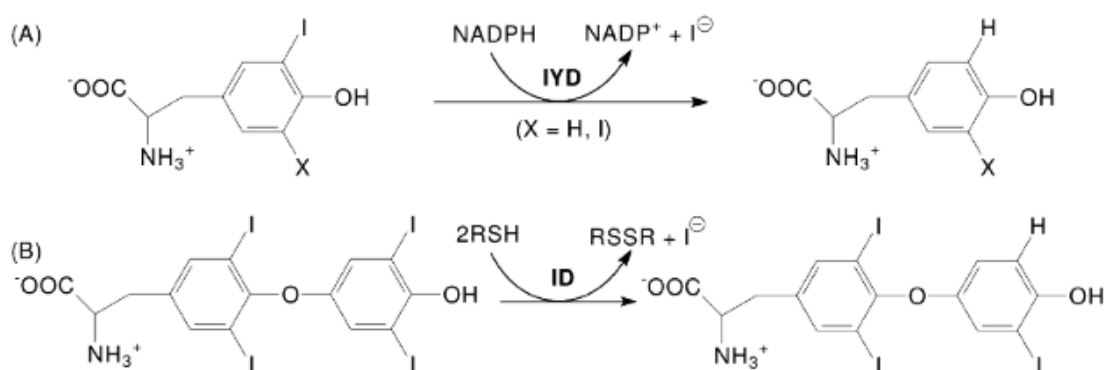


Figure 0-4: Deiodination catalyzed by (A) iodotyrosine deiodinase (IYD) and (B) iodothyronine deiodinase (ID) (source: Fournier, 2014)

The second type is represented by the reductive dehalogenases (RDHs) which can catalyze reactions with anthropogenic substrates making them enzymes of interest for bioremediation. One subfamily has been isolated from anaerobic bacteria and these RDHs utilize a broad range of organohalogenes as terminal electron acceptors in organohalide respiration chain, a particular energy-conserving metabolic process implicated in the global halogen cycle (Hug et al., 2013). In the other subfamily, glutathione S-transferase-like reductive dehalogenases are capable of dehalogenating toxic substrates by a catalytic attack of a cysteine thiolate on the halogen (**Figure 0-5A**). Examples of those enzymes involved in artificial chemical degradation are BphK from *Burkholderia xenovorans* strain LB400 (Fortin et al., 2006) and PcpC from *Flavobacterium sp.* strain ATCC39723 (Orser et al., 1993).

The third type of dehalogenating enzymes catalyze oxidative dehalogenation, such as dioxygenases. The catalytic mechanism involves the replacement of a halogen with a hydroxyl group derived from a molecular oxygen or hydrogen peroxide (**Figure 0-5B**) (for review: Arora & Bae, 2014, and references therein). This type of dehalogenating enzymes is mainly involved in the degradation of chlorophenols and their derivatives. For example, dioxygenases are involved in the bacterial degradation pathway of 4-chlorophenol from *Comamonas testosteroni* JH5 (Hollender et al., 1997).

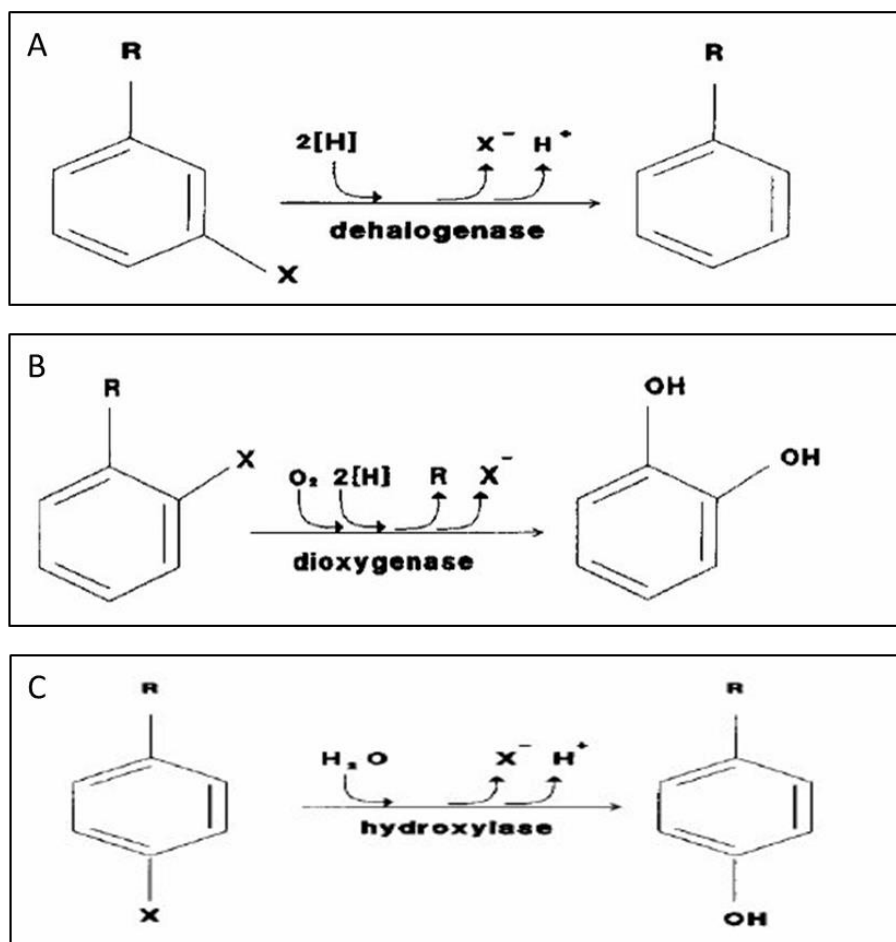


Figure 0-5: (A) reductive dehalogenation, (B) oxidative dehalogenation and, (C) hydrolytic dehalogenation (source: Sayyed & Patel, 2011).

The last type is represented by hydrolytic dehalogenases (HDHs) that encompass widely diverse hydroxylase enzymes. They catalyze the substitution of a halogen by a hydroxyl group derived either from a water molecule or from a vicinal alcohol (**Figure 5C**) (for review, [de Jong & Dijkstra, 2003](#)). The catalytic mechanisms of HDHs are named according to their substrate specificity. For example, the fluoroacetate dehalogenases are specific to fluorinated substrates, while the haloalcohol dehalogenases are specific to halohydrin substrates. The hydrolytic dehalogenation is commonly performed by haloalkane dehalogenases, 2-haloacid dehalogenases, 4-chlorobenzoyl-CoA dehalogenases and fluoroacetate dehalogenases (for reviews, [de Jong & Dijkstra, 2003](#); [Kurihara & Esaki, 2008](#)). The most studied are the haloalkane dehalogenases that are widely distributed in the tree of life and are certainly predominant in marine environment (for review, [Kunka et al., 2018](#)). The other largely expanded group is the 2-haloacid dehalogenases (for review, [Janssen et al., 2005](#)). This latter is further described in **paragraph 5**.

4. Vanadium-dependent haloperoxidases (VHPO)

4.1. Biochemical and structural characterization of VHPOs

The vanadium-dependent haloperoxidases (EC 1.11.1.10) catalyze the oxidation of halides (X^- : I $^-$, Br $^-$ or Cl $^-$) in the presence of hydrogen peroxide. During the catalytic cycle, the vanadate cofactor coordinates one molecule of H₂O₂ to form a stable peroxovanadate intermediate. This intermediate will then react with halide. After this step, the oxidized halogen intermediate (X^+ which is a mixture of different halogen species such as OX $^-$, X₃ or X₂) is very reactive and can halogenate a wide variety of nucleophilic organic substrates by a non-enzymatic reaction. In the absence of organic substrate, a second equivalent of H₂O₂ is oxidized to form an oxygen molecule and release the halide ion X $^-$ (**Figure 0-6**) (for review, [Leblanc et al. 2015](#)). The VHPOs are named according to the most electronegative halide they can oxidize. The vanadium-dependent chloroperoxidases (VCPO) can oxidize chloride, bromide and iodide; the vanadium-dependent bromoperoxidases (VBPO) can oxidize chloride and bromide; and the vanadium-dependent iodoperoxidases (VIPO) are specific to iodide oxidation (for reviews, [Winter & Moore, 2009](#); [Leblanc et al. 2015](#); and references through in).

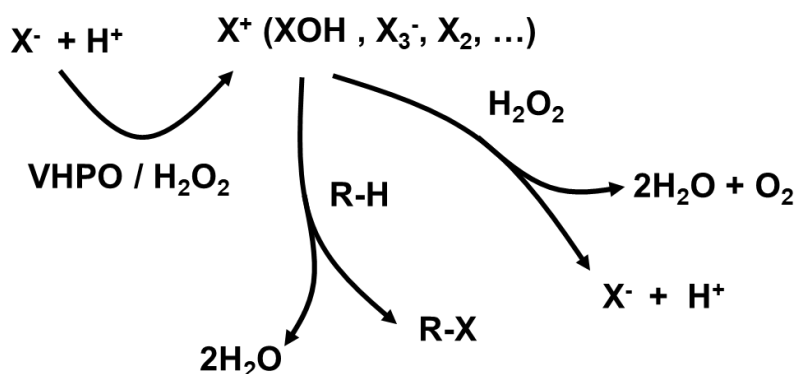


Figure 0-6: Reactions of the VHPO/H₂O₂ system. X: Br, Cl, I. R-H: organic compound. (Fournier and Leblanc, 2014)

In order to assess the VHPO enzymatic activities, a variety of sensible and reliable assays is available. The most common approach to determine VCPO and VBPO activities is the monitoring of monochlorodimedone (MCD) absorbance decrease at 290 nm ([De Boer & Wever, 1988](#)). It can detect halogenating activity quantitatively if the pH is below 6.5. Another qualitative method based on the halogenation of *o*-dianisidine can be used to determine chloro-, bromo- and iodo-peroxidase activities but only on native gels ([Jordan & Vilter, 1991](#)). The

phenol red dye can also be used to determine VBPO and VCPO activities at 590 nm but only qualitatively and is also very useful as a visual screening assay (De Boer et al., 1987). Another quantitative spectrophotometric assay, used to determine both VBPO and VIPO kinetic parameters, has been developed by Verhaeghe et al., 2008a. It is based on the halogenation of thymol blue by following the absorbance increase at 620 nm. This method is also pH dependent and reliable between pH 7 and 8. Moreover, thymol blue is a dye that changes color during its halogenation and thus can be used for rapid screening assay of VIPO or VBPO activities, in solution or directly in gel. VIPO activity was previously assessed by the spectrophotometric detection of triiodide (I_3^-) at 350 nm (Björkstén, 1968). I_3^- is one of the intermediates formed during the catalytic reaction. However, this assay has been shown to present important quantitative biases and be less reliable than thymol blue assay for biochemical studies of VIPO (Verhaeghe et al., 2008a). All these enzymatic assays were applied to characterize VHPO catalytic activities of purified native or recombinant enzymes from seaweeds, bacteria, fungi and cyanobacteria (Itoh et al., 1986; Sheffield et al., 1992; Hemrika et al., 1999; Colin et al., 2005; Wischang & Hartung, 2011; Johnson et al., 2011; Baharum et al., 2013; Fournier et al., 2014; Frank et al., 2016; Mckinnie et al., 2018). Up to this day, VHPOs from seaweeds have been shown to possess the highest catalytic activity compared to other organisms. According to Wischang et al. (2012) and Colin et al. (2005), VBPO-II from *Ascophyllum nodosum* and VIPO from *Laminaria digitata* have respective k_{cat} for iodide of 153 s^{-1} and 462 s^{-1} .

In terms of structural protein characterization, only 8 VHPOs from 7 different species have been studied, corresponding to 19 VHPO X-ray structures referenced in public databases up to now (listed in **Table 0-3**). These 3D structures correspond to either native, recombinant or derived enzyme forms (site-directed mutants, apo-proteins, etc) of VHPOs. Briefly, the tertiary structural foldings of VHPOs are highly conserved with helical bundles of alpha helices and identical arrangements of amino acid residues at the vanadium active sites, suggesting similar catalytic mechanisms. However, site-directed mutagenesis analyses of fungal VCPO, red algal VBPO and bacterial VIPO have shown that specific amino acids and hydrogen-bonding network around the vanadate center were both essential for catalytic properties and halide specificity (Fournier et al., 2014; for review, Leblanc et al. 2015). Other striking differences concern quaternary VHPO arrangements in solution between the different phyla, where monomers, covalently-bound homodimers, and homodimers self-rearranged into hexamers or dodecamers have been described (**Table 0-3**).

Table 0-3: Structural characterization of vanadium-dependent haloperoxidases (adapted from Leblanc et al 2015).

<i>Species</i>	<i>Activity</i>	<i>PDB Accession #</i>	<i>Structure</i>	<i>References</i>
Brown Alga				
<i>Ascophyllum nodosum</i>	VBPOI	1QI9	homodimer	Weyand et al., 1999
	VBPOII	5AA6	homo-hexamer	Radlow et al., 2018
Red Alga				
<i>Corallina officinalis</i>	VBPO	1QHB	dodecamer	Isupov et al., 2000
<i>Corallina pilulifera</i>	VBPO	1UP8	dodecamer	Garcia-Rodriguez et al., 2005
Fungi				
<i>Curvularia inaequalis</i>	VCPO	1VNC	monomer	Messerschmidt & Wever, 1996
Bacteria				
<i>Zobellia galactanivorans</i>	VIPO1	4CIT	monomer	Fournier et al., 2014
<i>Streptomyces</i> sp. CNQ-525	VCPO	3W35, 3W36	dimer	Liscombe et al., 2013 (unpublished)
<i>Acaryochloris marina</i>	VBPO	5LPC	dodecamer	Frank et al., 2016

VBPO: vanadium-dependent bromoperoxidase; VIPO: vanadium-dependent iodoperoxidase; VCPO: vanadium-dependent chloroperoxidase

4.2. Occurrence, evolution and putative biological roles of VHPOs

In the marine organisms, it appears that the VBPOs are the most common VHPOs, especially within red and brown macroalgae (for review, [Leblanc et al., 2015](#)). VBPO activities also occur in a variety of diatoms species ([Moore et al., 1996](#); [Hill and Manley, 2009](#)), *Cyanobacteria* ([Johnson et al., 2011](#); [Frank et al., 2016](#)) and planktonic communities ([Archer et al., 2019](#)). Some marine bacteria such as *Streptomyces* (for review, [Mckinnie et al., 2018](#)) and terrestrial fungi ([Simons et al., 1995](#); [Barnett et al., 1998](#)) feature VCPOs. The first VIPOs were characterized in brown macroalgae, belonging to *Laminariales*, and it was relevant as they are the strongest known accumulators of iodine, particularly *L. digitata* ([Küpper et al., 1998](#); [Colin et al. 2005](#)). More recently, it was also shown that the marine flavobacterium *Zobellia galactanivorans* possesses two VIPOs, and a third VHPO, more divergent in amino acid sequence, that is yet uncharacterized at the biochemical and structural levels ([Fournier et al., 2014](#); [Barbeyron et al., 2016](#)).

A previous phylogenetic analysis allowed the identification of numerous VHPO bacterial homologs in public protein databases and showed a large spreading of VHPO in bacterial lineages (**Figure 0-7**; [Fournier et al. 2014](#)). The phylogeny and conservation of 3D structures suggested a common origin for all VHPOs deriving from a marine bacterial ancestor, related to bacterial acid phosphatases. The algal VHPOs seem to be derived more precisely from VBPOs from *Cyanobacteria* (for review, [Leblanc et al., 2015](#); [Frank et al. 2016](#)). Moreover, the emergence of VIPOs, i.e. the specificity for iodide oxidation, would result in a convergent evolution of the divergent phyla of *Bacteroidetes* and *Laminariales* ([Fournier et al. 2014](#)).

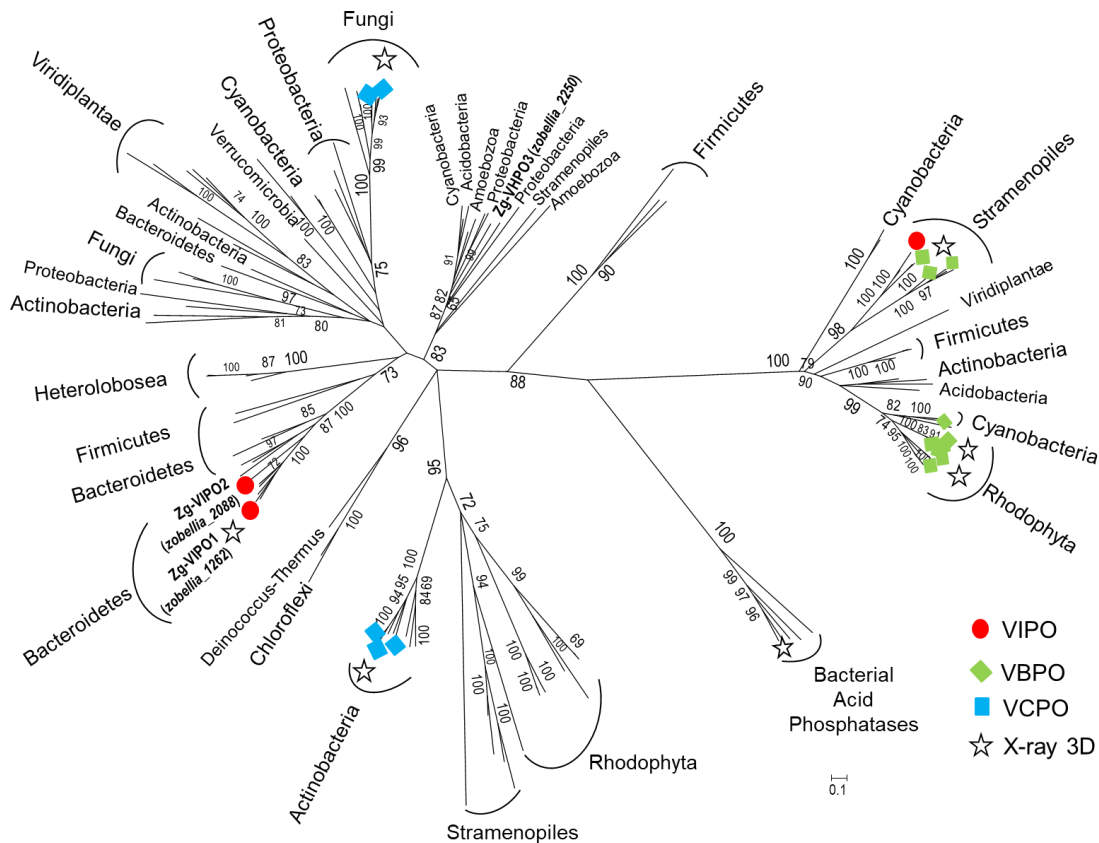


Figure 0-7: Phylogenetic analysis of VHPO proteins. A protein maximum likelihood (PML) tree was constructed using the multiple alignment of characterized and putative VHPO from 124 eukaryotic and selected bacterial species, and of five Bacterial Acid Phosphatases. When characterized at the biochemical level, the VHPO specificity towards halides is mentioned and refers to the legend code, i.e. iodo- (VIPO), bromo- (VBPO) or chloroperoxidase (VCPO) activity. The available 3D structures of VHPO are indicated by a star (from Fournier et al. 2014).

In macroalgae, some VHPOs were shown to be up-regulated at the transcriptomic level and to be part of antioxidative responses following a stress (cf. **paragraph 2.3**). For instance, their detoxifying role was pointed out in the red algae *Corallina officinalis* and *Gracilaria changii* where the expression of VBPO enzyme increases during an abiotic stress (Latham, 2008; Baharum et al., 2013). The same results were observed for the brown algae *L. digitata* and *E. siliculosus*, respectively, upon defense elicitation (Cosse et al., 2009) or during pathogen infection (Strittmatter et al., 2016).

Other studies on *Laminariales* have suggested the involvement of VIPOs in the accumulation of iodide in the apoplast of those kelps (Küpper et al., 1998, 2008; Verhaeghe et al., 2008b). The study of iodine distribution in *L. digitata* by cryofixation and chemical imaging showed that it was mainly located in the apoplast of the meristoderm and the outer cortex tissues

(Verhaeghe et al., 2008b). Following those results, it has been proposed a hypothesis about the direct involvement of an apoplastic VIPO into the highly selective H_2O_2 -based oxidation of iodide from seawater, allowing its uptake and sequestration in *L. digitata* cell walls (**Figure 0-8**). The biological role of this accumulated iodide stock would be to protect the cortical cell layers against oxidative stress (Verhaeghe et al. 2008b), reinforcing its proposed role as antioxidant (Küpper et al. 2008).

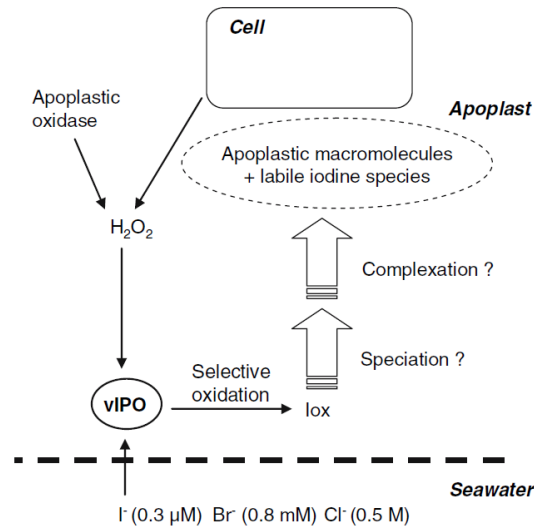


Figure 0-8: Hypothetic mechanisms of iodine uptake in *L. digitata* (from Verhaeghe et al. 2008b)

However, the biological roles of algal VHPOs, which form very large multigenic families in some kelps (Colin et al., 2003; Ye et al., 2015), are still not fully understood. Depending on their subcellular location, they could be involved in various physiological and metabolic processes. For instance, a recent study demonstrates the implication of VHPOs in phlorotannin incorporation into the cell wall of *Fucales*, as well as into the development of zygotes during embryogenesis (Lemesheva et al., 2020).

The biological role of VHPOs has also been explored in fungi such as *Curvularia inaequalis*. This plant pathogen fungus possesses VCPO and may use VCPO-produced hypochlorous acid to degrade lignocellulose in plant cell wall during hyphen penetration (Winter & Moore, 2009). This VCPO also possesses antimicrobial activity against *Enterococcus faecalis* biofilm (Persoon et al., 2012).

For biogeochemical cycling of halogens in marine environment (**paragraph 1.4**), VHPOs are likely to be some of key enzymes for producing biogenic halogenated compounds, emitted in marine environment. For instance, the VBPO activity has been linked to halocarbon emissions, especially methyl bromide (CH_3Br), in *Synechococcus* thanks to an insertional inactivation of

the gene (Johnson et al., 2015), but their specific biological roles have not been studied yet. In marine *Streptomyces* sp. strains, VCPOs catalyze a chlorination reaction leading to the biosynthesis of antibiotics such as napyradiomycin (Bernhardt et al., 2011) and merochlorin (Kaysser et al., 2012). In the marine flavobacteria *Zobellia galactanivorans* the presence of 3 VHPOs, including 2 VIPOs, could be related to the protection against algal chemical defenses or antioxidant responses (Fournier et al., 2014; Barbeyron et al., 2016). However, the biological roles of these VHPOs have yet to be confirmed experimentally.

5. Haloacid dehalogenases (HAD)

5.1. Classification of the HADs

There are several ways to classify the HADs according to their enzymatic or catalytic properties, and to their protein sequence or structure homologies.

First, they are ranged into three enzyme types based on their substrate specificities (for reviews Ang et al., 2018; Wang et al., 2018):

- The L-2-haloacid dehalogenases (L-2-HADs), also named (S)-2-haloacid dehalogenases, only act on L-2-haloalkanoic acids to produce the corresponding D-2-hydroxyalkanoic acids,
- The D-2-haloacid dehalogenases (D-2-HADs), also named (R)-2-haloacid dehalogenases, only act on D-2-haloalkanoic acids to produce the corresponding L-2-hydroxyalkanoic acids by a configuration-inverting mechanism,
- The DL-2-haloacid dehalogenases (DL-2-HADs) can use both D- and L-2-haloalkanoic acids, producing a mixture of DL-2-hydroxyalkanoic acids.

Secondly, these three types of HADs can be separated into two groups depending on their catalytic mechanism properties. In the case of L-2-HADs, it consists of a nucleophilic attack by a carboxylic amino acid followed by the hydrolysis of the esterified intermediate by a water molecule in a second step (**Figure 0-9A**). For the D-2-HADs and the DL-2-HADs, a direct nucleophilic attack mediated on the α -carbon by a hydrolytic water displaces the bound halogen of the substrate (**Figure 0-9B**).

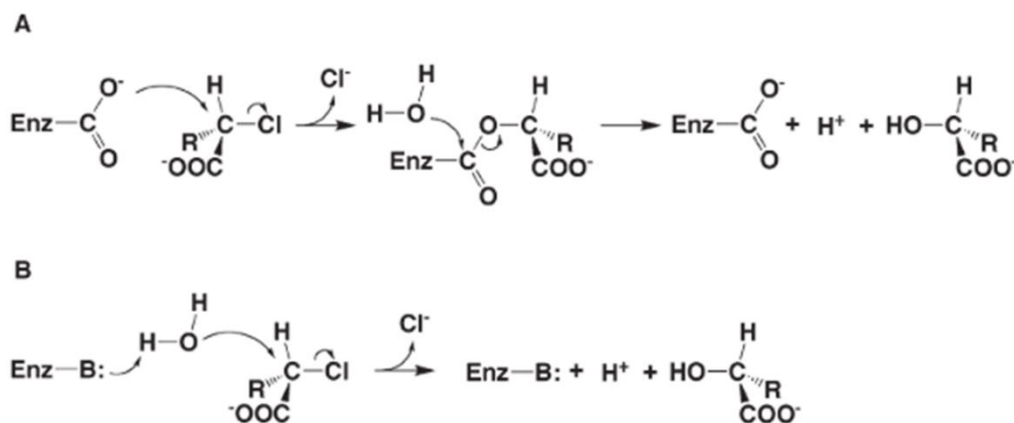


Figure 0-9: Mechanisms for hydrolytic dehalogenation of 2-haloacetic acids. (A) Reaction mechanism involving nucleophilic attack of an active site carboxylate group on the substrate leading to the formation of an ester intermediate. The reaction of L-2-haloacid dehalogenase (L-2-HAD) proceeds by this mechanism. (B) Reaction mechanism involving direct nucleophilic attack of water on the substrate. The reactions of D-2-haloacid dehalogenase (D-2-HAD) and DL-2-haloacid dehalogenase (DL-2-HAD) proceed by this mechanism. L-2-Haloalkanoic acid is shown as the substrate here, but D-2-haloalkanoic acid can also serve as a substrate for this DL-2-HAD (Source: [Kurihara & Esaki, 2008](#)).

Finally, the HADs are also phylogenetically classified into two groups ([Hill et al., 1999](#)). Similarly to catalytic regrouping, D-2-HAD and DL-2-HAD enzymes belong to the type I dehalogenases because of their high similarity in protein sequences. D-2-HADs and DL-2-HADs share about 30% similarities in their primary structures and α -helical hydrolase folding. Recent advances about structure/function characterization of D-2-HADs have shown that HadD, from *Pseudomonas putida* AJ1, crystallized as a homotetramer with a substrate binding pocket located at the interface between two repeats. The amino acids surrounding the active pocket participated in the enzyme-substrate binding. Two residues, an aspartate (Asp205) and an asparagine (Asn131) have been demonstrated to directly activate the nucleophilic water molecule involved in the catalytic dehalogenation ([Wang et al., 2018](#)).

The L-2-HAD enzymes (EC 3.8.1.2) belong to the type II dehalogenases and are part of a large hydrolase superfamily, with diverse substrate specificities and are widely distributed among living organisms. This superfamily, firstly described by an iterative approach of sequence homology, contains three conserved domains ([Koonin & Tatusov, 1994](#)). The HAD superfamily includes phosphatases, phosphonates, P-type ATPases, beta-phosphoglucosyltransferases, phosphomannosyltransferases, epoxide hydrolases, or dehalogenases, which are involved in a variety of cellular processes, ranging from amino acid biosynthesis to detoxification ([Burroughs et al., 2006](#)). These hydrolases have all in common their ability to

form a covalent enzyme-substrate intermediate via a conserved active site nucleophile aspartate, thus facilitating the cleavage of C-X (X = F, Cl, Br, I), P-C, or P-O bonds. Even if they gave their name to this superfamily, the L-2-HADs are the only “true” dehalogenases of the HAD superfamily enzymes. While the majority of enzymes in this superfamily requires a divalent metal ion cofactor for activity, the L-2-HADs are notable exceptions. Most superfamily members but not all have a cap domain, with variable folds and functions, in addition to a core domain always present (Glasner et al., 2006).

5.2. Structural features and enzymatic properties of the L-2-HADs

The biochemical and structure/function characterizations of L-2-HADs have been conducted during the past thirty years mainly on bacterial enzymes. Most structurally characterized L-2-HADs are dimers with two domains in each subunit: a characteristic alpha/beta core domain with a conserved alpha/beta hydrolase fold, similar to the “Rossmann-fold”, and a small cap domain. The helical domains provide a tight homodimeric interface and a confined active site which limit substrate access, and therefore specificity, to small C2-C3 molecules (Van der Ploeg et al., 1991; Hisano et al., 1996; Ridder et al., 1997). The determination of the molecular bases for L-2-HADs aggregation into dimers has shown the importance of a 17 amino acids sequence (Tsang & Pang, 2000). The exchanges of the residues 73 to 89 in DehCI protein (monomeric L-2-HAD) by the residues 74 to 90 of DehIVa protein (dimeric L-2-HAD) led to the dimerization of recombinant mutated DehCI and reciprocally to the production of recombinant mutated DehIVa monomers. The roles of Phe58, Thr65, Leu78, and Phe92 were also important for the dimerization of DehIVa (Tsang & Pang, 2000). The diversity of possible substrates identified for some biochemically characterized L-2-HADs is displayed in **Table 0-4**. The substrates tested were usually brominated and chlorinated, and more rarely iodinated. Not all of the enzyme activities listed in **Table 0-4** have been tested with iodinated substrates. The L-2-HADs are mostly specific towards short chained (C2-C3) mono-halogenated substrates, as shown for DehIVa (Murdiyatmo et al., 1992), DhIS5I (Köhler et al., 1998), dehDEH99 (Huang et al., 2011), DehCI and DehCII (Schneider et al., 1991; 1993). Other L-2-HADs, such as DehRhb (Novak et al., 2013a), DhIB (Van der Ploeg et al., 1991) or DehL (Cairns et al., 1996), can also catalyze the dehalogenation of di-halogenated substrates, and for DhIB, dibromo- and dichloroacetic acids have been described as preferred substrates. Only four enzymes were shown to catalyze C4 substrates (L-2-halobutyric acid): L-DEX YL (Liu et al., 1994), HadL (Barth et al., 1992), L-2-HAD from *P. ingrahamii* (Novak et al., 2013b) and

DehSft (Rye et al., 2009). The latter is even the unique known enzyme that can transform the L-2-bromohexanoic acid, with six carbons in its aliphatic chain. Up to now, only two L-2-HAD enzymes were shown to use fluorinated substrates: fluoroacetic acid can be dehalogenated by Bpro0530 and Rha0230 (Table 0-4, Chan et al., 2010).

Protein ID	Species	Substrate of dehalogenation	Metabolic pathway	Origin	PDB accession	References
DehRhb	<i>Marine Rhodobacteraceae</i>	bromoacetic acid chloroacetic acid L-2-bromopropionic acid L-2-chloropropionic acid dichloroacetic acid	unknown	marine	2YML	Novak et al., 2013
DehSft	<i>Sulfurisphaera tokodaii</i> (formerly <i>Sulfolobus tokodaii</i>)	L-2-chloropropionic acid L-2-bromopropionic acid L-2-bromobutyric acid L-2-bromohexanoic acid	unknown	hot spring	2W43	Bachas-Daunert et al., 2009 Rye et al., 2009
DehIVa	<i>Burkholderia cepacia</i> MBA4	bromoacetic acid chloroacetic acid L-2-bromopropionic acid L-2-chloropropionic acid	2-haloalkanoic acid degradation	soil	2NO4	Murdiyatmo et al., 1992 Pang & Tsang, 2001 Schmidberger et al., 2007
L-DEX YL	<i>Pseudomonas</i> sp. strain YL	L-2-chloropropionic acid bromoacetic acid iodoacetic acid chloroacetic acid dichloropropionic acid L-2-chlorobutyric acid	2-chloroacrylate degradation	soil	1JUD	Nardi-Dei et al., 1994 Liu et al., 1994
DhlB	<i>Xanthobacter autotrophicus</i> GJ10	dibromoacetic acid dichloroacetic acid chloroacetic acid bromoacetic acid L-2-chloropropionic acid	1,2-dichloroethane degradation	soil	1QQ5	Van der Ploeg et al., 1991 Ridder et al., 1997
Bpro0530	<i>Polaromonas</i> sp. JS666	fluoroacetic acid chloroacetic acid bromoacetic acid	unknown	soil	3UM9	Chan et al., 2010
Rsc1362	<i>Ralstonia solanacearum</i> GMI1000	chloroacetic acid bromoacetic acid	unknown	soil	3UMB	Chan et al., 2010
Rha0230	<i>Rhodococcus jostii</i> RHA1	fluoroacetic acid chloroacetic acid bromoacetic acid	unknown	soil	3UMG	Chan et al., 2010
DehDEH99	<i>Paracoccus</i> sp. DEH99	L-2-chloropropionic acid L-2-bromopropionic acid iodoacetic acid	2-haloalkanoic acid degradation	marine		Huang et al., 2011
	<i>Psychromonas ingrahamii</i>	bromoacetic acid chloroacetic acid L-2-chloropropionic acid L-2-bromopropionic acid dichloroacetic acid L-2-chlorobutyric acid	unknown	marine		Novak et al., 2013
DhlS5I	<i>Agrobacterium tumefaciens</i> RS5	chloroacetic acid iodoacetic acid bromoacetic acid L-2-chloropropionic acid dichloroacetic acid	unknown	soil		Köhler et al., 1998
H-2	<i>Moraxella</i> sp. strain B	bromoacetic acid iodoacetic acid chloroacetic acid L-2-chloropropionic acid dichloropropionic acid	unknown	soil		Kawasaki et al., 1981

HadL	<i>Pseudomonas putida</i> AJ1	L-2-chloropropionic acid L-2-chlorobutyric acid L-2-bromobutyric acid 2,3-dichloropropionic acid 2,3-dibromopropionic acid	unknown	soil	Barth et al., 1992 Jones et al., 1992
DehCI	<i>Pseudomonas</i> sp. CBS3	chloroacetic acid L-2-chloropropionic acid	unknown	soil	Schneider et al., 1991 Schneider et al., 1993
DehCII	<i>Pseudomonas</i> sp. CBS3	chloroacetic acid L-2-chloropropionic acid	unknown	soil	Schneider et al., 1991 Schneider et al., 1993
DehL	<i>Rhizobium</i> sp. RC1	L-2-chloropropionic acid dichloroacetic acid dibromoacetic acid	unknown	soil	Cairns et al., 1996

Table 0-4: Biochemically and structurally characterized L-2-HADs enzymes from bacteria

The structure determinations of recombinant L-2-HADs, complexed with their substrates, combined with site-directed mutagenesis analysis have allowed to identify the residues essential for the catalytic reaction processes (Kurihara et al., 1995; Pang & Tsang, 2001; Adamu et al., 2016). Nine amino acids (DTRSKYSND) around the active center are proposed to be involved in substrate binding and the formation of a hydrophobic halogen cradle (Kurihara et al., 1995; Ridder et al., 1997). The catalytic reaction starts by a nucleophilic attack on the alpha-carbon of the substrate by a conserved aspartic acid (Asp). This reaction results in cleaving the carbon-halogen bond, releasing one halide, and forming an enzyme-substrate ester bond. Then, an adjacent water molecule is activated by an Asp/Lys dyad to attack the intermediate's ester bond and to release the hydroxylated product (Schmidberger et al., 2007; Nakamura et al., 2009). This last step is different for the only structurally characterized L-2-HAD of marine origin, as the water molecule is activated by a His/Glu dyad (Novak et al., 2013). This enzymatic reaction occurs with an inversion of chirality of the final product.

5.3. Occurrence and putative biological roles of L-2-HADs

Up to now, most of the identified and characterized L-2-HADs are present in organisms from terrestrial origin and, only few of them have been characterized from marine species. Some terrestrial bacteria are able to catabolize halogenated xenobiotic compounds to detoxify or use them as carbon sources. These halocarbons include chemicals derived from industrial activities and released in the environment. L-2-HAD enzymes like L-DEX YL and DhIB have been shown to be part of metabolic pathways for the degradation of 1,2-dichloroethane (Janssen et al., 1994) and 2-chloroacrylate (Kurata et al., 2005), respectively.

In this context, some soil bacteria such as *Burkholderia cepacia* MBA4 or *Xanthobacter autotrophicus* GJ10 have been studied for their capacity to grow on and metabolize haloacid

compounds. They possess the genetic tools to internalize and degrade a large range of anthropogenic HOCs that are often toxic (Kwok et al., 2007; Mena-Benitez et al., 2008; Horisaki et al., 2011). In *B. cepacia* MBA4, the L-2-HAD-encoding gene, *dehIVa*, and the downstream permease-encoding gene, *dehIVp*, form an inducible operon that mediates the transformation and uptake of halogenated acids (Yu et al., 2007). More generally, the activities of HADs have also been related to natural detoxification processes. For instance, the decomposition of forest soil organic matter leads to the production of chloroacetic acid, which will need to be detoxified (Matucha et al., 2003; Laturnus et al., 2005), and the conversion of chloroacetic acid to glycolate has been reported for *X. autotrophicus* GJ10 thanks to a L-2-HAD (Torz and Beschkov, 2005).

The marine environment contains a large chemical diversity of natural halogenated compounds, some of them being highly specific and/or potentially toxic, as parts of marine algal chemical defenses (paragraph 2; Belkin, 1992; Paul et al., 2006). The halogenated compounds produced by kelps could be converted into haloacetic acids, and some red algae like *Asparagopsis taxiformis* contain haloacetic acids (Woolard et al., 1979; Fenical, 1982). However, very little is known about marine dehalogenase enzymes and more generally about the reactions involved in the catabolic pathways of halogenated compounds and their biological and ecological roles in marine organisms.

6. *Zobellia galactanivorans*, a model marine bacterium for studying specific metabolic pathways

Zobellia galactanivorans Dsij^T is a rod-shaped, Gram-negative, non-flagellated, marine *Flavobacterium* first isolated in Roscoff (France) from the red alga *Delesseria sanguinea* (Potin et al. 1991; Barbeyron et al., 2001). This bacterium produces flexirubine, a pigment that colors its colonies in yellow/orange (Figure 10). *Z. galactanivorans* is chemoorganotrophic and strictly aerobic (i.e., it needs organic compounds as carbon source and oxygen as final electron acceptor). To this day, six other *Zobellia* strains have been characterized: *Z. uliginosa*, *Z. amurskyensis* MAR_2009_138 (Barbeyron et al., 2001), *Z. russellii*, *Z. laminariae*, *Z. amurskyensis* KMM 3526^T (Nedashkovskaya et al., 2004) and *Zobellia* sp. OII3 (Harms et al., 2017). All of them were isolated from coastal marine habitats and live on the surface of green, red and brown macroalgae (Potin et al., 1991; Nedashkovskaya et al., 2004).

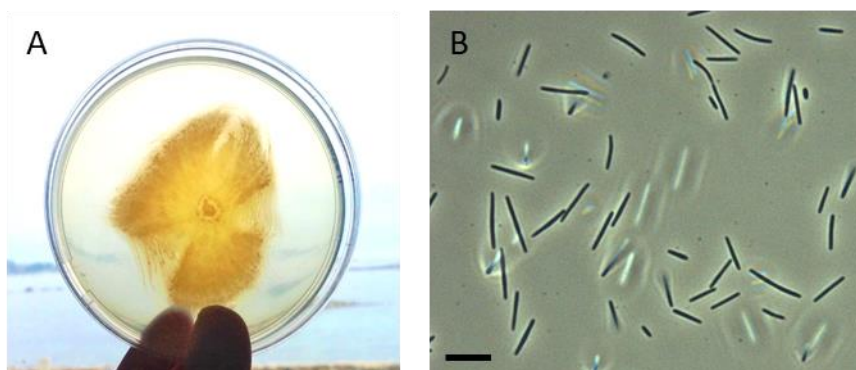


Figure 0-10: (A) Picture of *Z. galactanivorans* colonies on agar plate. (B) Phase contrast microscopy image of a *Z. galactanivorans* liquid culture (scale bar 6 μm).

Since its discovery, *Z. galactanivorans* has been studied in the past 20 years for its ability to degrade polysaccharides constituting algal cell walls, thanks to specialized enzymes such as glycoside hydrolases, polysaccharide lyases and carbohydrate esterases (Barbeyron et al., 2016). Experimental research on *Z. galactanivorans* has benefited from genomic resources and genetic tools, developed for functional studies on algal polysaccharide degradation (for review, Lami et al., 2021, in press). For instance, the first operons of marine origins, specific to alginate and mannitol utilizations, have been described in this model bacterium (Thomas et al., 2012; Groisillier et al., 2015). Its entire genome was sequenced in 2010 and has opened the door to numerous research opportunities. Many of those are linked to algal polysaccharides consumption (Thomas et al., 2012; 2013; 2017; Groisillier et al., 2015; Ficko-Blean et al., 2017; Dudek et al., 2020). The developments of functional genomics (transcriptomics, heterologous protein overexpression, site-directed mutagenesis,...) and structure/function approaches (resolution of 3D structures) were major advances to unravel the biochemical and biological roles of enzymes (Hehemann et al., 2010; 2012; Labourel et al., 2014; 2015; Ficko-Blean et al., 2015; Naretto et al., 2019). More recently, this panel was completed with knock-out mutagenesis, which was a powerful tool to establish the *in vivo* function of alginate lyases (Zhu et al., 2017).

Living in close interactions with seaweeds, *Z. galactanivorans* is expected to display many genetic adaptations to interact with macroalgae. During the degradation of brown algal alginate cell walls, bacteria have to deal with algal oxidative responses and iodine-based chemical defenses (Küpper et al., 2008; Cosse et al. 2009). It has been shown that exudates of *L. digitata* elicited by oligoguluronates positively stimulated the biofilm growth of *Z. galactanivorans* (Salaün et al., 2012). Moreover, the exposition of *Z. galactanivorans* cultures with diiodomethane (CH_2I_2) did not show strong effect on its biofilm formation (Salaün, 2015).

Iodinated volatile compounds, such as I₂ and CH₂I₂ were released by kelps in those conditions, and should indicate that *Z. galactanivorans* has developed enzymatic capacities to survive in the presence of toxic halogenated metabolites, even the iodinated ones.

Indeed, the genes encoding putative enzymes related to halogenation and dehalogenation metabolisms were annotated on *Zobellia*'s genome (Barbeyron et al., 2016): three vanadium-dependent haloperoxidases, two of which already characterized as iodoperoxidases (VIPOs); one cofactor-free haloperoxidase (HPO), one iodotyrosine deiodinase (IYD), and one haloacid dehalogenase (HAD). While the first bacterial VIPOs were biochemically and structurally described in *Z. galactanivorans* (Fournier et al., 2014), no further analyses have been performed on the other putative enzymes. In addition, besides the presence of putative iodination-related enzymes, *Z. galactanivorans* can accumulate iodine compared to other planktonic bacteria and surrounding medium, up to a hundred times more than the seawater concentration (Barbeyron et al., 2016).

7. Thesis project and outline

In the biogeochemical cycle of halogens, a wide diversity of actors are expected to be involved, from seaweeds to phytoplankton in oceans, to terrestrial plants, soil microbes and human industry on lands. The role of marine bacteria could be of importance in this cycle, especially in coastal regions, where they are living in close interactions with macroalgae, known to actively produce both brominated and iodinated compounds. However, very few information is available on enzymes connected to this metabolism, or even the biological and ecological importance of this metabolism for marine bacteria.

Z. galactanivorans represents a very interesting marine bacterial laboratory model to further explore its halogen metabolism, and more specifically that related to iodine. Based on previous work conducted in the Roscoff's team (Fournier, 2014) and current knowledge at the beginning of my thesis, a hypothetical model of the biochemical roles for the enzymes related to halogen metabolism in *Z. galactanivorans* was adapted and is presented in **Figure 11**. Besides the biochemical and structural characterization of the first two VIPOs (Fournier et al., 2014), it illustrates that most of the identified enzymes, through genomic annotation, still have putative biochemical and biological functions in *Z. galactanivorans*, and especially during interactions with *L. digitata*.

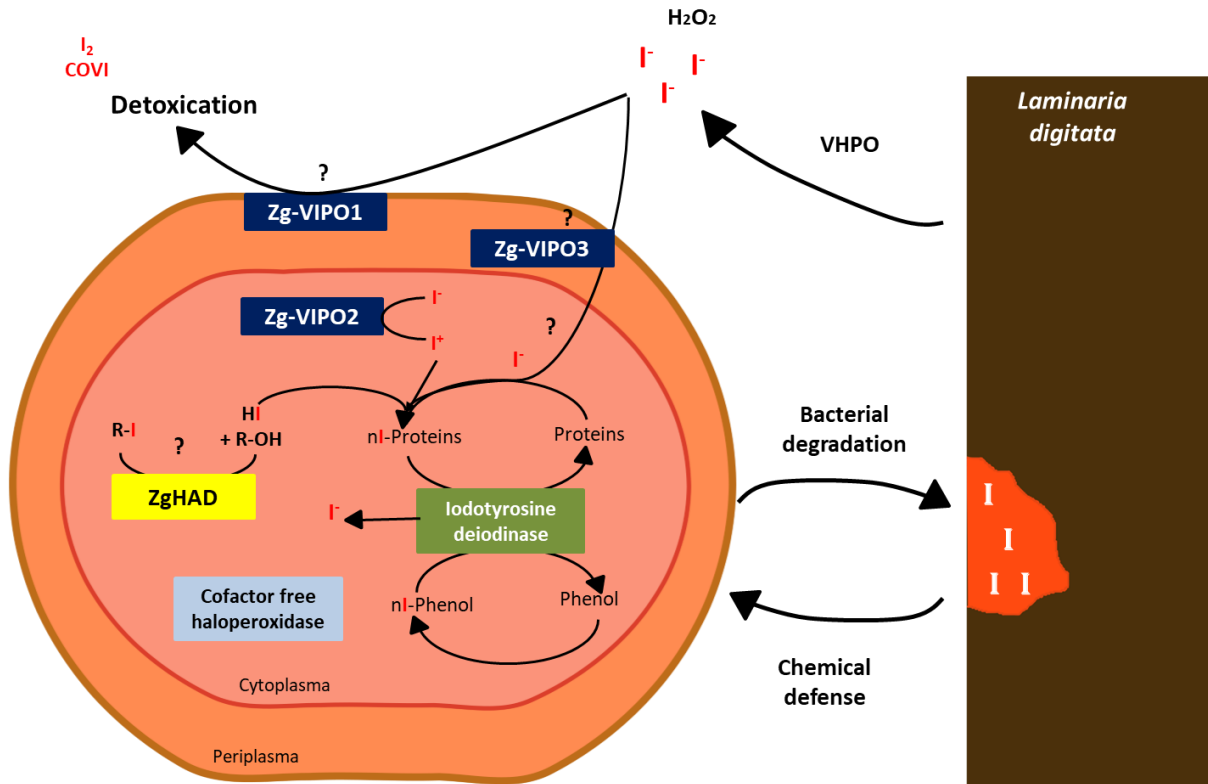


Figure 0-11: Hypothetical model of iodine metabolism within *Z. galactanivorans* and its interaction with the brown alga *L. digitata* (adapted from Fournier, 2014).

In this context, I addressed the following questions during my thesis, focusing my work on two key enzymes of *Z. galactanivorans*:

- What are the biochemical and structural properties of the putative haloacid dehalogenase enzyme (ZgHAD)? Are there conserved features in marine L-2-HADs, when no L-2-HAD from the *Bacteroidetes* phylum was known to date? In which metabolic pathway is this enzyme involved and what is its biological role in *Z. galactanivorans*?
- Concerning halogenating enzymes, what is Zg-VHPO3 halogen specificity and how distant its structure is from the two other VIPOs, characterized in *Z. galactanivorans*?
- Where in the bacterium are these enzymes active and what are their biological roles? Are these enzymes involved in HOCs biosynthesis or catabolism, detoxication process and protection against chemical algal defenses? How is the bacterial halogen metabolism regulated during alga-bacterium interactions?

For that purpose, I developed different methodological approaches during my thesis, which are presented in four chapters, followed by a synthetic “conclusion and perspectives” part.

In chapter 1, I present the investigation of the enzymatic properties of the recombinant HAD enzyme of *Z. galactanivorans* (ZgHAD), in order to determine its biochemical characteristics and specific substrates. I produced a knock-out mutant, by deleting the corresponding gene and compared different cultures of the wild-type and mutant strains on selected halogenated compounds, in order to explore the biological role of ZgHAD. A second part of this chapter deals with the phylogenetic analysis of ZgHAD and the environmental distribution of homologous proteins.

In chapter 2, I focus on the structure resolution of ZgHAD. Site-directed mutagenesis and computational docking were performed to identify key amino acids involved in substrate fixation and in the water molecule activation during the catalytic reaction.

The third chapter is dedicated to the biochemical and structural studies of *Z. galactanivorans* VHPO3. Colorimetric assays were used to determine its halide specificity and crystallography tests were performed in the hope of solving its 3D structure. In view of this difficulty, structural models were built to explore the monomeric and dimeric folding of the protein.

Finally, the fourth chapter focuses on investigating the localization of Zg-VIPO1 enzyme within the bacterium, through Western-blot analysis, as well as its potential biological roles using the knock-out mutant approach. The ability to detoxify and/or accumulate iodine was explored in both cultures of wild-type and mutant strains, in particular using *in vitro* cultures with radioactive I¹²⁵ during a short research stay in the laboratory of Prof. Seigo Amachi in Japan.

Chapter 1:

**Functional characterization of a L-2-haloacid dehalogenase
from *Zobellia galactanivorans* suggests a role in haloacetic acid
catabolism and a wide distribution in marine environment**

Chapter presentation

This chapter is dedicated to the first functional characterization of a L-2-haloacid dehalogenase (L-2-HAD) from a bacterium of the *Bacteroidetes* phylum, combining biochemical and gene knockout approaches. I showed that the unique L-2-HAD of *Zobellia galactanivorans* was involved in bromo- and iodoacetic acid catabolism, providing a potential selective advantage to this marine coastal *Bacteroidetes*.

Phylogeny and distribution analyses of homologous L-2-HADs in environmental sequence databases revealed an unexpected wide marine diversity, amongst which we identified two distinct clades of *Bacteroidetes* L-2-HADs. All these results provide insights towards a potential ecological role of *Bacteroidetes* L-2-HADs during biotic interactions in marine habitats.

Article in preparation

Functional characterization of a L-2-haloacid dehalogenase from *Zobellia galactanivorans* suggests a role in haloacetic acid catabolism and a wide distribution in marine environment

Eugénie Grigorian, Agnès Groisillier [#], François Thomas, Catherine Leblanc*, Ludovic Delage*

Sorbonne Université, CNRS, UMR8227, Integrative Biology of Marine Models, Station Biologique de Roscoff, CS 90074, Roscoff, France

* Corresponding authors.

* For correspondence. Ludovic Delage. Address: Station Biologique de Roscoff, Place Georges Teissier, 29680 Roscoff, France. Email: ludovic.delage@sb-roscoff.fr.

[#] Université de Nantes, CNRS, UFIP, UMR6286, F-44000 Nantes, France

Running Head: Biological function of L-2-HAD in *Zobellia*

ABSTRACT

L-2-halocid dehalogenases (L-2-HADs) were mainly characterized in terrestrial polluted environments, and could be essential for detoxification of halocarbons also predominant in marine environment. A global phylogenetic analysis showed an unexpected diversity of homologous L-2-HADs, especially among those belonging to marine bacteria. While the already biochemically characterized terrestrial L-2-HADs were part of a monophyletic group (group A), including proteins of terrestrial and marine origin, another branch grouped together, mostly marine L-2-HADs (group B), with two distinct clades of *Bacteroidetes* homologs, closely linked to *Proteobacteria* ones. This study focused on the characterization of the unique L-2-HAD from the flavobacterium *Zobellia galactanivorans* Dsij^T (ZgHAD), included in one of these Group B clades. The recombinant ZgHAD was shown to convert bromo- and iodoacetic acids into glycolate, and the functional study by gene knockout revealed a direct role of ZgHAD in tolerance against both haloacetic acids in *Z. galactanivorans*. Interestingly, the analyses of environmental sequence databases confirmed that the group A homologs were well-represented in bacteria from both terrestrial and marine habitats, whereas the ZgHAD (group B) homologs were mainly present in marine bacteria, and particularly in host-associated species. Our results suggest that ZgHAD homologs could be key enzymes for marine *Bacteroidetes*, by conferring selective advantage for the recycling of toxic halogen compounds produced in particular marine habitats, and especially during macroalgal interactions.

INTRODUCTION

Halogenated metabolites are widely distributed on Earth. They are defined as organic compounds that covalently bind one or several halogen atom(s) such as fluorine, chlorine, bromine or iodine. Over 5,000 different natural organohalogens have been described, mainly from the marine environment (Gribble, 2015). They can be produced abiotically (Dong *et al.*, 2021), but also derived from many different biogenic sources. For example, some chlorinated metabolites are found in land plants and fungi, while brominated metabolites have been mainly related to marine sources such as red and brown algae, or sponges (Amsler, 2008; Cabrita *et al.*, 2010; Bialonska *et al.*, 2009; El-Demerdash *et al.*, 2019). Furthermore, during the last century and with industrial developments, man-made polyhalogenated organic products were synthesized and are now persistent organic environmental pollutants (Agarwal *et al.*, 2017; Ang *et al.*, 2018). To mitigate this environmental issue, nature-based solutions are a promising alternative for bioremediation. During the last four decades, research efforts have identified microorganisms that can catabolize diverse mono or polyhalogenated compounds, and characterized a broad range of dehalogenases (Hardman and Slater, 1981; Janssen *et al.*, 1994; Copley S., 1998). These enzymes are highly diverse in terms of structure and biochemistry, but they all share the enzymatic capacity of cleaving carbon-halogen bonds. Depending on their catalytic mechanisms and substrates, they are classified in large superfamilies (Janssen *et al.*, 2005; Ang *et al.*, 2018).

This haloacid dehalogenase (HAD) superfamily includes mostly enzymes that hydrolyze carbon-phosphorus or oxygen-phosphorus bonds, such as phosphoesterases, phosphonatasases, P-type ATPases, or nucleotidasases. Widely conserved among living

organisms, they are involved in a variety of cellular processes ranging from amino acid biosynthesis to detoxification (Burroughs *et al.*, 2006). In plant pathogen bacteria, HADs might also be involved in biofilm formation during biotic interactions (Li and Wang, 2011). The “true” dehalogenases of the HAD superfamily are categorized into two types. Type I contains both HADs that have an enantioselective dehalogenating activity on D-2-haloacids (D-2-HADs), and those that have non-stereospecific mechanism accepting both D- or L-2-haloacids as substrates (DL-2-HADs). Enzymes from type II specifically act on L-2-haloacids (L-2-HADs) to produce the corresponding hydroxyalkanoic acids with an inverted chirality (Ang *et al.*, 2018). The L-2-HADs are phylogenetically unrelated to D-2-HADs and DL-2-HADs exhibiting a distinct protein fold and catalytic mechanism (Hill *et al.*, 1999).

Many genes encoding L-2-HADs have previously been identified in the genomes of bacteria from contaminated soils or freshwater environments (Copley S., 1997; Kurihara *et al.*, 2008). Biochemical and structure/function characterizations of L-2-HAD enzymes have been conducted during the past thirty years to identify new enzymatic or biotechnological processes for detoxification of halogenated pollutants. The large majority of characterized L-2-HADs originate from terrestrial *Proteobacteria* such as DehIVa from *Burkholderia cepacia* MBA4 (Schmidberger *et al.*, 2007), Dh1B from *Xanthobacter autotrophicus* GJ10 (Van der Ploeg *et al.*, 1991), or L-DEX from *Pseudomonas* sp. strain YL (Nardi-Dei *et al.*, 1994). The *dhlB* gene has been engineered into land plants by transformation, allowing effective treatment of soil and groundwater contaminated with halogenated solvents (Mena-Benitez *et al.*, 2008).

The biological roles of these HADs in terrestrial and/or freshwater bacteria are mostly related to their adaptations to degrade xenobiotic compounds, derived from industrial activities and released in the environment (Copley, S., 1998; Hill *et al.*, 1999; Janssen *et al.*, 2005). However, sampling efforts for HAD-containing microorganisms mostly focused on polluted matrices, potentially biasing the overall representation of these enzymes. Therefore, the phylogenetic diversity and biological roles of HADs might be underestimated in non-polluted environments (Janssen *et al.*, 2005).

The marine environment contains a large range of natural halogenated compounds, some of them being highly specific and/or potentially toxic, as parts of chemical defenses of marine invertebrates or algae. For instance, while iodinated compounds are relatively rare on Earth, brown macroalgae are main producers of volatile iodocarbons that play a notable role in atmospheric chemistry (Carpenter *et al.*, 2012). Other natural sources of marine halogenated compounds could include volcanoes and organic matter efflux in estuaries (Jordan *et al.*, 2000; Gribble, 2003; Gordon *et al.*, 2015). Very little is currently known about marine dehalogenase enzymes, and even less about the metabolic pathways involved in the catabolism of halogenated compounds by marine microorganisms. To date, only four marine L-2-HADs have been biochemically characterized: DehRhB from a *Rhodobacteraceae* bacterium associated to marine *Polychaeta* (Novak *et al.*, 2013a); two enzymes from the sponge-associated *Paracoccus* sp. DEH99 and *Pseudomonas stutzeri* DEH130 (Huang *et al.*, 2011; Zhang *et al.*, 2013); and one from the psychrophilic strain *Psychromonas ingrahamii* DehPsi (Novak *et al.*, 2013b). The best-studied marine L-2-HAD so far is DehRhB, whose structure and catalytic properties notably differ from soil enzymes (Novak *et al.*, 2013a).

In this context, this paper reports on the occurrence of L-2-HAD homologous proteins in microorganisms, *i.e.* marine bacteria and archaea, through large in silico genomic surveys; on the phylogeny of such proteins in the *Bacteroidetes* phylum, and on the biochemical characterization of the only haloacid dehalogenase identified on the genome of the marine flavobacterium *Zobellia galactanivorans* Dsij^T. This bacterium has been developed as a laboratory model for marine *Bacteroidetes*, because of its capacities to degrade algal polysaccharides. Its genome also features several genes related to halogen metabolism (Fournier *et al.*, 2014; Barbeyron *et al.*, 2016). Thanks to a recent protocol development (Zhu *et al.*, 2017), a genetic knockout approach was conducted, demonstrating the potential *in vivo* protective role of this L-2-HAD when *Z. galactanivorans* was exposed to toxic halogenated substrates. In addition, the distribution and expression of phylogenetically distinct L-2-HADs were analyzed using metagenomic and metatranscriptomic datasets, highlighting an underexplored marine biodiversity. Finally, the laboratory functional characterization of *Z. galactanivorans* L-2-HAD and environmental survey results on homologous proteins are discussed in light of the biological and ecological roles of these enzymes in marine *Bacteroidetes* in their natural coastal habitats.

RESULTS

Phylogenetic analysis of bacterial L-2-HADs

The phylogenetic analysis of microbial L-2-HAD proteins was based on a subset of 352 protein sequences, including the biochemically and structurally characterized enzymes (Table S1) and their closest counterparts, in addition to the closest relatives of ZgHAD, identified by BlastP search on protein databases (Table S2). L-2-HAD proteins mainly

clustered into two well-supported groups (**Fig. 1**), with an additional small clade of proteobacterial sequences related to the L-2-DhlB of *Ancylobacter aquaticus* UV5. The first group (group A) mostly comprises proteobacterial L-2-HAD sequences (122/182 sequences) that are divided into four clades, respectively containing the biochemically characterized L-2-HADs L-DEX, DhlB, DehIVa and DehPsi. Two other clades in group A contained archaeal proteins: one features terrestrial extremophile L-2-HADs together with the DehSft protein; the second clade contains a mix of *Euryarchaea* and *Actinobacteria* putative L-2-HADs. Most L-2-HAD homologs from group A have been identified in species of terrestrial or freshwater origins, but also few in marine species (**Table S2**). By contrast, the second phylogenetic group (group B) contains, almost exclusively (138/150 sequences), L-2-HAD protein sequences belonging to microorganisms either from saline or from marine origins (**Table S2**). The group B is constituted of three well-supported clades and an isolated proteobacterial putative L-2-HAD from *Halomonas* (**Fig. 1**). A clade groups all other proteobacterial L-2-HAD proteins, including DehRhB. Interestingly, the *Bacteroidetes* L-2-HAD homologs are separated into two phylogenetic groups, named HAD1 and HAD2 clades. No *Bacteroidetes* L-2-HAD was yet biochemically characterized before this study. The two phylogenetic types of *Bacteroidetes* L-2-HADs share between 40 to 45% amino acid identity.

The phylogenetic group A (**Fig. 1**) features most of the biochemically characterized L-2-HADs (**Table S1**), and these enzymes share around 30% of identity at the protein sequence level. Furthermore, a motif of 9 amino acids (DTRSKYSND) essential for enzyme activity and substrate binding ([Adamu et al., 2016](#)) was strictly conserved between all the characterized L-2-HADs of group A (**Fig. S1**).

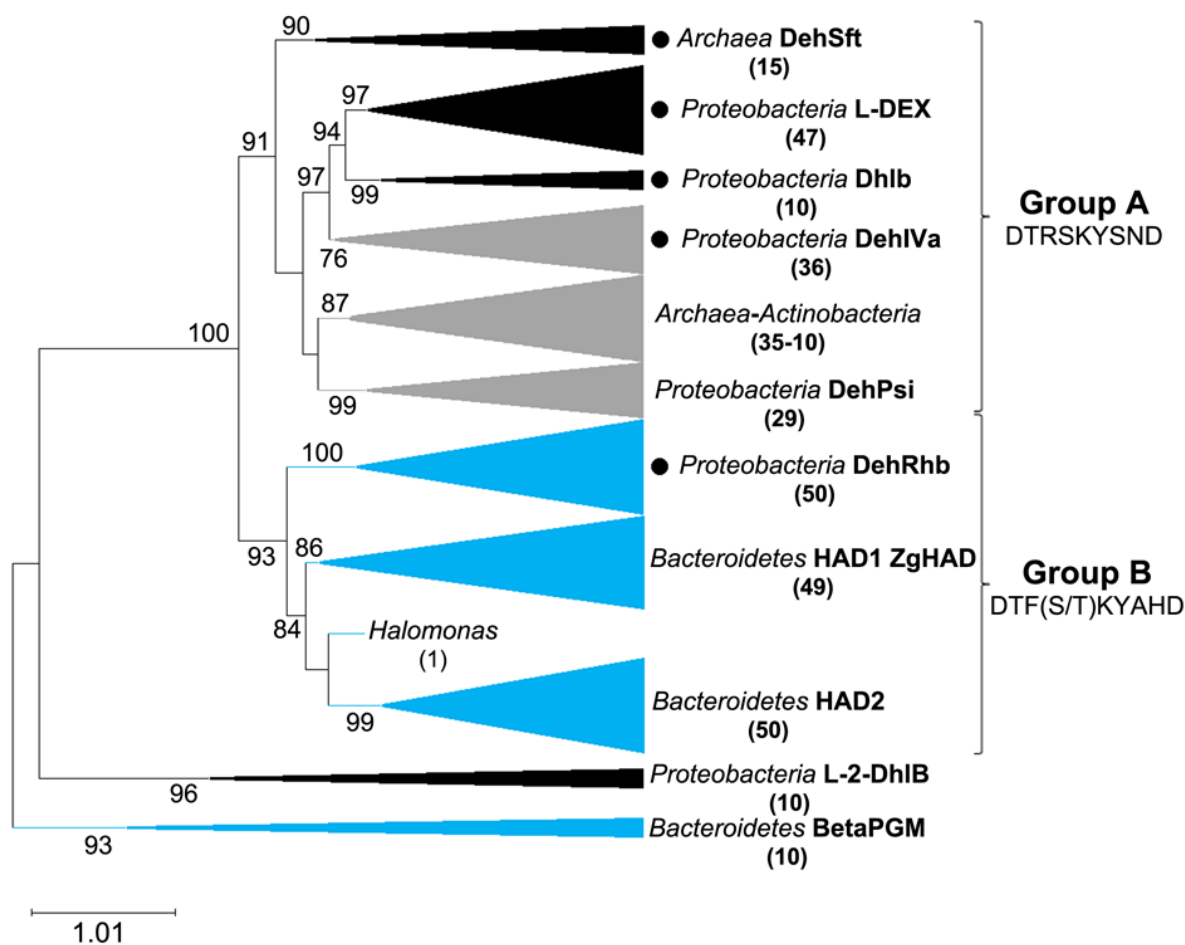


Figure 1: Representative phylogenetic tree of the L-2-HAD proteins. This PhyML tree was constructed through an automated pipeline at the NGphylogeny.fr website including 352 archaeal and bacterial sequences (see **Table S2**). Only bootstrap values (100 replicates) > 70 % are provided. The tree is rooted by an outgroup of beta-phosphoglucosyltransferase proteins, a distinct and closely related group of the HAD superfamily. Black colored circles indicate groups with at least an available 3D structure of L-2-HAD. Black branches represent putative L-2-HAD proteins from terrestrial or freshwater organisms, blue branches represent those from marine organisms and grey ones are those for mixed terrestrial/marine groups. The number of sequences in each group is indicated in brackets. DehSft, L-DEX, DhIb, DehIVa, DehPsi, DehRhb, ZgHAD, L-2-DhIB and BetaPGM proteins are indicated in their clade of belonging. Group A and group B define the two major phylogenetic groups, for which nine specifically conserved amino acids of the catalytic site are shown. The two distinct clades of *Bacteroidetes* L-2-HADs are named HAD1 and HAD2.

The closest biochemically characterized protein homolog of ZgHAD is DehRhb from a marine *Rhodobacteraceae*, present in the group B, but they only share 31% of amino acid sequence identity (**Table S1**). Reciprocally, a motif of nine conserved amino acids

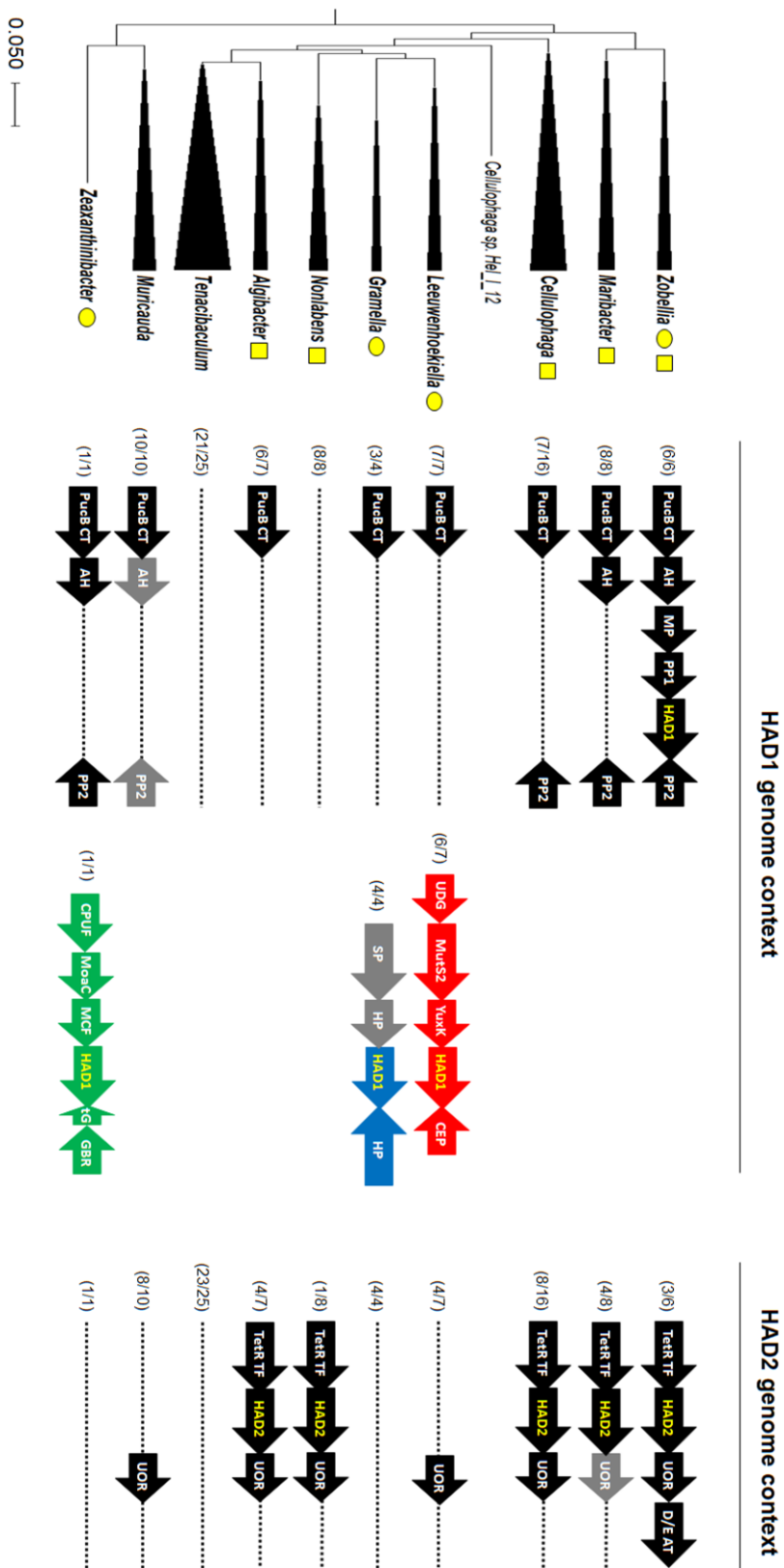
(DTF(S/T)KYAHD) present in the group B are equivalent to those of group A (**Fig. S1**). Eight of those amino acids are strictly conserved in the sequences of DehRhb and ZgHAD. Only a T124 present in DehRhb is replaced by a S131 in ZgHAD in this pattern (**Fig. S1**).

Study of the genomic context of ZgHAD and among *Flavobacteriaceae*

The phylogenetic analysis has shown that most *Bacteroidetes* featured only one L-2-HAD belonging to either the HAD1 or the HAD2 phylogenetic clade, but some of them also exhibited both L-2-HAD sequences (**Table S2**). Some intra-species variations occur: for example, *Zobellia amurskyensis* MAR_2009_138 (formerly *Zobellia uliginosa*; Chernysheva *et al.*, 2019) possesses two different L-2-HAD-encoded genes whereas the *Z. galactanivorans* genome only encodes for ZgHAD, belonging to the HAD1 phylogenetic clade. The occurrence and genomic context of the different L-2-HAD-encoded genes were further analyzed in genomes of *Zobellia* species and closely related members of the *Flavobacteriaceae* family (**Fig. 2**). The HAD1-type gene (relative to the phylogenetic HAD1 clade) was present on the genome of all the 6 *Zobellia* strains among a conserved succession of 8 ORFs followed by 3 genes in the other orientation (**Fig. S2**). The analysis of the publicly available RNAseq data for *Z. galactanivorans* (Ficko-Blean *et al.*, 2017) showed continuous transcript coverage over the three genes *zgal_4181-zgal_4183* encoding MP/PP1/ZgHAD with a clear drop in coverage upstream *zgal_4181* (**Fig. S3**), supporting the hypothesis that they might form an operon. The genetic context in the same genomic region for *Maribacter* and *Zeaxanthibacter* genomes showed the absence of the 3 homologous genes including the HAD1-type gene. The same situation was found in *Cellulophaga* genomes where a fourth gene (amidohydrolase) was also missing. Indeed,

the genomes of *Leeuwenhoekiella* (6 strains), *Gramella* (4 strains) and *Zeaxanthibacter* (one strain) have homologs of the ZgHAD gene, but without any genomic context conservation (**Fig. 2** and **Fig. S2**). Only 3 of the 6 *Zobellia* strains feature a second L-2-HAD-encoding gene, belonging to the HAD2 phylogenetic clade, on their genomes (**Fig. 2**). The analysis of the genetic region showed that 3 genes are conserved around HAD2-type gene, namely a transcriptional regulatory protein from the TetR family (TetR TF) upstream and an uncharacterized oxidoreductase (UOR) and an Asp/Glu aminotransferase (D/E AT) downstream (**Fig. 2** and **Fig. S2**). The comparison with the genomes of other genera (*Maribacter*, *Cellulophaga*, *Algibacter* and *Nonlabens*) showed that they sometimes present a HAD2-type gene homolog but never a HAD1-type gene. It revealed also that the synteny of the TetR TF, HAD2-type and UOR encoding genes were always conserved. Furthermore, this study showed that some genera of *Flavobacteriaceae* like *Tenacibaculum* or *Muricauda* had no L-2-HAD-encoding gene.

Figure 2: Genetic context of the two types of haloacid dehalogenases identified in *Flavobacteriaceae*. On the left, the phylogenetic tree of 10 genus clades was constructed using the comparative genomics tool for genome clustering of MaGe website. The yellow round and square symbols indicated the presence of homologs genes belonging, respectively, to HAD1 or HAD2 phylogenetic groups. The middle part represents the genetic context around HAD1-type genes found in *Zobellia* genomes. The synteny in this genomic region of other genera is indicated below (in black). In addition, the specific genomic context around HAD1-type genes is shown in *Leeuwenhoekiella*, *Gramella* and *Zeaxanthinibacter* genomes, respectively, in red, blue and green. At the right of the panel, the gene synteny is shown around HAD2-type gene. Conserved genes between species are shaded in black, partially conserved genes are shaded in grey and absent genes are represented by dotted lines. PucB CT = PucB-like cytidyltransferase, AH = Amidohydrolase, MP = metallopeptidase, PP1 = putative protein 1, PP2 = putative protein 2, UDG = Uracyl-DNA-Glycolase, MutS2 = Recombination inhibitory protein, YuxK = Putative DCC family thiol-disulfide oxidoreductase, CEP = Conserved exported protein of unknown function, SP = Secreted protein, HP = Hypothetical protein, CPUF = Conserved protein of unknown function, MoaC = Molybdenum cofactor biosynthesis protein, MCF = Molybdopterin converting factor, tG = trnaGly, GBR = Glyoxalase/bleomycin resistance, Tet TF = Tetracyclin transcription factor, UOR = Uncharacterized oxidoreductase, D/E AT = Asp/Glu amidotransferase. Arrow representations of genes indicate the orientation of the ORFs.



Production, purification and enzymatic characterization of the recombinant ZgHAD

To characterize the biochemical activity of ZgHAD, the recombinant ZgHAD enzyme was produced in *E. coli* and purified to homogeneity (**Fig. S4**), yielding 300 mg.L⁻¹ culture. SDS-PAGE confirmed the purity and correct size of the protein that appeared as a unique band at the expected 26.3 kDa molecular mass (**Fig. S4**). Based on size exclusion chromatography, the protein eluted as a homodimer in solution. A standard colorimetric assay solution based on phenol red was used to first determine the substrate specificity of recombinant ZgHAD. Thirteen substrates with different carbon chain lengths (C2 to C4) and halogen atom nature, position and number were tested (**Fig. 3**). Within 30 minutes, the recombinant ZgHAD showed activity only towards L-enantiomer substrates with short carbon chains (C2 and C3). The enzyme was active towards substrates, that were monoiodinated, monobrominated or monochlorinated on the α -carbon position. The recombinant ZgHAD enzyme was then able to react with iodoacetic acid (IAA), bromoacetic acid (BAA), chloroacetic acid (CAA), L-2-bromopropionic acid and L-2-chloropropionic acid (**Fig. 3**). The fastest activity was observed with IAA and BAA, leading to an acidic yellow coloration within 5 min. The chloroacetic acid (CAA) and the L-2-bromopropionic acid were turned partially into their corresponding alcohols at the same time, giving an orange coloration. They were totally transformed between 10 and 30 min (**Fig. 3**). The conversion of the L-2-chloropropionic acid was achieved after more than 30 min. Longer incubations up to 16 hrs did not evidence activity on the 8 other substrates (data not shown), confirming that the D-2-haloacids, multi-chlorinated or brominated acetic acids, and the halobutyric acids cannot be processed by the recombinant ZgHAD. To further compare the catalytic properties on both iodinated and brominated compounds,

IAA and BAA were used as substrates to calculate kinetic parameters of ZgHAD. The V_{max} and K_m value with IAA were $1.12 \mu\text{M}\cdot\text{sec}^{-1}$ and 0.31 mM , respectively and with BAA they were $1.70 \mu\text{M}\cdot\text{sec}^{-1}$ and 0.46 mM , respectively.

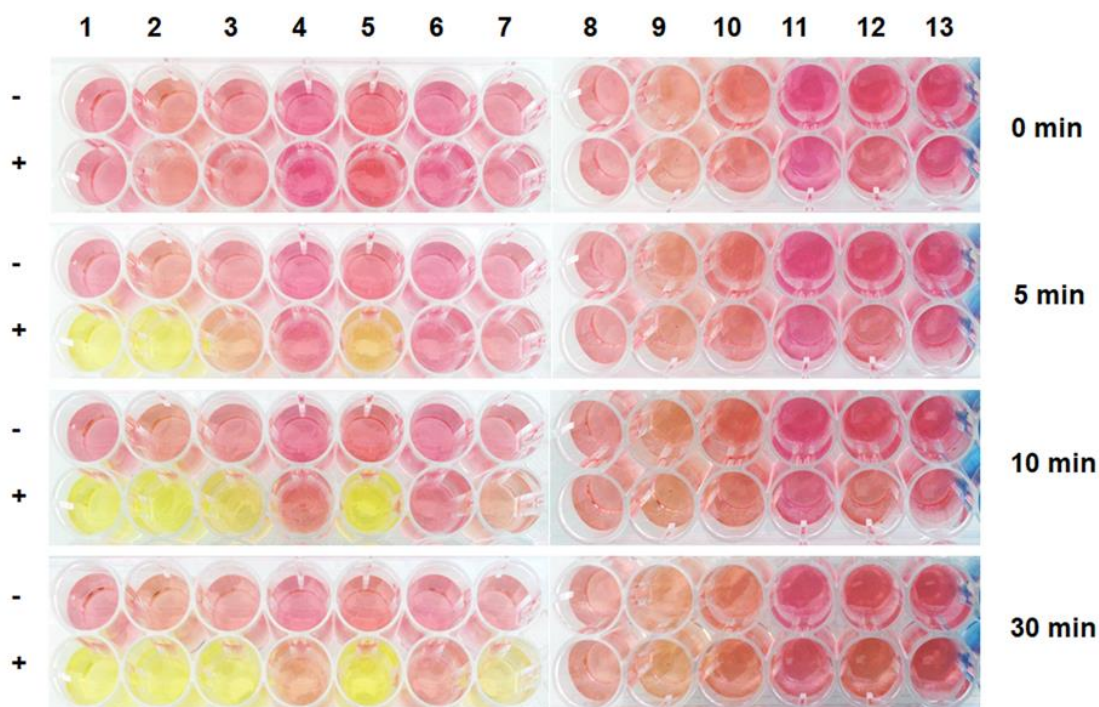


Figure 3: Screening of ZgHAD specificity towards different halogenated substrates based on colorimetric assays. Pictures were taken after 0, 5, 10 and 30 minutes of enzymatic reaction. Substrates are : (1) iodoacetic acid ; (2) bromoacetic acid ; (3) chloroacetic acid ; (4) D-2-bromopropionic acid ; (5) L-2-bromopropionic acid ; (6) D-2-chloropropionic acid ; (7) L-2-chloropropionic acid ; (8) trichloroacetic acid ; (9) 3-iodopropionic acid ; (10) 3-bromopropionic acid ; (11) 2-chlorobutyric acid ; (12) iodoacetamide ; (13) dibromoacetic acid ; (-) no enzyme ; (+) with enzyme.

Effects of haloacetic acids on growth of different bacterial strains

The growth of *Z. galactanivorans* in the presence of BAA and IAA was compared to that of two *Tenacibaculum* bacterial species (*T. discolor* and *T. gallaicum*), which are phylogenetically closely-related to *Z. galactanivorans* (85.7% and 86.35% 16S rRNA identity respectively) but do not possess any L-2-HAD homolog gene. Bacterial cultures

were grown in liquid ZoBell medium with the highest concentrations of BAA (10 mM) or IAA (2 mM) tolerated by *Z. galactanivorans*. After 16 h, cell densities of both *Tenacibaculum* strains were < 5% in presence of BAA and IAA compared to unamended ZoBell medium. By contrast, the cell densities of *Z. galactanivorans* WT were still 20% with BAA and 30% with IAA compared to the unamended ZoBell condition. (**Fig. 4A**). Therefore, the presence of a L-2-HAD-encoding gene in *Z. galactanivorans* compared to *Tenacibaculum* strains suggests an increased resistance to BAA and IAA.

In order to test this hypothesis, we investigated the effect of the *zghad* gene deletion on the *Z. galactanivorans* tolerance to haloacids. On solid medium, BAA or IAA induced clear growth inhibition zones for the wild-type strain (WT), with apparent diameters of 1.3 and 3.4 cm, respectively (**Fig. 4B**). No inhibition zone was observed with the buffer alone. Compared to the WT, the inhibition zones observed for the *zghad*-deleted strain, Δhad , were larger, showing an increase of 85% for the BAA (apparent diameter 2.4 cm) and 35% for the IAA (4.6 cm). Consequently, the deletion effect appeared to be more pronounced with BAA than IAA. To confirm these results, we compared the growth rates of the WT and Δhad strains in liquid ZoBell medium supplemented with increasing concentrations of BAA or IAA, until reaching the upper toxic limit. For both halogenated compounds, all the culture conditions showed a reduced cell density for the Δhad mutant compared to the WT (**Fig. 4C** and **4D**). The greatest effect of the *zghad* deletion was obtained with 1 mM BAA where the growth of the WT strain was still 60% and that of the Δhad strain was only 10% compared to the control culture conditions without haloacid. Above 2 mM of BAA, the growth rate of the WT strain dropped at 25%, and reached 15% for 4 mM of BAA, whereas that of the Δhad strain remained under 10% of the corresponding control growth rate. The

growth rates of both WT and *Δhad* strains were close to 0% after incubation with 8 mM of BAA. More than 2 mM of IAA was lethal for both strains. However, the WT strain growth was higher than the *Δhad* mutant between 0.2 and 0.4 mM of IAA (**Fig. 4D**).

In order to further test the role of ZgHAD in haloacid tolerance, the recombinant *E. coli* expression strain (ZgHAD-BL21) was grown in parallel with a control *E. coli* strain transformed with an empty pFO4 plasmid (pFO4-BL21) (**Fig. 4E**). The control pFO4-BL21 strain did not grow with the upper BAA and IAA concentrations (4.9% and 6.4% of the relative growth compared to that of an unamended LB medium) while the ZgHAD-BL21 strain was able to reach 86% and 77%, respectively. The pFO4-BL21 strain was also strongly inhibited in the presence of 0.5 mM of BAA with 57% relative growth, compared to the ZgHAD-pFO4 strain, which showed no difference compared to the control (94% relative growth).

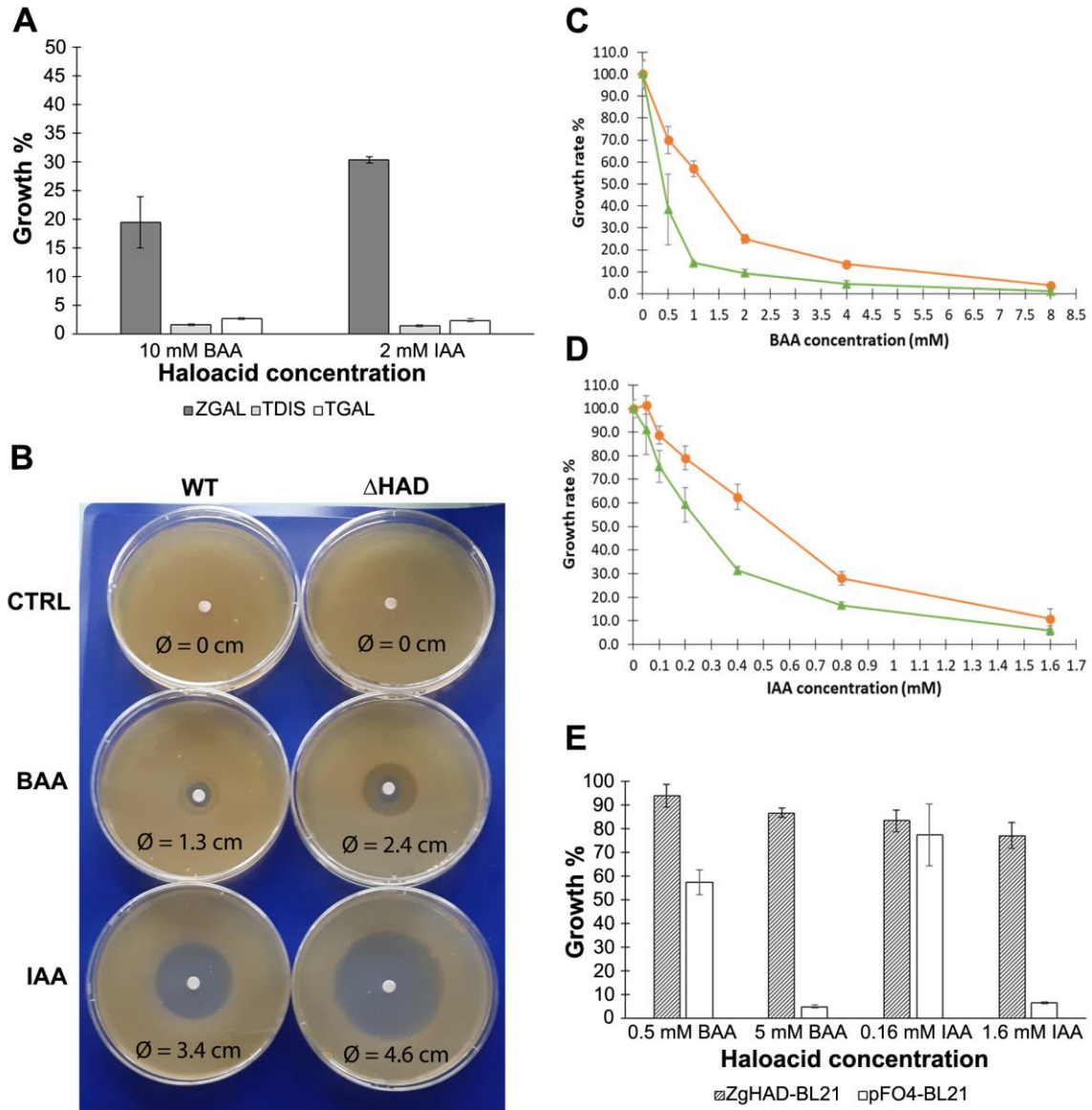


Figure 4: Comparison of bacterial growth of different marine strains, *Z. galactanivorans* HAD knockout mutant and *E. coli* recombinant clones in presence of haloacetic acids (A) Growth rates of *Tenacibaculum* strains (*T. discolor* : TDIS and *T. gallaicum* : TGAL) compared to *Z. galactanivorans* wild type (ZGAL) in liquid cultures supplemented with 10 mM bromoacetic acid (BAA) and 2 mM iodoacetic acid (IAA). **(B)** *Z. galactanivorans* WT and Δ had growth on solid medium with BAA and IAA solutions deposited on a filter at the center of the plate. The diameter of inhibition around the disk was measured for each plate after 3 days of incubation at 20 °C. CTRL: negative control. **(C, D)** Growth rates of *Z. galactanivorans* wild-type and Δ had mutant in liquid cultures with different concentrations of BAA (C) and IAA (D). *Z. galactanivorans* (orange line, round dots) and Δ had mutant (green line, triangle dots). **(E)** Percentage of growth of ZgHAD-expressing recombinant clones of *E. coli* (ZgHAD-BL21) compared to *E. coli* control strain (pFO4-BL21) in liquid cultures supplemented with either 0.5 or 5 mM BAA and 0.16 or 1.6 mM of IAA.

Distribution of the two L-2-HAD major phylogenetic groups in the environment

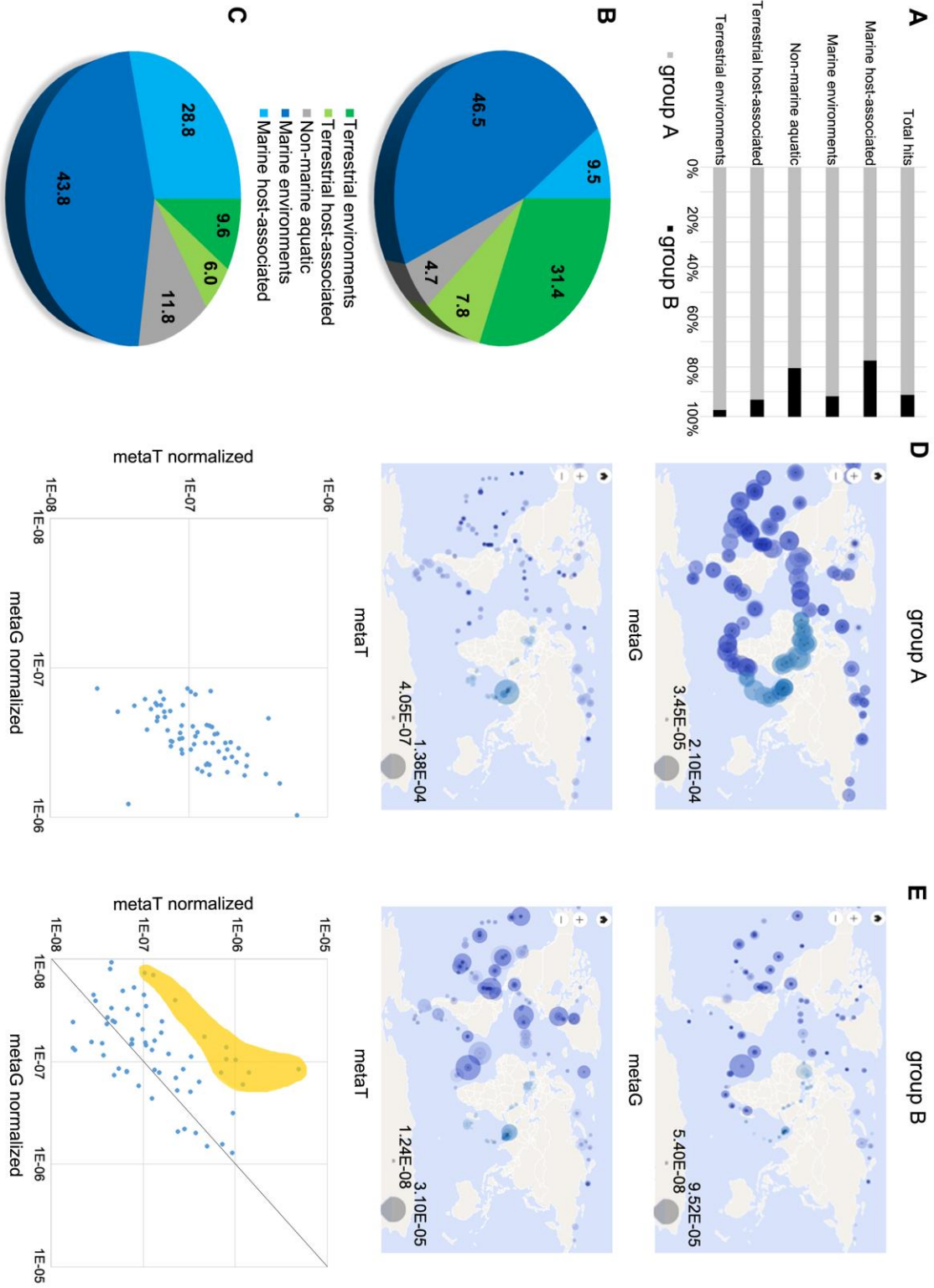
Our phylogenetic analysis suggested that the two different phylogenetic groups A and B, showing different conserved amino-acid signatures, could be differently distributed in the terrestrial and marine environments (**Fig. 1**). To test this hypothesis, we investigated (i) the overall metagenomic abundance distribution of L-2-HAD homologs in contrasted ecosystems using IMG/MER database (IMG/MER) and (ii) the specific marine distribution of the L-2-HADs through their gene number and gene expression using the Ocean Gene Atlas database (OGA). Among the 25 analyzed ecosystems corresponding to 2,500 metagenomes of IMG/MER (**Table S3**), a total of 4,265 hits were found. The group A L-2-HAD sequences were ten times more frequent (3,800 hits) than the group B L-2-HAD sequences (365 hits). This preponderance of group A L-2-HADs was verified for all the five major ecosystems of terrestrial, aquatic non-marine and marine habitats with 75 to 95% of the overall hit identification represented by the group A L-2-HAD sequences (**Fig. 5A**). Nevertheless, the environmental distribution differed in the 5 datasets (**Fig. 5B-C**). The group A L-2-HAD sequences were almost equally distributed between the non-marine and marine fractions (43.9 and 56%, **Fig. 5B**). By contrast, the majority of group B hits originated from marine biotopes (72.6% altogether, **Fig. 5C**). As shown in **Table S3**, the group A L-2-HADs are encountered mostly in marine intertidal (764 hits) and coastal (554 hits) zones and in forest soils (560 hits). Moreover, they seemed to be more present in free-living environments (1768 sequences representing 46.5% and 1195 sequences representing 31.4% for marine and terrestrial environments, respectively) than in host-associations (9.5% and 7.8% for marine and terrestrial hosts only). By contrast, the group B L-2-HADs were found in bacteria closely linked to marine hosts (28.8% of all the group B hits)

compared to terrestrial hosts (6% of hits, **Fig. 5C**). Furthermore, they were particularly found in association with marine macroalgae (76 hits, representing 72.6% of the marine host-associated subset and 20.8% of all the group B hits). Other characteristics of this group B L-2-HADs revealed that these sequences are also principally present in the marine coastal and in the non-marine saline/alkaline environments (51 and 39 hits respectively, 31.9% and 90.7% of their subset, 14% and 10.7% of all the group B hits) (**Table S3**).

The distribution of the group A and group B L-2-HADs was assessed more precisely in marine environment using OGA (**Table S4**). Interestingly, a similar order of magnitude of group A sequences was obtained when the marine DehPsi and DehDEH99 proteins were used as queries (166 and 214 hits) while a highest number of hits (about 3 to 7 fold) was retrieved using the 15 terrestrial sequences. The three selected L-2-HAD protein sequences from the phylogenetic group B (ZgHAD, DehRhb and WP_038235908) allowed to retrieve 204 to 234 hits (**Table S4**), which all feature the conserved amino acid consensus DETF(S/T)KYAHD. The group A hits were detected in the metagenomes of 66 stations worldwide with an overall gene abundance of at least 10^{-4} (**Fig. 5D**). Group A homologs were more abundant in temperate and tropical zones than in arctic and subarctic zones. By comparison, the group B hits were detected in the metagenomes of 64 stations also well-distributed around the globe but with lower abundances (**Fig. 5E**). We further evaluated the expression of these L-2-HAD homologs by searching hits in the OGA metatranscriptomes. Overall, the representation of group A sequences in metatranscriptomes was low compared to their corresponding detection in metagenomes. The scatterplot of the normalized abundance in metatranscriptomes vs. metagenomes showed that all but one station fell below the 1:1 line, confirming a comparatively low

expression of the group A L-2-HAD-encoding genes in most oceanic regions (**Fig. 5D**). Conversely, the metatranscriptomic abundance of group B L-2-HADs was more heterogeneous, and often higher than the corresponding metagenomic abundance for Atlantic and Pacific stations (**Fig. 5E**). The scatterplots demonstrated that the ratio of group B L-2-HAD-encoding genes abundance in metatranscriptomes vs. metagenomes was ≥ 1 for 75% of the 64 stations, suggesting a consistent gene expression. In particular, the ratios of 11 stations fell well above the 1:1 line (orange colored zone, **Fig. 5E**), with a metatranscriptome abundance exceeding 5 to 40 fold that in metagenome. The sample exhibiting the highest expression level for the group B (MetaT/MetaG ratio > 40) was located at the station 137 (sample TARA_B100001964, TARA_137_DCM) in the Pacific Ocean at about 500 km west off the coast of Mexico. It corresponds to water collected during late autumn at 40 m depth in the deep chlorophyll maximum layer. The temperature of the water was 20.5 °C and pigment detection indicated that chlorophyll a, fucoxanthin, lutein and zeaxanthin were present in the sample. The exploration of individual results for all group B L-2-HAD hits found in this particular sample suggests that mainly two homolog genes (corresponding to OM-RGC.v2.011753063 and OM-RGC.v2.014543634) are highly expressed. Both hits were affiliated to the *Gammaproteobacterium Alteromonas australica*.

Figure 5: Analysis of environmental and oceanic distributions of L-2-HADs into IMG/MER metagenomes and OGA databases. (A) Global abundance representation of the group A homologs and group B homologs among L-2-HADs hit number in the full set of IMG/MER metagenomes. (B-C) Distribution of the group A (B) and the group B (C) sequence hits in 5 IMG/MER ecosystems sets. (D-E) Geographic distribution of group A (D) and group B (E) homolog relative abundances into metagenomic (metaG) and metatranscriptomic (metaT) OGA databases and scatterplots of the corresponding normalized gene abundance in metaT vs. metaG. Global abundance scales are represented by the grey circles at the bottom right of the maps.



DISCUSSION

A bacterial protein named ZgHAD was identified based on its amino acid sequence as the unique L-2-HAD coded in the genome of *Z. galactanivorans*, a marine bacterium belonging to the *Bacteroidetes* phylum. Although L-2-HAD protein homologs are distributed in numerous bacteria and archaea, only four enzymes have been previously described from marine bacteria, and little was known about their biological functions and potential ecological role(s) and distribution in marine environment.

The biochemical properties of this newly characterized marine L-2-HAD were compared to other previously characterized L-2-HADs, mostly in *Proteobacteria*. As also shown by the phylogenetic analysis, a poor conservation of amino acid sequences between L-2-HADs from group A and group B suggested differences in the conservation of the global protein folding, but also in the biochemical properties. ZgHAD exhibited highest activity towards C2 and C3 carbon-chain substrates with a preference for bromo and iodoacetate, similar to DehRhb (Novak *et al.*, 2013a), DehIVa (Schmidberger *et al.*, 2007), DehPsi (Novak *et al.*, 2013b) and H-2 (Kawasaki *et al.*, 1981) which use BAA as best substrate. ZgHAD did not show any activity towards substrates with a longer carbon-chain or towards dihalogenated acid substrates, contrasting with other L-2-HADs like DehSft (Rye *et al.*, 2009), Dh1B (Ridder *et al.*, 1997), DehPsi (Novak *et al.*, 2013b) from the phylogenetic group A, suggesting some enzymatic specificities of the marine L-2 HADs from the phylogenetic group B. The K_m value of ZgHAD for BAA was 0.46 mM, whereas it varied from 1.1 to 6.72 mM for other L-2-HADs. Notably its closest relative DehRhb showed a higher K_m value of 6.72 mM (Novak *et al.*, 2013a) revealing a lower affinity for BAA compared to ZgHAD. The K_m of ZgHAD for IAA was lower (0.31 mM) compared to

BAA suggesting a higher affinity of ZgHAD for the iodinated substrate. The IAA has been previously shown to be a substrate for several L-2-HADs of the phylogenetic group A like DEH99 (Zhang *et al.*, 2014), L-DEX (Liu *et al.*, 1994), DhIS5I (Köhler *et al.*, 1998), and H-2 (Kawasaki *et al.*, 1981). Previous assays with the characterized L-2-HADs did not always include iodinated substrates. As iodide is a better leaving group than bromide or chloride, it is likely that most L-2-HAD enzymes, are also active on IAA and therefore on both brominated and iodinated short carbon chains, especially those from seawater origin, as the halocarbons are predominant in the marine environment. However it is the first time that IAA was reported to be a best substrate than other haloacids for a L-2-HAD. It would be interesting to confirm that by the calculation of enzymatic parameters with IAA for other L-2-HADs. In contrast, DEH130 of *Pseudomonas stutzeri*, isolated from the marine sponge *Hymeniacidon perlevis*, was unable to transform iodoacetic acid (Zhang *et al.*, 2013).

Z. galactanivorans was able to grow in the presence of higher concentrations of BAA and IAA than its *Δhad* knockout mutant and, than both fish pathogens *T. discolor* and *T. gallaicum*. The strong growth inhibition induced by BAA and IAA in strains lacking a L-2-HAD gene suggested it could confer a selective advantage to *Z. galactanivorans* in the presence of toxic haloacetic acids in its environment. This potential benefit was confirmed by the improved tolerance of the *E. coli* cells expressing ZgHAD to these haloacids. As ZgHAD enzyme was produced inside the *E. coli* cells (as it is also predicted for *Z. galactanivorans*), this result suggested that these bacteria could import BAA and IAA into their cytoplasm for detoxification. Soil bacteria such as *Burkholderia cepacia* MBA4 or *Xanthobacter autotrophicus* GJ10 have been studied for their capacity to grow on and

metabolize haloacid compounds. They possess the genetic tools to internalize and degrade a large range of organic halogenated compounds that are often toxic (Kwok *et al.*, 2007; Mena-Benitez *et al.*, 2008; Horisaki *et al.*, 2011). In *B. cepacia* MBA4, the dehalogenase gene *dehIVa* and the downstream permease gene *dehIVp* were shown to form an inducible operon that mediates the transformation and uptake of halogenated acids (Yu *et al.*, 2007). No clear haloacid operon, permease gene or equivalent transport system were identified within *Z. galactanivorans* genome. Nevertheless, the detoxification of haloacetic acids was efficient in *Z. galactanivorans* suggesting that an unidentified transport system might exist. The haloacetic acids are converted to glycolate by the L-2-HADs. The enzymes catalyzing the glycolate catabolism (Zgal_4160/Zgal_4169 and Zgal_4659) are predicted to be encoded by the genome of *Z. galactanivorans* as shown in its KEGG metabolic network and schematized in **Fig. 6**. They might link BAA and IAA degradations either to the glyoxylate cycle or to the vitamin B6 metabolism via glycolaldehyde (**Fig. 6**). The Δhad mutant of *Z. galactanivorans* resisted better to haloacetic acids than the *Tenacibaculum* strains lacking L-2-HAD. Other unidentified genes could therefore be involved in the resistance against haloacetic acids in *Z. galactanivorans*, as it was previously demonstrated for BAA resistance in *E. coli* (Desai and Miller, 2010). Altogether, our functional results and gene mining in *Z. galactanivorans* suggested that a complete degradation pathway of short carbon chain haloacids could be potentially present inside the cell, downstream of ZgHAD (**Fig. 6**). It would be interesting to further compare transcriptomic regulations in *Z. galactanivorans* and in its Δhad mutant in the presence of BAA or IAA to elucidate all the metabolic processes involved in haloacid intracellular degradation.

All the available sequenced *Zobellia* isolates have one or two copies of L-2-HAD-encoding gene in their genome, a trait that might be a selective advantage linked to the presence of short haloacetic acids, in their natural environment. Indeed, coastal ecosystems could host a permanent natural production of toxic haloacids through various processes (**Fig. 6**). First, low-molecular-weight organic acids such as acetic acids are ubiquitous in seawater, produced either *via* respiration, microbial degradation of lipids or photochemical breakdown of dissolved organic matter (Liang *et al.*, 2020). They might be converted to the corresponding halogenated acetic acids abiotically or biotically, as reported previously for other environments. For example, the decomposition of forest soil organic matter leads to the production of CAA (Matucha *et al.*, 2003; Laturmus *et al.*, 2005), potentially due to the action of fungal and bacterial chloroperoxidases (Wever *et al.*, 2017). In line with this, we hypothesize that the combination of vanadium-haloperoxidases and L-2-HADs could also contribute to the recycling of acetic acids dissolved in seawater through the production of BAA and IAA intermediates (**Fig. 6**). Second, brominated or iodinated compounds are produced by some other marine bacteria, and also by a range of marine macro-organisms living in close association with bacteria (e.g. corals, sponges, macroalgae) (Gribble, 2010). In particular, marine macroalgae are known to release organic brominated and iodinated toxic compounds in the seawater (Belkin, 1992; Paul *et al.*, 2006). Some red algae like *Asparagopsis taxiformis* have been reported to produce haloacetic acids (Woolard *et al.*, 1979; Fenical, 1982). Moreover, haloalkanes like diiodoethane produced by kelps in biotic interactions could be sequentially transformed into haloacetic acids similarly to the dichloroethane degradation found in *Xanthobacter autotrophicus* GJ10 (Van der Ploeg *et al.*, 1991). Since all known *Zobellia* species live with or close to macroalgae, including red

algae such as *Delesseria sanguinea* (Barbeyron *et al.*, 2001) and brown algae such as *Fucales* and *Laminariales* (Nedashkovskaya *et al.*, 2004a; Martin *et al.*, 2015), it is likely they regularly experience the release of haloacetic acids or haloalkanes (Fig. 6). The haloacetic acids present in the coastal seawater might also result from anthropogenic activities (e.g. agriculture, water-treatment stations). Chlorine residuals and humic acids of effluents can react with bromide-rich coastal seawaters (0.8 mM) to form BAA (Gordon *et al.*, 2015). Similar reactions might occur for the IAA formation, as seawater contains 0.3 μM of iodide (La Barre *et al.*, 2010). The catabolic properties towards both BAA and IAA might reflect the genetic adaptation of *Zobellia* to these halogen-rich marine ecological niches, and especially those formed by the coastal macroalgal beds (Fig. 6).

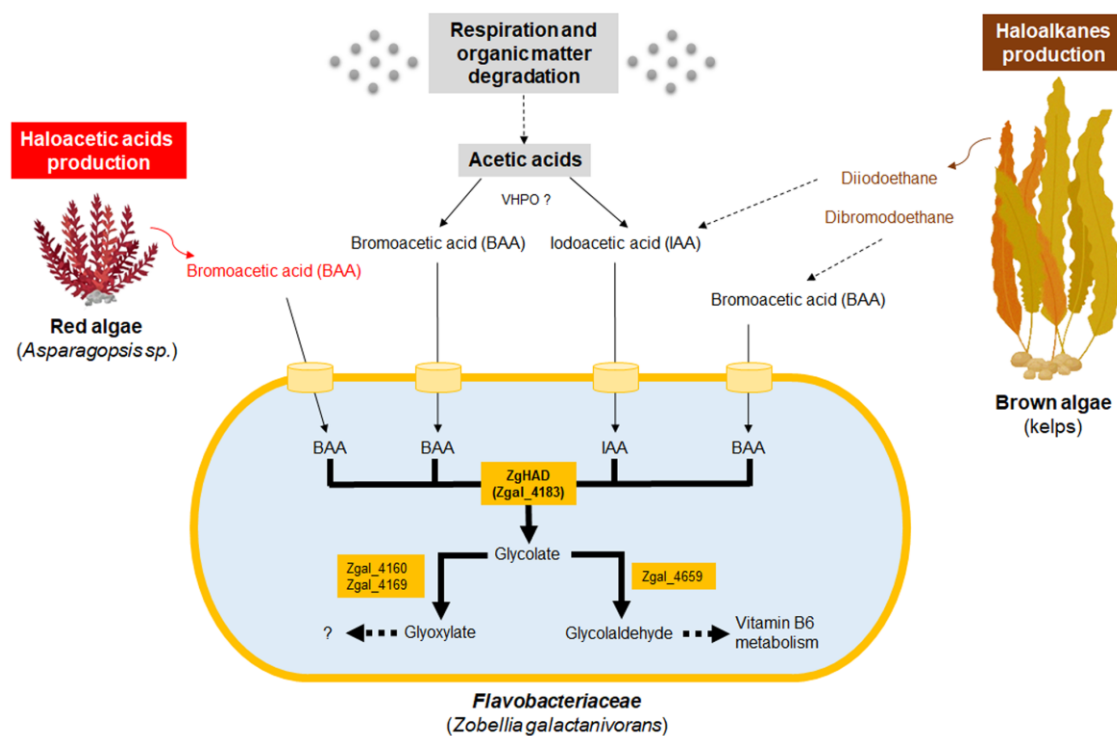


Figure 6: Hypothetical scheme of production and biotransformation of haloacetates by *Z. galactanivorans*, in macroalgae-dominated coastal habitats. ZgHAD and Zgal_4183 = L-2-Haloacid dehalogenase of *Z. galactanivorans*; BAA = bromoacetic acid; IAA = iodoacetic acid; Zgal_4160 = glyoxylate/hydroxypyruvate reductase; Zgal_4169 = glyoxylate reductase; Zgal_4659 = glycolaldehyde dehydrogenase; VHPO = vanadium-haloperoxidases. Dotted arrows

refer to multistep enzymatic transformations. Oceanic biomass, red algal and brown algal transformation and productions are respectively colored in grey, red and brown. Specific toxic compounds produced by red and brown algae are also in red and brown fonts. Orange cylinder models the putative BAA and IAA transporters.

The phylogenetic tree of L-2-HADs revealed two major distinct phylogenetic groups that were correlated to a specific amino acid signature corresponding to differences in catalytic sites. The phylogenetic group A contained a majority of terrestrial but also marine sequences and the phylogenetic group B was essentially composed of marine ones. Furthermore, the group B showed a separation of two distinct *Bacteroidetes* L-2-HAD clades, namely HAD1 (including ZgHAD) and HAD2. The comparative genomics in the *Flavobacteriaceae* family and transcriptomic analysis in *Z. galactanivorans* suggested that *zghad* featured a 3-gene operon with *zgal_4181* and *zgal_4182*. Comparative genomics also demonstrated that the HAD1-type genes did not have the same genomic context in different *Flavobacteriaceae*. It brought to light that HAD1-type gene might be a mobile element in flavobacterial genomes or might have been acquired by multiple independent horizontal gene transfers. By contrast, the HAD2-type gene is often surrounded by the same two genes (TetR TF and UOR) suggesting a conserved genomic organization within *Flavobacteriaceae*. With the fact that its presence was frequent in *Flavobacteriaceae* genomes, this conserved pattern put forward the hypothesis that the HAD2-type gene was an ancestral gene, which still need to be characterized at the biochemical level. Additional functional and transcriptomic analyses would be necessary to further test these hypotheses. This phylogenetic overview was enlarged with environmental analyses through oceanic (OGA) and multi-ecosystemic (IMG/MER) data. Group A L-2-HADs are more widespread than group B, irrespective of the biotope. These group A L-2-HADs are almost equally

distributed between terrestrial and marine habitats. Moreover, the analyses of ocean genomic data revealed that these L-2-HADs were more frequent in the marine environment than initially thought, often exceeding group B sequences. The group B L-2-HADs appeared to be less frequent in nature but they are very selectively present in the marine environments, in particular in close association with macroalgae. Overall, the presence of toxic haloacids in marine environments likely drove the selection and evolution of L-2-HAD genes. Indeed, the strong prevalence of L-2-HADs in metagenomes from macroalgae or hypersaline waters suggests that these enzymes could be involved in the elimination of haloacetic acids favored in these particular environments. Considering a larger point of view, the important representation of L-2-HAD genes in oceanic stations could reflect strong biomass production spots like microalgal blooms. Metatranscriptomic analyses of OGA data revealed that group A L-2-HADs have a homogeneously low expression level around the globe while group B expression is likely induced in certain zones in response to yet-unknown stimuli. The high expression of group B L-2-HADs affiliated to *Alteromonas* at station TARA_137 where chlorophyll a, fucoxanthin, lutein and zeaxanthin were detected might suggest an association with microalgae and *Flavobacteriaceae*.

CONCLUSION

Biochemical and functional characterizations of the only L-2-HAD encoded in the genome of *Z. galactanivorans* (ZgHAD) have shown its key role in the catabolism of IAA and BAA in this marine *Bacteroidetes*. ZgHAD could confer a selective advantage to live in haloacetic acid-producing niches, such as those formed by coastal macroalgae. An extensive phylogenetic analysis has revealed the occurrence of two sister groups of L-2-

HADs, namely group A and group B. When the well-represented group A contains both terrestrial and marine sequences, the minor group B was mainly composed of marine L-2-HADs and contained two distinct *Bacteroidetes* clades. The search for group A and group B L-2-HADs homologs in environmental databases further confirmed world-wide, but distinct ecological distribution and expression levels of these two L-2-HAD groups, according to geographical origins, suggesting different ecological functions. For instance, the presence of homologs of ZgHAD could be the functional signature of bacterial haloacetic acid catabolism, especially during micro- and macroalgal interactions.

Our study also highlighted the important frequency and diversity of marine L-2-HADs, especially of those belonging to the phylogenetic group A, which are still to be characterized as being important actors of halogenated compounds biotransformation and halogen biogeochemical cycle in open marine environments.

MATERIAL AND METHODS

Chemicals

Iodoacetic acid (I4386), bromoacetic acid (17000), chloroacetic acid (C19627), D-2-bromopropionic acid (18165), L-2-bromopropionic acid (38551), D-2-chloropropionic acid (306800), L-2-chloropropionic acid (306797), trichloroacetic acid (91233), 3-iodopropionic acid (I10457), 3-bromopropionic acid (101281), 2-chlorobutyric acid (24008), iodoacetamide (I1149), dibromoacetic acid (242357) were obtained from Merck.

Bacterial strains and plasmids

All the bacterial strains and plasmids used in this study are listed in **Table S6**.

Phylogenetic analysis

The selected set of L-2-HAD proteins was derived from NCBI BlastP queries against the RefSeq database. Sequences were loaded into the NGPhylogeny.fr “A la carte” pipeline and analyzed as follows. A total of 352 protein sequences were aligned using MAFFT under default parameters then cleaned with trimAl resulting in 165 informative positions over the 400 aligned positions (see **Table S2** for complete information). A maximum likelihood phylogenetic analysis was carried out using default parameters of the PhyML-SMS tool allowing the best substitution model selection. Bootstrap analysis with 100 replicates was used to provide estimates for the phylogenetic tree topology and it resulted in a newick file formatted with the program MEGA v10.1.1 to obtain the corresponding simplified dendrogram tree figure.

Environmental IMG/MER data analyses

L-2-HAD homologs were searched by BlastP in the environmental metagenomic IMG/MER database at the JGI website (<https://img.jgi.doe.gov/cgi-bin/mer/main.cgi?section=FindGenesBlast&page=geneSearchBlast>), using DehIVa and ZgHAD sequences as the representative sequences of the phylogenetic group A and group B respectively. A stringent e-value cutoff of 10^{-50} was selected to identify reliable hits of group A and group B with at least 38% amino acid identity into five datasets (Terrestrial environments, Terrestrial host-associated, Non-marine aquatic, Marine environments, Marine host-associated). Each dataset was constituted of 5 subsets comprising 100 selected metagenomes (**Table S3**). The BlastP results of group A and group B sequences were expressed as hit number abundances in each dataset and subset, and as overall percentages.

Oceanic distribution and expression in OGA databases

The BlastP searches were carried out with the 20 representative L-2-HAD sequences against the Ocean Gene Atlas (OGA) database (<http://tara-oceans.mio.osupytheas.fr/ocean-gene-atlas>), comprising metagenomic OM-RGCv2+G and metatranscriptomic OM-RGCv2+T data collections from the Tara Oceans stations (Villar *et al.*, 2018). A stringent e-value cutoff of 10^{-30} was selected in order to cover a majority of each phylogenetic clade (Table S4). In a second step, we focused on the DehIVa and ZgHAD BlastP hits respectively as representative sequences of the phylogenetic group A and group B, to compare their geographic repartition, relative gene abundance (metaG) and relative gene expression (metaT) levels. All the data for BlastP searches can be downloaded and extracted at the website. Relative abundance values were calculated based on the sum of all the hits found at a precise site and showed on geographical maps. Relative abundance was further normalized by the number of hits in order to evaluate the average of gene abundance and gene expression for every OGA stations. The “global abundance / hits number” were calculated for each station and predicted as log10 correlation plots analyses of 66 and 64 spots respectively for DehIVa (group A) and ZgHAD (group B) homologs. Finally, environmental parameters were compared using the bubble plots tools available on the OGA website platform.

Genomic context decryption

The *had* gene context in *Flavobacteriaceae* was analyzed by the selective tool of synteny reconstruction on the Genoscope platform: Microscope (MaGe; <https://mage.genoscope.cns.fr/microscope/home/>). All the genomic regions containing a

had gene (listed in **Table S5**) were then aligned to allow the identification of the conserved neighboring genes and the varying ones.

Gene cloning

The ZgHAD-encoding gene sequence (*zgal_4183*) was cloned from the genomic DNA of *Zobellia galactanivorans* Dsij^T (Barbeyron *et al.*, 2001), using primers Zgal_4183fw and Zgal_4183rv (**Table S6**). The PCR product was ligated into the pFO4 vector, using *Bam*HI and *Eco*RI restriction sites and the T4 DNA ligase protocol (New England Biolabs). The recombinant vector was transformed firstly into *Escherichia coli* DH5 α for sequence verification and secondly into *E. coli* BL21 (DE3) expression strain.

Overexpression and purification

The recombinant *E. coli* strain expressing ZgHAD was grown in LB medium containing 100 $\mu\text{g}\cdot\text{ml}^{-1}$ ampicillin at 37 °C to an optical density of ~ 1.0 , then the temperature was lowered to 20 °C for 1 hour followed by a 20 h induction of protein production by the addition of 0.5 mM IPTG. After centrifugation (3,000 *g*, 30 min, 4 °C), the bacterial pellet was stored at -20 °C, then resuspended in 50 mM Tris (pH 7.5), 500 mM NaCl, bovine DNase I (500 U/ μL), 0.1 mg/mL lysozyme, CompleteTM Protease Inhibitor Cocktail (Merck) and 6 mM MgCl₂ and lysed using a French press and the lysate was centrifuged at 23,000 *g* during 30 min and 4°C. The recombinant protein was purified by a two-step chromatography carried on an ÄKTA Avant purification system (GE Healthcare Life Sciences). The first step was performed on an immobilized nickel affinity HisTrapTM column (GE Healthcare Life Sciences) using an equilibration buffer composed of 50 mM

Tris (pH 7.5), 500 mM NaCl and 50 mM imidazole and an elution buffer containing 500 mM imidazole instead of 50 mM. Proteins were eluted with a constant gradient of imidazole concentration. The pooled fractions of the elution peak were concentrated on Centriprep devices and the protein sample was injected on a gel filtration HiLoad™ 16/600 Superdex™ 200 pg column (GE Healthcare Life Sciences). The purified protein was stored in a buffer containing 20 mM Tris (pH 8.0) and 150 mM NaCl. The purity of the recombinant protein was analyzed by SDS-PAGE (Bio-Rad Mini-PROTEAN® precast gels and systems).

Substrate specificity and kinetic enzymatic parameters determination

The ZgHAD enzyme specificity was determined by adapting the colorimetric assay from [Holloway *et al.*, 1998](#). The detection was based on a pH decrease when the halogenated substrate was reduced to a hydroxyalkanoic acid. Upon dehalogenation, the release of halide ions X^- decreased the pH inducing a color transition of the phenol red pH indicator (from pink to orange to yellow) that was monitored visually. The assay solution contained final concentrations of 0.3 mg.ml⁻¹ recombinant ZgHAD enzyme, 1 mM HEPES, 1 mM EDTA, 20 mM sodium sulfate and 56 μM of phenol red (pH 8.2). The assay was adapted for 48-well plates to test 13 different substrates at 10 mM (iodoacetic acid, bromoacetic acid, chloroacetic acid, D-2-bromopropionic acid, L-2-bromopropionic acid, D-2-chloropropionic acid, L-2-chloropropionic acid, trichloroacetic acid, 3-iodopropionic acid, 3-bromopropionic acid, 2-chlorobutyric acid, iodoacetamide, dibromoacetic acid) in 1 mL final volume. The plates were incubated at 20 °C during 30 min then photographed and left 16 h at 20 °C to check for long-term variations.

The colorimetric assay was further used for measuring enzymatic kinetic parameters towards IAA or BAA as substrates. All reactions were performed in triplicates at 20 °C. Each assay was carried out in a 180 µL reaction mixture. The final concentration of purified ZgHAD protein was 0.3 mg.ml⁻¹. The kinetics of the reaction was followed by measuring the decrease of absorbance at 560 nm for 10 minutes on a Spark® multimode microplate reader (Tecan Group Ltd. Switzerland). A standard curve was produced by mixing the assay solution with 1 M HCl to final concentrations of 0-2 mM in a total volume of 200 µL. The Lineweaver-Burke plots were used to calculate the Km and Vmax steady-state kinetic parameters.

Deletion of ZgHAD gene in *Zobellia galactanivorans*

A deletion mutant of the *zghad* gene was constructed following the previously described method from [Zhu et al., 2017](#). A 2.2-kb fragment corresponding to the first 36 bp of the *zghad* gene with the region directly upstream was amplified using the primers OEG007 and OEG009 (**Table S6**). The fragment was digested with *Xba*I and *Sal*I and ligated into the pYT313 vector cut with the same enzymes to generate the vector pEG1. Similarly, a 2.3-kb fragment corresponding to the last 35 bp of the *zghad* gene and the region directly downstream was amplified with the primers OEG008 and OEG010 (**Table S6**). The fragment was inserted between *Bam*HI and *Xba*I sites of pEG1 to generate the suicide plasmid pEG3. Suicide plasmid was introduced into the wild type *Z. galactanivorans* Dsij^T by conjugation with *E. coli* S17-1 λpir strain. Erythromycin resistance was used to select the cells having integrated the plasmid in their genome. Resulting colonies were grown overnight in *Cytophaga* medium (per liter: 1.0 g yeast extract, 1.0 g tryptone, 24.7 g NaCl,

0.7 g KCl, 6.3 g MgSO₄·7H₂O, 4.6 g MgCl₂·6H₂O, 1.2 g CaCl₂·2H₂O, 0.2 g NaHCO₃) without antibiotics at 30 °C to allow the loss of the plasmid. The cells were then plated onto *Cytophaga*-agar containing 5% sucrose. The sucrose-resistant colonies were checked for erythromycin sensitivity. The deletion of the *zghad* gene was confirmed by PCR using primer pairs OEG011-OEG012 (**Table S6**) and then verified by Sanger sequencing at the GENOMER platform (FR2424; Roscoff Biological Station).

Growth inhibition analyses of marine *Flavobacteriaceae* and phenotyping of the *Z. galactanivorans* Δ had mutant

The ability to grow and resist to increasing haloacid concentrations was tested using an antibiogram-like method. *Z. galactanivorans* wild type (WT) and its deleted *had* gene mutant (Δ had) were grown on ZoBell 2216-agar plates with a Whatman paper disc at the center. The paper was impregnated with 25 μ l solution of either 500 mM BAA or IAA (shown to be *in vitro* substrates of ZgHAD) or Tris-glycine 100 mM pH 8.0 as negative control. The haloacid effect was determined by monitoring the size of the inhibition zone after 72 h at 20 °C. This experiment was realized two times independently.

Z. galactanivorans WT and both *Tenacibaculum* species (*T. discolor* DSM 18842^T and *T. gallaicum* DSM 18841^T) were grown in 3 mL ZoBell 2216 liquid medium with high concentrations of BAA and IAA (2 mM) buffered by 20 mM HEPES buffer pH 7.0 and during 16 h at 20 °C. Each medium was initially inoculated at 1/100 dilution with a two-day preculture. *Z. galactanivorans* WT strain and the mutant Δ had strain were also grown in ZoBell liquid medium in the same conditions with different concentration ranges of IAA or BAA dissolved in 200 mM HEPES buffer pH 7.0. The final concentrations were defined

from 0 to 1.6 mM and 0 to 8 mM respectively for IAA and BAA. Each concentration was tested in biological triplicates. The bacterial growth was measured by the mean of OD₆₀₀ in the respect of technical duplicates. The growth rates were calculated from the slopes of the growth curves between 15 and 20 h, during the exponential phase. They were expressed as a percentage of the standard growth rate in ZoBell medium for each corresponding strain.

Phenotyping of recombinant *E. coli* tolerance to BAA and IAA

The *E. coli* BL21 expression strains containing the pFO4 vector alone (pFO4-BL21 strain) or recombined with the *zghad* gene (ZgHAD-BL21 strain) were grown in LB medium containing 100 µg.ml⁻¹ ampicillin and IPTG overnight at 20 °C. These precultures were used to inoculate a fresh LB/Ampicillin medium supplemented with 0.5 mM IPTG at 1/100 dilution. Two concentrations distant of ten folds were tested in triplicates as follows, 0.5 and 5 mM for BAA and 0.16 and 1.6 mM for IAA. After 15 h of incubation at 20 °C, the final OD₆₀₀ was measured and reported to that of an equivalent culture in standard conditions, without haloacids.

ACKNOWLEDGMENT

We would like to thank Tristan Barbeyron for giving us access to *Tenacibaculum* strains. This work benefited from the support of the French Government via the National Research Agency investment expenditure program IDEALG (ANR-10-BTBR-04) and via the Centre National de la Recherche Scientifique (CNRS). The PhD project of EG was also supported by Region Bretagne (ARED 2017, projet MHALIN).

REFERENCES

- Adamu, A., Wahab, R.A., Huyop, F. (2016) 1-2-Haloacid dehalogenase (DehL) from *Rhizobium* sp. RC1. Springerplus 5: 695.
- Agarwal, V., Miles, Z., Winter, J., Eustaquio, A., El Gamal, A., and Moore, B. (2017) Enzymatic halogenation and dehalogenation reactions: pervasive and mechanistically diverse. *Chem Rev* 117: 5619-5674.
- Amsler, C.D. (2008) *Algal Chemical Ecology*.
- Ang, T.F., Maiangwa, J., Bakar Salleh, A., Normi, Y., and Leow, T.C. (2018) Dehalogenases: from improved performance to potential microbial dehalogenation applications. *Molecules*. 23: 1-40.
- Barbeyron, T., L'Haridon, S., Corre, E., Kloareg, B., and Potin, P. (2001) *Zobellia galactanovorans* gen. nov., sp. nov., a marine species of *Flavobacteriaceae* isolated from a red alga, and classification of [*Cytophaga*] *uliginosa* (ZoBell and Upham 1944) Reichenbach 1989 as *Zobellia uliginosa* gen. nov., comb. nov. *Int J Syst Evol Microbiol* 51: 985–997.
- Barbeyron, T., Thomas, F., Barbe, V., Teeling, H., Schenowitz, C., Dossat, C., *et al.* (2016) Habitat and taxon as driving forces of carbohydrate catabolism in marine heterotrophic bacteria: example of the model algae-associated bacterium *Zobellia galactanivorans* Dsij^T. *Environ Microbiol* 18: 4610-4627.
- Belkin, S. (1992) Biodegradation of haloalkanes. *Biodegradation* 3: 299-313.
- Bialonska, D., and Zjawiony, J.K. (2009) Aplysinopsins – marine indole alkaloids: chemistry, bioactivity and ecological significance. *Mar Drugs* 7: 166-183.
- Burroughs, A.M., Allen, K.N., Dunaway-Mariano, D., and Aravind, L. (2006) Evolutionary Genomics of the HAD Superfamily: Understanding the Structural Adaptations and Catalytic Diversity in a Superfamily of Phosphoesterases and Allied Enzymes. *J Mol Biol* 361: 1003–1034.
- Cabrita, M.T., Vale, C., and Rauter, A.P. (2010) Halogenated compounds from marine algae. *Mar Drugs* 8: 2301-2317.
- Carpenter, L.J., Archer, S.D., and Beale R. (2012) Ocean-atmosphere trace gas exchange. *Chem Soc Rev* 41: 6473-6506.

- Chernysheva, N., Bystritskaya, E., Stenkova, A., Golovkin, I., Nedashkovskaya, O., and Isaeva, M. (2019) Comparative genomics and CAZyme genome repertoires of marine *Zobellia amurskyensis* KMM 3526^T and *Zobellia laminariae* KMM 3676^T. *Mar Drugs* 17: 661.
- Copley, S.D. (1997) Diverse mechanistic approaches to difficult chemical transformations: microbial dehalogenation of chlorinated aromatic compounds. *Chem Biol* 4: 169-174.
- Copley, S.D. (1998) Microbial dehalogenases: enzymes recruited to convert xenobiotic substrates. *Curr Opin Chem Biol* 2: 613-617.
- Desai, K.K., and Miller, B.G. (2010) Recruitment of genes and enzymes conferring resistance to the non-natural toxin bromoacetate. *Proc Natl Acad Sci U S A* 107: 17968-17973.
- Dong, Y., Peng, W., Liu, Y., Wang, Z. (2021) Photochemical origin of reactive radicals and halogenated organic substances in natural waters: A review. *J Hazard Mater* 401: 123884.
- El-Demerdash, A., Atanasov, A., Horbanczuk, O., Tammam, M., Abdel-Mogib, M., Hooper, J., *et al.* (2019) Chemical diversity and biological activities of marine sponges of the genus *Suberea*: a systematic review. *Mar Drugs* 17: 115.
- Fenical, W. (1982) Natural products chemistry in the marine environment. *Science* 215: 923-928.
- Ficko-Blean, E., Préchoux, A., Thomas, F., Rochat, T., Larocque, R., Zhu, Y., *et al.* (2017) Carrageenan catabolism is encoded by a complex regulon in marine heterotrophic bacteria. *Nature Commun* 8: 1685.
- Fournier, J-B., Rebuffet, E., Delage, L., Grijol, R., Mesclet-Cladière, L., Rzonca, J., *et al.* (2014) The vanadium iodoperoxidase from the marine *Flavobacteriaceae* species *Zobellia galactanivorans* reveals novel molecular and evolutionary features of halide specificity in the vanadium haloperoxidase enzyme family. *Appl Environ Microbiol* 80: 7561-7573.
- Gordon, A.R., Richardson, T.L., and Pinckney J.L. (2015) Ecotoxicology of bromoacetic acid on estuarine phytoplankton. *Environ Pollut* 206: 369-375.
- Gribble (2003). The diversity of naturally produced organohalogenes. *Chemosphere* 52:289-297.

Gribble, G.W. (2010) Naturally Occurring Organohalogen Compounds - A Comprehensive Update.

Gribble, G.W. (2015). A recent survey of naturally occurring organohalogen compounds. *Envir Chem* 12: 396-405.

Hardman D.J., and Slater J.H (1981). Dehalogenases in soil bacteria. *J Gen Microbiol* 123: 117–128.

Hill, K.E., Marchesi, J.R., and Weightman, A.J. (1999) Investigation of two evolutionarily unrelated halocarboxylic acid dehalogenase gene families. *J Bacteriol* 181: 2535–2547.

Holloway, P.A. (1998) Colorimetric assay for detecting haloalkane dehalogenase activity. *J Microbiol Methods* 32: 31-36.

Horisaki, T., Yoshida, E., Sumiya, K., Takemura, T., Yamane, H., and Nojiri, H. (2011) Isolation and characterization of monochloroacetic acid-degrading bacteria. *J Gen Appl Microbiol* 57: 277-284.

Huang, J., Xin, Y., and Zhang, W. (2011) Isolation, characterization and identification of a *Paracoccus* sp. 2-haloacid-degrading bacterium from the marine sponge *Hymeniacidon perlevis*. *J Basic Microbiol* 51: 318-324.

Janssen, D., Pries, F., and Van der Ploeg, J. (1994) Genetics and biochemistry of dehalogenating enzymes. *Annu Rev Microbiol* 48: 163-191.

Janssen, D., Dinkla, I., Poelarends, G., and Terpstra, P. (2005) Bacterial degradation of xenobiotic compounds: evolution and distribution of novel enzyme activities. *Environ Microbiol* 7: 1868-1882.

Jordan A., Harnisch J., Borchers R., Le Guern F., and Shinohara H. (2000) Volcanogenic Halocarbons. *Environ Sci Technol* 34: 1122.

Kawasaki, H., Yahara, H., and Tonomura, K. (1981) Isolation and Characterization of Plasmid pUOI Mediating Dehalogenation of Haloacetate and Mercury Resistance in *Moraxella* sp. B. *Agric Biol Chem* 45: 1477-1481.

Köhler, R., Brokamp, A., Schwarze, R., Reiting, R.H., and Schmidt, F.R. (1998) Characteristics and DNA-sequence of a cryptic haloalkanoic acid dehalogenase from *Agrobacterium tumefaciens* RS5. *Curr Microbiol* 36: 96-101.

Kurihara, T., and Esaki, N. (2008) Bacterial hydrolytic dehalogenases and related enzymes: occurrences, reaction mechanisms, and applications. *Chem Rec* 8: 67-74.

- Kwok, S-Y., Siu, A., Ngai, S-M., Che, C-M., and Tsang, J. (2007) Proteomic analysis of *Burkholderia cepacia* MBA4 in the degradation of monochloroacetate. *Proteomics* 7: 1107-1116.
- La Barre, S., Potin, P., Leblanc, C., and Delage, L. (2010) The halogenated metabolism of brown algae (Phaeophyta), its biological importance and its environmental significance. *Mar Drugs* 8: 988-1010.
- Laternus, F., Fahimi, I., Gryndel, M., Hartmann, A., Heal, M.R., Matucha, M., *et al.* (2005) Natural Formation and Degradation of Chloroacetic Acids and Volatile Organochlorines in Forest Soil. *Environ Sci and Pollut Res.* 12: 233-244.
- Li, J., and Wang, N. (2011) Genome-wide mutagenesis of *Xanthomonas axonopodis* pv. *citri* reveals novel genetic determinants and regulation mechanisms of biofilm formation. *PLoS One* 6: e21804.
- Liu, J.Q., Kurihara, T., Hasan, A.K., Nardi-Dei, V., Koshikawa, H., Esaki, N., and Soda K. (1994) Purification and characterization of thermostable and nonthermostable 2-haloacid dehalogenases with different stereospecificities from *Pseudomonas* sp. strain YL. *Appl Environ Microbiol* 60: 2389-93.
- Ludewig, H., Molyneux, S., Ferrinho, S., Guo, K., Lynch, R., Gkotsi, D.S., and Goss, R.J. (2020) Halogenases: structures and functions. *Curr Opin Struct Biol* 65: 51-60.
- Martin, M., Barbeyron, T., Martin, R., Portetelle, D., Michel, G., and Vandenbol, M. (2015) The cultivable surface microbiota of the brown alga *Ascophyllum nodosum* is enriched in macroalgal-polysaccharide-degrading bacteria. *Front Microbiol* 6: 1487.
- Matucha, M., Gryndler, M., Forczek, S.T., Uhlirova, H., Fuksova, K., and Schröder, P. (2003) Chloroacetic acids in environmental processes. *Environ Chem Lett* 1: 127-130.
- Mena-Benitez, G., Gandia-Herrero, F., Graham, S., Larson, T., McQueen-Mason, S., French, *et al.* (2008) Engineering a catabolic pathway in plants for the degradation of 1,2-dichloroethane. *Plant Physiol* 147: 1192-1198.
- Mena-Benitez, G., Gandia-Herrero, F., Graham, S., Larson, T., McQueen-Mason, S., French, C., Rylott, E., and Bruce, N. (2008) Engineering a catabolic pathway in plants for the degradation of 1,2-dichloroethane. *Plant Physiol* 147: 1192-1198.
- Nardi-Dei, V., Kurihara, T., Okamura, T., Liu, J-Q., Koshikawa, H., Ozaki, H., *et al.* (1994) Comparative studies of genes encoding thermostable L-2-haloacid dehalogenase from

Pseudomonas sp. strain YL, other dehalogenases, and two related hypothetical proteins from *Escherichia coli*. Appl Environ Microbiol 60: 3375-3380.

Nedashkovskaya, O.I., Suzuki, M., Vancanneyt, M., Cleenwerck, I., Lysenko, A.M., Mikhailov, V.V., and Swings, J. (2004a) *Zobellia amurskyensis* sp. nov., *Zobellia laminariae* sp. nov. and *Zobellia russellii* sp. nov., novel marine bacteria of the family *Flavobacteriaceae*. Int J Syst Evol Microbiol 54: 1643-1648.

Novak, H.R., Sayer, C., Isupov, M.N., Paszkiewicz, K., Gotz, D., Spragg, A.M., and Littlechild, J.A. (2013a) Marine *Rhodobacteraceae* L -haloacid dehalogenase contains a novel His / Glu dyad that could activate the catalytic water. FEBS J 280: 1664–1680.

Novak, H.R., Sayer, C., Panning, J., and Littlechild, J.A. (2013b) Characterisation of an L-haloacid dehalogenase from the marine psychrophile *Psychromonas ingrahamii* with potential industrial application. Mar Biotechnol 15:695-705.

Ridder, I.S., Rozeboom, H.J., Kalk, K.H., Janssen, D.B., and Dijkstra, B.W. (1997) Three-dimensional structure of L-2-haloacid dehalogenase from *Xanthobacter autotrophicus* GJ10 complexed with the substrate-analogue formate. J Biol Chem 272: 33015–33022.

Rye, C.A., Isupov, M.N., Lebedev, A.A. and Littlechild, J.A. (2009) Biochemical and structural studies of a l-haloacid dehalogenase from the thermophilic archaeon *Sulfolobus tokodaii*. Extremophiles 13: 179–190.

Schmidberger, J.W., Wilce, J.A., Tsang, J.S., and Wilce, M.C. (2007) Crystal structures of the substrate free-enzyme, and reaction intermediate of the HAD superfamily member, haloacid dehalogenase DehIVa from *Burkholderia cepacia* MBA4. J Mol Biol 368: 706-17.

Van der Ploeg, J., Van Hall, G., and Janssen, D. (1991) Characterization of the haloacid dehalogenase from *Xanthobacter autotrophicus* GJ10 and sequencing of the *dhlB* gene. J Bacteriol 173: 7925-7933.

Villar, E., Vannier, T., Vernet, C., Lescot, M., Cuenca, M., Alexandre, A., *et al.* (2018) The Ocean Gene Atlas: exploring the biogeography of plankton genes online. Nucleic Acids Res 46: W289-W295.

Wever, R., and Barnett, P. (2017) Vanadium Chloroperoxidases: The Missing Link in the Formation of Chlorinated Compounds and Chloroform in the Terrestrial Environment? Chem Asian J 12: 1997-2007.

Woolard, F.X., Moore, R.E., and Roller, P.P. (1979) Halogenated acetic and acrylic acids from the red alga *Asparagopsis taxiformis*. *Phytochemistry* 18: 617-620.

Yu, M., Faan, Y-W., Chung, W., and Tsang, J. (2007) Isolation and characterization of a novel haloacid permease from *Burkholderia cepacia* MBA4. *Appl Environ Microbiol* 73: 4874-4880.

Zhang, J., Cao, X., Xin, Y., Xue, S., and Zhang, W. (2013) Purification and characterization of a dehalogenase from *Pseudomonas stutzeri* DEH130 isolated from the marine sponge *Hymeniacidon perlevis*. *World J Microbiol Biotechnol* 29: 1791-1799.

Zhang, J., Xin, Y., Cao, X., Xue, S., and Zhang, W. (2014) Purification and characterization of 2-haloacid dehalogenase from marine bacterium *Paracoccus* sp. DEH99, isolated from marine sponge *Hymeniacidon perlevis*. *J Ocean Univ China* 13: 91-96.

Zhu, Y., Thomas, F., Larocque, R., Li, N., Duffieux, D., Cladière, L., *et al.* (2017) Genetic analyses unravel the crucial role of a horizontally acquired alginate lyase for brown algal biomass degradation by *Zobellia galactanivorans*. *Environ Microbiol* 19: 2164–2181.

SUPPORTING INFORMATION

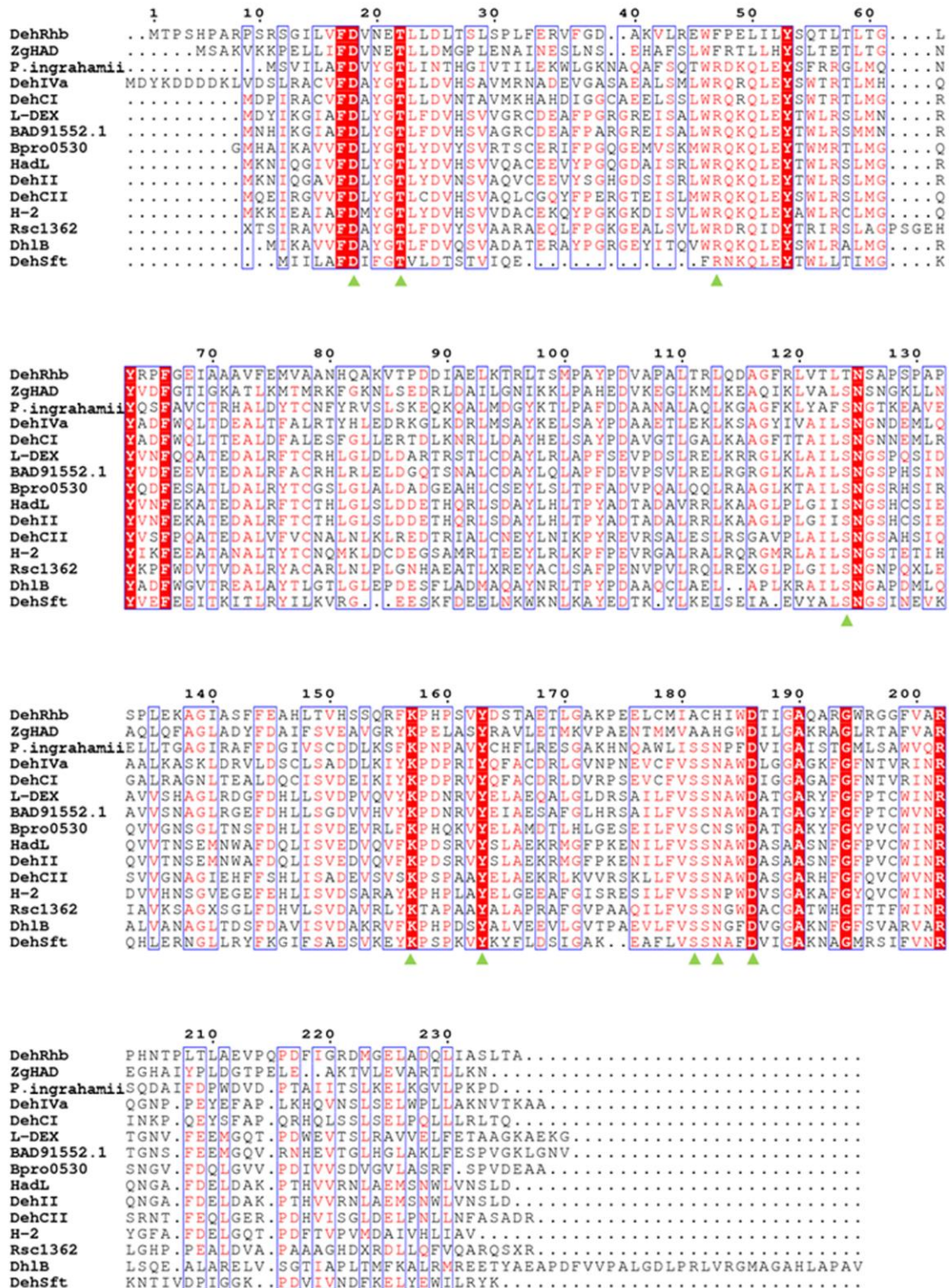


Fig. S1. Amino-acid sequence alignment of ZgHAD and 14 L-2-HAD homologs.

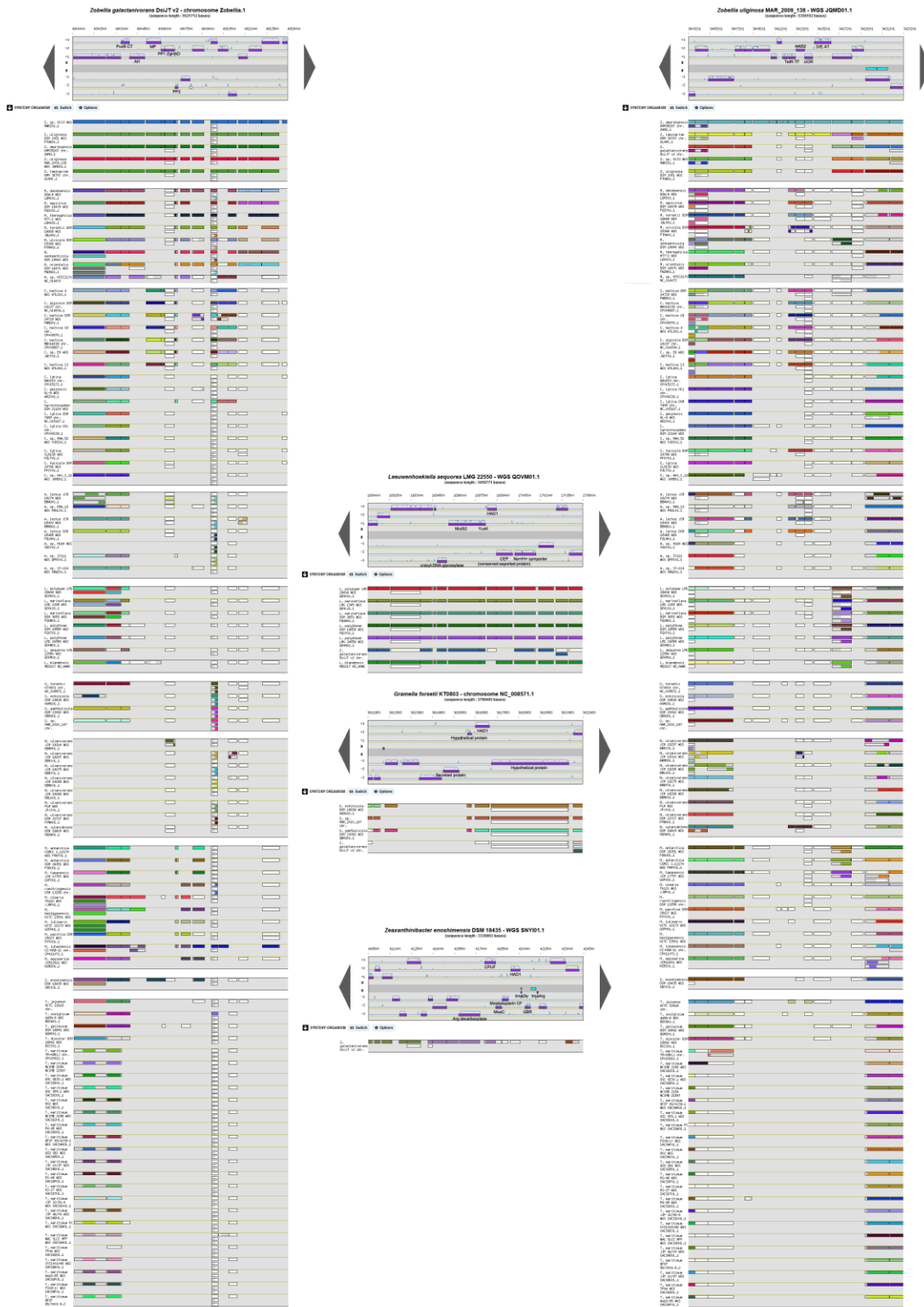


Fig. S2. Detailed analysis of the genetic context for the haloacid dehalogenases HAD1 and HAD2 in *Flavobacteriaceae*. All the screenshots of synteny overlaps were obtained from the MaGe platform.

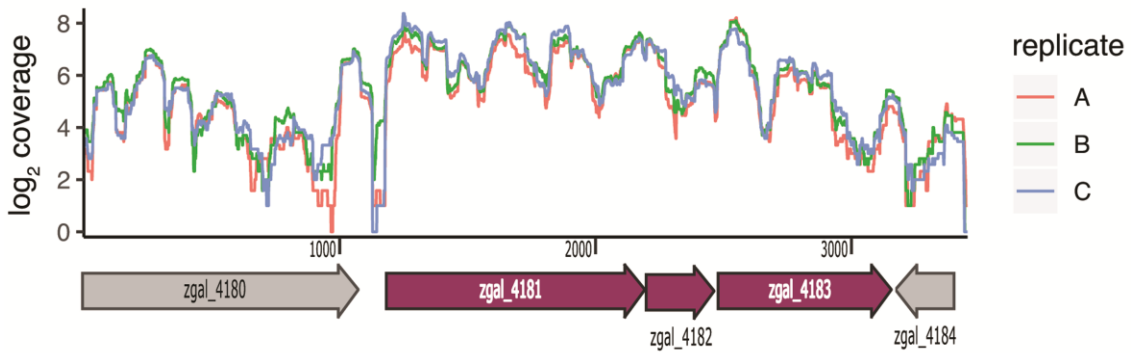


Fig. S3. Genomic map and transcript coverage of the region encoding ZgHAD in *Z. galactanivorans*. Transcriptomic data was retrieved from a publicly available RNA-seq dataset with GEO accession number: GSE101142 (Ficko-Blean *et al.*, 2017). Triplicate cultures of *Z. galactanivorans* were grown in minimum medium with galactose as the sole carbon source and harvested in the exponential phase. The base-per-base transcript coverage is shown on a log scale.

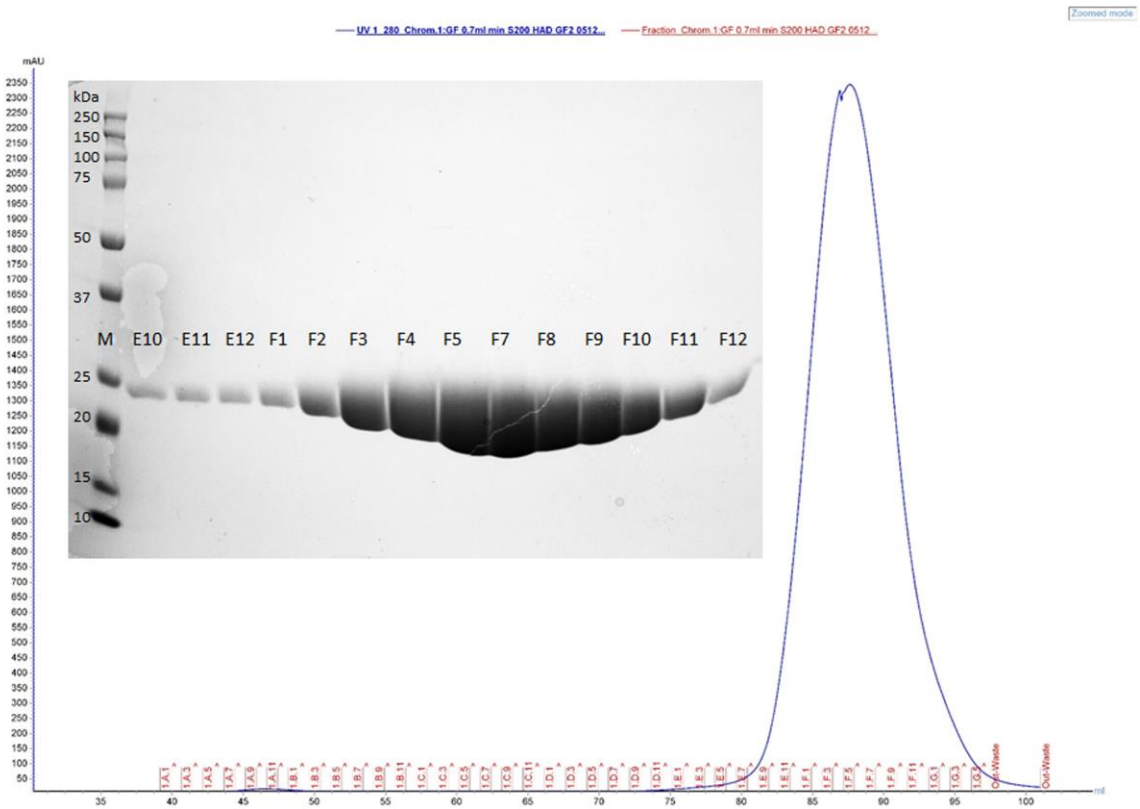


Fig. S4. Chromatogram and SDS-PAGE analyses of ZgHAD purification by size exclusion chromatography. The polyacrylamide gel was stained with Coomassie Brilliant Blue R-250, revealing the presence of the recombinant protein in eluted fractions of the A280 peak (lanes E10 to F12). M = marker Precision Plus Protein™ Standards (Bio-Rad Laboratories) and the molecular masses are indicated on the left of the lane.

Table S1. Dataset of biochemically and/or structurally characterized L-2-HAD enzymes.

Enzyme	Organism	Phylum	Origin	Main reference	Accession	Conserved domain	MAFFT ALIGNMENT	
							% identity aa	% similarity aa
ZgHAD	<i>Zobellia galatinarivorus</i>	Bacteroidetes	surface of marine red alga, Roscoff, FRA	This paper	WP_013995506	TIGR01428	100	100
DehRhb	Marine Rhodobacteraceae	Alphaproteobacteria	marine polychaeta worm on the beach, Argyl, UK	Novak <i>et al.</i> , 2013a	AFX88327.1	TIGR01428	31	50
DehSt	<i>Sulfurisphaera tokodaii</i> (formerly <i>Sulfilobus tokodaii</i>)	Archaea (Crenarchaeota)	hot spring	Rye <i>et al.</i> , 2009	WP_010980655.1	TIGR01428	28	47
DehVa	<i>Burkholderia cepacia</i> MBA4	Betaproteobacteria	soil	Murdiatno <i>et al.</i> , 1992	Q51645.3	TIGR01428	25	43
L-DEX VL	<i>Pseudomonas</i> sp. strain VL	Gammaproteobacteria	soil	Nardi-Dei <i>et al.</i> , 1994	AA832245.1	TIGR01428	23	45
DhbB	<i>Xanthobacter autotrophicus</i> GJ10	Alphaproteobacteria	soil	Ridder <i>et al.</i> , 1997	AAA27590.1	TIGR01428	23	39
HadI	<i>Pseudomonas putida</i> AJ1	Gammaproteobacteria	soil exposed to 2-MCPA, Billingham, UK	Barth <i>et al.</i> , 1992	AAA25832.1	TIGR01428	23	44
DehH109	<i>Pseudomonas putida</i> 109	Gammaproteobacteria	soil	Kawasaki <i>et al.</i> , 1994	BAAD4474.1	CD02588	24	43
DehI	<i>Pseudomonas putida</i> PP3	Gammaproteobacteria	soil microbial community growing on the herbicide Dalapon	Hill <i>et al.</i> , 1999	Q97323	TIGR01428	23	43
DehCI	<i>Pseudomonas</i> sp. CBS3	Gammaproteobacteria	soil	Schneider <i>et al.</i> , 1991	AAA63640.1	TIGR01428	25	40
DehCII	<i>Pseudomonas</i> sp. CBS3	Gammaproteobacteria	soil	Schneider <i>et al.</i> , 1991	AAA25833.1	TIGR01428	21	40
H-2	<i>Moraxella</i> sp. strain B	Gammaproteobacteria	soil	Kawasaki <i>et al.</i> , 1992	BAA14413.1	TIGR01428	22	44
Bpr00530	<i>Polaromonas</i> sp. JS666	Betaproteobacteria	from a granular activated-carbon filter treating chloroethane-contaminated groundwater	Chan <i>et al.</i> , 2010	3UM9A	TIGR01428	22	40
RscI362	<i>Ralstonia solanacearum</i> GMI1000	Betaproteobacteria	from tomato in French Guyana, pathogen	Chan <i>et al.</i> , 2010	3UM8A	TIGR01428	23	39
Rha0230	<i>Rhodococcus jostii</i> RHA1	Actinobacteria	soil, potent polychlorinated biphenyl-degrading	Chan <i>et al.</i> , 2010	3UMGA	TIGR01428	19	34
DehDEH99	<i>Paracoccus</i> sp. DEH99	Alphaproteobacteria	marine sponge Hymeniacidon perlewis	Huang <i>et al.</i> , 2011	ACS54860.1	CL31108	17	29
BA091552.1	<i>Burkholderia</i> sp. WS	Betaproteobacteria	soil	Kurata <i>et al.</i> , 2005	BA091552.1	TIGR01428	22	42
DhISSI	<i>Agrobacterium tumefaciens</i> RSS	Alphaproteobacteria	dichloropropionate-contaminated soil	Köhler <i>et al.</i> , 1998	P60527.1	CD02388	23	44
No name (DehPsi)	<i>Psychromonas ingrahamii</i>	Gammaproteobacteria	marine (psychrophilic)	Novak <i>et al.</i> , 2013b	WP_01177159.1	TIGR01428	27	44
L-2-DhbB	<i>Anchlobacter aquaticus</i> UV5	Alphaproteobacteria	contaminated site in South Africa	Kumar <i>et al.</i> , 2015	WP_126279759.1	CD07526	17	30
Dehalogenase II	<i>Pseudomonas stutzeri</i> DEH130	Gammaproteobacteria	marine sponge Hymeniacidon perlewis	Zhang <i>et al.</i> , 2013	several accessions, unclear	nd	nd	nd

Marine enzymes are shown in light blue

Chapter 1

Accession	Organism	Environment	Location	Country
hahadcf:dehIVa-like type II (C. albifrons parvulus) WP_08722046.1	GROUP A	terrestrial	soil	Japan
hahadcf:dehIVa-like type II (B. thalassius) sp. (hah77) WP_09839113.1	GROUP A	terrestrial	soil of Arabidopsis thaliana	Netherlands (Nunck)
DehIVA (Burkholderia cepacia M8A4-G1545_3)	GROUP A	terrestrial	forest soil	Taiwan
hahadcf:dehIVa-like type II (Paraburkholderia sp.) WP_08468187.1	GROUP A	terrestrial	acidic forest soil	Japan (Baraki, Tsukuba)
hahadcf:dehIVa-like type II (Paraburkholderia sp. 8466-G176) WP_118121245-1	GROUP A	terrestrial	soil	Indonesia
hahadcf:dehIVa-like type II (Paraburkholderia sp. SC51) WP_071315148-1	GROUP A	terrestrial	tomato rhizosphere	Australia (Brisbane)
hahadcf:dehIVa-like type II (Paraburkholderia sp.) WP_081208891-1	GROUP A	terrestrial	acidic forest soil	Japan (Baraki, Tsukuba)
hahadcf:dehIVa-like type II (Biodiversity Institute bacterium 1951) 000141 WP_118652119-1	GROUP A	terrestrial	leaves	China
hahadcf:dehIVa-like type II (T. apiculatus geminus) WP_13204643-1	GROUP A	aquatic	runoff of a hot spring	Portugal (Azores Island)
hahadcf:dehIVa-like type II (M. luteus) WP_05191171-1	GROUP A	phage/capsid	Marine macroalgae Laminaria saccharina	Guernsey (Belle Isle)
hahadcf:dehIVa-like type II (Desulfobacterium autotrophicum) WP_019001209-1	GROUP A	marine	marine mud	Bahia, Venice
hahadcf:dehIVa-like type II (Desulfobacterium autotrophicum) WP_142994180-1	GROUP A	marine	soil	China (Nanning)
hahadcf:dehIVa-like type II (Pseudomonas putida A1) AAA21832_1	GROUP A	terrestrial	soil exposed to 2,4-DCA	UK
hahadcf:dehIVa-like type II (Pseudomonas chloritiformans) WP_021446682-1	GROUP A	environmental	ureaH reactor	Netherlands (Wageningen)
hahadcf:dehIVa-like type II (Paraburkholderia sp. Merced) WP_012078762-1	GROUP A	aquatic	ultra-pure water used in hemodialysis units	USA
hahadcf:dehIVa-like type II (Hermisporium sp. K9W02) WP_124171311-1	GROUP A	aquatic	Dugesiya japonica (plantarum)	Japan
hahadcf:dehIVa-like type II (Hermisporium sp. 0018) WP_013870039-1	GROUP A	environmental	industrial water waste treatment plant contaminated with arsenic	Germany
hahadcf:dehIVa-like type II (Mantella eximiosa) WP_099292551-1	GROUP A	aquatic	ice core from glacier	China (Sizhuang Province, Muozhuang glacier)
hahadcf:dehIVa-like type II (Mantella vietnamensis) WP_099800444-1	GROUP A	aquatic	Tamshui glacier	China (Sizhuang Province)
hahadcf:dehIVa-like type II (Mantella sp. S02) WP_12607285-1	GROUP A	terrestrial	soil	China (Hubei)
hahadcf:dehIVa-like type II (Mantella guoyinghai) WP_299914827-1	GROUP A	aquatic	ice core from glacier	China (Sizhuang Province, Muozhuang glacier)
1-2-CHB (Acetivibrio aquaticus) 1951 WP_131818462-1	L-2-CHB	aquatic	lake	Germany
1-2-CHB (Acetivibrio aquaticus) 1951 WP_131818462-1	L-2-CHB	terrestrial	roots of Spartina anglica	China (Jiangsu Province)
1-2-CHB (Acetivibrio aquaticus) 1951 WP_131818462-1	L-2-CHB	aquatic	Lake Washington	USA
1-2-CHB (Acetivibrio aquaticus) 1951 WP_131818462-1	L-2-CHB	aquatic	Lake Taihu	China
1-2-CHB (Acetivibrio aquaticus) 1951 WP_131818462-1	L-2-CHB	terrestrial	Phragmites of a salt meadow greater plantain	Germany (Mainberg, Hessen)
1-2-CHB (Acetivibrio aquaticus) 1951 WP_131818462-1	L-2-CHB	environmental	Strangford Lough	Ireland (Monroe)
1-2-CHB (Acetivibrio aquaticus) 1951 WP_131818462-1	L-2-CHB	environmental	Florida	USA
1-2-CHB (Acetivibrio aquaticus) 1951 WP_131818462-1	L-2-CHB	aquatic	Lake Taihu	China
1-2-CHB (Acetivibrio aquaticus) 1951 WP_131818462-1	L-2-CHB	terrestrial	soil	China
1-2-CHB (Acetivibrio aquaticus) 1951 WP_131818462-1	L-2-CHB	aquatic	water	Taiwan
beta-phage-like (Zobellia galapagensis) CAZ95206-1	BetaPAGM	marine/macroalgae	red alga	France (Rocqufort)
beta-phage-like (Zobellia galapagensis) CAZ95206-1	BetaPAGM	marine/macroalgae	red alga	France (Rocqufort)
beta-phage-like (Zobellia galapagensis) CAZ95206-1	BetaPAGM	marine/coastal	Saccharina japonica	Russia (Vladivostok, Troitsa Bay)
beta-phage-like (Zobellia galapagensis) CAZ95206-1	BetaPAGM	marine/macroalgae	red alga	France (Rocqufort)
beta-phage-like (Zobellia galapagensis) CAZ95206-1	BetaPAGM	marine	seawater	Russia (Vladivostok, Amursky Bay)
beta-phage-like (Zobellia galapagensis) CAZ95206-1	BetaPAGM	marine/coastal	Yellow Sea	China
beta-phage-like (Zobellia galapagensis) CAZ95206-1	BetaPAGM	marine	microbial mat culture pond	China
beta-phage-like (Zobellia galapagensis) CAZ95206-1	BetaPAGM	marine/coastal	tidal flat sediment of the Yellow Sea	South Korea
beta-phage-like (Zobellia galapagensis) CAZ95206-1	BetaPAGM	marine	North Sea	Netherlands
beta-phage-like (Zobellia galapagensis) CAZ95206-1	BetaPAGM	terrestrial	rusty iron plate	South Korea (Taejeon)

Table S3. Identification of the representative L-2-HAD sequences by BlastP searches in the IMG/MER database.

Datasets	Ecosystems	Hit number 1E-50	
		DehIVa-like (group A)	ZgHAD-like (group B)
Terrestrial environments	Forest soil	560	15
	Agricultural land	60	0
	Grasslands	296	9
	Permafrost	48	4
	Peat	231	7
Terrestrial host-associated	Insecta associated	3	5
	Human associated	0	0
	Mammals associated	1	0
	Birds associated	0	0
	Plant associated	294	17
	River	33	1
Non-marine aquatic	Lake	73	1
	Groundwater	12	0
	Non-marine saline and alkaline	38	39
	Hot springs	22	2
	Oceanic	292	32
Marine environments	Coastal	554	51
	Intertidal zone	764	24
	Pelagic	45	29
	Hydrothermal vents	113	24
Marine host-associated	Macroalgae associated	223	76
	Microalgae/Plankton/unclassified associated	7	5
	Annelida associated	76	17
	Cnidaria/Tunicates/Sponges associated	54	3
	Mollusca associated	1	4
Overall		3800	365

Chapter 1

Table S4. Identification of the representative L-2-HAD sequences by BlastP searches in the OGA database.

Enzyme	AA sequence	9 aa signature	Conserved domain	Group	*Hit number 1E-30
ZgHAD	MSAKVKPELLIFDVNETLLDMGLENAINESLNSEHAFSLWFRLLHYSLETTLTGNVYDFGTIGKATLKMTRKFKGNLSEDRDLDAILGNIKKLPAHEDVKEGLKMLKEAQIKLVALSNSNGKLLNAQLQFAGLADYFDALFVSEAVGRYKPELASYRAVLETMKVPAENTMMVAAHGWDILGAKRAGLRTAFVAREGHAIYPLDGTPELEAKTVLEVARTLLKN	DTFSKYAHD	TIGR01428	B	224
WP_038235908 (HAD2 phylogenetic clade)	MKKNRRDFIKKTAALSLAGATIPQFGMAANELIKEANMSLEVRPKVLPFDVNETLLDLTAMKESVGAIGLNRDLDLPLWFTTMLQYSLVTTVGRQVNDFGIIGAAALQMVASNNGIKLTKETQRTREAILGPIRSLPTHDPVKPALQQLKADGYKLVSTFNSNKGVETQFTNAGLLDYFPEERLSIEDMGKFKPDADAYAWAARKMGIQPNCEMLVAAGWDIAGAVWANWRGAFVSRPSAQLYPLAPNPEINEPNLKPITAKHLISLK	DTFTKYAHD	TIGR01428	B	234
DehRhb	MTPSHPARPSRSGILVFDVNETLLDLTSLSPLEFVFDGAKVLEWRFPELILYSQTLTLTGLYRPFGEIAAAVFMVAANHQAKVTPDDIAELKRLTSMFATPDVAPALTRLQDAGPRLVITLNSAPSPAPSPLEKAGIASFPEAHLTVHSQRFPKHPVSYDSTABETLGAKEPEELCMIACHIWDITIGAQAQRGWRGGFVARPHNTPLTLAEVPPQDFPIGRDMGELADQLIASLTA	DTFTKYAHD	TIGR01428	B	204
DehSft	MIILAFDIFGTVLDTSTVIQEFRNKQLEYTWLLTIMGKYVEFEEITKILTRYILKVRGEESEKDFEELNKNKLNKAYEDTKYLKEISEIAEVYALSNGSINEVQKHLERNGLLRYFKGIFSAESVKEYKPSPKVYKYLDSI GAKEAFVSSNAFDVIGAKNAGMRSIFVNRKNTIVDPDIGKPDVIVNDFKELYEWILRYK	DTRSKYSND	TIGR01428	A	5
DehIva	MDYKDDDDKLVDSLRACVFDAYGTLDDVHSAVMRNAMEVGSABEALSMLWRQRQLEYSWTRTLMHQYADFQWLTDEALTALRTYHLEDRKGLKDRMSAYKELSAYPDAAEATLEKLLKSAGYIVAILNSNGNDEMQLQALKASKLDRVLDSCLSADDLKIYKPDPIYQFACDRLGVNPNVCFVSSNAWDLGGAGKGFNTVIRINRQGNPEYEFAPLKHQVNSLSELWPLLAKNVTKAA	DTRSKYSND	TIGR01428	A	1476
L-DEX YL	MDYIKGIAFDLYGTLFDVHVVGRCD EAFPGRGREISALWRQKQLEYTWLRSMLMNRVYVNFQQATEDALRFTCRHLGLDLDARTRSTLCDAYLRLAPFSEVPDLSRELKRRGLKLAIALNSGSPQSIDAVVSHAGLRDGFHLLSVDPVQVYKPNRVSLSAEKQALGLDRSAILFVSSNAWDTGARYFGFPTCWINRTGNVFEEMGQTPDWEVTSRAVVELFETAAGKAEG	DTRSKYSND	TIGR01428	A	1498
DhIB	MIKAVVFDAYGTLFDVQSVADATERAYPGRGEYITQVWRQKQLEYSWLRALMGRYADFWGVTREALAYTLGTLGLEPDESFLADMAQYNRTPYPDAQAQCLAEALAPLKRAILSNGAPDMLQALVANAGLTDSDAVISVDAKRVFKPHPDSYALVEEVLGVTPAEVLVSSNGFDVGGAKNFGFSVARVARLSQEALARELVSGTIAPLTMFKALRMREETAAEAPDFVVPALGDLPRLVGMAGHLAPAV	DTRSKYSND	TIGR01428	A	935
HadL	MKNIQGI VFDLYGTLVDVHVVQACEEYVPGQDAISRLWRQKQLEYTWLRSMLMGRYVNF EKATEDALRFTCTHLGLSDDETHQRLSDAYLHLTPYADTADAVRRLKAAGLPLGIISNGSHCSIEQVVTNSEMNWAFDQLISVEDVQVFKPDSRVYSLAEKRMGFPKENILFVSSNAWASAANSFGFPVCWINRQNGAFDELDAKPTHVVRNLAEMSNWLVNSLD	DTRSKYSND	TIGR01428	A	1378
DehH109	MQPIEGIVFDLYGTLVDVHVVQACESAYPGQGEAISRLWRQKQLEYTWLSSLMGRYASFEQRTEEARLYTCKHGLATDETTLRQLGQAYLHLAPHDPTTAALRRLKASGLPMAIASNGSHHSIEQVVSVDGWFADHLISVETVVKFKNRVSLSAEQTMATIPDRLLFVSSNSWDATGARHFGFPVCWVNRQGA VDFELGATPTREVRDLGEMSDWLLD	DTRSKYSND	CD02588	A	1207
DehII	MKNIQGA VFDLYGTLVDVNSVAQVCEEVYSGHGD SISRWRQKQLEYTWLRSMLMGRYVNF EKATEDALRFTCTHLGLSDDETHQRLSDAYLHLTPYADTADALRRLKAAGLPLGIISNGSHCSIEQVVTNSEMNWAFDQLISVEDVQVFKPDSRVYSLAEKRMGFPKENILFVSSNAWASAANSFGFPVCWINRQNGAFDELDAKPTHVVRNLAEMSNWLVNSLD	DTRSKYSND	TIGR01428	A	1395
DehCI	MDPIRACVFDAYGTLVDVNTAVMKHAHDIGGCAEELSSLRQKQLEYSWTRTLMGRYADF WQLTTEALDPALESFGLLERTDLKNRLDAYHLESAYPDVAVTGLGALKAAAGFTTALISNGNNEMLRAGLRAGNLTEALDQCSVDEIKIYKPDPRVYQFACDRLDVRPSEVCFVSSNAWIGGAGAFGNTVIRINRINKPQEYSPAPQRHQLSSLSLPLQLLLRLTQ	DTRSKYSND	TIGR01428	A	1499
DehCII	MQEIRGVVFDLYGTLCDVHVSVAQLCGQYFPERGTEISLMWRQKQLEYSWLRSLMGQYVSFPQATEDALVFCNALNKLKREDTRIALCNEYLNIPKYREVRSALESLSRGAVPLAILNSGSAHSIQSVGNAGIEHFFSHLISADEVSVSKPSAPAYELAEKRLKVVRSKLLFVSSNAWASGARHFGFQVCWVNRSRNTFEQLGERPDHVISGLDELPLNLLNFASADR	DTRSKYSND	TIGR01428	A	1211
H-2	MKKIEAIAFDMYGTLVDVHVVVDACEKQYPGKGD ISVLWRQKQLEYAWLRCLMGQYIKFEEATANALTYTCNQMKLDCDEGSAMRLTEEYLRKFPPEVVRGALRALRQGMRLAILNSGSTETIHDVVHNSGVGEFEHLISVDSARAYKPHPLAYELGEEAFGISRESILFVSSNPWDVSGAKAFGYQVCWINRYGFAFDELGQTPDFTVPMDAIVHLIAV	DTRSKYSND	TIGR01428	A	1150
Bpro0530	GMHAIKAVVFDLYGTLVDVSVRTSCERIFPGQGMVSKMWRQKQLEYTWMTLMGQYQDFESATLDALRYTCGSLGLADADAGEAHLCEYLSLTPFADVPQALQQLRAAGLKTAILNSGSRHSIRQVVGNSGLTNSFDHLISVDEVRLFKPHQKVEYELAMDTLHGESEILFVSCNSWDATGAKYFGYPVCWINRNSGVFDLQGVVDPDIVSDVGVLASRFSVPDEAA	DTRSKYSND	TIGR01428	A	1313
Rsc1362	XTSIRAVVFDAYGTLFDVYSVAARAEQLFPGKGEALSVLWRDRQIDYTRIRSLAGPSGEHYKFPFDVTVDALRYACARLNLPLGNHAEATLXREYACLSAFPENVPVLRQLREXGLPLGILSNGNPQXLEIAVKSAGXSLFDHVLSDAVRLYKTAPAAALAPRAFVPAQILFVSSNGWDACGATWHGFTTFWINRGLHGPPEALDVAAPAAAGHDXRDLQLQFVQARQSR	DTRSKYSND	TIGR01428	A	855
Rha0230	MAGVFRSPSTGRNVRAVLFDTFGTVVDWRTGIATAVADYAAHQLEVDVAFAADRWRAR YQPSMDAILSGAREFVTLDI LHRENLDVFLRESGIDPTNHDSGELDELARAWHVLTPWPDVSPGLTAIKAEYIIGPLSNGNTSLLLDMAKNAGIPWDVIGSDINRKYKPDQAYLRTAQVLGLHPGVMLEAAAHNGDLEAAHATGLATAFILRPVEHGHQTDLDLAPTGSWDISATDITDLAAQLRAGSTGFR	DTRSKYSHD	TIGR01428	A	625

Chapter 1

DehDEH99 (partial sequence)	WRQQQLEYSWLRRAITGDHADFWQVTS DALDWA AERHGASREQATRLLDLYRRLPAYPEIP AMLDRLRAAGGATAIFSNGLMLADATQSAGLSDRDLALLSVETAGRFKPSDEGYRIVT DHFGCEAAQITPVSSNTC	--RSKYSN-	CL31108	A	214
BAD91552.1	MNHIKGIAPFDLYGTLFDVHVSVAGRCDEAFPARGREISALWRQKQLEYTWLRSMMNRYVDF EEVTE DALRFACRHLRLELDGQTSNALCDAYLQLAPFDEVPSVLRRLRGRGLKLA ILSNG SPHSINAVVSNAGLRGEFDHLLSGDVVHVYKPNRVYIEAESAFGLHRSAILFVSSNAWD ATGAGYFGFPPTCWNRTGNSFEEMGQVRNHEVTGLHGLAKLFESVVGKLGTV	DTRSKYSND	TIGR01428	A	1442
DhISSI	MKHIKAIAPFDLYGTLFDVHVSVIDQCEKRFPGRGREVSTLWRQKQLEYTWLRSMMNRYVTF EQATEDALRYTCRHLGPFALDDAACTVLC DAYLRLQAPPEVPPRLRELRNRGLQAVLSNG SPHSIGAVVGNAGIRDEFDHLLSVDVVRVYKPHDRAYGLAEEAFGLARTSILFVSSNGWD ATGARYFGFPPTCWINRGGNVFEEMGQTPDWDLGIDEIVRLPDSAEGSAPSV	DTRSKYSND	CD02588	A	1332
DehPsi	MSVILAFDVYGTILNTHGIVTILEKWLGNKAQAFSQTWRDKQLEYSFRRLGMQNYQSFV CTRHALDYTCNPFYRVLSLSEKQKQALMDGYKTLPAFDDAANALQKAGFKLYAFSNGTK EAVEELLTGAGIRAFFDGI VSCDDLKSFKNPAVYCHFLRESGAKHNQAWLISSNPFVDI GAISTGMLSAWVRSQDAIFDPWDVDTAIIITSLKELKGVLPKPD	DTRSKYSND	TIGR01428	A	166
L-2-DhIB	MRPGLFIFDCDGVLI DSEMLAARALIDELACHGVAVDMDFVARHF IGRAHTVIRTEVTAR FGRELPA SFEDDYSRLLAGFEAGLAPMEGAREALALTVPFCLATSSPPRLAASLRIV GLAELFAGRAFTASQVARGKPADLFLYAAAQMGADPAACVVVEDSAGIAAGLAGMEV WHFVGGAHFAGMDMPLPADVSPHRRFAGFSEIRAAMP TLFHAPPDIADPT	DVVTKFESG	CD07526	Outgroup	283

*prokaryotic OM-RGC_v2_metaG

Marine enzymes are shown in light blue

Chapter 1

Table S5. List of bacterial strains, plasmids and genomes used in this study.

Bacterial strain name	Description	References
<i>Zobellia galactanivorans</i> Dsjj ^T	Wild type	Barbeyron <i>et al.</i> , 2001
<i>Zobellia galactanivorans</i> ΔHAD	Zghad deletion in strain DsjjT	this study
<i>Tenacibaculum gallaicum</i> DSM 18841	Wild type	Pineiro-Vidal <i>et al.</i> , 2008
<i>Tenacibaculum discolor</i> DSM 18842	Wild type	Pineiro-Vidal <i>et al.</i> , 2008
<i>Escherichia coli</i> DH5α	Strain used for general cloning	Chen <i>et al.</i> , 2018
<i>Escherichia coli</i> BL21(DE3)	strain used for overexpression	Jeong <i>et al.</i> , 2009
<i>Escherichia coli</i> S17-1 λ pir	strain used for conjugation	De Lorenzo and Timmis, 1994
Plasmid name		References
pFO4	AmpR, T7lac promoter, His.Tag	Groisillier <i>et al.</i> , 2010
pYT313	Suicide vector carrying sacB; sacB with F. johnsoniae ompA promoter amplified with primers 1769 and 1770 from pMS75 and cloned into EcoRI site of pLYL03; Apr (Emr)	Zhu <i>et al.</i> , 2017
pEG1	2.2 kbp region upstream of <i>Z. galactanivorans</i> ZgHAD amplified with primers OEG007 and OEG009 and cloned into XbaI and Sall sites of pYT313; Apr (Emr)	this study
pEG3	Construct used to delete <i>Z. galactanivorans</i> ZgHAD; 2.3 kbp region downstream of ZgHAD amplified with primers OEG008 and OEG010 and cloned into BamHI and XbaI sites of pEG1; Apr (Emr)	this study
Bacterial genomes	NCBI Genome ID	References
<i>Zobellia galactanivorans</i> Dsjj ^T	1396	Barbeyron <i>et al.</i> , 2001
<i>Zobellia</i> sp. OII3	56876	Harms <i>et al.</i> , 2017
<i>Zobellia amurskyensis</i> KMM3526T	85943	Nedashkovskaya <i>et al.</i> , 2004a
<i>Zobellia laminariae</i> KMM3676T	85944	Nedashkovskaya <i>et al.</i> , 2004a
<i>Zobellia uliginosa</i> DSM 2061	33171	Barbeyron <i>et al.</i> , 2001
<i>Zobellia amurskyensis</i> MAR_2009_138	33171	Barbeyron <i>et al.</i> , 2001
<i>Maribacter thermophilus</i> HT7-2	38427	Hu <i>et al.</i> , 2015
<i>Maribacter dokdonensis</i> DSW-8	16889	Kwak <i>et al.</i> , 2005
<i>Maribacter orientalis</i> DSM 16471	49845	Nedashkovskaya <i>et al.</i> , 2004b
<i>Maribacter aquavivus</i> DSM 16478	50780	Nedashkovskaya <i>et al.</i> , 2004b
<i>Maribacter sedimenticola</i> DSM 19840	55937	Nedashkovskaya <i>et al.</i> , 2004b
<i>Maribacter forsetii</i> DSM 18668	33159	Barbeyron <i>et al.</i> , 2008
<i>Maribacter ulvicola</i> 15366	52440	Nedashkovskaya <i>et al.</i> , 2004b
<i>Maribacter</i> sp. HTCC2170	13656	Oh <i>et al.</i> , 2011
<i>Cellulophaga algicola</i> DSM 14237	2470	Abt <i>et al.</i> , 2011
<i>Cellulophaga baltica</i> NNO16038	18310	Johansen <i>et al.</i> , 1999
<i>Cellulophaga lytica</i> HI1	3018	Asahina and Hadfield, 2014
<i>Cellulophaga lytica</i> DSM 7489	3018	Pati <i>et al.</i> , 2011
<i>Cellulophaga geojensis</i> KL-A	17619	Shan <i>et al.</i> , 2014
<i>Cellulophaga</i> sp. E6	34157	Lafleur <i>et al.</i> , 2015
<i>Cellulophaga baltica</i> 18	18310	Johansen <i>et al.</i> , 1999
<i>Cellulophaga baltica</i> 13	18310	Johansen <i>et al.</i> , 1999
<i>Cellulophaga lytica</i> DAU203	3018	Lee and Choi, 2017
<i>Cellulophaga fucicola</i> DSM 24786	50534	Johansen <i>et al.</i> , 1999
<i>Cellulophaga baltica</i> 4	18310	Johansen <i>et al.</i> , 1999
<i>Cellulophaga</i> sp. Hel_1_12	34157	Lafleur <i>et al.</i> , 2015
<i>Cellulophaga baltica</i> DSM 24729	18310	Johansen <i>et al.</i> , 1999
<i>Cellulophaga lytica</i> Cl8139	3018	Chapelais-Baron <i>et al.</i> , 2017
<i>Cellulophaga tyrosinoydans</i> DSM 21164	54056	Kahng <i>et al.</i> , 2009
<i>Cellulophaga</i> sp. RHA_52	34157	Lafleur <i>et al.</i> , 2015
<i>Algibacter lectus</i> JCM 19300	34172	Takatani <i>et al.</i> , 2014
<i>Algibacter lectus</i> JCM 19274	34172	Takatani <i>et al.</i> , 2014
<i>Algibacter lectus</i> DSM 15365	34172	Nedashkovskaya <i>et al.</i> , 2004c
<i>Algibacter</i> sp. RHA_19	40511	unpublished
<i>Algibacter</i> sp. XY-114	40511	unpublished
<i>Algibacter</i> sp. H164	40511	unpublished
<i>Leeuwenhoekia marinoflava</i> DSM 3653	50747	Nedashkovskaya <i>et al.</i> , 2005; Nedashkovskaya <i>et al.</i> , 2014
<i>Leeuwenhoekia palythoae</i> DSM 19859	50714	Nedashkovskaya <i>et al.</i> , 2009
<i>Leeuwenhoekia marinoflava</i> LMG 1345	50747	Nedashkovskaya <i>et al.</i> , 2005; Nedashkovskaya <i>et al.</i> , 2014
<i>Leeuwenhoekia palythoae</i> LMG 24856	50714	Nedashkovskaya <i>et al.</i> , 2009
<i>Leeuwenhoekia polynya</i> LMG 29608	75305	Si <i>et al.</i> , 2015
<i>Leeuwenhoekia aequorea</i> LMG 22550	75306	Nedashkovskaya <i>et al.</i> , 2014
<i>Leeuwenhoekia blandensis</i> MED217	1298	Pinhassi <i>et al.</i> , 2006
<i>Gramella forsetii</i> KT0803	715	Bauer <i>et al.</i> , 2006
<i>Gramella</i> sp. MAR_2010_147	15109	Tully <i>et al.</i> , 2018
<i>Gramella echinicola</i> DSM 19838	16158	Panschin <i>et al.</i> , 2016
<i>Gramella gaetbulicola</i> DSM 23082	68883	Panschin I <i>et al.</i> , 2017
<i>Nonlabens ulvanivorans</i> JCM 19275	32542	Kopel <i>et al.</i> , 2014; Nakanishi <i>et al.</i> , 2014
<i>Nonlabens ulvanivorans</i> JCM 19296	32542	Kopel <i>et al.</i> , 2014; Nakanishi <i>et al.</i> , 2014
<i>Nonlabens ulvanivorans</i> JCM 19297	32542	Kopel <i>et al.</i> , 2014; Nakanishi <i>et al.</i> , 2014
<i>Nonlabens ulvanivorans</i> JCM 19298	32542	Kopel <i>et al.</i> , 2014; Nakanishi <i>et al.</i> , 2014
<i>Nonlabens ulvanivorans</i> JCM 19314	32542	Kopel <i>et al.</i> , 2014; Nakanishi <i>et al.</i> , 2014
<i>Nonlabens ulvanivorans</i> PLR	32542	Kopel <i>et al.</i> , 2014; Nakanishi <i>et al.</i> , 2014
<i>Nonlabens xylanidelens</i> DSM 16809	67204	Yi and Chun, 2012
<i>Muricauda ruestringensis</i> DSM 13258	3119	Huntemann <i>et al.</i> , 2012
<i>Muricauda lutaonensis</i> CC-HSB-11	36724	Arun <i>et al.</i> , 2009
<i>Muricauda antarctica</i> CGMCC1.12174	49929	Wu <i>et al.</i> , 2013

Chapter 1

<i>Muricauda pacifica</i> DSM 25027	67499	Zhang <i>et al.</i> , 2015
<i>Muricauda lutimaris</i> KCTC 22173	72559	Yoon <i>et al.</i> , 2008
<i>Muricauda taenensis</i> JCM 17757	72567	Kim <i>et al.</i> , 2013
<i>Muricauda beolgyonensis</i> KTCC 17757	74978	Lee <i>et al.</i> , 2012
<i>Muricauda aquimarina</i> JCM 11811	74981	Yoon <i>et al.</i> , 2005
<i>Muricauda olearia</i> Th120	75875	Hwang <i>et al.</i> , 2009
<i>Muricauda antarctica</i> DSM 26351	49929	Wu <i>et al.</i> , 2013
<i>Zeaxanthibacter enoshimensis</i> DSM 18435	77824	Asker <i>et al.</i> , 2007
<i>Tenacibaculum jejuense</i> KCTC 22618	56398	Oh <i>et al.</i> , 2012
<i>Tenacibaculum ovoleticum</i> da5A-8	16550	Suzuki <i>et al.</i> , 2001
<i>Tenacibaculum gallaicum</i> DSM 18841	71520	Pineiro-Vidal <i>et al.</i> , 2008
<i>Tenacibaculum discolor</i> DSM 18842	72939	Pineiro-Vidal <i>et al.</i> , 2008
<i>Tenacibaculum maritimum</i> TM-KORJJ	16243	Suzuki <i>et al.</i> , 2001
<i>Tenacibaculum maritimum</i> NCIM 2154T	16243	Suzuki <i>et al.</i> , 2001
<i>Tenacibaculum maritimum</i> USC SE30.1	16243	Suzuki <i>et al.</i> , 2001
<i>Tenacibaculum maritimum</i> USC-SP9.1	16243	Suzuki <i>et al.</i> , 2001
<i>Tenacibaculum maritimum</i> NCIMB 902	16243	Suzuki <i>et al.</i> , 2001
<i>Tenacibaculum maritimum</i> NCIMB 2158	16243	Suzuki <i>et al.</i> , 2001
<i>Tenacibaculum maritimum</i> P4-45	16243	Suzuki <i>et al.</i> , 2001
<i>Tenacibaculum maritimum</i> DPIF 89/0239-1	16243	Suzuki <i>et al.</i> , 2001
<i>Tenacibaculum maritimum</i> UCD SB2	16243	Suzuki <i>et al.</i> , 2001
<i>Tenacibaculum maritimum</i> JIP 10/97	16243	Suzuki <i>et al.</i> , 2001
<i>Tenacibaculum maritimum</i> P2-48	16243	Suzuki <i>et al.</i> , 2001
<i>Tenacibaculum maritimum</i> P2-27	16243	Suzuki <i>et al.</i> , 2001
<i>Tenacibaculum maritimum</i> JIP 32/91-4	16243	Suzuki <i>et al.</i> , 2001
<i>Tenacibaculum maritimum</i> JIP 46/00	16243	Suzuki <i>et al.</i> , 2001
<i>Tenacibaculum maritimum</i> FC	16243	Suzuki <i>et al.</i> , 2001
<i>Tenacibaculum maritimum</i> NAC SLCC MFF	16243	Suzuki <i>et al.</i> , 2001
<i>Tenacibaculum maritimum</i> TFA4	16243	Suzuki <i>et al.</i> , 2001
<i>Tenacibaculum maritimum</i> CVI1001048	16243	Suzuki <i>et al.</i> , 2001
<i>Tenacibaculum maritimum</i> Aq16-85	16243	Suzuki <i>et al.</i> , 2001
<i>Tenacibaculum maritimum</i> FS08(1)	16243	Suzuki <i>et al.</i> , 2001
<i>Tenacibaculum maritimum</i> DPIF 89/3001-6.2	16243	Suzuki <i>et al.</i> , 2001

Table S6. Sequences of primers used for ZgHAD gene cloning and knockout mutant production.

Primer name	Primer sequence
Zgal_4183fw	GGGGGGGGATCCTCGGCAAAAGTAAAGAAACCCGAG
Zgal_4183rv	CCCCCGAATTCTTAGTTCTTCAATAAGGTTCTGGGCTAC
OEG007	TTTTTTGTCGACTAGCCAAAACCTATCCCAATCGATT
OEG008	TTTTTTGGATCCCCAAAGCCTTCGCTTAAGATTCGT
OEG009	TTTTTTCTAGAAATCAGTAGCTCGGGTTTCTTTACT
OEG010	TTTTTTCTAGATTTTGAAGTAGCCCGAACCTTATT
OEG011	TATTCCAAGCAATTTGAAGGGGAA
OEG012	ACGGATCGAAAATACAGATATACATTT

Supplementary references

- Abt, B., Lu, M., Misra, M., Han, C., Nolan, M., Lucas, S., *et al.* (2011) Complete genome sequence of *Cellulophaga algicola* type strain (IC166). *Stand Genomic Sci* 4: 72-80.
- Arun, A.B., Chen, W.M., Lai, W.A., Chao, J.H., Rekha, P.D., Shen, F.T., *et al.* (2009) *Muricauda lutaonensis* sp. nov., a moderate thermophile isolated from a coastal hot spring. *Int J Syst Evol Microbiol* 59: 2738-2742.
- Asahina, A.Y., and Hadfield, M.G. (2014) Complete genome sequence of *Cellulophaga lytica* H11 using PacBio single-molecule real-time sequencing. *Genome Announc* 2: 6–7.
- Asker, D., Beppu, T., and Ueda, K. (2007) *Zeaxanthinibacter enoshimensis* gen. nov., sp. nov., a novel zeaxanthin-producing marine bacterium of the family *Flavobacteriaceae*, isolated from seawater off Enoshima Island, Japan. *Int J Syst Evol Microbiol* 57: 837-843.
- Barbeyron, T., Carpentier, F., L'haridon, S., Schüler, M., Michel, G., and Amann, R. (2008) Description of *Maribacter forsetii* sp. nov., a marine *Flavobacteriaceae* isolated from North Sea water, and emended description of the genus *Maribacter*. *Int J Syst Evol Microbiol* 58: 790-797.
- Barth, P.T., Bolton, L., and Thomson, J.C. (1992) Cloning and partial sequencing of an operon encoding two *Pseudomonas putida* haloalkanoate dehalogenases of opposite stereospecificity. *J Bacteriol* 174: 2612-2619.
- Bauer, M., Kube, M., Teeling, H., Richter, M., Lombardot, T., Allers, E., *et al.* (1996) Cloning, sequencing and expression in *Escherichia coli* of two *Rhizobium sp.* genes encoding haloalkanoate dehalogenases of opposite stereospecificity. *Eur J Biochem* 235: 744-749.
- Chan, W.Y., Wong, M., Guthrie, J., Savchenko, A.V., Yakunin, A.F., Pai, E.F., *et al.* (2010) Sequence- and activity-based screening of microbial genomes for novel dehalogenases. *Microb Biotechnol* 3: 107-120.
- Chapelais-Baron, M., Goubet, I., Duchaud, E., and Rosenfeld, E. (2017) Draft Genome Sequence of the Iridescent Marine Bacterium *Cellulophaga lytica* CECT 8139. *Am Soc Microbiol* 5: 1–3.
- Chen, J., Li, Y., Zhang, K., and Wang, H. (2018) Whole-Genome Sequence of Phage-Resistant Strain *Escherichia coli* DH5alpha. *Genome Announc* 6:e00097-18.
- Choudhuri, J.V., Meyer, F., Reinhardt, R., Amann, R.I., and Glöckner, F.O. (2006) Whole genome analysis of the marine Bacteroidetes '*Gramella forsetii*' reveals adaptations to degradation of polymeric organic matter. *Environ Microbiol* 8: 2201-2213.
- Corpet, F. (1988) Multiple sequence alignment with hierarchical clustering. *Nucleic Acids Res* 16: 10881-10890.
- De Lorenzo, V., and Timmis, K.N. (1994) Analysis and construction of stable phenotypes in gram-negative bacteria with Tn5- and Tn10-derived minitransposons. *Methods Enzymol* 235: 386-405.
- Groisillier, A., Hervé, C., Jeudy, A., Rebuffet, E., Pluchon, P.F., Chevlot, Y., *et al.* (2010) MARINE-EXPRESS: taking advantage of high throughput cloning and expression strategies for the post-genomic analysis of marine organisms. *Microb Cell Fact* 9: 45.
- Harms, H., Poehlein, A., Thürmer, A., König, G.M., and Schäberle, T.F. (2017) Draft Genome Sequence of *Zobellia sp.* Strain OII3, Isolated from the Coastal Zone of the Baltic Sea. *Genome Announc* 5: e00737-17.
- Hu, J., Wang, F., Han, S.B., Wu, S.L., Wu, M., and Xu, X.W. (2015) Genome sequence of facultatively anaerobic marine bacterium *Maribacter thermophilus* strain HT7-2(T). *Mar Genomics* 3:265-268.

- Huntemann, M., Teshima, H., Lapidus, A., Nolan, M., Lucas, S., Hammon, N., *et al.* (2012) Complete genome sequence of the facultatively anaerobic, appendaged bacterium *Muricauda ruestringensis* type strain (B1(T)). *Stand Genomic Sci* 6: 185-193.
- Hwang, C.Y., Kim, M.H., Bae, G.D., Zhang, G.I., Kim, Y.H., and Cho, B.C. (2009) *Muricauda olearia* sp. nov., isolated from crude-oil-contaminated seawater, and emended description of the genus *Muricauda*. *Int J Syst Evol Microbiol* 59: 1856-1861.
- Jeong, H., Barbe, V., Lee, C.H., Vallenet, D., Yu, D.S., Choi, S.H., *et al.* (2009) Genome sequences of *Escherichia coli* B strains REL606 and BL21(DE3). *J Mol Biol* 394: 644-652.
- Johansen, J.E., Nielsen, P., and Sjøholm, C. (1999) Description of *Cellulophaga baltica* gen. nov., sp. nov. and *Cellulophaga fucicola* gen. nov., sp. nov. and reclassification of [*Cytophaga*] *lytica* to *Cellulophaga lytica* gen. nov., comb. nov. *Int J Syst Bacteriol* 49: 1231-1240.
- Jones, D.H., Barth, P.T., Byrom, D., and Thomas, C.M. (1992) Nucleotide sequence of the structural gene encoding a 2-haloalkanoic acid dehalogenase of *Pseudomonas putida* strain AJ1 and purification of the encoded protein. *J Gen Microbiol* 138: 675-683.
- Kahng, H-Y., Chung, B.S., Lee, D-H., Jung, J.S., Park, J.H., and Jeon, C.O. (2009) *Cellulophaga tyrosinoxydans* sp. nov., a tyrosinase-producing bacterium isolated from seawater. *Int J Syst Evol Microbiol* 59: 654-657.
- Kawasaki, H., Tsuda, K., Matsushita, I., and Tonomura, K. (1992) Lack of homology between two haloacetate dehalogenase genes encoded on a plasmid from *Moraxella* sp. strain B. *J Gen Microbiol* 138:1317-1323.
- Kawasaki, H., Toyama, T., Maeda, T., Nishino, H., and Tonomura, K. (1994) Cloning and sequence analysis of a plasmid-encoded 2-haloacid dehalogenase gene from *Pseudomonas putida* No. 109. *Biosci Biotechnol Biochem* 58: 160-163.
- Kim, J.M., Jin, H.M., and Jeon, CO. (2013) *Muricauda taeansensis* sp. nov., isolated from a marine tidal flat. *Int J Syst Evol Microbiol* 63: 2672-2677.
- Köhler, R., Brokamp, A., Schwarze, R., Reiting, R.H., and Schmidt, F.R. (1998) Characteristics and DNA-sequence of a cryptic haloalkanoic acid dehalogenase from *Agrobacterium tumefaciens* RS5. *Curr Microbiol* 36: 96-101.
- Kopel, M., Helbert, W., Henrissat, B., Doniger, T., and Banin, E. (2014) Draft Genome Sequence of *Nonlabens ulvanivorans*, an Ulvan-Degrading Bacterium. *Genome Announc* 2: e00793-14.
- Kumar, A., Pillay, B., and Olaniran, A.O. L-2-Haloacid dehalogenase from *Ancylobacter aquaticus* UV5: Sequence determination and structure prediction. *Int J Biol Macromol* 83: 216-225.
- Kurata, A., Kurihara, T., Kamachi, H., and Esaki, N. (2005) 2-Haloacrylate reductase, a novel enzyme of the medium chain dehydrogenase/reductase superfamily that catalyzes the reduction of a carbon-carbon double bond of unsaturated organohalogen compounds. *J Biol Chem* 280: 20286-20291.
- Kwak, M-J., Lee, J., Kwon, S-W., and Kim, J.F. (2017) Genome Information of *Maribacter dokdonensis* DSW-8 and Comparative Analysis with Other *Maribacter* Genomes. *J Microbiol Biotechnol* 27: 591-597.
- Lafleur, J.E., Costa, S.K., Bitzer, A.S., and Silby, M.W. (2015) Draft Genome Sequence of *Cellulophaga* sp. E6, a Marine Algal Epibiont That Produces a Quorum-Sensing Inhibitory Compound Active against *Pseudomonas aeruginosa*.
- Lee, S.Y., Park, S., Oh, T.K., and Yoon, J.H. (2012) *Muricauda beolgyonensis* sp. nov., isolated from a tidal flat. *Int J Syst Evol Microbiol* 62: 1134-1139.

- Murdiyato, U., Asmara, W., Tsang, J.S., Baines, A.J., Bull, A.T., and Hardman, D.J. (1992) Molecular biology of the 2-haloacid halohydrolyase IVa from *Pseudomonas cepacia* MBA4. *Biochem J* 284: 87-93.
- Lee, Y.S., and Choi, Y.L. (2017) Complete genome sequence and analysis of three kinds of β -agarase of *Cellulophaga lytica* DAU203 isolated from marine sediment. *Mar Genomics* 35: 43–46.
- Nakanishi, M., Meirelles, P., Suzuki, R., Takatani, N., Mino, S., Suda, W., *et al.* (2014) Draft Genome Sequences of Marine Flavobacterium *Nonlabens* Strains NR17, NR24, NR27, NR32, NR33, and Ara13. *Genome Announc* 2: e01165-14.
- Nedashkovskaya, O.I., Kim, S.B., Han, S.K., Lysenko, A.M., Rohde, M., Rhee, M.S., *et al.* (2004b) *Maribacter* gen. nov., a new member of the family *Flavobacteriaceae*, isolated from marine habitats, containing the species *Maribacter sedimenticola* sp. nov., *Maribacter aquivirus* sp. nov., *Maribacter orientalis* sp. nov. and *Maribacter ulvicola* sp. nov. *Int J Syst Evol Microbiol* 54: 1017–1023.
- Nedashkovskaya, O.I., Kim, S.B., Han, S.K., Rhee, M.S., Lysenko, A.M., Rohde, M., *et al.* (2004c) *Algibacter lectus* gen. nov., sp. nov., a novel member of the family *Flavobacteriaceae* isolated from green algae. *Int J Syst Evol Microbiol* 54: 1257–1261.
- Nedashkovskaya, O.I., Vancanneyt, M., Dawyndt, P., Engelbeen, K., Vandemeulebroecke, K., Cleenwerck, I., *et al.* (2005) Reclassification of [*Cytophaga*] *marinoflava* Reichenbach 1989 as *Leeuwenhoekiella marinoflava* gen. nov., comb. nov. and description of *Leeuwenhoekiella aequorea* sp. nov. *Int J Syst Evol Microbiol* 55: 1033–1038.
- Nedashkovskaya, O.I., Vancanneyt, M., Kim, S.B., Zhukova, N.V., Han, J.H., and Mikhailov, V.V. (2009) *Leeuwenhoekiella palythoae* sp. nov., a new member of the family *Flavobacteriaceae*. *Int J Syst Evol Microbiol* 59: 3074-3077.
- Nedashkovskaya, O.I., Kukhlevskiy, A.D., Zhukova, N.V., and Kim, S.B. (2014) *Flavimarina pacifica* gen. nov., sp. nov., a new marine bacterium of the family *Flavobacteriaceae*, and emended descriptions of the genus *Leeuwenhoekiella*, *Leeuwenhoekiella aequorea* and *Leeuwenhoekiella marinoflava*. *Antonie Van Leeuwenhoek* 106: 421-429.
- Oh, H-M., Kang, I., Yang, S-J., Jang, Y., Vergin, K.L., Giovannoni, S.J., and Cho, J-C. (2011) Complete genome sequence of strain HTCC2170, a novel member of the genus *Maribacter* in the family *Flavobacteriaceae*. *J Bacteriol* 193: 303-304.
- Oh, Y.S., Kahng, H.Y., Lee, D.H., and Lee, S.B. (2012) *Tenacibaculum jejuense* sp. nov., isolated from coastal seawater. *Int J Syst Evol Microbiol* 62: 414-419.
- Panschin, I., Huang, S., Meier-Kolthoff, J.P., Tindall, B.J., Rohde, M., Verburg, S., *et al.* (2016) Comparing polysaccharide decomposition between the type strains *Gramella echinicola* KMM 6050(T) (DSM 19838(T)) and *Gramella portivictoriae* UST040801-001(T) (DSM 23547(T)), and emended description of *Gramella echinicola* Nedashkovskaya *et al.* 2005 emend. Shahina *et al.* 2014 and *Gramella portivictoriae* Lau *et al.* 2005. *Stand Genomic Sci* 11: 37.
- Panschin, I., Becher, M., Verburg, S., Spröer, C., Rohde, M., Schüler, M., *et al.* (2017) Description of *Gramella forsetii* sp. nov., a marine *Flavobacteriaceae* isolated from North Sea water, and emended description of *Gramella gaetbulicola* Cho *et al.* 2011. *Int J Syst Evol Microbiol* 67: 697-703.
- Pati, A., Abt, B., Teshima, H., Nolan, M., Lapidus, A., Lucas, S., *et al.* (2011) Complete genome sequence of *Cellulophaga lytica* type strain (LIM-21). *Stand Genomic Sci* 4: 221-232.

- Piñeiro-Vidal, M., Riaza, A., and Santos, Y. (2008) *Tenacibaculum discolor* sp. nov. and *Tenacibaculum gallaicum* sp. nov., isolated from sole (*Solea senegalensis*) and turbot (*Psetta maxima*) culture systems. *Int J Syst Evol Microbiol* 58: 21-25.
- Pinhassi, J., Bowman, J.P., Nedashkovskaya, O.I., Lekunberri, I., Gomez-Consarnau, L., and Pedrós-Alió, C. (2006) *Leeuwenhoekiella blandensis* sp. nov., a genome-sequenced marine member of the family *Flavobacteriaceae*.
- Robert, X. and Gouet, P. (2014) Deciphering key features in protein structures with the new ENDscript server. *Nucleic Acids Res* 42: W320-W324.
- Schneider B, Müller R, Frank R, Lingens F. (1991) Complete nucleotide sequences and comparison of the structural genes of two 2-haloalkanoic acid dehalogenases from *Pseudomonas* sp. strain CBS3. *J Bacteriol* 173: 1530-1535.
- Shan, D., Ying, J., Li, X., Gao, Z., Wei, G., and Shao, Z. (2014) Draft Genome Sequence of the Carrageenan-Degrading Bacterium *Cellulophaga* sp. Strain KL-A, Isolated from Decaying Marine Algae. *Genome Announc* 2: e00145-14.
- Si, O.-J., Kim, S.-J., Jung, M.-Y., Choi, S.-B., Kim, J.-G., Kim, S.-G., *et al.* (2015) *Leeuwenhoekiella polynya* sp. nov., isolated from a polynya in western Antarctica. *Int J Syst Evol Microbiol* 65: 1694-1699.
- Suzuki, M., Nakagawa, Y., Harayama, S., and Yamamoto, S. (2001) Phylogenetic analysis and taxonomic study of marine *Cytophaga*-like bacteria: proposal for *Tenacibaculum* gen. nov. with *Tenacibaculum maritimum* comb. nov. and *Tenacibaculum ovolyticum* comb. nov., and description of *Tenacibaculum mesophilum* sp. nov. and *Tenacibaculum amyolyticum* sp. nov. *Int J Syst Evol Microbiol* 51: 1639-1652.
- Takatani, N., Nakanishi, M., Meirelles, P., Mino, S., Suda, W., Oshima, K., *et al.* (2014) Draft Genome Sequences of Marine Flavobacterium *Algibacter lectus* Strains SS8 and NR4. *Genome Announc* 2: e01168-14.
- Tully, B.J., Graham, E.D., and Heidelberg, J.F. (2018) The reconstruction of 2,631 draft metagenome-assembled genomes from the global oceans. *Sci Data* 5: 170203.
- Wu, Y.H., Yu, P.S., Zhou, Y.D., Xu, L., Wang, C.S., Wu, M., *et al.* (2013) *Muricauda antarctica* sp. nov., a marine member of the *Flavobacteriaceae* isolated from Antarctic seawater. *Int J Syst Evol Microbiol* 63: 3451-3456.
- Yi, H., and Chun, J. (2012) Unification of the genera *Nonlabens*, *Persicivirga*, *Sandarakinotalea* and *Stenothermobacter* into a single emended genus, *Nonlabens*, and description of *Nonlabens agnitus* sp. nov. *Syst Appl Microbiol* 35: 150-155.
- Yoon, J.H., Lee, M.H., Oh, T.K., Park, Y.H. (2005) *Muricauda flavescens* sp. nov. and *Muricauda aquimarina* sp. nov., isolated from a salt lake near Hwajinpo Beach of the East Sea in Korea, and emended description of the genus *Muricauda*. *Int J Syst Evol Microbiol* 55: 1015-1019.
- Yoon, J.H., Kang, S.J., Jung, Y.T., and Oh, T.K. (2008) *Muricauda lutimaris* sp. nov., isolated from a tidal flat of the Yellow Sea. *Int J Syst Evol Microbiol* 58: 1603-1607.
- Zhang, Z., Gao, X., Qiao, Y., Wang, Y., and Zhang, X.H. (2015) *Muricauda pacifica* sp. nov., isolated from seawater of the South Pacific Gyre. *Int J Syst Evol Microbiol* 65: 4087-4092.

Chapter 2:

Purification, crystallization and structural analyses of ZgHAD, a

L-2-haloacid dehalogenase from the marine flavobacterium

Zobellia galactanivorans

Article in preparation

This chapter presents the structural characterization of recombinant ZgHAD, as well as the structure of two site-directed mutant of this protein: H179A and H179N. Computational docking has also been performed to study to substrate fixation in the active site of the enzyme. These data have been obtained thanks to the collaborative work of Mirjam Czjzek and Thomas Roret from the platform of crystallography in Roscoff.

INTRODUCTION

The haloacid dehalogenases (HAD) superfamily includes dehalogenating enzymes together with diverse enzymes that hydrolyze carbon-phosphorus bonds, such as epoxide hydrolases, phosphatases, phosphomutases, or nucleotidases. Widely conserved among living organisms, they are involved in a variety of cellular processes ranging from amino acid biosynthesis to detoxification (Burroughs *et al.*, 2006). Since the industrial boom, halogenated xenobiotic pollutants are contaminating soils and aquatic environments. The accumulation of those toxic compounds led to the research of new tools for detoxification and bioremediation.

The “true” dehalogenases of the HAD superfamily are categorized into two types. Type I represents both HADs that have an enantioselective dehalogenating activity on D-2-haloacids (D-2-HADs), and those that have non-stereospecific mechanism accepting both D- or L-2-haloacids as substrates (DL-2-HADs). Enzymes from type II specifically act on L-2-haloacids (L-2-HADs, E.C. 3.8.1.2) to produce the corresponding alcohols with an inverted chirality (Hill *et al.*, 1999; Ang *et al.*, 2018). Those enzymes degrade the substrate molecule by a nucleophilic attack on its halogenated C α by an aspartic acid group that forms an ester bond and release the halide ion. The enzyme-substrate ester bond is then hydrolyzed by another nucleophilic attack by an activated water molecule. This reaction occurs with an inversion of chirality of the final product (Liu *et al.*, 1995; Nardi-Dei *et al.*, 1997).

There are currently five crystal structures of L-2-HADs available: L-DEX YL from *Pseudomonas* sp. (Hisano *et al.*, 1996), DhIB from *Xanthobacter autotrophicus* GJ10 (Ridder *et al.*, 1997), DehIVa from *Burkholderia caribensis* (Schmidberger *et al.*, 2007; Pan *et al.*, 2015), DehSft from *Sulfolobus tokodaii* (Rye *et al.*, 2009) and DehRhb from *Rhodobacteraceae* (Novak *et al.*, 2013). HAD proteins are dimers with two domains in each subunit: a characteristic alpha/beta core domain with a conserved alpha/beta hydrolase fold, similar to the “Rossmann-fold”, and many of them have a small cap domain exhibiting varying folds and

functions. This cap domain is responsible for the diversification of chemistry within HAD superfamily (Lahiri *et al.*, 2004). Those enzymes transform the substrate(s) molecule(s) according to a conserved nucleophilic substitution involving a conserved aspartic acid group that forms an ester bond. In the case of L-2-HADs, that are the only true dehalogenases of the HAD superfamily, the enzyme-substrate ester bond is then hydrolyzed by another nucleophilic attack with an activated water molecule (Liu *et al.*, 1995 ; Nardi-Dei *et al.*, 1997). In contrast to HAD in general, the cap domain is similar in all L-2-HADs and is composed of a four-helix bundle and the active site is flanked by a hydrophobic residue cavity between the core and cap domain (Ridder *et al.*, 1997 ; Schmidberger *et al.*, 2007 ; Rye *et al.*, 2009).

The complete genome sequence of the marine flavobacterium *Zobellia galactanivorans*, revealed the presence of a type II HAD enzyme. Following cloning and purification, the biochemical characterization of the recombinant ZgHAD enzyme has been performed (Grigorian *et al.*, in prep). Briefly, it is specific towards L-enantiomer substrates with short carbon chain (C2 and C3) and iodinated, brominated or chlorinated on the α -carbon position. The fastest activity was observed with iodoacetic acid and bromoacetic acid, while the reaction with chloroacetic acid and L-2-bromopropionic acid was much slower. Thus, ZgHAD is a L-2-HAD.

In this paper, we describe the crystal structure resolution of ZgHAD. We present the high-resolution three-dimensional structure of this mesophilic dehalogenase together with site-directed mutagenesis, computational docking and comparison with other related enzymes previously described. The thermostability and solvent stability of this enzyme has also been assessed, in view of potential biotechnological applications.

MATERIALS AND METHODS

Gene cloning and site-directed mutagenesis

The ZgHAD gene sequence (Zobellia_4183) was cloned from the genomic DNA of *Zobellia galactanivorans* as described by [Barbeyron *et al.*, 2001](#); using primers Zgal_4183fw and Zgal_4183rv (**Table S2**) The PCR product was ligated into pFO4 vector using *Bam*HI and *Eco*RI restriction sites and the T4 DNA ligase protocol (New England Biolabs). The recombinant vector was transformed firstly into *Escherichia coli* DH5 α for sequence verification and secondly into *E. coli* BL21(DE3) expression strain.

ZgHAD mutants H179A and H179N were produced using QuickChange Lightning Site-directed Mutagenesis (Agilent Technologies). Primers used are listed in **Table S2** from supplementary data.

Protein overexpression and purification

As described in Chapter 1.

Thermal unfolding experiments

The proteins were diluted to a final concentration of 10 μ M. For each condition, 10 μ L of sample per capillary were prepared. The samples were loaded into UV capillaries and experiments were carried out using the Prometheus NT.48 (NanoTemper Technologies) that can detect changes in the fluorescence of tryptophan (Trp) residues in the proteins. The temperature gradient was set to an increase of 2 $^{\circ}$ C/min in a range from 20 $^{\circ}$ C to 95 $^{\circ}$ C. Protein unfolding was measured by detecting the temperature-dependent change in tryptophan fluorescence at 330 and 350 nm emission wavelengths. The increase of the ratio of Trp fluorescence emission between 350 and 330 nm indicates the thermal unfolding transition midpoint of the protein.

Thermostability measurements

The thermostability of the protein was determined by incubation in the presence of monochloroacetic acid (MCA) at different temperatures between 10 and 90°C for 30 minutes. The assay solution was added then incubated on ice for 1h. The solvent stability was investigated by incubating the enzyme in the presence of monochloroacetic acid and with ethanol, methanol, acetonitrile and dimethylsulfoxide (DMSO) at concentrations between 10% and 80% for 1h at room temperature. The assay solution was added then incubated on ice for 1h. The activity was determined by measuring the absorbance at 560 nm as previously described.

Crystallization, data collection, structure determination and refinement

The purified L-haloacid dehalogenase (ZgHAD) and its variants (ZgHAD H179A and ZgHAD H179N) were concentrated using a 10 kDa membrane Amicon Ultra-15 centrifugals Filters (Mercks Millipore) at 3600 g and 4°C until a final concentration of 15 mg/mL was reached. Hanging drops were prepared by mixing 2 μ L of ZgHAD (15 mg/mL) and 1 μ L of reservoir, and were equilibrated by vapor diffusion at 20°C. Diffraction-quality crystals appeared after approximately three days in a condition containing 0.33 M potassium thiocyanate and 31% (w/v) PEG3350 for ZgHAD and ZgHAD H179A; and containing 25% (w/v) PEG3350, 0.1 M Tris-HCl pH 8.5 and 0.2 M NaCl for ZgHAD H179N. Crystals were soaked in their reservoir solutions supplemented with 10% (v/v) glycerol before flash-freezing in liquid nitrogen. Diffraction data were collected at 100 K at microfocus beamline Proxima 2-A (Soleil, France). The data were processed using XDS (Kabsch, 2010) and scaled with Aimless from the CCP4 program package (Winn *et al.*, 2011). The structure of ZgHAD was solved by molecular replacement with the CCP4 suite program MolRep (Vagin & Teplyakov, 2010) using the marine *Rhodobacteraceae* L-Haloacid Dehalogenase as the starting model (PDB code: 2YML).

Iterative rounds of model building and refinement were carried out using Coot ([Emsley *et al.*, 2010](#)) and the Phenix.Refine module of PHENIX ([Adams *et al.*, 2010](#)). The validation of the crystal structures was performed with MolProbity ([Chen *et al.*, 2010](#)).

Computational docking

Computational docking of haloacetic acids (Cl-, Br- and I-) and of the 2-Bromopropionic acid to ZgHAD X-ray structure was performed using AutoDock Vina ([Trott & Olson, 2010](#)). The initial coordinates of these molecules were generated from the SMILES string using PHENIX.eLBOW ([Liebschner *et al.*, 2019](#)). The ZgHAD protein was kept rigid during docking. A docking grid with dimensions 25 Å × 25 Å × 25 Å, encompassing the entire active site, was used. The calculation yielded 9 possible models, of which the one with the highest ranking was selected as the most likely. Then the complexes were energy minimized using the Yasara energy minimization server ([Krieger *et al.*, 2009](#)).

RESULTS

Thermostability and solvent stability

A temperature gradient between 20°C and 95°C was applied in the aim to evaluate the stability zone of the protein fold with the Prometheus NT.48 (Nanotemper). ZgHAD is denaturated between 60 and 70°C with a melting temperature of 65°C (**Fig. 1A**). A similar experiment was achieved by Dynamic Light Scattering (DLS) measurement and exhibited a denaturing peak confirming the melting temperature of 65°C (data not shown). These correlated results suggest that ZgHAD is thermostable up to the maximal temperature of 65°C. The thermal stability of the enzymatic activity was investigated between 10°C and 90°C and measured after 30 minutes of incubation. The remaining activities were plotted as a percentage of initial activity (**Fig. 1B**). ZgHAD activity was found to be stable up to 50°C and decreased strongly between 60°C and 70°C, from 80% remaining activity to a complete loss of activity. Again, both experiments, on protein denaturation and activity, correlate and show that ZgHAD turns completely inactive and unfolded at 70°C.

The solvent stability of ZgHAD was assessed by incubating the enzyme with different concentrations of ethanol, methanol, acetonitrile and dimethyl sulfoxide (DMSO) for one hour before testing the residual activity (**Fig. 1C**). The effects of ethanol and methanol treatments are very similar. The activity of the enzyme is conserved up to 80% when 0% to 20% of these organic solvents were added. Then, the activity decreased to 20% in presence of 20% to 40% of alcohols. Above 40% of methanol or ethanol, the activity was almost zero. DMSO had the least inhibitory effect of all the solvent tested. Only 20% of activity loss was observed by the addition of up to 40% DMSO. The activity decreased to 60% with 50% of DMSO and higher concentrations drastically reduced the activity to 10% of the standard without any solvent. In acetonitrile the activity of ZgHAD was drastically reduced to 20% already in 10% of solvent. It was completely inhibited between 20 and 30% of acetonitrile, and surprisingly it increased

again for higher concentrations tested, with a stabilization allowing about 20% of residual activity in presence of 60 to 80% of acetonitrile solvent.

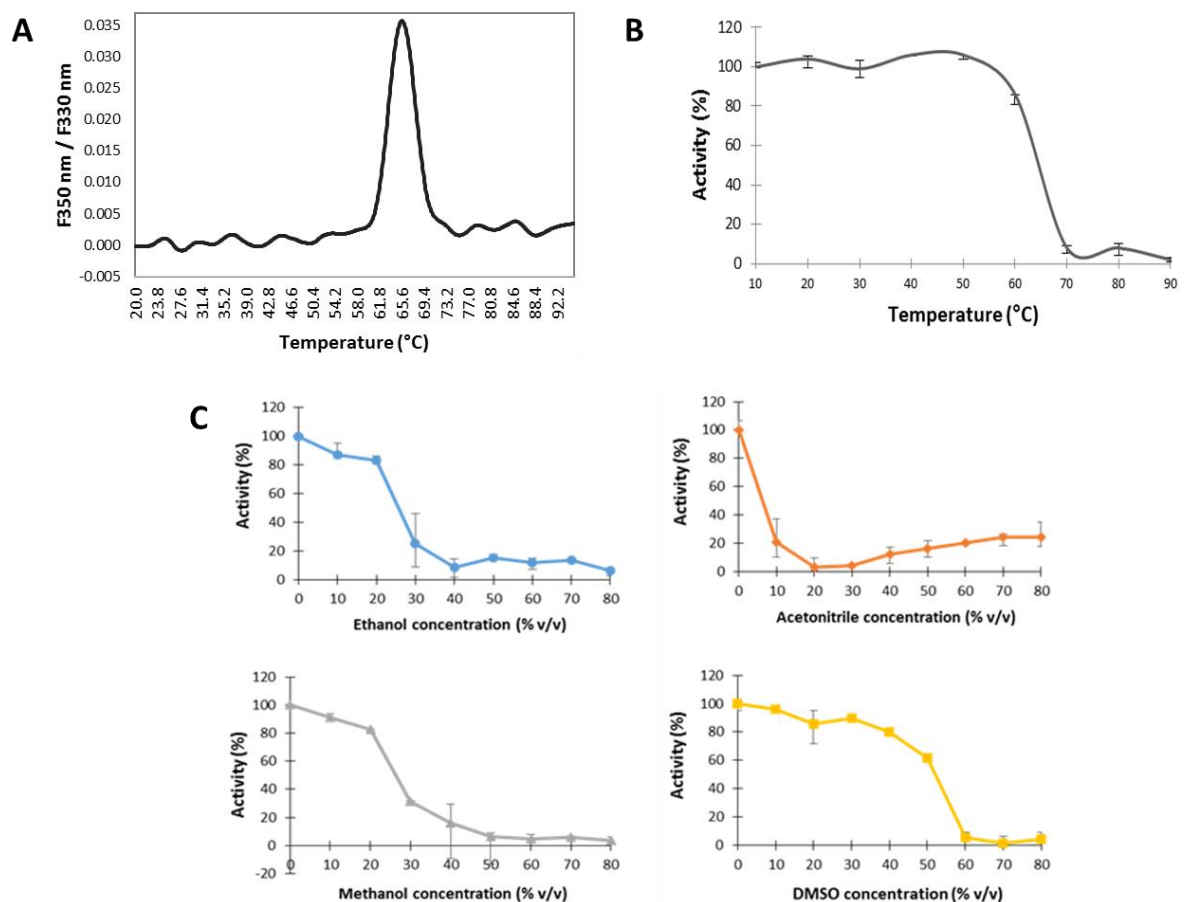


Figure 1: (A) Thermal break point of ZgHAD as determined by the Prometheus NT.48. (B) Thermal stability of ZgHAD as determined by the incubation of the enzyme at varying temperatures for 30 minutes. (C) Solvent stability of ZgHAD as determined by the activity of the enzyme after exposure to different concentrations of ethanol, methanol, acetonitrile and DMSO for 1h.

Overall structure of ZgHAD

The crystal structure of ZgHAD was solved by the molecular replacement method at 1.6 Å, using the closest structural representative, which is DehRhb (PDB accession: 2YML) from a marine *Rhodobacteraceae*. The two proteins share 31% identity and 50% similarity in their amino acid sequences. ZgHAD crystallized with the space group P2₁2₁2₁, and unit cell parameters are reported in **Table 1**.

<i>Data collection</i>	ZgHAD wt	ZgHAD H179A	ZgHAD H179N
Beam line	PROXIMA-2A	PROXIMA-2A	PROXIMA-2A
Space group	P 2 ₁ 2 ₁ 2 ₁	P 2 ₁ 2 ₁ 2 ₁	P 2 ₁
Average unit cell (Å)	59.53 68.83 103.74	59.716 71.655 116.009	76.17 132.79 275.70
Wavelength (Å)	0.97986	0.980116	0.980114
Resolution (Å)	45.03 to 1.60	45.874 to 1.716	49.46 to 2.72
R_{merge}	0.098 (0.745)	0.080 (0.872)	0.132 (1.471)
R_{meas}	0.102 (0.774)	0.083 (0.908)	0.143 (1.612)
R_{pim}	0.028 (0.208)	0.023 (0.252)	0.054 (0.643)
No. unique reflections	41657 (2364)	41318 (2628)	144,483 (4,343)
Mean $I/\sigma I$	15.2 (3.1)	21.6 (3.5)	9.6 (0.9)
CC _{1/2}	0.998 (0.896)	0.999 (0.925)	0.998 (0.447)
Completeness (%)	100 (100)	100 (100)	98.0 (60.1)
Average redundancy	13.5 (13.7)	13.0 (13.1)	6.9 (5.6)
<i>Refinement</i>			
Resolution (Å)	1.78	1.88	2.72
$R_{\text{free}}/R_{\text{work}}$	0.1774/0.1552	0.1991/0.1680	0.2363/0.1938
Total number of atoms	7481	7415	44949
Water	473	413	56
Average B factor	24.7	29.6	73.31
Ligands	PO4 ; SCN	PO4 ; SCN	PO4
<i>R.m.s deviations</i>			
Bonds	0.010	0.017	0.035
Angles	1.034	1.388	2.100
<i>MolProbity analysis</i>			
Clashscore, all atoms	3.14	2.14	4
MolProbity score	1.21	1.02	1.21
PDB entry	7ARP	7ASZ	7XXX

Table 1: Data collection and refinement statistics for ZgHAD. Values in parentheses refer to the outer resolution shell.

ZgHAD is a homodimer and its monomeric unit folds into two domains, comprising a core domain, formed by the residues 18-30 and 110-238, and a cap domain, formed by the residues 31-109 (**Fig. 2**). The core domain has a typical “Rossmann fold” which consists of six parallel β -strands surrounded by five α -helices and three 3_{10} helices. All strands show β -strand α -helix β -strand connectivity, except for β -strands 5 and 6, which are connected by a β -turn. 3_{10} helices are found before and after strand β 3. The cap domain is composed of four α -helices and a 3_{10} helix is inserted into the core domain between strand β 1 and helix α 5. The active site is located between the core and the cap domains, right after strand β 1. The four helices of the cap domain shield the top of the active site cavity from the solvent (**Fig. 2A**).

The core and the cap domains of ZgHAD are similar to those of DehRhb (2YML), DehSft (2W43), DehIVa (2NO4) and L-DEX YL (1ZRM) with rmsd values between matching C α positions of 1.21 Å over 212, 1.65 Å over 194, 1.77 Å over 213 and 1.30 Å over 203 residues, respectively.

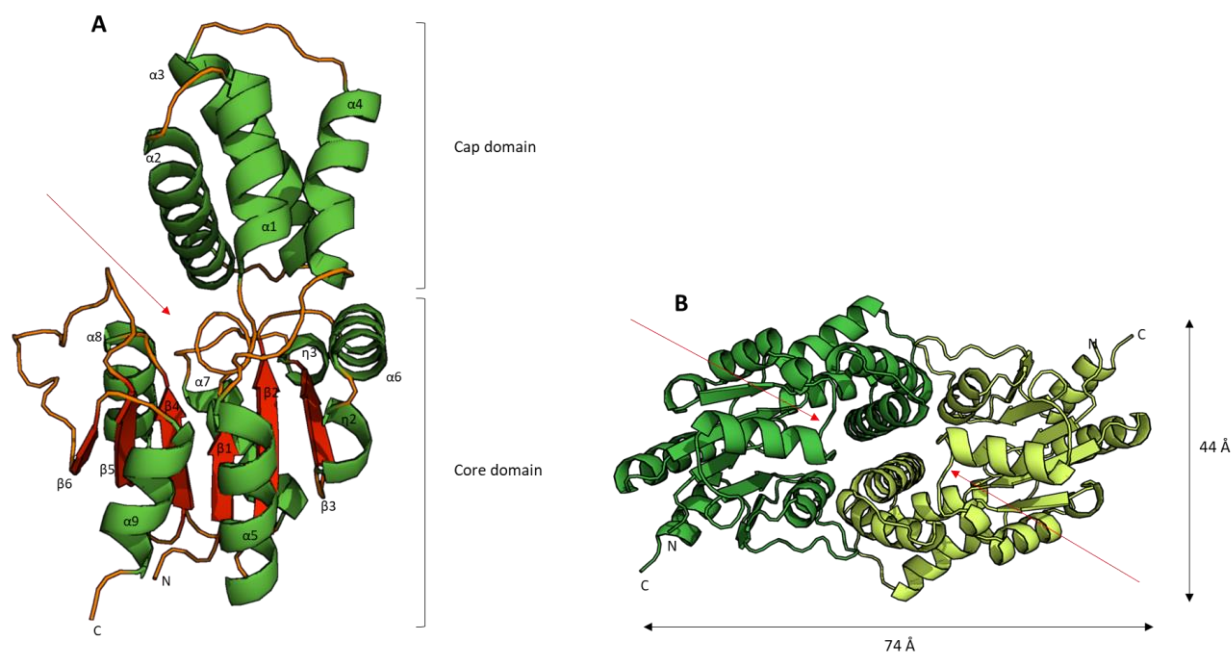


Figure 2: (A) Overall fold of ZgHAD monomer presented as a ribbon diagram colored by secondary structure elements. The α helices, β strands and loops are colored in green, red and orange respectively. (B) Ribbon diagram of ZgHAD dimer viewed with the two-fold horizontal axis. Each subunit is shown in a different color. The red arrows indicate the position of the catalytic site.

The ZgHAD protein crystallizes as a homodimer, with dimensions of 74 x 35 x 44 Å (**Fig. 2B**). This oligomeric state is in agreement with the estimated size of the protein in solution as determined by gel filtration during the purification steps as referred in [Grigorian et al., 2021](#). Up to date, all other L-2-HADs (DehRhb, DehSft, DehIVa and DhIB) have been reported to occur as homodimers, as well. Similar to the dimers of other L-2-HADs, the two subunits are related by a two-fold symmetry axis running nearly parallel to the $\alpha 2$ helix. On dimer formation, 16% of each monomer's accessible surface is buried in comparison with 18.7% in DehRhb, 13.4% in DehSft, 13.5% in L-DEX-YL and 19% in DhIB. The subunit interface of ZgHAD is

mainly formed by helices $\alpha 2$ and $\alpha 3$. In addition, a salt bridge between glutamate E53 of helix $\alpha 2$ of one subunit and arginine R188 of helix $\alpha 8$ of the other (and vice versa) reinforce the interaction between the two monomers.

Active site of ZgHAD

ZgHAD shares 31% of identical amino acids with DehRhb. Consequently there are 69% of differences in primary sequence between them. However, the active site of ZgHAD is strictly conserved with DehRhb except for one amino acid that changes from a serine (S120) in ZgHAD to a threonine (T124) in DehRhb (**Fig. 3A**). This corresponds to a minor difference, as both amino acids are exchangeable with a conservative function. Previous site-directed mutagenesis performed on other L-2-HADs has shown that nine amino acids are essential and conserved within those enzymes ([Adamu et al., 2016](#)). Those essential amino acids are highlighted in a protein alignment of structurally characterized dehalogenases (**Fig. S1** and **Table S1**). There are three amino acids that are different in ZgHAD. The positively charged arginine that binds and stabilizes the halide ion in the active site of Dh1B (R39) and L-DEX (R42) ([Ridder et al., 1997](#) ; [Kondo et al., 2014](#)) is replaced by a non-polar phenylalanine (F43) in ZgHAD. In L-DEX and DehIVa, a serine residue (S175 and S176, respectively) is described to form a hydrogen bond with the catalytic aspartate (D10 and D11, respectively) to maintain a suitable orientation of its carboxyl group for the nucleophilic attack on the substrate ([Hisano et al., 1996](#) ; [Schmidberger et al., 2007](#)). In ZgHAD and DehRhb, this serine is replaced by an alanine (A177) that cannot bind with the catalytic D14. Instead, a threonine (T18) and a lysine (K153) form a hydrogen bond with the carboxyl group of the catalytic aspartate (D14). In DehRhb, a histidine (H183) was proposed to participate to the activation of the catalytic water molecule instead of the conserved asparagine in other characterized L-2-HADs ([Novak et al., 2013](#)). Like DehRhb, ZgHAD possesses a potential catalytic histidine at position 179 as part of the

hydrophobic pocket around the active site, which is an asparagine in the other L-2-HADs. This histidine in ZgHAD has been changed to alanine and asparagine by site directed mutagenesis to generate respectively ZgHAD_H179A and ZgHAD_H179N mutant enzymes. Both mutants were shown to be inactive using the colorimetric assay adapted from [Holloway *et al.*, 1998](#) (data not shown). To analyze potential structural rearrangements due to these mutations, we have also crystallized and solved the crystal structures of both ZgHAD_H179A and ZgHAD_H179N. No major structural differences were observed for the H179N and H179A mutants, except for the position of glutamate E17. In both cases, the main chain of E17 moved from 1 Å to 2 Å towards the active site and the side chain displayed an alternative conformer that moved the functional group by 6 Å closer to the catalytic residues, which may possibly interfere with substrate binding or water activation (**Fig. 3B** and **3C**). In the case of the mutant ZgHAD_H179N, the crystal structure revealed 13 dimers displaying a helical arrangement within the asymmetric unit, as shown in **Figure 4A**. Notably, the same space group and large unit cell parameters as for ZgHAD_H179N were also observed for certain wild-type ZgHAD crystals, indicating that this spatial arrangement (dependent on the pH of the crystallization condition) is also possible for the native protein. But due to diffraction at low resolution (i.e. 3.5 - 3.2 Å), these crystals were not investigated further, since better diffracting crystals were obtained for the wild-type protein. For ZgHAD_H179N, when all independent dimers of the asymmetric unit are superimposed based on one monomer, these monomers match well with an rmsd between 0.288 and 0.445 (**Fig. 4B**). However, the other monomers, which are not included in the superimposition calculations, appear to display different relative positions with respect to the first monomer, with largest main chain distances of up to 2.7 Å (**Fig. 4C**) for the outer structural elements. This indicates that the dimer arrangement has some flexibility, allowing a rotational freedom at the interface of the two monomers.

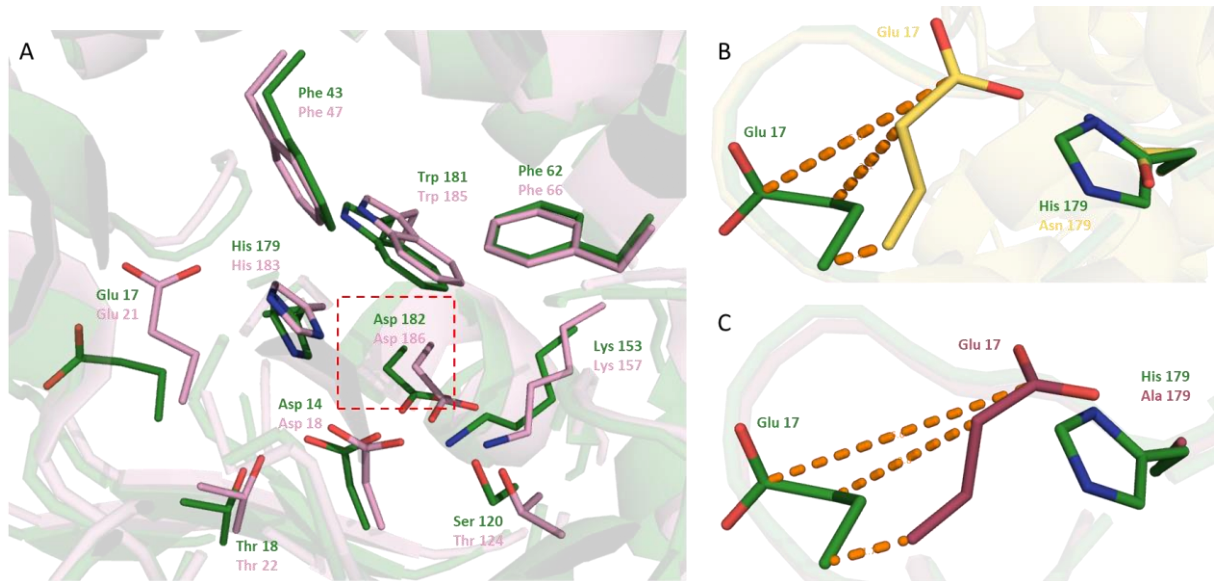


Figure 3: Ribbon representation showing the active site residues in the structures of ZgHAD and DehRhb. The side chains of selected residues are shown as sticks (carbons are colored in green, pink, yellow or purple, oxygen red and nitrogen blue). (A) Superimposition of the structures of ZgHAD (green) and DehRhb (pink). (B) Superimposition of ZgHAD (green) and mutant H179N (yellow). (C) Superimposition of ZgHAD (green) and mutant H179A (purple). The red square shows the fixation site of the substrate. Orange dotted lines highlight the distance of the movement of Glu17 between wild-type and mutant proteins.

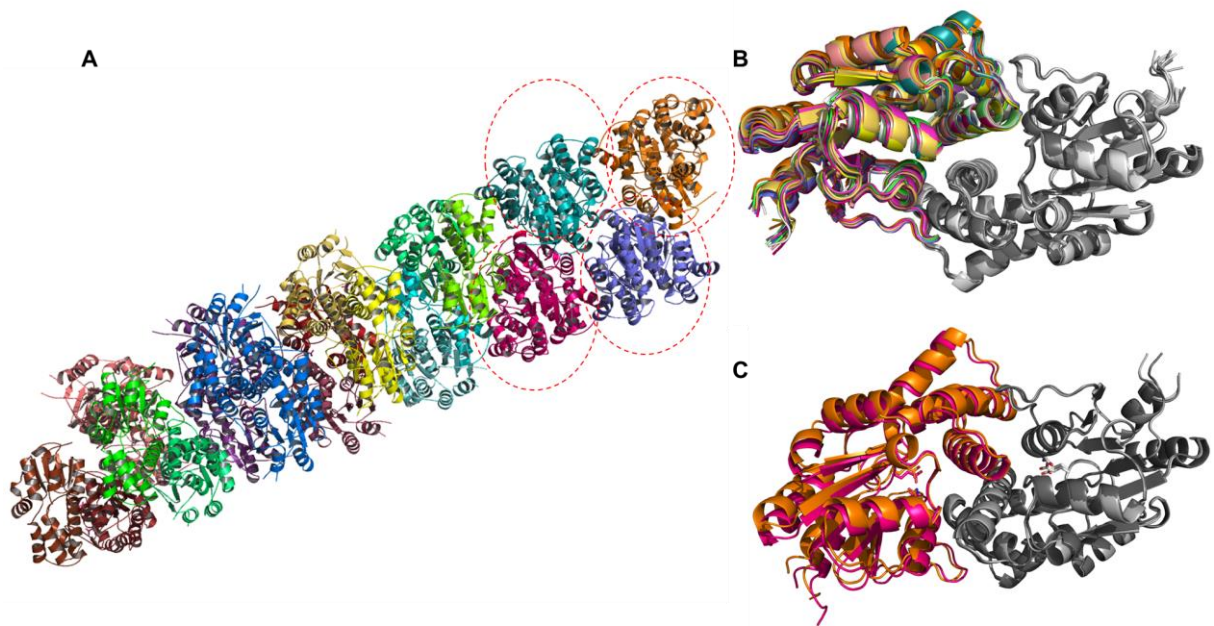


Figure 4: (A) Ribbon representation of the 13 ZgHAD_H179N dimers present in the asymmetric unit. The individual monomers of each dimer are colored with similar colors, highlighting the helical arrangement of the dimers. At one end, each circle of dotted lines surrounds one dimer. (B) Superimposition of all dimers based on the calculation of a single monomer of each (grey). The colored monomers highlight the variability of relative position to the gray monomers, which in contrast are almost identical. (C) Two of the dimers from (B), displaying the most distant relative orientations, are presented as ribbons and the amino acids E17 and N179, represented as sticks, highlight the position of the respective catalytic active sites.

Putative binding residues and docking analysis

Docking analyses with IAA, BAA, CAA and 2-BPA were undertaken. The binding energy of those substrates was comprised between -5.6 and -6.1 kcal/mol, meaning they can all be considered as preferable substrates for ZgHAD. The complexes with the best conformation were selected from nine docking positions for each ligand. V15, N16, S120, N121 and K153 were found to interact directly with each substrate through hydrogen bonding (**Fig. 5**). They each interact by forming a hydrogen bond to an oxygen atom of the carboxylate group present in the different substrates. There is no hydrogen bond observed between V15 and 2-BPA. N16 forms two hydrogen bonds with BAA and 2-BPA but only one with IAA and CAA.

According to [Novak *et al.*, 2013](#), a ‘halogen cradle’ is formed by the side chains of residues F47, I51, F66, N125 and W185. The corresponding amino acids in ZgHAD (F43, L47, F62, N121 and W181) are identically conserved and appear to be similarly involved in stabilizing the halogen atom. In the complexes obtained by docking, the catalytic D14 is hydrogen bonded to T18 and K153, with D14-OD1 also at a distance of 3.0 Å from the C2 of substrate molecules (for IAA, BAA and CAA) and 4.6 Å from 2-BPA (**Fig. 5**).

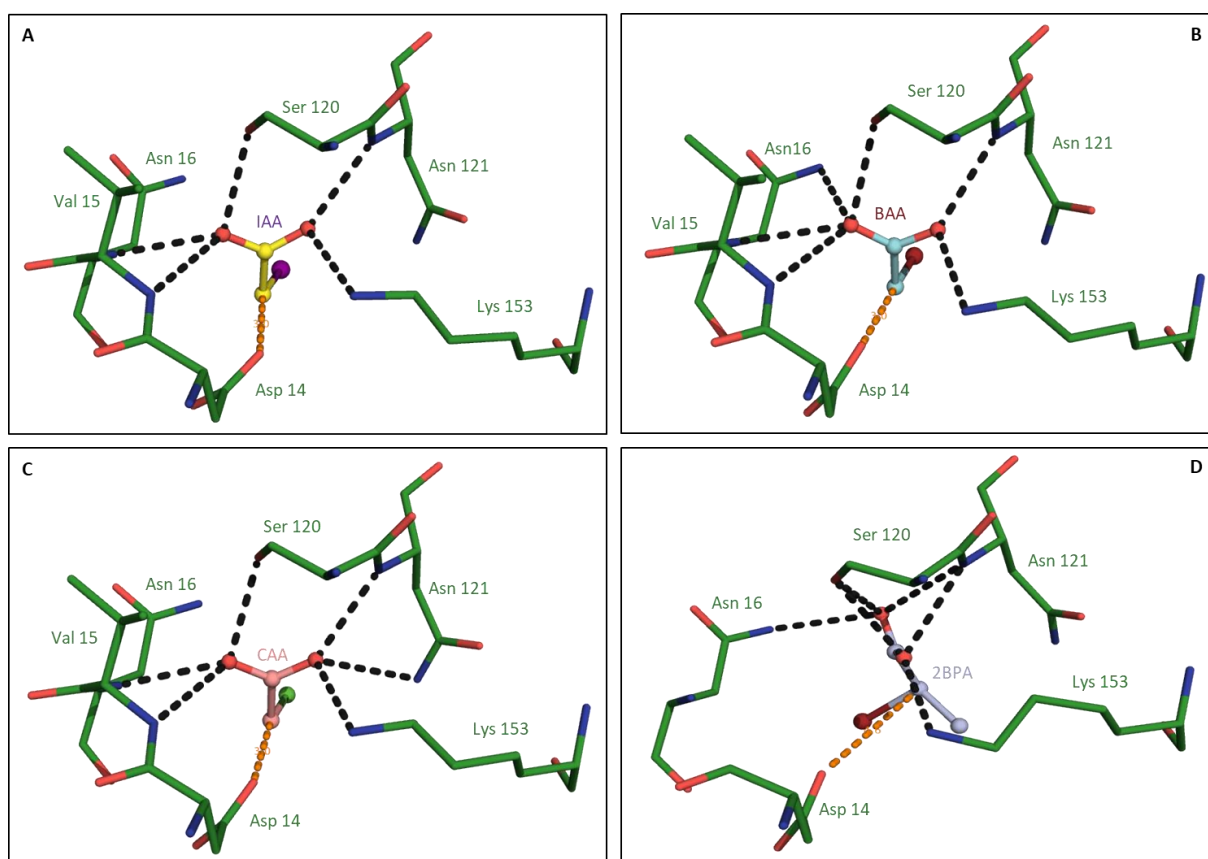


Figure 5: Illustration of the molecular docking calculations of various substrate molecules in the active site of ZgHAD. Selected residues are shown as sticks. (A) Docking of IAA (yellow) in ZgHAD (green) structures. (B) Docking of BAA (cyan) in ZgHAD (green) structure. (C) Docking of CAA (pink) in ZgHAD (green) structure. (D) Docking of 2BPA (purple) in ZgHAD (green) structure. Orange dotted line represent the distance between Asp 14 and the carbon 2 of the substrate. Black dotted lines represent hydrogen bonds of the substrates with surrounding amino acids.

DISCUSSION

L-2-HADs were shown to be robust enzymes as they have a high degree of thermostability and resistance in organic solvents. L-DEX from *Pseudomonas sp.* YL retained 100% of its activity when incubated at 60°C for 30 minutes (Liu *et al.*, 1994) and DehRhb from *Rhodobacteraceae* retained 90% activity when incubated at 55°C (Novak *et al.*, 2013). Similarly, we also observe a high thermal stability for ZgHAD as it conserves 100% of its activity when incubated up to 55°C. On the other hand, while ZgHAD was shown to be quite stable in ethanol, methanol, acetonitrile and DMSO at low concentrations, it is rapidly inactivated at high concentrations. Similar results were presented for DehRhb (Novak *et al.*, 2013) and DehSft (Rye *et al.*, 2009). ZgHAD and DehRhb appear to be more stable than DehSft, when incubated with the same organic solvents. The optimum pH was not determined since the activity assay is pH dependent, but according to previous studies, L-2-HADs proteins were generally reported to be alkaline (Van der Ploeg *et al.*, 1991; Liu *et al.*, 1994). In this respect, it is interesting to note the possible flexibility at the interface of the dimer at alkaline pH, as shown by the dimer positional variability of ZgHAD_H190N crystallized at pH 8.5 that could be important for the catalytic turnover.

The overall dimeric ZgHAD is similar to other L-2-HADs, but there are main differences regarding lengths of loops and interface interactions. The global structure is most similar to DehRhb (Novak *et al.*, 2013), as indicated by the rmsd of 1.21 Å. In the same line, interactions involved in dimerization of ZgHAD are most similar to those of DehRhb and different from DehSft (Rye *et al.*, 2009), L-DEX (Hisano *et al.*, 1996) and Dh1B (Ridder *et al.*, 1997), as described by Novak *et al.*, 2013. Nevertheless, some interesting differences between DehRhb and ZgHAD can be seen at the entrance of the active site.

ZgHAD shares low sequence identity (between 20 and 30 %) with the other characterized L-2-HADs. Interestingly, the marine ZgHAD confirms the differences of catalytic features

described for DehRhb, in contrast to L-2-HAD originating from soil bacteria. While the aspartate D14 (ZgHAD numbering) performing the first step of the reaction is the main catalytic amino acid for all of these enzymes, the activation of a water molecule is done by a His/Glu dyad for both ZgHAD and DehRhb, whereas an Asp/Lys dyad is responsible of this step in the other structurally characterized enzymes (Novak *et al.*, 2013 ; Schmidberger *et al.*, 2007 ; Nakamura *et al.*, 2009). A similar His/Glu dyad is well-known to operate in a same manner in haloalkane dehalogenases that are widespread in the marine environment (Janssen, 2004).

Among the nine residues depicted to be most important for catalytic activity (**Table S1**), the multiple alignment analysis shows that lysine and aspartic acid are fully conserved, while serine and tyrosine are less systematically conserved, but present in all bacterial and archaeal sequences (**Fig. S1**). Previous reports on site directed mutagenesis have already shown the importance of these amino acids for protein activity (Kurihara *et al.*, 1995; Pang & Tsang, 2001; Nakamura *et al.*, 2009). Here we describe the high resolution structure of ZgHAD in the unbound state and computationally analyzed the structure by docking the substrate molecules into the active site. The catalytic amino acids are well-conserved with DehRhb and the overall structure showed a dimer with mixed α/β core domain and a four helix bundle cap domain. The catalytic site is located in a cavity between the core and cap domains. The core domain contributes to the catalytic residues and the cap domain stabilizes the substrate and determines substrate specificity (Lahiri *et al.*, 2004). Its 3D model structure is highly similar to the crystal structure of DehRhb from *Rhodobacteraceae* family (Novak *et al.*, 2013). Only two important residues for substrate binding or catalysis are different between both proteins (L47 and S121 of ZgHAD vs. I51 and T124 of DehRhb). Since serine and threonine are neutral polar amino acids, the substitution between them is unlikely to introduce a strong significant change of the catalytic activity. The same conservative replacement could result for the exchange of hydrophobic amino acids isoleucine to leucine in ZgHAD. The recombinant ZgHAD was shown to have

preferable activity towards short-carbon-chain substrates and most specifically for C2 compared to C3 haloalkanoic acids. Iodoacetic acid and bromoacetic acid were found to be the best substrates and the catalytic turnover rates were similar for both substrates (Grigorian *et al.*, [in prep](#)). When compared with DehRhb, we found that ZgHAD is more efficient to convert the bromoacetic acid. Consequently the replacement of these two amino acids mentioned earlier, which are the only underlined differences among those enzymes, might be associated with substrate affinity. Leucine 47 is located in the cap domain, which is responsible for substrate recognition and binding. However, this hypothesis requires further experimental examination such as site-directed mutagenesis. The high structural similarities, between ZgHAD and DehRhb, suggests that the equivalent His/Glu dyad might be responsible for water activation.

REFERENCES

- Adams, P. D., Afonine, P. V., Bunkoczi, G., Chen, V. B., Davis, I. W., Echols, N., et al. (2010) PHENIX: a comprehensive Python-based system for macromolecular structure solution. *Acta Crystallogr D Biol Crystallogr* **66**: 213-221.
- Adamu, A., Wahab, R.A., and Huyop, F. (2016) L-2-Haloacid dehalogenase (DehL) from *Rhizobium* sp. RC1. *Springerplus* **5**:695.
- Ang, T.F., Maiangwa, J., Salleh, A.B., Normi, Y.M., and Leow, T.C. (2018) Dehalogenases: From improved performance to potential microbial dehalogenation applications. *Molecules* **23**: 1–40.
- Barbeyron, T., L'Haridon, S., Corre, E., Kloareg, B., and Potin, P. (2001) *Zobellia galactanovorans* gen. nov., sp. nov., a marine species of *Flavobacteriaceae* isolated from a red alga, and classification of [*Cytophaga*] *uliginosa* (ZoBell and Upham 1944) Reichenbach 1989 as *Zobellia uliginosa* gen. nov., comb. nov. *Int J Syst Evol Microbiol* **51**: 985–997.
- Burroughs, A.M., Allen, K.N., Dunaway-Mariano, D., and Aravind, L. (2006) Evolutionary Genomics of the HAD Superfamily: Understanding the Structural Adaptations and Catalytic Diversity in a Superfamily of Phosphoesterases and Allied Enzymes. *J Mol Biol* **361**: 1003–1034.
- Chen, V. B., Arendall, W. B., Headd, J. J., Keedy, D. A., Immormino, R. M., Kapral, G. J., et al. (2010) MolProbity: all-atom structure validation for macromolecular crystallography. *Acta Crystallogr D Biol Crystallogr* **66**: 12-21.
- Emsley, P., Lohkamp, B., Scott, W. G., Cowtan, K. (2010) Features and development of Coot. *Acta Crystallogr D Biol Crystallogr* **66**: 486-501.
- Hill, K.E., Marchesi, J.R., and Weightman, A.J. (1999) Investigation of two evolutionarily unrelated halocarboxylic acid dehalogenase gene families. *J Bacteriol* **181**: 2535–2547.
- Hisano, T., Hata, Y., Fujii, T., Liu, J.-Q., Kurihara, T., Esaki, N., and Soda, K. (1996) Crystal structure of a 2-haloacid dehalogenase from *Pseudomonas* sp. YL. *J Biol Chem* **271**: 20322–30230.
- Holloway, P. (1998) A colorimetric assay for detecting haloalkane dehalogenase activity. *J Microbiol Methods*. **32**: 31-36.
- Janssen, D.B. (2004) Evolving haloalkane dehalogenases. *Curr Opin Chem Biol* **8**: 150–159.
- Kabsch, W. (2010) XDS. *Acta Crystallogr D Biol Crystallogr* **66**: 125-132.

Kondo, H., Nakamura, T. & Tanaka, S. (2014) A significant role of Arg41 residue in the enzymatic reaction of haloacid dehalogenase L-DEX YL studied by QM/MM method. *J. Mol. Catal. B Enzym.* **110**: 23–31.

Krieger, E, Joo, K., Lee, J., Lee, J., Raman, S., Thompson, J., Tyka, M., Baker, D. and Karplus, K. (2009) Improving physical realism, stereochemistry, and side-chain accuracy in homology modeling: Four approaches that performed well in CASP8. *Proteins* **9**: 114-122.

Kurihara, T., Liu, J.Q., Nardi-dei, V., Koshikawa, H., Esaki, N., and Soda, K. (1995) Comprehensive site-directed mutagenesis of L-2-halo acid dehalogenase to probe catalytic amino acid residues. *J Biochem* **117**: 1317–1322.

Lahiri, S.D., Zhang, G., Dai, J., Dunaway-Mariano, D., and Allen, K.N. (2004) Analysis of the Substrate Specificity Loop of the HAD Superfamily Cap Domain. *Biochemistry* **43**: 2812–2820.

Liebschner, D., Afonine, P. V., Baker, M. L., Bunkóczi, G., Chen, V. B., Croll, T. I., et al. (2019) Macromolecular structure determination using X-rays, neutrons and electrons: recent developments in Phenix. *Acta Crystallogr D Struct Biol* **75**: 861-877.

Liu, J.Q., Kurihara, T., Hasan, A.K., Nardi-Dei, V., Koshikawa, H., Esaki, N., and Soda, K. (1994) Purification and characterization of thermostable and nonthermostable 2-haloacid dehalogenases with different stereospecificities from *Pseudomonas* sp. strain YL. *Appl Environ Microbiol* **60**: 2389–93.

Liu, J.Q., Kurihara, T., Miyagi, M., Esaki, N., and Soda, K. (1995) Reaction mechanism of L-2-haloacid dehalogenase of *Pseudomonas* sp. YL: Identification of Asp10 as the active site nucleophile by ¹⁸O incorporation experiments. *J Biol Chem* **270**: 18309–18312.

Nakamura, T., Yamaguchi, A., Kondo, H., Watanabe, H., Kurihara, T., Esaki, N., et al. (2009) Roles of K151 and D180 in L-2-Haloacid Dehalogenase from *Pseudomonas* sp. YL: Analysis by Molecular Dynamics and Ab Initio Fragment Molecular Orbital Calculations. *J Comput Chem* **30**: 2625–2634.

Nardi-Dei, V., Kurihara, T., Park, C., Esaki, N., and Soda, K. (1997) Bacterial DL-2-haloacid dehalogenase from *Pseudomonas* sp. strain 113: Gene cloning and structural comparison with D- and L-2-haloacid dehalogenases. *J Bacteriol* **179**: 4232–4238.

Novak, H.R., Sayer, C., Isupov, M.N., Paszkiewicz, K., Gotz, D., Spragg, A.M., and Littlechild, J.A. (2013) Marine *Rhodobacteraceae* L -haloacid dehalogenase contains a novel His / Glu dyad that could activate the catalytic water. *FEBS J* **280**: 1664–1680.

Pan, Y., Kong, K.F., and Tsang, J.S.H. (2015) Complete genome sequence and characterization of the haloacid-degrading *Burkholderia caribensis* MBA4. *Stand Genomic Sci* **10**: 4–11.

Pang, B.C.M. and Tsang, J.S.H. (2001) Mutagenic analysis of the conserved residues in dehalogenase IVa of *Burkholderia cepacia* MBA4. *FEMS Microbiol Lett* **204**: 135–140.

Ridder, I. S., Rozeboom, H. J., Kalk, K. H., Janssen, D. B. and Dijkstra, B. W. (1997) Three-dimensional structure of L-2-haloacid dehalogenase from *Xanthobacter autotrophicus* GJ10 complexed with the substrate-analogue formate. *J. Biol. Chem.* **272**: 33015–33022.

Rye, C.A., Isupov, M.N., Lebedev, A.A., and Littlechild, J.A. (2009) Biochemical and structural studies of a l-haloacid dehalogenase from the thermophilic archaeon *Sulfolobus tokodaii*. *Extremophiles* **13**: 179–190.

Schmidberger, J.W., Wilce, J.A., Tsang, J.S.H., and Wilce, M.C.J. (2007) Crystal Structures of the Substrate Free-enzyme, and Reaction Intermediate of the HAD Superfamily Member, Haloacid Dehalogenase DehIVa from *Burkholderia cepacia* MBA4. *J Mol Biol* **368**: 706–717.

Trott, O. and Olson, A. J. (2010) AutoDock Vina: improving the speed and accuracy of docking with a new scoring function, efficient optimization, and multithreading. *J Comput Chem* **31**: 455-461.

Vagin, A. and Teplyakov, A. (2010) Molecular replacement with MOLREP. *Acta Crystallogr D Biol Crystallogr* **66**: 22-25.

Van der Ploeg, J., Van Hall, G., and Janssen, D.B. (1991) Characterization of the haloacid dehalogenase from *Xanthobacter autotrophicus* GJ10 and sequencing of the dhlB gene. *J Bacteriol* **173**: 7925–7933.

Winn, M. D., Ballard, C. C., Cowtan, K. D., Dodson, E. J., Emsley, P., Evans, P. R., Keegan, R.M., et al. (2011) Overview of the CCP4 suite and current developments. *Acta Crystallogr D Biol Crystallogr* **67**: 235-242.

Supporting information

Figure S1: Amino-acid sequence alignment of ZgHAD and his homologues DehRhb from *Rhodobacteraceae*, DehIVa from *B. cepacia* MBA4, L-DEX from *Pseudomonas sp.* YL, Deh1B from *X. autotrophicus* and DehSft from *S. tokodaii* and using the programs MultAlin (Corpet, 1988) and ESPript (Robert & Gouet 2014). Identical residues are shown in red boxes and residues with similar properties are in blue boxes. The green triangles highlight the residues that have been shown to be important for catalytic activity and substrate recognition (see Table S1).

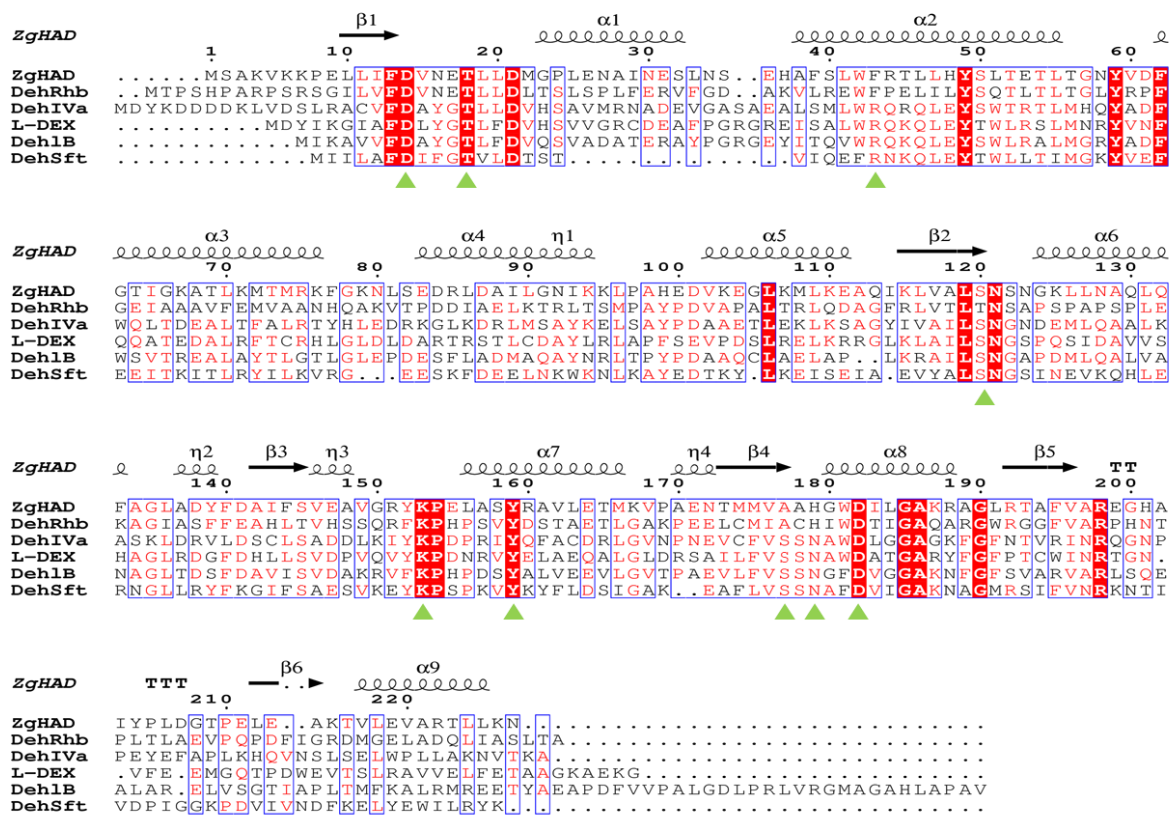


Table S1: Conserved essential amino acids for catalysis in L-DEX, Dh1B, DehIVa, DehSft, DehRhb and ZgHAD

L-DEX	Dh1B	DehIVa	DehSft	DehRhb	ZgHAD
D10	D8	D11	D7	D18	D14
T14	T12	T15	T11	T22	T18
R41	R39	R42	R23	F47	F43
S118	S114	S119	S95	T124	S120
K151	K147	K152	K128	K157	K153
Y157	Y135	Y158	Y134	Y163	Y159
S175	S171	S176	S150	A181	A177
N177	N173	N178	N152	H183	H179
D180	D176	D181	D155	D186	D182

Chapter 3:

Biochemical and structural characterization of Zg-VIPO3

I. Introduction

During the annotation of *Zobellia galactanivorans* genome, 3 homologous VHPO-encoding genes were identified (Barbeyron et al., 2016). Two of them coded for Zg-VIPO1 and Zg-VIPO2, which were previously biochemically characterized as being VHPOs strictly specific to iodide oxidation and were used in structure/function analyses for studying the bases of iodide specificity (Fournier et al., 2014). Their kinetic parameters were measured, showing a high affinity to iodide (Table 3-1). The 3D structure of Zg-VIPO1 was obtained as a monomer, unlike algal VBPOs that are mostly homodimers, hexamers or dodecamers. The other bacterial VHPOs characterized up to now are the dimeric VCPO from *Streptomyces* sp. CNQ-525 (Liscombe et al., unpublished) and the dodecameric VBPO from *Acaryochloris marina* (Frank et al., 2016).

Enzymes	K _m ^{I⁻} (mM)	K _{cat} ^{I⁻} (sec ⁻¹)
Zg-VIPO1	0.22 ± 0.01	1.98 ± 0.05
Zg-VIPO2	0.22 ± 0.02	2.04 ± 0.08

Table 3-1: Kinetic parameters of Zg-VIPO1, and Zg-VIPO2 (Fournier et al., 2014).

The presence of several distinct VHPO activities was assessed earlier for macroalgae, based on protein purification, biochemical and structural characterizations: at least two VBPOs for *Ascophyllum nodosum* (Wischang and Hartung, 2011; Wischang et al., 2012), two VBPOs for *Corallina pilulifera* (Itoh et al., 1986; Carter et al., 2002), one VBPO and one VIPO for *Laminaria digitata* (Jordan et al., 1991; Colin et al., 2005). Moreover the marine bacterium *Streptomyces* sp. CNQ-525 possesses three characterized VCPOs (McKinnie et al., 2018).

The third putative VHPO-encoding gene, *zobellia_2250*, only featured 28% of identity at the amino acid level with Zg-VIPO1 or Zg-VIPO2, while those latter shared 48% of identity. The main goal of this chapter is to characterize the biochemical function and the halide specificity of the third VHPO of *Z. galactanivorans*, as well as trying to obtain its 3D structure and compare it to Zg-VIPO1.

II. Material and methods

II. 1. Zobellia_2250 gene cloning, overexpression and purification

Zobellia_2250 was cloned from the genomic DNA of *Z. galactanivorans* as described by [Barbeyron et al., 2001](#). Specific oligonucleotides were designed according to carry *SphI* and *PstI* restriction sites. The forward and reverse primer sequences were 5'- ACCATCACGGATCCGCATGCCAGAAAAACCAAGAAGAACCAAGAGG-3' and 5' CTAATTAAGCTTGGCTGCAGCTATTGACCTAGGTGTTTGTGTAG-3' respectively. The PCR product was ligated into a linearized pQE80L vector and then transformed into *Escherichia coli* Stellar cells. Then, the extracted recombinant vector was firstly sequenced to ensure a correct DNA construction and secondarily transformed into *E. coli* BL21(DE3) expression cells, to produce the recombinant protein without the first 21 amino acids of the wild-type *Zobellia_2250*.

The recombinant bacteria were grown in LB medium in the presence of 100 µg/mL ampicillin at 37°C to an optical density of ~1.0, then the temperature was lowered to 20°C for 1 h followed by a 20 h induction of the protein production by the addition of 0.5 mM IPTG. The culture was then centrifuged at 3,000 g for 30 min at 4°C. The bacterial pellet was treated with a buffer containing 50 mM Tris-HCl pH 7.5, 500 mM NaCl, 500 U/µl bovine DNase I, 0.1 mg/mL lysozyme, Complete™ Protease Inhibitor Cocktail (Merck) and 6 mM MgCl₂. The bacterial cells were harvested using a French press and the lysate was centrifuged at 23,000 g for 30 min and 4°C. Then, the recombinant protein was purified by a two-step chromatography carried on an ÄKTA Avant purification system (GE Healthcare Life Sciences). The first step was performed on an immobilized nickel affinity HisTrap™ column (GE Healthcare Life Sciences) using an equilibration buffer composed of 50 mM Tris (pH 7.5), 500 mM NaCl and 50 mM imidazole and an equivalent elution buffer containing 500 mM imidazole instead of 50 mM. The proteins were eluted with a constant gradient of imidazole concentration. The pooled

fractions of the elution peak were concentrated on Centriprep devices to 3 mL and the protein sample was injected on a gel filtration HiLoad™ 16/600 Superdex™ 200 pg column (GE Healthcare Life Sciences). Two independent peaks of purified protein were obtained and pooled separately. Then, they were stored in a buffer containing 20 mM Tris/HCl pH 8.0 and 150 mM NaCl. The purity of the recombinant protein was analyzed using SDS-PAGE (Bio-Rad Mini-PROTEAN® precast gels and systems) and aliquots were frozen at -80°C. A second two-step chromatography purification was performed several months later with a thawed protein sample and a buffer containing 20 mM Tris/HCl pH 8.0 and 50 mM NaCl for the gel filtration. Dynamic Light Scattering (DLS) measurement were performed on 20 µL of purified protein in a quartz cuvette using ZetaSizer Nano-S instrument (Malverne Instruments).

Protein concentration was determined by measuring absorbance at 280 nm and by using the Beer-Lambert law: $A = \epsilon * l * c$. The molar attenuation coefficient (ϵ) was determined from the protein sequence on ProtParam server (<https://web.expasy.org/protparam/>) and was equal to 83690 M⁻¹.cm⁻¹.

II.2. Native gel and spectrophotometric haloperoxidase activity measurements

The VHPO activities were tested on native electrophoresis gels using the *o*-dianisidine as revealing agent. The running gel was prepared from 0.375 M Tris/HCl buffer pH 8.8 and 12% bis-acrylamide. The stacking gel consisted of 0.125 M Tris/HCl buffer pH 6.8 and 3.8% bis-acrylamide. The polymerization was achieved chemically by the addition of 1 mM ammonium persulphate in the presence of 40 pM N,N,N',N'-tetramethyl- 1,2-diaminoethane (TEMED) as catalyst accelerator. The samples were supplemented with a native buffer of 0.3 M Tris/HCl pH 6.8, 50% glycerol and 0.05% bromophenol blue. After migration, the gel was incubated in 0.1 mM of *o*-dianisidine solution, containing 100 mM potassium phosphate pH 7.4 and either 10 mM of potassium chloride, or bromide, or iodide, or no halide, for 2 h at room temperature

with gentle shaking. The gel was rinsed with distilled water and placed in a solution of 0.37 mM hydrogen peroxide for revelation during few minutes to several hours.

The spectrophotometric assays used for the enzymatic activity measurements are based on the iodination of thymol blue (TB) and the production of a stable molecule, diiodothymolsulfonphthalein (TBI₂), with spectral properties different from those of TB, as described by [Verhaeghe et al., 2008b](#). Briefly, 10 µg of purified enzyme were added to the 250 µL reaction mixture, consisting of 0.1 M phosphate buffer pH 7.2, 100 µM TB, 80 µM to 2.5 mM KI, and 0.42 mM H₂O₂. The absorbance at 620 nm was recorded on a Safire2 spectrophotometer (Tecan Group Ltd., Switzerland) for 5 min. All reactions were performed in triplicate at 20°C in clear flat-bottomed 96-well microplates (Greiner UV-Star 96-well plates). The Lineweaver-Burke plots were used to calculate the K_m and k_{cat} steady-state kinetic parameters.

II.3. Protein stability and activity analysis

The Prometheus NT.48 (Nanotemper) measures the protein thermal unfolding by detecting smallest changes in the fluorescence emission of the tryptophans (ratio 330/350 nm). The Zg-VHPO3 protein was concentrated to 1 µM then centrifuged at 13,000 g for 5 minutes at 4°C. The thermal unfolding experiments were carried out at a heating rate of 1°C/min. The F350/F330 measurements of the proteins, contained in glass capillaries, were performed by increasing temperature during 90 min.

The protein denaturing was also explored by heating 1 µg of proteins in a thermocycler (Bio-Rad) at different temperatures (from 10°C to 90°C) for 30 minutes. The samples were cooled on ice for 1 h then deposited on a native acrylamide gel. The running gel was prepared from 0.375 M Tris/HCl buffer pH 8.8 and 10% bis-acrylamide. The stacking gel consisted of 0.125 M Tris/HCl buffer pH 6.8 and 3.8% bis-acrylamide. The polymerization was achieved

chemically by the addition of 1 mM ammonium persulphate 10% in the presence of 40 pM of the catalyst accelerator, N,N,N',N'-tetramethyl- 1,2-diaminoethane (TEMED). After migration, the gel was briefly rinsed with milliQ water and incubated for 1 h in the elution buffer with 1 mM thymol blue and 15 μ M potassium iodide. Then the precedent solution was discarded and replaced by 0.42 mM hydrogen peroxide for iodoperoxidase activity revelation.

II.4. Crystallogensis

Prior to crystallization experiments by a vapor diffusion method, the purified proteins were concentrated at 11.6 mg/mL using a centrifugal filter 30K (Amicon Ultra) within a buffer containing 20 mM Tris-HCl pH 8.0 and 150 mM NaCl. The crystallization experiment was carried out as follows: a drop of the protein sample was mixed with one drop of a crystallization solution containing a precipitant reagent with or without a buffer, salts, organic solvents, polymers. This mixture was deposited next to a reservoir of the crystallization solution at a temperature of 18°C and the vapor diffusion between the drop and the reservoir led to the formation of crystals. This process was very slow and often the crystallization solution was either under-saturated (which prevented any crystal formation) or supersaturated (which generated an amorphous precipitate) (**Figure 3-1**).

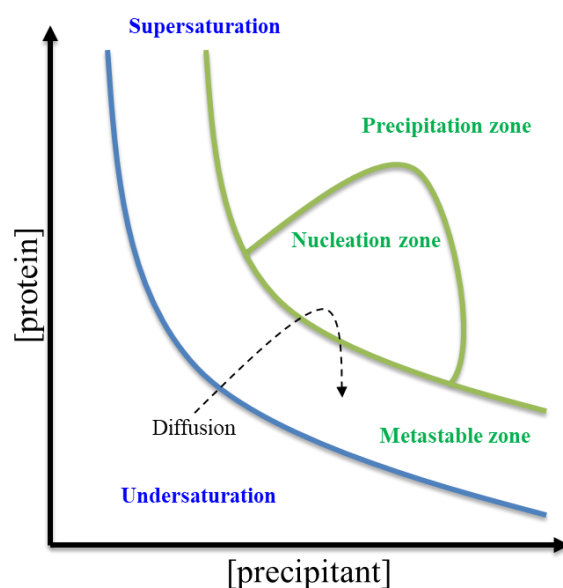


Figure 3-1: Phase diagram of the conditions needed for crystallization by vapor diffusion. In the undersaturation area: the drop remained clear. The goal was to find the right ratio and the good protein/precipitant reagent concentrations in order to reach the nucleation area and promote crystal growth.

First, crystallization trials using the sitting-drop vapor-diffusion (**Figure 3-2A**) method were performed at room temperature using a Crystal Gryphon (Art Robbins Instruments). This pipetting robot allowed to automatically test 96 crystallization solutions at a time per plate. The tested commercial screens were PACT premier™, JCSG-*plus*™, Classics™, PEGs™, PEGs II™, SaltRx™, Natrix™ and pHClear™ (QIAGEN). The crystallization drops were composed of 0.1 μ L of purified protein and 0.2 μ L of crystallization solution that were deposited on a corning crystallization plate (Molecular Dimensions) and then sealed. After a few days, each well was observed with CrysCam™ Digital Microscope System (Art Robbins Instruments). The best crystallization conditions were then manually reproduced and optimized on a 24-well XRL plate (Molecular Dimensions) for mass production with the hanging drop technic (**Figure 3-2B**). The goal was to produce a single crystal, with sufficient size and quality in order to perform X-ray diffraction experiments at a Synchrotron beamline.

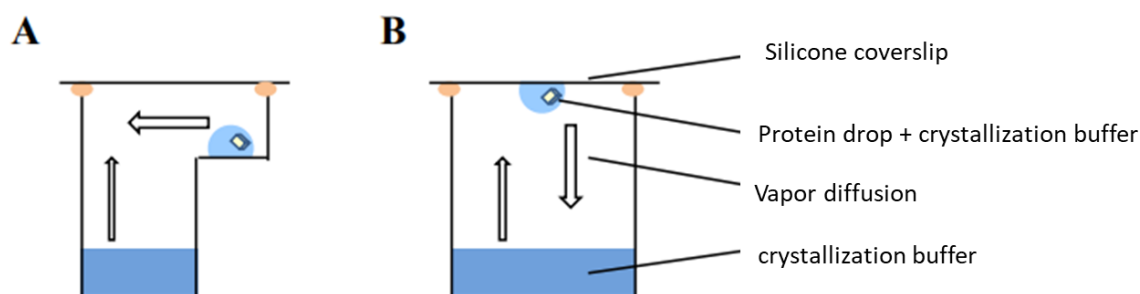


Figure 3-2: Crystallization techniques (A) sitting drop vapor diffusion and (B) hanging drop vapor diffusion (François Thomas, 2011)

II.5. Structure modelling

The 3D structure modelling of Zg-VHPO3 was performed using Zg-VIPO1 structure (PDB: 4CIT, 28% of sequence identity) and NapH1 (PDB: 3W35, 31% of sequence identity) as models with SWISS-MODEL server (<https://swissmodel.expasy.org/interactive>). The figures were constructed by using PyMOL v2.0.6. Protein-protein interface analysis was performed on PDBePISA v1.52 server (<https://www.ebi.ac.uk/pdbe/pisa/>).

III. Results and discussion

III.1. Purification of the third vanadium-dependent haloperoxidase from *Z. galactanivorans*

The third *vhp* homologous gene (*zobellia_2250*) was heterologously expressed in *E. coli* and the recombinant protein was purified by a two-step chromatography using IMAC and gel filtration. One unique peak was obtained from the first chromatography (data not shown), but the enzyme was separated as a mixture of two major distinct peaks by gel filtration (**Figure 3-3A**). The first minor peak of gel filtration corresponded to high-size protein aggregations, the second peak was eluted as a protein of about 100 kDa, and the third peak as a protein of about 50 kDa (according to a calibration range with reference proteins) (**Figure 3-3A**). The theoretical molecular weight of the recombinant Zg-VHPO3 was calculated as being 53.5 kDa. Further electrophoresis analysis of each fraction led to the identification of single 50-kDa bands on denaturing polyacrylamide gel (**Figure 3-3A**), suggesting that the second and third peaks corresponded to dimeric and monomeric forms of the protein, respectively. The fractions of each peak were separately pooled to produce two dimer and monomer batches. Another step of gel filtration was performed several months later with 1 mL sample of the thawed dimeric batch. It showed a major peak corresponding to the dimeric protein as well as a small peak

corresponding to the monomeric protein (**Figure 3-3B**). Those results suggest that the separation between dimer and monomer batches is relatively stable. The smaller peak corresponding to the monomeric protein might be a minor contamination occurring during gel filtration separation. After this purification step, the dimer batch was concentrated up to 11.6 mg/mL and the monomer batch up to 5.3 mg/mL. The DLS analysis allowed to identify hydrodynamic diameters of 6.34 nm for the monomer batch and 7.4 nm for the dimer batch, which are also in agreement with monomer and dimer purifications (data not shown).

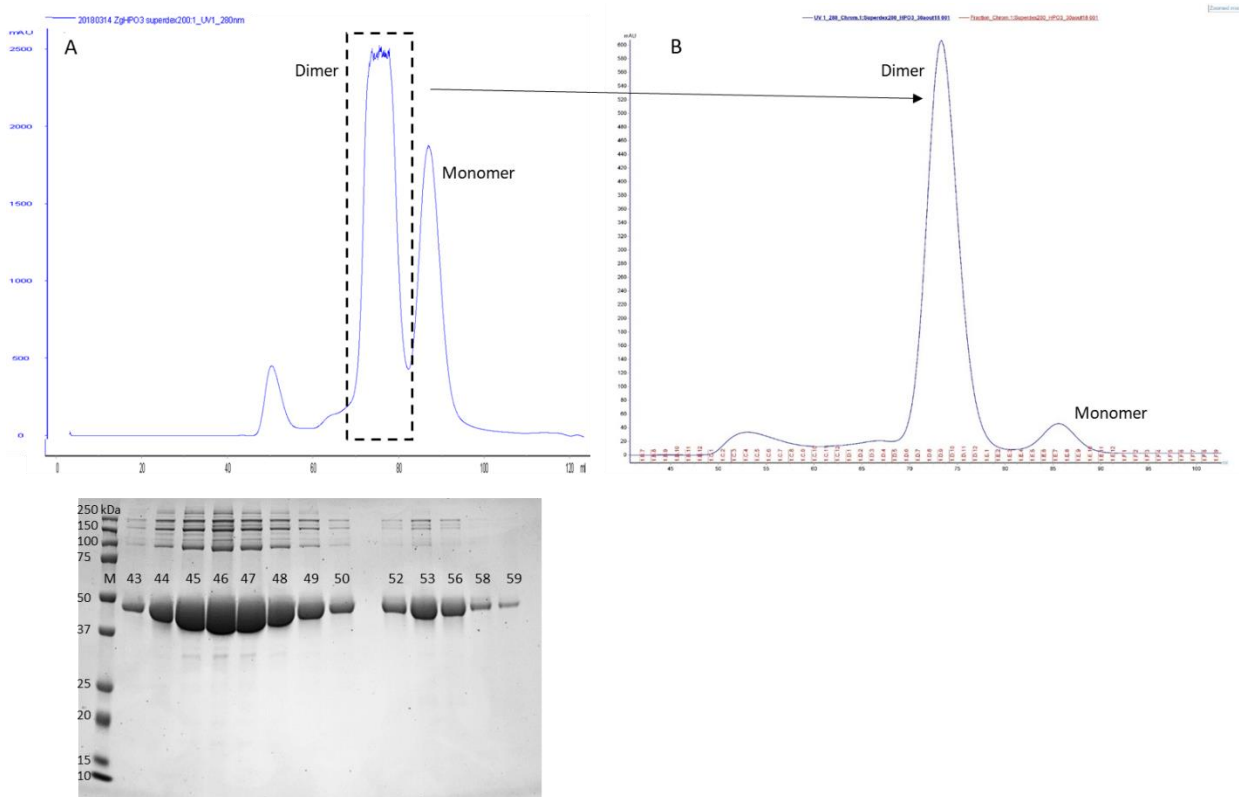


Figure 3-3: (A) Chromatogram and SDS-PAGE analyses of Zg-VHPO3 purification fractions by size exclusion chromatography. Elution buffer: 20 mM Tris/HCl, pH 8.0 and 150 mM NaCl. The polyacrylamide gel was stained with Coomassie Brilliant Blue R-250, revealing the presence of the recombinant protein in eluted fractions of the A280 peak (lanes 43 to 50 and 52 to 59). M = Precision Plus Protein™ Standards marker (Bio-Rad Laboratories) and molecular masses were indicated on the left of the lane. (B) Chromatogram analysis of the first peak from the previous size exclusion chromatography. Elution buffer: 20 mM Tris/HCl, pH 8.0 and 150 mM NaCl. Black dotted rectangle surrounded the 2nd peak of the size exclusion chromatograph in A, corresponding to the dimeric form.

The recombinant Zg-VIPO1 and Zg-VIPO2 were both purified as strictly monomeric proteins (Fournier et al., 2014). The recombinant Zg-VHPO3 purified here appeared to have two

possible protein forms, dimeric or monomeric, in solution. In order to evaluate the impact of salt concentration on the Zg-VHPO3 protein folding, another two-step chromatography purification was performed by lowering the NaCl concentration of the elution buffer to 50 mM in the gel filtration chromatography (instead of 150 mM previously). As shown in **Figure 3-4**, there were still the major two peaks following the gel filtration, but the monomer peak was dominant in this case, according to UV absorbance and SDS-PAGE gel. It appears that low NaCl concentration favors monomeric folding in solution.

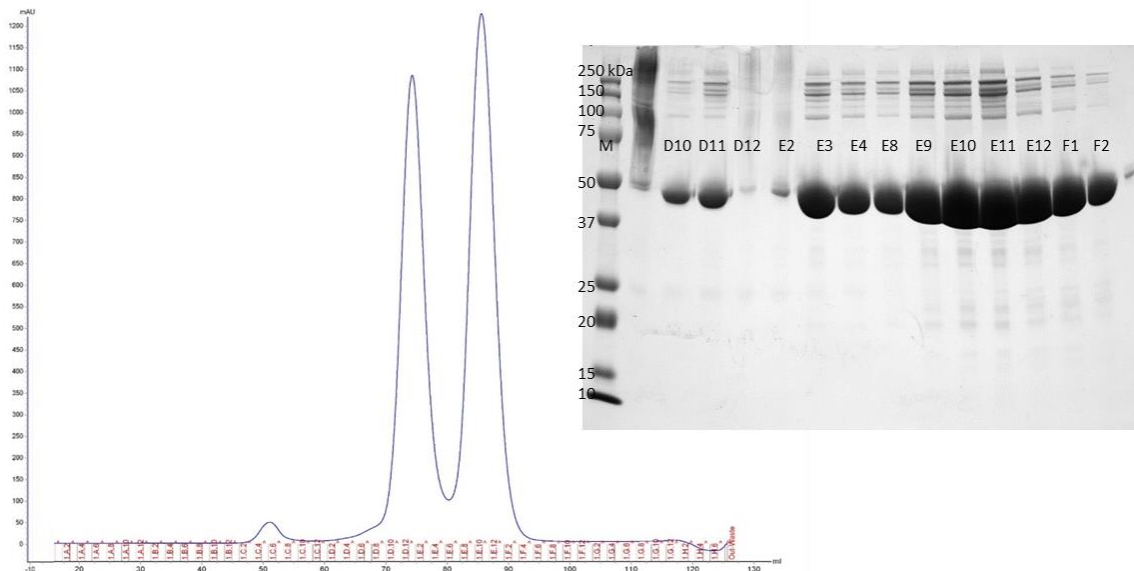


Figure 3-4: Chromatogram and SDS-PAGE analyses of Zg-VHPO3 purification by size exclusion chromatography. Elution buffer: 20 mM Tris/HCl, pH 8.0 and 50 mM NaCl. The polyacrylamide gel was stained with Coomassie Brilliant Blue R-250, revealing the presence of the recombinant protein in eluted fractions of the A280 peak (lanes D10 to E4 and E8 to F2). M = Precision Plus Protein™ Standards marker (Bio-Rad Laboratories) and molecular masses were indicated on the left of the lane.

The Tris/NaCl elution buffer had a pH of 8, which was higher than the theoretical isoelectric point ($pI = 6.16$) of the recombinant Zg-VHPO3, and led to negatively charged proteins after purification. Protein-protein interactions usually increased in that case, which could explain the higher peak corresponding to the prevalence of dimeric folds in solution. The protein stability at different pH was also tested using DLS, but the purified recombinant Zg-VHPO3 was either

aggregating at pH < 6 or precipitating at pH > 8 (data not shown). A clear effect of the pH on the dimeric or monomeric folding of Zg-VHPO3 cannot be concluded for now, as the nature of the buffer also impacted protein conformations: for example HEPES buffer at pH 8.0 induced protein precipitation, but not Tris buffer (data not shown).

III.2. Substrate specificity of Zg-VHPO3 and determination of steady-state kinetic parameters

The halogen specificity of the purified recombinant Zg-VHPO3 was determined by an *o*-dianisidine assay (Jordan & Vilter, 1991) on native protein electrophoresis gel. A red-brown color was only detected in the presence of iodide but not with bromide, chloride, or without halide showing a strict specificity of the enzyme towards iodide (Figure 3-5).

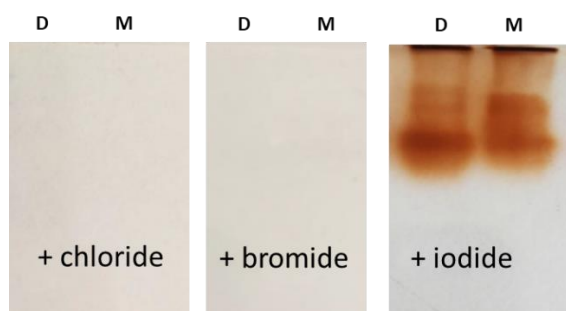


Figure 3-5: *O*-dianisidine assay on native polyacrylamide electrophoresis gel of the recombinant protein Zg-VHPO3, purified as monomer (M) and dimer (D) batches. The assay was performed in presence of potassium chloride, bromide or iodide.

A second experiment was performed using the thymol blue assay (Verhaeghe et al. 2008a). This colorimetric assay revealed changes of color, from yellow to blue, when oxidation occurred and only with iodide, for both enzyme batches (Figure 3-6). The recombinant protein Zg-VHPO3 was then renamed Zg-VIPO3 as it was specific to iodide oxidation. With the same amount of protein, the resulting assay coloration was bright blue with the dimeric batch and green for the monomeric batch suggesting a faster and stronger reactivity of the dimeric enzyme compared to the monomeric one.



Figure 3-6: Thymol blue colorimetric assay of the recombinant protein Zg-VHPO3, purified as monomer and dimer batches. The assay was performed at room temperature for 1 h in clear flat-bottomed microplate wells, in presence of potassium iodide or potassium bromide. The negative control was performed without enzyme.

Using this thymol blue assay, the steady-state kinetic parameters of the Zg-VIPO3 enzyme batches were determined. Both monomeric and dimeric purified batches were separately used, immediately after the purification steps (**Table 3-2**). As suggested by the in-well colorimetric assay (**Figure 3-6**), the monomeric enzyme batch was less active than the dimeric one. Indeed, the kinetic parameters showed that even though the two batches had similar K_m , *i.e.* similar iodide affinity, the k_{cat} of monomeric enzyme batch was about 14 times lower than the dimeric one, confirming a more efficient activity of this latter form (**Table 3-2**). The most active batch, enriched in dimeric form, was kept for complete and further biochemical analyses. Compared to Zg-VIPO1 and Zg-VIPO2 kinetic parameters (**Table 3-2**), those of Zg-VIPO3 suggested that the iodide affinity was poor, with a higher K_m value, and a catalytic turnover much lower, leading to a k_{cat}/K_m ratio for iodide more than 128-fold lower for Zg-VIPO3.

Enzymes	K_m ¹⁻ (mM)	k_{cat} ¹⁻ (sec ⁻¹)
Zg-VIPO3 (monomer)	1.11	0.0065
Zg-VIPO3 (dimer)	1.36 ± 0.07	0.09 ± 0.02
Zg-VIPO1	0.22 ± 0.01	1.98 ± 0.05
Zg-VIPO2	0.22 ± 0.02	2.04 ± 0.08

Table 3-2: Kinetic parameters of Zg-VIPO1, VIPO2 and VIPO3 (Fournier et al., 2014)

Those results suggested that Zg-VIPO3 functions differently than its two homologues within *Z. galactanivorans*. Further investigation on its 3D structure might be of great interest to study a potentially different enzymatic mechanism.

III.3. Effect of temperature on the folding of Zg-VIPO3

The structure stability analysis by thermal shift of the freshly purified dimer and monomer batches revealed two different melting temperatures comprised between 39.2°C and 40.3°C for the first peak and between 53.2°C and 55.7°C for the second one (**Figure 3-7**). These two peaks represented protein unfolding steps of the dimeric and monomeric forms, respectively, and suggested that the two batches had to be considered as mixtures of both forms in different equilibria. In parallel, to study the effect of temperature on the enzymatic activity, each batch was submitted to an increasing gradient of temperature for 30 min, and deposited on native gels to assess remaining activity using a thymol blue colorimetric assay. The results showed a better activity stability of the monomer form (still active after 50°C treatment) compared to the dimer form (fully active up to 30°C incubation) (**Figure 3-8**). This suggested that Zg-VIPO3 as a dimer was first denatured and lost enzymatic activity with lower temperature than as a monomer. The monomeric form might be more stable in solution and better for *in vitro* experiments.

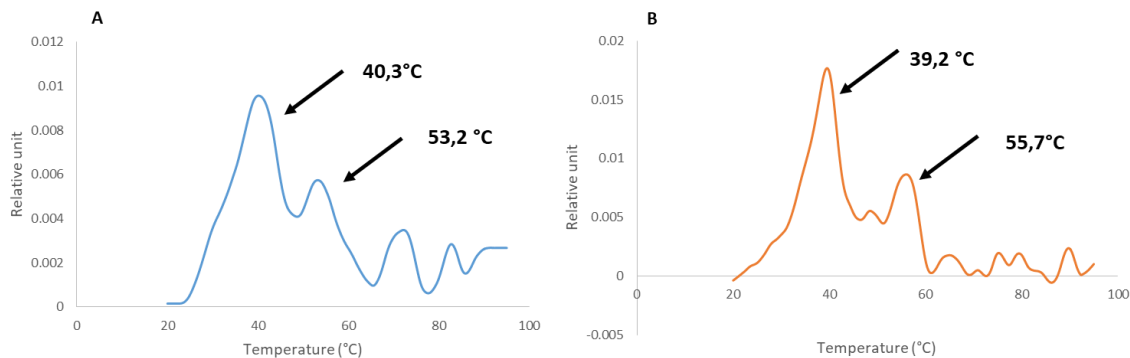


Figure 3-7: Thermal denaturing analysis using Nanotemper NT48 of recombinant protein Zg-VIPO3, purified as (A) Dimer batch, or (B) Monomer batch. Each peak represented denaturing protein step.

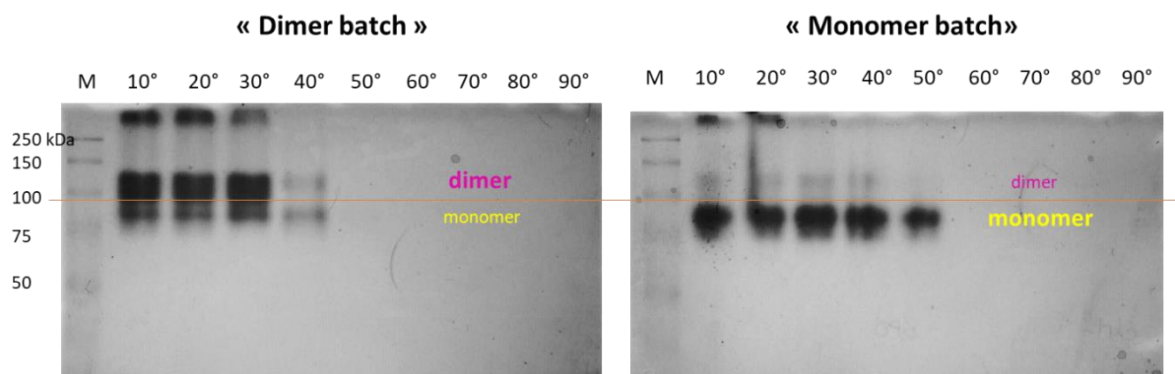


Figure 3-8: SDS-PAGE gel revealing the iodoperoxidase activities of recombinant protein in dimeric or monomeric batches, after heating treatment at 10°C to 90°C for 30 minutes. The native polyacrylamide electrophoresis gel was stained with thymol blue. M = Precision Plus Protein™ Standards marker (Bio-Rad Laboratories) and molecular masses were indicated on the left of the lane.

III.4. 3D structural studies of Zg-VIPO3

In order to determine the 3D structure of Zg-VIPO3, crystallographic tests were performed on the crystallography platform of the Station Biologique at Roscoff. First, many conditions were automatically tested with commercially available screening kits from QIAGEN. Both monomeric and dimeric purified protein batches were used.

After a few days, no crystal was formed with the monomeric batch, the drops stayed clear. On the other hand, half of the screens performed with the dimeric protein batch precipitated, especially in the SaltRx™ screen. It appeared that the dimeric form was very sensitive to high salt concentration, which was in contradiction with the fact that the monomeric form was dominant after purification with decreased NaCl concentration.

For the Zg-VIPO3 dimeric batch, only one microcrystal was obtained using the PEGs™ screen (0.1 M Tris-HCl pH 8.5 and 25% (w/v) PEG 4000). This condition was manually optimized with the hanging drop technic to obtain bigger crystals, but only an amorphous precipitate was obtained after few days. The nanocrystal was then frozen in liquid nitrogen and transported to Synchrotron SOLEIL to perform X-Ray diffraction, but it did not persist to the freezing process and melted. After unsuccessfully testing 768 crystallization conditions, no further investigation

was performed according to these difficulties to obtain and keep stable crystals. Instead, it was decided to study a computational model of the recombinant Zg-VIPO3 protein.

Based on the protein sequence, two structural 3D models of Zg-VIPO3 were build using the two closest 3D VHPO available structures: the monomer of Zg-VIPO1 and the dimer of NapH1 (**Figure 3-9**). The latter was characterized as a VCPO from the marine bacterium strain, *Streptomyces* sp. CNQ-525 (McKinnie et al., 2018). The first model, based on Zg-VIPO1, showed a global structure folded into 11 α -helices, four 3_{10} -helices and no β -sheet. The vanadium-binding active site was located at the C-terminus and seemed to be easily accessible through a large tunnel on the surface (**Figure 3-9A,C**). The second model, based on NapH1, showed a global structure folded into 12 α -helices, three 3_{10} -helices and six β -sheets. Both active sites were found on opposing sides and seemed to be less accessible than in the first model (**Figure 3-9B,D**).

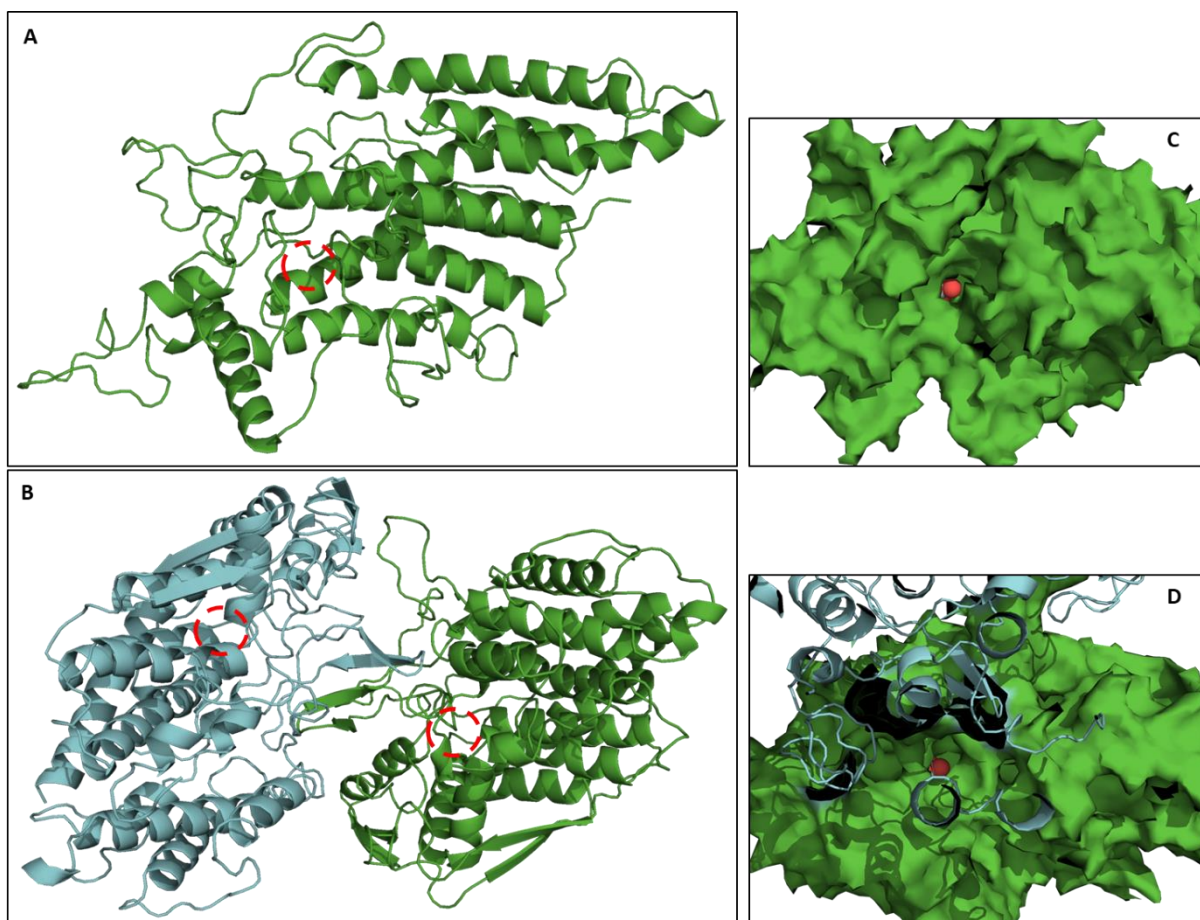


Figure 3-9: Ribbon-type representation of Zg-VIPO3 3D model as monomer (A) based on Zg-VIPO1 (PDB accession number 4CIT) and as dimer (B) based on NapH1 (VCPO, PDB accession number 3W35). One monomer was colored in cyan and the other one in green. Red dotted circles showed the localization of the active sites. Corresponding surface representations of the monomer (C) and of the dimer (D) in side view with the vanadate molecule, represented in red.

The dimeric structures were further compared by protein-protein interface analysis using PDBePISA tool (**Table 3-3**). The analyses performed on X-ray dimeric structures of NapH1 and An-VBPOI showed high Complex Formation Significance Score (CSS) scores of 1 and 0.92, respectively. 1 being the maximum score for complex formation, these results suggested that protein-protein interfaces are highly relevant for dimerization in both VHPOs. On the contrary, for Zg-VIPO3 model, the CSS score was null. This score is based on the total free energy of binding belonging to the interface in stable assemblies (Δ^iG), and takes into account the number of hydrogen bonds, disulfide bonds and salt bridges. All those factors (**Table 3-3**) suggested that the interface did not play any role in dimer formation for Zg-VIPO3. Even though NapH1 was the closest homologue of Zg-VIPO3, this VCPO was structurally and biochemically quite different from Zg-VIPO1 ([Fournier et al., 2014](#)).

	Zg-VIPO3 model	3W35 (NapH1)	1QI9 (An-VBPOI)
Solvent-accessible area	7.0%	10.4%	23.5%
Number of residues in the interface	10.3%	13.2%	24.1%
Number of residues in the surface	93.4%	89%	91.2%
Solvation free energy Δ^iG (kcal/mol)	-7	-15.6	-47.6
Hydrogen bonds	11	30	87
Salt bridges	1	8	9
Disulfide bond	0	0	2
Complex Formation Significance Score	0	1	0.92

Table 3-3: Protein-Protein interface analysis performed using PDBePISA online tool for the structure of Zg-VIPO3 dimeric model, VCPO of *Streptomyces* sp. CNQ-525 (NapH1, PDB accession number 3w35) and VBPOI of *Ascophyllum nodosum* (An-VBPOI, PDB accession number 1QI9).

IV. Conclusions

The main goal of this chapter was to biochemically and structurally characterize the third VHPO from *Z. galactanivorans*. After purification of the recombinant protein, overexpressed in *E. coli*, colorimetric tests based on *o*-dianisidine and thymol blue halogenation showed that the enzyme was active and strictly specific to iodide oxidation and therefore, this new iodoperoxidase was renamed Zg-VIPO3. The recombinant proteins were purified as either monomers or dimers, stable in solution. By contrast, the two other VIPOs of *Z. galactanivorans* were shown to be strictly monomeric. The phenomena of multimerization in solution were already observed for other VHPOs of macroalgae, such as *L. digitata* (Colin et al., 2003), *A. nodosum* (Wishang et al., 2012) or *C. pilulifera* (Isupov et al., 2000). Changes in buffer salinity, pH and temperature during purification were explored to stabilize Zg-VIPO3 folding as monomer or as dimer only. The decrease of salinity might help to increase monomer folding in certain conditions of buffer and pH. The other tested parameters did not seem to influence the dimeric or monomeric folding state in solution, but some led to protein aggregation or precipitation.

The kinetic parameters showed that the catalytic turnover of the dimeric enzyme was up to 10 times faster than that of the monomeric Zg-VIPO3, but compared to the other characterized iodoperoxidases from *Z. galactanivorans* or *Laminaria digitata*, this VIPO was much less efficient to oxidize iodide. A potential reason for that would be a completely different biological role of Zg-VIPO3 compared to its homologues. In order to verify this hypothesis, a first step would be to solve the 3D structure of this enzyme and investigate the amino acids involved in its catalytic mechanism.

A lot of crystallogenesis experiments were attempted but did not lead to obtain adequate crystals for subsequent X-Ray data acquisitions. The experiments were performed at 18°C, and decreasing the temperature to 4°C may help to stabilize and homogenize protein folding during

crystal generation and growth. In absence of X-ray data, the 3D model of Zg-VIPO3 was used to investigate dimer interface on PISA server. However this approach only suggested that the dimeric model was not naturally possible and the dimerization of Zg-VIPO3 would occur more likely by a different way. These modelling results were not conclusive, certainly because of significant structural divergences between Zg-VIPO3 and the other closest VHPO 3D structures. Further investigations will be necessary to better understand the self-organization of Zg-VIPO3 in solution, to progress on its 3D structure resolution and to elucidate the molecular bases of dimerization.

Chapter 4:

Studies on VIPO localization and biological roles in *Zobellia*

galactanivorans

I. Introduction

Numerous bacterial strains have been isolated and characterized based on their capacity to interact with iodine or metabolize iodinated compounds. According to [Amachi et al., 2005b](#), they are grouped into three categories: iodide-volatilizing bacteria belonging to *Proteobacteria* and *Cytophaga-Flexibacter-Bacteroidetes* (CFB) group ([Amachi et al., 2004](#)), iodine-accumulating bacteria, such as the *Flavobacteriaceae Arenibacter* sp. strain C-21 ([Ito et al., 2016](#)) and iodide-oxidizing bacteria, such as *Iodidimonas* sp. Q-1 ([Ehara et al., 2014](#)) or *Roseovarius* sp. A-2 ([Yuliana et al., 2017](#)). A multicopper oxidase activity was linked to the iodide-oxidation activity for the two latter bacteria ([Yuliana et al., 2017](#); [Taguchi et al., 2018](#)).

Zobellia galactanivorans was shown to accumulate iodine ([Barbeyron et al, 2016](#)), and to encode three vanadium-dependent iodoperoxidases (VIPOs), specific for iodide oxidation ([Fournier et al., 2014](#); **Chapter 3**). The presence of three VIPOs and of other proteins potentially related to iodine metabolism such as a L-2 haloacid dehalogenase (**Chapter 1**) suggests that *Z. galactanivorans* has developed an active iodine metabolism, which may be related to antioxidant protection and its capacity to degrade algal polysaccharides and to cope with the high concentrations of iodide in brown algal cell walls ([Barbeyron et al, 2016](#)).

Up to now, however, the biological roles of such iodide-specialized enzymes have been poorly documented, especially in bacteria and in relation to iodine-rich environments. Taking advantage of biochemical and genetic tools developed in *Zobellia* in our laboratory, this chapter reports on the localization and expression of one of these VIPO proteins through immunolabelling and Western-blot analyses. Functional comparisons of the wild-type and the *zg-vipo1* knock-out mutant strains were conducted to explore the role of the Zg-VIPO1 protein in iodine-rich medium and in relation to iodine uptake.

II. Materials and methods

II.1. Chemicals and antibodies

The monoclonal anti-polyHistidine–Peroxidase antibody (anti-His tag) produced in mice was obtained from Merck (reference: A7058). The rabbit polyclonal anti-Zg-VIPO1 (batch number: 1230005, New Zealand White rabbit) was produced by Covalab using the purified native recombinant protein. The total IgG fraction was purified using protein A beads column and stored at 4°C with a 0.02% (w/v) sodium azide preservative. The final concentration was 2.46 mg.ml⁻¹.

The secondary antibody coupled to Peroxidase was obtained from Bio-Rad. This anti-rabbit IgG (H + L)-HRP Conjugate was produced in goats (reference: 170-5046).

Protein A gold conjugates (15 nm) for electronic microscopy were purchased from Cell Microscopy Center, Utrecht, Netherland.

II.2. Bacterial strains and culture conditions

All cultures of marine bacterial strains were carried out at 25°C with shaking at 180 rpm. Strains *Arenibacter sp.* C-21 (NBRC culture collection, Chiba, Japan), *Cellulophaga fucicola* and *Zobellia galactanivorans* Dsij^T (Roscoff culture collection, Roscoff, France) were grown in ZoBell (per liter: 1.0 g yeast extract, 5.0 g tryptone, sea water) or artificial ZoBell (per liter: 1.0 g yeast extract, 5.0 g tryptone, 24.7 g NaCl, 0.7 g KCl, 6.3 g MgSO₄.7H₂O, 4.6 g MgCl₂.6H₂O, 1.2 g CaCl₂.2H₂O, 0.2 g NaHCO₃) media supplemented with or without 0.1 μM of KI.

II.3. In silico prediction of protein subcellular localization

The subcellular localization of Zg-VIPOs was predicted using the following generic tools: PSORTb 3.0 (Yu et al., 2010), CELLO2GO (Yu et al., 2014), SOSUI-GramN (Imai et al., 2008), LocTree3 (Goldberg et al., 2014), iLoc-Gneg (Xiao et al., 2011), PSLpred (Bahsin et al., 2005) and ProtCompB (<http://www.softberry.com>). The determination of the presence of a

signal peptide or a lipoprotein signal was done using SignalP 5.0 (Armenteros et al., 2019), PrediSi (Hiller et al., 2004), Phobius (Käll et al., 2004), SOSUIsignal (Gomi et al., 2004), SecretomeP (Bendtsen et al., 2005), Signal-3L (Zhang et al., 2020), Signal-BLAST (Frank and Sippl, 2008), LipoP (Juncker et al., 2003), DOLOP (Babu and Sankaran, 2002) and SPEPLip (Fariselli et al., 2003). All of these programs are freely available on web server addresses.

II.4. Protein subcellular fractionation

After three days of bacterial cultures (corresponding to the end of the exponential growth phase), the pellet was collected by centrifugation at 9,000 *g* for 15 min, and rinsed twice with a wash buffer (19.45 g/L NaCl, 5.9 g/L MgCl₂, 0.3 g/L CaCl₂, 10 mM potassium phosphate pH 7.0). The pellet was then resuspended in (5mL/g of pellet) lysis buffer (3 mM EDTA, 100 mM Tris, 500 mM sucrose, pH 6.8) with 15 mg/mL of lysozyme and incubated for 20 min at 30°C with stirring. An equal volume of distilled water was added and incubated at 30°C for an additional 20 min with stirring. After centrifugation at 20,000 *g* for 20 min at 4°C, the supernatant was collected as the periplasmic fraction. The resulting precipitate was resuspended in 50 mM Tris pH 7.5 buffer. The mixture was sonicated using a sonifier device to achieve lysis. After centrifugation for 1h at 20,000 *g* at 4°C, the supernatant corresponding to the cytoplasm and the precipitate corresponding to the membranes were separated. The latter fraction was resuspended with 1 mL of 50 mM Tris pH 7.5 buffer. The total protein concentration was determined by a colorimetric test with the Bio-Rad Protein Assay Dye Reagent according to standard recommendations. Aliquots of all the fractions were kept at -20°C before use.

II.5. Western blot analysis

An equal amount of protein fraction was deposited in each well of SDS-PAGE. Two gels were loaded and run in parallel to compare the immunorevelation signals with the protein quantities,

revealed by a Coomassie blue coloration. The fractionated protein samples were supplemented with a 6-fold concentrated loading buffer (360 mM Tris HCl pH 6.8; 45% glycerol; 9% SDS; 9% DTT; 0.12% bromophenol blue) and they were previously denatured at 95°C for 5 min before being charged on a 12% SDS-PAGE (Bio-Rad system). Following the separation, the proteins were electro-transferred from the polyacrylamide gel to a nitrocellulose membrane (GE Healthcare) using Trans-Blot Turbo Transfer System (Bio-Rad). The membrane was first incubated for 5 min with 5% milk in TBS-T buffer (20 mM Tris pH 7.6; NaCl 150 mM; 1% tween 20) to block free sites on the membrane. The immunodetection of target protein was realized either with the commercial anti-His tag directly to HRP for detection or with the anti-Zg-VIPO1. Both antibodies were diluted at 1/5000 in TBS-T buffer and incubated 1 h at room temperature with a gentle shaking. The membrane was then rinsed 3 times with TBS-T buffer for 5 min before adding the secondary antibody directed against rabbit IgG and couple with HRP at a final dilution of 1/5000 following the incubation with anti-Zg-IPO1. After 30 min of incubation, the membrane was washed again 3 times during 5 min with TBS-T buffer. The protein-antibody interaction was then revealed by ECL reagents (100 mM Tris pH 8.5; 44.3 mg/mL luminol; 14.8 mg/mL coumaric acid; 30% H₂O₂) and visualized by a Fusion FX camera using ChemiCapt software (Vilber Lourmat).

II.6. Deletion of the Zg-VIPO1-encoding gene

Single deletion mutant of *zg-vipo1* (*zobellia_1262*) was constructed following the previously described method from [Zhu et al., 2017](#). A 2.0-kb fragment corresponding to the first 30 bp of *zobellia_1262* with the region directly upstream was amplified using the primers OEG001 (TTTTTTGGATCCAGATGAACAACACCAAGCTTATGGA) and OEG003 (TTTTTTCTGCAGCGATATTAGTGCGATAAGAATCTTCT). The fragment was digested with *Bam*HI and *Pst*I and ligated into pYT313 that had been digested with the same enzymes, to generate pEG1. Similarly, a 2.0-kb fragment corresponding to the last 30 bp of *zg-vipo1* and

the region directly downstream was amplified with the primers OEG002 (TTTTTTGCATGCGGTTGCCCAAAGAAAATTCCAAAGA) and OEG004 (TTTTTTCTGCAGCTATCCGATAAGAAAGTAGCCCAA). The fragment was inserted between *Pst*I and *Sp*HI sites of pEG1 to generate the suicide plasmid pEG3. Suicide plasmid was introduced into the wild type *Z. galactanivorans* Dsij^T by conjugation with *E. coli* S17-1 λ *pir* strain. Erythromycin resistance was used to select cells with the plasmid integrated in the genome. Resulting colonies were grown overnight in *artificial ZoBell* medium without antibiotics at 30°C to allow the loss of the plasmid. The cells were then plated onto *artificial ZoBell*-agar containing 5% sucrose. Sucrose-resistant colonies were checked for erythromycin sensitivity. The deletion of *zg-vipol* was confirmed by PCR using primer pairs:

OEG005 (TATTTTGGCGTTAAACCCTATCATGG) and

OEG006 (GGGTAAGTGTACTGGTGAAGTCC) and then verified by sequencing.

II.7. Iodine accumulation assays

The strains *Z. galactanivorans* Dsij^T, *Δipo1* and *C. fucicola* were cultured aerobically in 100 mL of artificial Zobell containing iodide (0.1 μM). After cultivation for 48 h, each culture was centrifuged at 4°C for 30 min at 10,000 g. Fresh pellets were then lyophilized, together with 50 mL of artificial ZoBell medium. The dried powder samples were analyzed for total iodine content using Inductively Coupled Plasma Mass Spectrometry (ICP-MS) at the LABOCEA chemical analysis laboratory (Brest, France).

The C-21, *Z. galactanivorans* Dsij^T, *Δipo1* and *C. fucicola* strains were cultured aerobically in 100 mL of artificial ZoBell containing nonradioactive iodide (0.1 μM) and ¹²⁵I⁻ (74 kBq mL⁻¹). After cultivation for 24 h, 700 μL of each culture was sampled and put on a silicone oil layer (500 μL; 35:65 mixture of SH556 and SH550; Toray Dow Corning Silicone) that had been placed over 100 μL of distilled water in a microcentrifuge tube. After centrifugation at 4°C for 3 min at 13,000 g, 50 μL of the supernatant sample was removed and placed in a scintillation

vial. The distilled water layer containing the cell pellets were frozen at -40°C . The pellets in the microcentrifuge tubes were cut with dog nail clippers and were transferred to another scintillation vial. The activity of ^{125}I in each sample was measured with a NaI scintillation counter (Auto well gamma system ARC-370M, Aloka) for 10 min every 24h over 3 days. At the starting point (before bacterial cultivation), the medium was sampled to quantify the initial ^{125}I amount and then subsequent measurement values were subtracted to calculate the net uptake by the bacterial cells.

II.8. Mass spectrometry analysis of the iodine-enriched protein fractions

After 3-days cultures in the presence of ^{125}I , wild-type and mutant pellet cultures of *Z. galactanivorans* were fractionated using the method described earlier. The radioactivity of ^{125}I in each fraction was measured with the NaI scintillation counter for 10 min. The protein fraction, with the most radioactive signal, was denatured at 100°C for 5 min and loaded on a 12% SDS-PAGE. After migration, the gel was placed on a miniGita scanning device (Elysia-Raytest) to determine which gel lanes and zones were the most radioactive. Then another SDS-PAGE gel was run with the corresponding protein fractions but coming from a non-radioactive culture. The corresponding Coomassie-blue bands were subsequently cut and sent for trypsin digestion and Liquid Chromatography coupled to tandem Mass Spectrometry (LC-MS/MS) analysis of the peptides (Integrale Co, Ltd, Japan). The results of these proteomic data were analyzed by the freeware Scaffold Viewer 4.11.1, in particular for the iodination modifications.

II.9. Structure modelling

A 3D structure modelling of the *Z. galactanivorans* OmpA-like protein (Zobellia_1580) was performed using the OmpA protein from *Capnocytophaga gingivalis* (PDB accession: 5WTL, 60% sequence similarity) as a template using the SWISS-MODEL server (<https://swissmodel.expasy.org/interactive>). The figures were constructed using PyMOL 2.0.6.

III. Results and discussion

III.1. Subcellular localization prediction of Zg-VIPOs

In silico localization predictions were realized with the most accurate generalist program tools for Gram-negative bacteria allowing identification of protein assignment between several compartments (Goudenège et al., 2010; Lertampaiporn et al., 2019). The results of the seven different analyses showed that there was no prediction consensus for any of the 3 VIPO proteins (Table 4-1). Zg-VIPO1 would be likely assigned to periplasmic space but other secondary subcellular destinations were also predicted such as cytoplasm and outer membrane. Similarly, Zg-VIPO2 would be likely assigned in the cytoplasm, however, the periplasm and the outer membrane were also predicted as possibilities. Zg-VIPO3 had a higher probability of being localized in periplasm. Overall, there was relatively low agreement between programs. This difficulty to address a single compartment and to find a consensus between all the programs is illustrated by the results of PSORTb. This software is described as being the most effective generalist tool available (Peng & Gao, 2014) but it was unable to predict a clear localization for Zg-VIPO1 and Zg-VIPO3.

Protein	PSORTb	CELLO2GO	LocTree3	SOSUI-GramN	iLoc-Gneg	PSLpred	ProtCompB
Zg-VIPO1	Not determined	Periplasmic	Periplasmic	Cytoplasmic	Outer membrane	Cytoplasmic	Periplasmic
Zg-VIPO2	Cytoplasmic	Cytoplasmic	Periplasmic	Periplasmic	Outer membrane	Cytoplasmic	Membrane
Zg-VIPO3	Not determined	Periplasmic	Periplasmic	Periplasmic	Cytoplasmic	Periplasmic	Extracellular

Table 4-1: Predictions of Zg-VIPOs subcellular protein localization using 7 different generalist tools developed to discriminate the sorting between 4 or 5 compartments (membranes are not dissociated for ProtCompB whereas outer and inner membranes are separated in others). More detailed results are provided in Table S4-1.

Taking into account the difficulty in assigning the VIPOs into one subcellular compartment, a second approach was used to determine the presence and the nature of signal peptides using bioinformatic tools specialized for secretory pathway prediction, for lipoprotein sequence detection or for both (**Table 4-2**). The SignalP program is the most performant to date ([Armenteros et al., 2019](#)) as it can discriminate between three types of bacterial signal peptides, corresponding to different secretory pathways, and also predict a peptide cleavage site. The summary of prediction results (last column, **Table 4-2**) suggested that the three Zg-VIPOs might have a potential cleavable N-terminal signal peptide, although not all programs predicted them.

		Secretory Pathway tools						Lipoprotein tools			Both	
		PrediSi	Phobius	SOSUIsignal	SecretomeP	Signal-3L	Signal-BLAST	LipoP	DOLOP	SPEPLip	SignalP	Total
Zg-VIPO1	signal peptide	no SP	SP	no SP	no SP	SP	SP	LPSP	no SP	no SP	LPSP	SP 5/10
	SP type							SP II			SP II	
Zg-VIPO2	signal peptide	no SP	SP	no SP	no SP	SP	SP	LPSP	no SP	no SP	LPSP	SP 5/10
	SP type							SP II			SP II	
Zg-VIPO3	signal peptide	SP	SP	no SP	SP	SP	SP	SP	no SP	no SP	SP	SP 7/10
	SP type							SP I			SP I	

Table 4-2: Predictions of the presence/absence of signal peptides (SP) and the type of these signals in Zg-VIPOs protein sequences using 10 different specialized tools. The best predictions are summarized in the total predictions column. Legend: type I signal peptide (SPI), type II signal peptide (SPII). More detailed results are given in table S4-2.

According to LipoP and SignalP, Zg-VIPO1 and Zg-VIPO2 were predicted to possess a signal peptide of type II (SPII) corresponding to a lipoprotein formation whereas Zg-VIPO3 could be

exported by a signal peptide of type I (SPI). The length of the Zg-VIPO3 cleavable peptide might be of 21 amino acids with a cut between an alanine and a glutamine respectively in positions 21 and 22. In contrast, several sizes and cutting sites were proposed by the different programs for Zg-VIPO1 and Zg-VIPO2 signal peptides. The lipoproteins from Gram-negative bacteria are synthesized in the cytoplasm and then exported to the inner or to the outer membranes. The characteristic feature of all lipoproteins is a signal peptide sequence in the N-terminal end, followed by a cysteine residue (Hayashi & Wu, 1990). Consequently, the serine-cysteine peptide linkages, in positions 16-17 and 17-18 respectively, for Zg-VIPO1 and Zg-VIPO2, appeared to be the most reliable cleavage sites. Furthermore, the program Signal-BLAST, used to detect N-terminal peptides by homology with other known peptides of lipoproteins, indicated that Zg-VIPO1 had a signal peptide homologous to the penicillin-binding protein activator LpoB of *Xenorhabdus nematophila* (D3VIE0). This protein LpoB is located in the outer membrane where it activates bacterial cell wall polymerases (Paradis-Bleau et al., 2010). Additionally the first twenty amino acids of Zg-VIPO2 were found to be similar to the lipoprotein Blc of *Vibrio cholerae serotype O1* (Q08790), which has been demonstrated to be part of the outer membrane in *E. coli* (Campanacci et al., 2006).

The amino acid in +2 position after the signal cleavage site was found to be essential to assign lipoproteins either to the inner or the outer membrane (Seydel et al, 1999). The nature of this particular amino acid can change drastically the destination of the lipoprotein and also the orientation side of the protein in the corresponding membrane (cytoplasm or periplasm for the inner membrane and extracellular medium or periplasm for the outer membrane). The analysis of the +2 amino acids of Zg-VIPO1 and Zg-VIPO2 done by LipoP revealed, respectively, a lysine and a glycine at this position. Considering that the SPII pathway of *Z. galactonivorans* could strictly function as its equivalent in *E. coli*, it would direct Zg-VIPO1 in the outer membrane with an orientation to periplasmic space and Zg-VIPO2, equally into inner and outer

membranes, and also exposed to the periplasmic space (as deduced from the study of Seydel *et al.*, 1999).

Taken together, these *in silico* subcellular targeting results tend to predict Zg-VIPO1 and Zg-VIPO2 as anchored lipoproteins in the outer membrane, turned towards the periplasmic space. Zg-VIPO2 could also be present at the inner membrane surface. In contrast, Zg-VIPO3 would be a periplasm-released protein, after cleavage of a SPI peptide signal.

The *in vivo* expression and localization of Zg-VIPO1 in *Z. galactanivorans* was investigated using a polyclonal antibody, shown to be specific for Zg-VIPO1 detection, as revealed by a 50 kDa band at the expected size of the recombinant protein (**Figure 4-1**). The anti-Zg-VIPO1 was also able to recognize some epitopes of Zg-VIPO2 as it cross-reacted at about 15% of intensity with this recombinant protein (**Figure 4-1**). Contrastingly, the anti-Zg-VIPO1 western blotting analysis exhibited no immunodetection signal with the recombinant Zg-VIPO3, being more distant in amino acid sequence than Zg-VIPO1 and Zg-VIPO2 (**Figure 4-1**).

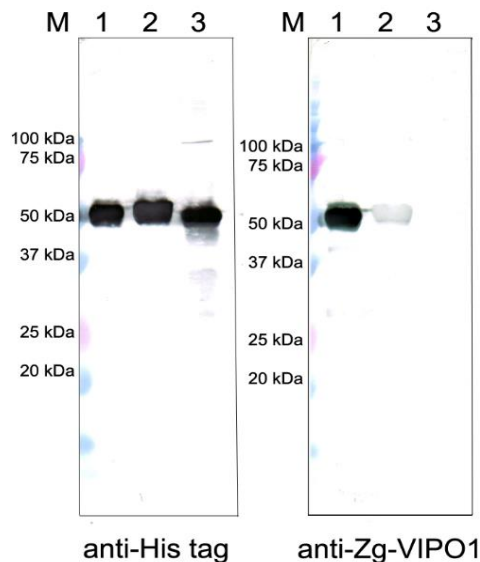


Figure 4-1: Western blot analysis of the three recombinant Zg-VIPO proteins with antibodies recognizing the N-terminal 6xHis tag sequence (left panel) and the entire protein Zg-IPO1 (right panel). The same quantities (10 μ g) of purified proteins were loaded into the wells of the SDS-PAGE before electro transfer onto nitrocellulose blotting membranes. (M) protein size marker; (1) Zg-VIPO1; (2) Zg-VIPO2; (3) Zg-VIPO3.

The fractionation of *Z. galactanivorans* subcellular compartments led to the separation of the periplasmic space, the cytoplasm and the total membranes. When no immunolabelling signal was revealed in periplasmic protein fractions, major 50 kDa bands were mainly detected in the membrane protein fraction and weakly in the cytoplasm (**Figure 4-2**). Since the inner and the outer membranes were not separated during protein fractionation and fell into the same fraction, it was impossible to conclude in which membrane *Zg*-VIPO1 was located. Nevertheless, those results were in accordance with the previous *in silico* analyses that might signify a possible outer membrane lipoprotein signal for *Zg*-VIPO1. The signal detected in the cytoplasm might be due to a contamination of the cytoplasm compartment by the membrane proteins as they are separated during the last step of fractionation by pipetting. We could also suppose that a part of the *Zg*-VIPO1 protein might stay in the cytoplasm where it is initially produced. As the predictor tools did not provide full evidence for a discriminant localization, it is possible that the cytoplasm might be the second place of residence of *Zg*-VIPO1. Further work on subcellular fractionation between all the bacterial compartments using sucrose gradients could help explore this in more detail.

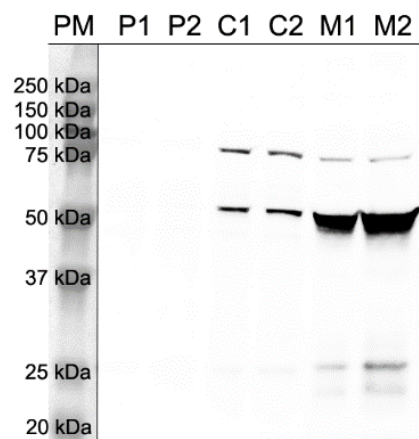


Figure 4-2: Anti-*Zg*-VIPO1 western blot analysis of the fractionated cellular compartments of *Z. galactanivorans*. 10 µg of protein samples were loaded in each well. Legend: periplasmic (P1, P2), cytoplasmic (C1, C2) and membrane (M1, M2) duplicates. Precision Plus Protein™ Dual Color Standard Marker (PM).

III.2. Effects of an iodide increase on the wild-type and the *Δipo1* knock-out mutant bacterial growth

In order to explore *in vivo* the biological roles of Zg-VIPO1 protein, a knock-out mutant of *Z. galactanivorans* was produced by deleting the *zobellia_1262* gene. The growth of cultures exposed to a gradient of increasing iodide concentrations, from 10 mM to 400 mM, was compared for both *Z. galactanivorans* wild-type (WT) and *Δipo1* mutant strains. No major differences in growth curves were observed between the two strains, when comparing under control condition, or in the presence of each iodide concentration from 10 to 200 mM (**Figure 4-3 A and B**). During the one week of culture, the OD (optical density) of both strains was approximately similar at the concentrations of 0 mM and 10 mM iodide (orange and light blue curves, **Figure 4-3**). From the second day at 100 mM and from the third day at 200 mM iodide, the two strains seemed to have similarly increased growth compared to the control (ZoBell medium only). Up to 200 mM of iodide, there seem to be no effect on the growth of either strain. (**Figure 4-3**). In the cultures with 400 mM iodide, a growth stagnation was observed for both the WT and the *Δipo1* mutant strains (green curves, **Figure 4-3**) during the 7 day kinetics. The bacterial OD was lower during the first day and the first 72 h of cultures with 200 mM and 300 mM of iodide, respectively, suggesting a slowing-down of growth for both strains at these concentrations (yellow and dark blue curves, **Figure 4-3**). At the fourth day of culture with 300 mM iodide, cell densities of the WT strain appeared to reach those of the control condition, whereas the *Δipo1* mutant cultures remained lower in comparison. This latter result suggested that the *Δipo1* mutant strain could be more affected by a concentration of 300 mM iodide than the WT strain. Nevertheless, the growth level of the mutant strain was comparable to the WT strain under the same conditions and to the control after one week (light and dark blue curves, **Figure 4-3**). These results suggested a progressive adaptation of the strains to strong iodide concentrations or a possible transformation and iodovolatilisation to resist these unusual and

unnatural quantities of iodine. Moreover, these experiments showed that a concentration of 300 mM iodide (1 million-fold higher than the concentration found in seawater) is the threshold beyond which cell division of *Z. galactanivorans* is no longer possible in a rich culture medium. The fact that both WT and $\Delta ipo1$ mutant strains had similar growth in the presence of 0 to 200 mM iodide demonstrated that the Zg-VIPO1 protein is potentially not involved in the tolerance of *Z. galactanivorans* to high amounts of iodide (up to 200 mM). However, this enzyme could participate in bacterial recovery when iodide concentrations of culture medium are closer to the tolerance limit (e.g. after 4 days with 300 mM iodide).

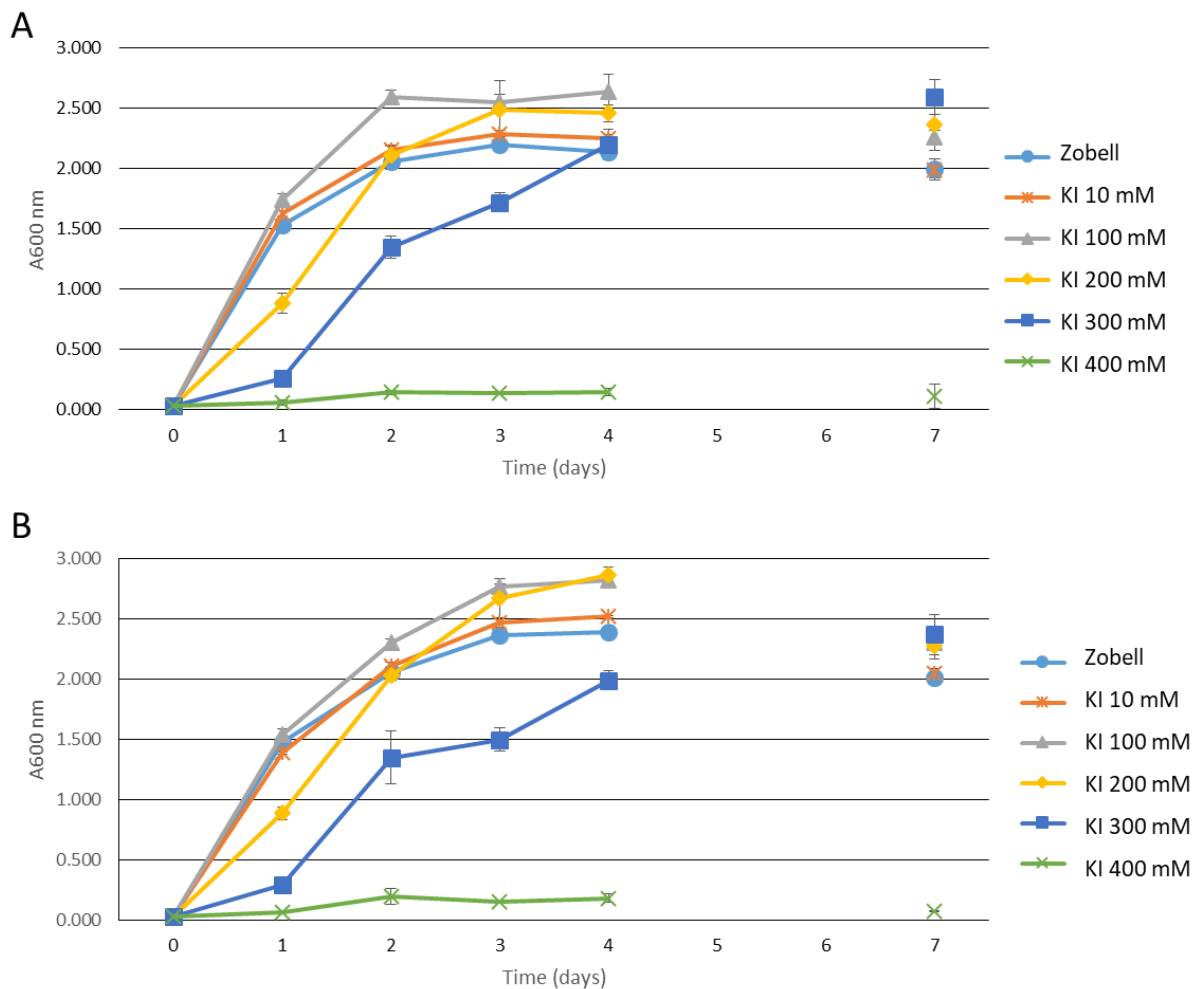


Figure 4-3: Growth curves of *Z. galactanivorans* wild-type (A) and $\Delta ipo1$ mutant (B) cultures with increasing concentrations of KI for 7 days. Values are mean \pm s.e.m.

III.3. Comparison of iodine accumulation and uptake in wild-type and *Δipo1* knock-out mutant strains

To monitor the iodine accumulation after 2 days of bacterial cultures and to test the potential involvement of Zg-VIPO1 in this process, ICP-MS analyses were performed on pellets of *Z. galactanivorans* WT and *Δipo1* mutant strains. In addition, another *Bacteroidetes* strain of *Cellulophaga fucicola* which does not possess any VHPO-encoding gene was used to compare the results. *Z. galactanivorans* pellets featured iodine contents of 6.85 ± 0.35 $\mu\text{g/g}$ (**Table 4-3**), whereas *Δipo1* mutant and *C. fucicola* strains showed lower iodine concentration in their cell pellets (1.5 ± 0.00 $\mu\text{g/g}$ and <1 $\mu\text{g/g}$ respectively).

Sample name	Total iodine content ($\mu\text{g/g}$ of pellet)
Artificial ZoBell medium	below the detection threshold
<i>Zobellia galactanivorans</i> WT	6.85 ± 0.35
<i>Zobellia galactanivorans Δipo1</i>	1.5 ± 0.00
<i>Cellulophaga fucicola</i>	<1

Table 4-3: Total iodine content of lyophilized bacterial pellets analyzed by ICP-MS for the *Z. galactanivorans* WT and *Δipo1* mutant, and *C. fucicola* strains after 2-days cultured in artificial ZoBell medium. Values are mean \pm std deviation.

In order to monitor iodine uptake in bacterial strains, the same culture conditions were performed for three days, in collaboration with Haruka Nakazawa, a Master student in the group of Prof. Seigo Amachi, who has a strong expertise in the use of radioactive iodide ^{125}I as a tracer. The *Arenibacter* sp. C-21 strain was used as a positive control for the iodide uptake experiment (Amachi et al., 2005a). The separated bacterial pellets and surrounding media were measured each day for radioactivity. As shown in **Figure 4-4**, for *C. fucicola* and *Δipo1* mutant strains, the radioactive iodine contents remained stable in the medium, around 0.1-0.12 μM , between 24 h and 72 h (**Figure 4-4A**). In comparison, based on the radioactive measurements,

the iodide concentration decreased very rapidly in surrounding media of both *Z. galactanivorans* WT and *Arenibacter* sp. C-21 strains, up to 0.02 μM , and remained at this low level for the duration of the experiment. In parallel, after 24 h of culture, the radioactive iodide content significantly increased in the cell pellets of *Arenibacter* sp. C-21 and *Z. galactanivorans* WT strains (168 and 160 pmol per mg of dry cells respectively, **Figure 4-4B**). At 48 h and 72 h of culture, the iodide content decreased slightly in the cell pellets of *Z. galactanivorans* WT and almost by half for the C-21 strain. For *C. fucicola*, the maximum iodide content in cell pellets reached only 0.48 ± 0.06 pmol per mg of dry cells after 48h of culture. The mutant strain *$\Delta ipo1$* cultures showed small increases of iodide content after 72h with 14 ± 0.33 pmol per mg of dry cells (**Figure 4-4B**).

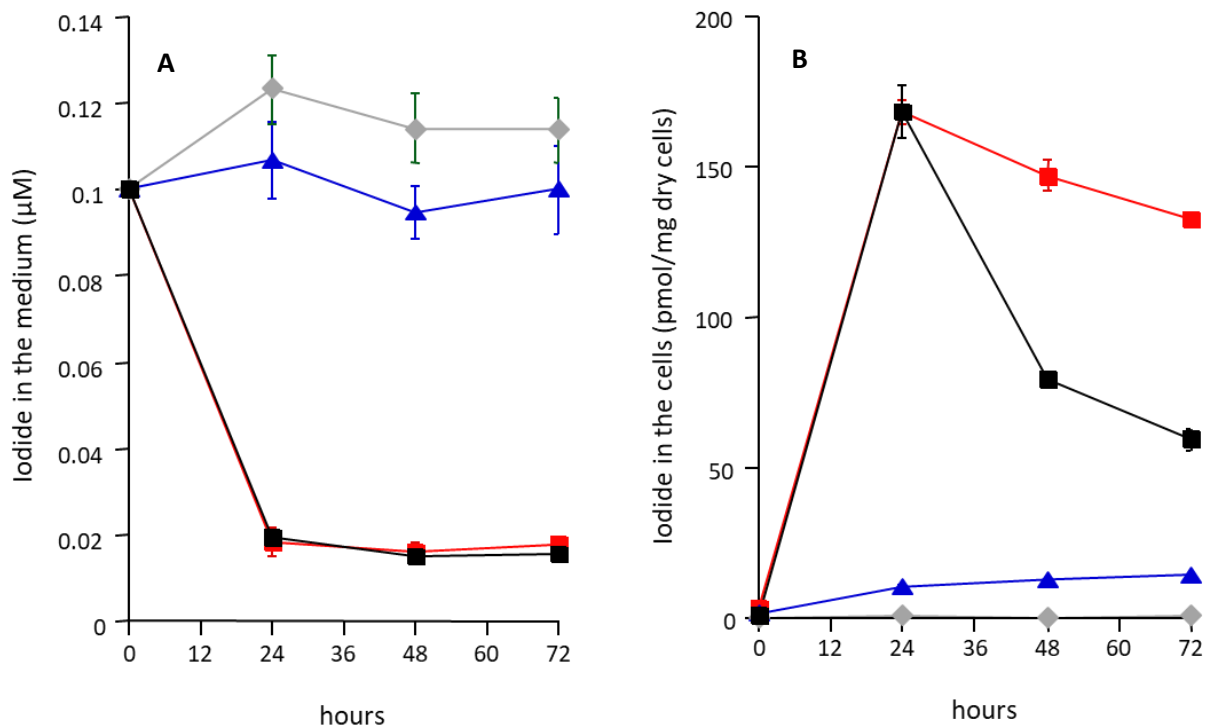


Figure 4-4: Time course of iodide accumulation by *Arenibacter* sp. C-21 (black squares), *Zobellia galactanivorans* Dsjj^T WT (red squares), *Zobellia galactanivorans* $\Delta ipo1$ (blue triangles) and *Cellulophaga fucicola* (grey diamond-shape) strains grown in artificial ZoBell medium containing iodide ^{125}I . The results are expressed as the means \pm standard deviations of triplicate analyses. (A) Relative iodide content in the culture medium. (B) Measure of the radioactive iodide concentration in culture pellets during 3 days of culture.

For the *Z. galactanivorans* WT strain, around 80% of total iodide was removed from the medium after 24h and transferred to cells, whereas almost no iodide was accumulated in the *Δipo1* mutant cells, demonstrating that the deletion of *zg-vipo1* gene provoked a decrease of internal iodine contents. Furthermore, the content of iodine in the cells of *C. fucicola* was null during the 72 h experiment and below the curve of the *Δipo1* mutant. These results are in clear agreement with the precedent ICP-MS analyses and therefore strongly suggests that Zg-VIPO1 plays a key role in iodine concentration mechanism(s) in *Z. galactanivorans*.

In addition, based on the ICP-MS and radioactivity flux analyses, weak differences between the *Z. galactanivorans* *Δipo1* mutant and *C. fucicola* could suggest an implication, albeit to a much lesser extent, of one of the other Zg-VIPOs, and more likely Zg-VIPO2 given its biochemical and structural similarities with Zg-VIPO1, in addition to its subcellular localization prediction.

III.4. Localization and LC-MS/MS analysis of iodine-enriched protein fractions

To further explore the iodine accumulation mechanisms in the different cell compartments, after 72 h, the ^{125}I -containing pellets of the *Z. galactanivorans* WT and *Δipo1* mutant strains were separated and extracted into three protein samples corresponding to cytoplasm, periplasm, and total membrane-enriched fractions. Each protein fraction was then measured for radioactivity. The highest radioactivity levels were detected in the membrane fractions for both strains, with significantly higher values for the *Z. galactanivorans* WT compared to the mutant (8.4-fold higher, **Table 4-4**). For the cytoplasmic-enriched fractions, there were approximately the same ratios of iodine content between the *Z. galactanivorans* WT and *Δipo1* mutant samples (9.3-fold higher, **Table 4-4**), but the ^{125}I measurements were ~ 40-fold lower than for membrane fractions. As discussed above, this labelling in cytoplasm fractions might be due to 1) an artifact of a slight contamination of the cytoplasmic compartment by membrane debris occurring during fractionation, or 2) a real presence of radioactive iodine in the cytoplasmic compartment. This

latter hypothesis remains to be demonstrated as in this case the iodide would need to be internalized by crossing the inner membrane by an energetic transport. The differences between the WT and *Δipo1* mutant membrane and cytoplasmic-enriched fractions in iodide content and the simultaneous presence of Zg-VIPO1 in these fractions suggest that iodide could be associated directly or indirectly with this enzyme.

	Periplasm	Cytoplasm	Membranes
Zobellia galactanivorans	1,239.0 ± 58.3	11,354.7 ± 1,008.9	450,180.4 ± 11,818.7
<i>ΔIPO1</i> mutant	818.2 ± 17.4	1,220.6 ± 31.4	53,207.2 ± 3,236

Table 4-4: Radioactive iodide detected in periplasm, cytoplasm and membranes fractions of *Z. galactanivorans* and *Δipo1* mutant. Values are mean ± std deviation.

In order to further investigate the nature of iodine-labelled proteins, the membrane-enriched protein fractions of both *Z. galactanivorans* and *Δipo1* mutant strains were analyzed by electrophoresis and the radioactivity was measured along the migration pattern. Only a background radioactivity was detected in the lane loaded with the protein fractions from the *Δipo1* mutant strain (**Figure S4-1**). A uniquely high-level zone of ^{125}I radioactivity was detected on the radioactive gel loaded with the WT membrane-enriched protein fractions (**Figure S4-2**), corresponding to the migration position of a band triplet, around 50 kDa, detected by Coomassie Blue in the equivalent non-radioactive gel run in parallel (**Figure 4-5**). Each band was cut on both gels and the radioactivity level was measured on those derived from radioactive gel (**Figure 4-5**).

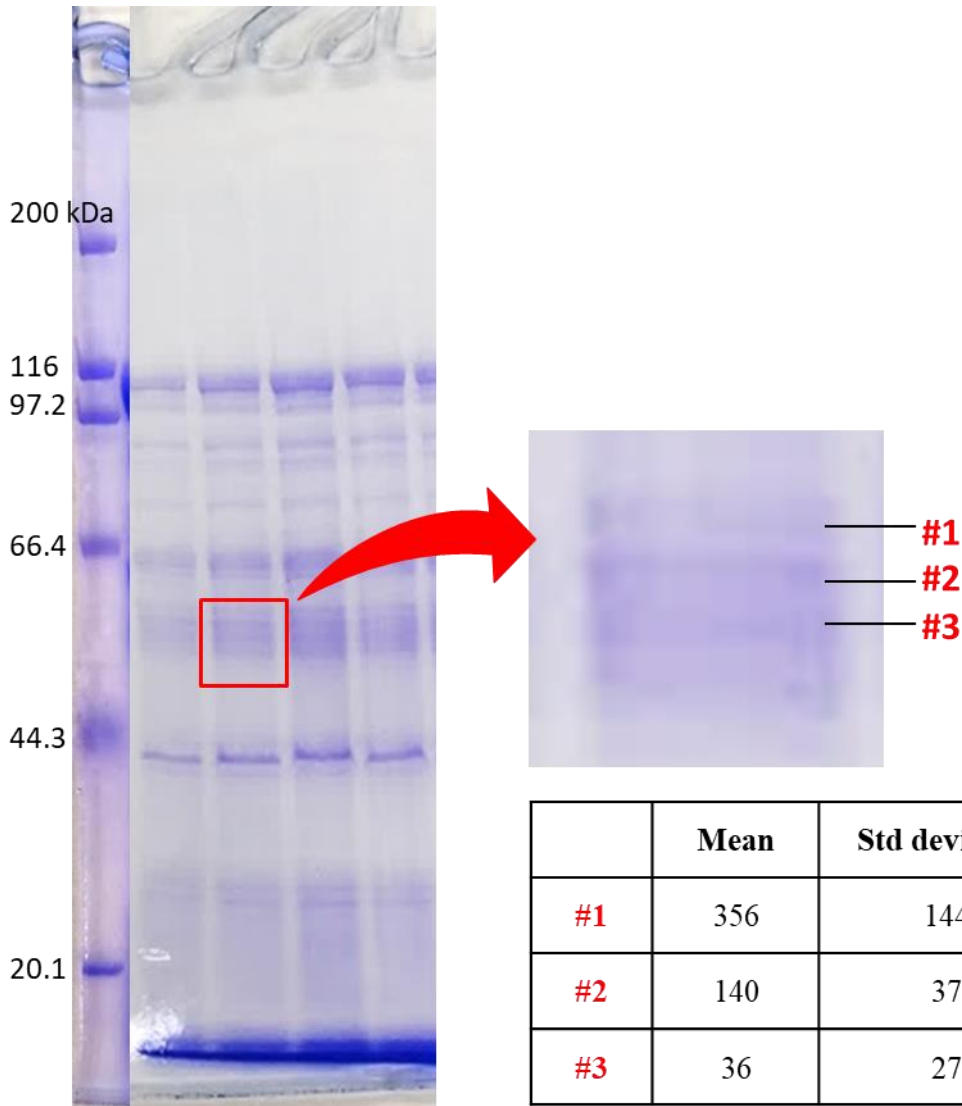


Figure 4-5: Picture of the SDS-PAGE polyacrylamide gel, stained by Coomassie Blue and loaded with 20 μ L of *Z. galactanivorans* membrane fractions (5 deposits). In the corresponding gel charged with radioactive fractions, the bands #1, #2 and #3 showed the most intense signal and then cut in the non-radioactive gel. The ^{125}I radioactivity values correspond to the mean and standard deviation of five independent measurements for each.

The highest radioactivity was recorded in band #1 and the corresponding proteins in the gel sample, unlabeled by ^{125}I , were analyzed by LC-MS/MS by our colleagues, H. Nakazawa and Prof. S. Amachi in Chiba University. According to the results, only one protein, identified as OmpA-like protein, was found to be iodinated on a tyrosine, in the following C-terminal peptide motif, LSAIGYGE EK.

The OmpA-like protein (*Zobellia_1580* locus; CAZ95635.1 or WP_013992944.1 protein IDs) was annotated by an expert manual annotation of the genome of *Z. galactanivorans*, with a

putative N-terminal peptide signal assigning the protein to the external membrane or to the periplasm, which was in agreement with its detection in the total membrane protein fraction. Zobellia_1580 corresponded to the most abundant protein detected in the band#1 gel sample, as it represented about 2.7% of all the peptide spectra. A total of 18 spectra corresponding to the iodinated zone of Zobellia_1580 were detected in the LS-MS/MS data, with two peptide motifs LSAIGYGEEK and LSAIGYGEEKPIASNTR, but only one was found to be iodinated on the tyrosine (Tyr425). This suggests that Zobellia_1580 is probably partly iodinated with a minor percentage of at least 5.5%. OmpA proteins are well-studied outer membrane proteins in *E. coli* and possess many biological functions such as adhesion, host cell penetration and even participation in biofilm formation (Smith et al., 2007).

A 3D structure model of Zobellia_1580 was built with SWISS MODEL using the OmpA protein structure from *Capnocytophaga gingivalis* (CgOmpA; PDB accession: 5WTL) as a template (**Figure 4-6**). Only the second half of the protein was modeled (from glycine193 to lysine452) as the PDB structure of CgOmpA featured only 261/455 amino acids corresponding to the C-terminal domain. Zobellia_1580 featured a high degree of conservation with its counterpart: 63.6% of sequence identity and 57% of sequence coverage (51.5% of sequence identity for the overall sequence coverage). The N-terminal domain of the Zobellia_1580 protein was not modeled but a conserved domain possibly related to a putative MetA-pathway of phenol degradation was predicted in this region (Evalue of 1.17e-06 for a pfam 13557 domain in the region 47-191 of Zobellia_1580). Moreover, this N-terminal region was also similar to the TIGR04565 domain, OMP_myx_plus, known to form a transmembrane β -barrel structure embedded in the bacterial outer membrane. The central part of Zobellia_1580 (**Figure 4-6**, left part) could be considered as a linker region comprising five consecutive thrombospondin type 3 repeats (TT3Rs). This TT3R domain was shown to be an efficient calcium ion (Ca^{2+}) binding motif in CgOmpA (Dai et al., 2017). The C-terminal modeled domain of Zobellia_1580

corresponded to an α/β fold of a peptidoglycan binding domain (**Figure 4-6**, right part). This latter domain could allow the anchoring of the outer membrane to the bacterial cell wall and ensure the cohesion of bacterial envelope supramolecular assembly (Park et al., 2012). According to their global structural conservation, the two OmpA-like proteins from *Z. galactanivorans* and *C. gingivalis* could feature conserved functions and cellular locations. In addition, the iodinated Tyr425 residue of Zobellia_1580 would be located in the peptidoglycan attachment domain, bathed in the periplasmic space.

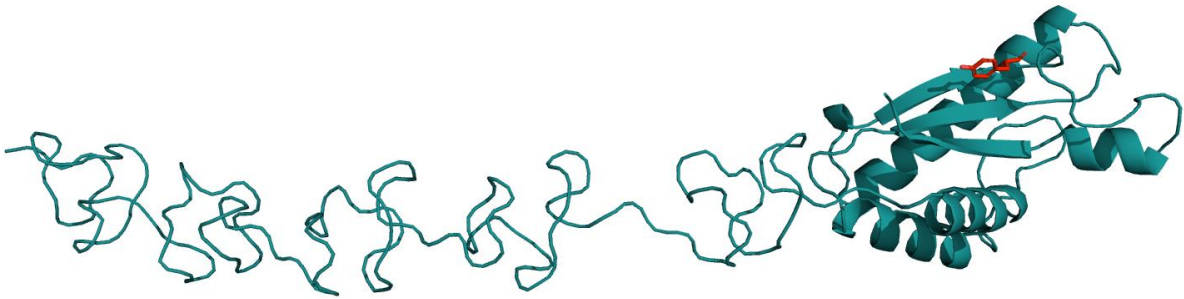


Figure 4-6: 3D model representation of zobellia_1580 OmpA-like protein based on CgOmpA (PDB accession: 5WTL). The overall structure is colored in turquoise and shown as ribbons. The Tyr425 is colored in red and shown as sticks.

The level of Tyr425 iodination was very low therefore it was difficult to distinguish between a real, functional iodination of this protein or a putative artifact linked to a side effect of an iodinating enzyme like Zg-VIPO1. Four other OmpA-like proteins were also detected in the same dataset of LC-MS/MS spectra, but no peptide with a similar C-terminal iodinated tyrosine was obtained. As the number of spectra for these proteins was very low and the number of peptides identified in their C-terminal was minor, it was not excluded that some of them could also be iodinated. Nevertheless, as the OmpA-like protein ZoBellia_1580 and Zg-VIPO1 were isolated and identified in the same subcellular fraction, a close relationship might exist and remains to be demonstrated.

According to [Feiters et al. \(2005\)](#), surface tyrosines of the *Ascophyllum nodosum* An-VBPO1 were found to be partially brominated and could also incorporate iodine to a lesser extent. Our precedent hypothesis was that Zg-VIPO1 could also present some tyrosine residues susceptible to be iodinated, particularly in a loop near the active site entry. Within that context, the Tyr263 was an interesting candidate, to explore a functional role of iodination, and its mutations with Ala/Phe/Ser affected the kinetic constants of the enzyme. One of the mutants even developed an activity towards bromide ([Fournier et al., 2014](#)).

As expected in this range of sizes (~50 kDa), peptides corresponding to both Zg-VIPO1 and Zg-VIPO2 proteins were detected from the trypsin digested band#1 extract in LC-MS/MS data, but no iodinated residue was identified. Unfortunately, no peptide including the Tyr263 residue was identified in this dataset, implying further tests are needed to validate this hypothesis of a potential Zg-VIPO1 iodination.

IV. Conclusions

The online prediction tools showed a low consensus for a clear and unique localization of each VIPO from *Z. galactanivorans*. It appeared probable that Zg-VIPO1 and Zg-VIPO2 could have a more similar but not identical localization, due to their predicted lipoprotein signal peptide, therefore anchored in a membrane (either outer, or inner). However, Zg-VIPO3 appeared to be more commonly predicted in the periplasm due to its potential SPI signal peptide. Even if these VIPOs belonged to the same enzyme class and shared the same substrate specificity, they may not display the same *in vivo* function because of their possible different localizations.

Nonetheless, the *in silico* approaches have their limits and setting up *in vitro* experiments was necessary. The bacterial subcellular fractionation and the Zg-VIPO1 protein immunodetection allowed investigation of protein localization in the bacteria. Zg-VIPO1 protein was experimentally confirmed to be predominantly present in the membrane-enriched protein fractions (either the inner or the outer membrane), suggesting a biological role at the interface of the two membranes. However, no role in iodide detoxification was clearly unraveled, based on growth comparison between wild-type and $\Delta ipo1$ mutant strains, although the capacity of *Z. galactanivorans* to cope with high concentrations of iodide revealed that another VIPO, or other enzymatic pathways, might be involved in this protection mechanism. The gene knockout approach was particularly successful for exploring the potential role of VIPO in iodine uptake and concentration. Indeed, our results showed that Zg-VIPO1 was essential for a maximum iodide accumulation in the bacterium and that this accumulation seemed to be associated with the membranes. However, it was not proven that iodine was directly bound to any amino acid of this protein, only that the loss of Zg-VIPO1 enzyme led to a drastic reduction in iodine accumulation. This illustrated that the iodine trapping was achieved via mechanisms involving the oxidation of iodide via VIPO activity and probably a secondary iodination of molecules present in the same compartment. Zg-VIPO1 is certainly essential, however, it is not the only

key player. The participation of other protein actors in this mechanism like the OmpA-like protein will need further experiments to be validated. The *Δipo1* mutant concentrated iodine to a lesser extent than *Z. galactanivorans* WT suggesting that Zg-VIPO1 could not be fully replaced by another VIPO. Thus Zg-VIPO2 or Zg-VIPO3 might also be involved in iodine uptake but differences in precise localization, reactivity or expression level of these proteins could explain their low contribution to the process.

A conserved chemical trapping by the cell wall structures in the apoplast of kelps as proposed by [Verhaeghe et al. \(2008b\)](#) could be different in *Z. galactanivorans* as these components are absent and the iodine concentration factor is very weak in comparison. Nevertheless, molecular structures present in the same compartment as Zg-VIPO1 could potentially play a role as iodine acceptors and explain the accumulation rate of iodine.

V. Supporting information

Protein	Subcellular compartments	PSORTb	CELLO2GO	LocTree3	SOSUI-GramN	iLoc-Gneg	PSLpred	ProtCompB	Total predictions
---------	--------------------------	--------	----------	----------	-------------	-----------	---------	-----------	-------------------

Zg-IPO1	Cytoplasmic	0	1.986	nd	Yes	nd	53.10%	0.56	2
	Periplasmic	2.5	3.092	89%	nd	nd	nd	9.02	3
	Outer membrane	2.5	1.089	nd	nd	Yes	nd	nd	1
	Inner membrane	2.5	0.596	nd	nd	nd	nd	nd	0
	Membrane	nd	nd	nd	nd	nd	nd	0	0
	Extracellular	2.5	0.237	nd	nd	nd	nd	0.42	0

Zg-IPO2	Cytoplasmic	8.96	3.342	nd	nd	nd	68.10%	3.28	3
	Periplasmic	0.26	1.698	89%	Yes	nd	nd	0.46	2
	Outer membrane	0.01	0.494	nd	nd	Yes	nd	nd	1
	Inner membrane	0.51	1.276	nd	nd	nd	nd	nd	0
	Membrane	nd	nd	nd	nd	nd	nd	6.26	1
	Extracellular	0.26	0.19	nd	nd	nd	nd	0	0

Zg-IPO3	Cytoplasmic	2	0.841	nd	nd	Yes	nd	0	1
	Periplasmic	2	4.114	91%	Yes	nd	68.10%	2.03	4
	Outer membrane	2	0.571	nd	nd	nd	nd	nd	0
	Inner membrane	2	0.475	nd	nd	nd	nd	nd	0
	Membrane	nd	nd	nd	nd	nd	nd	0.87	0
	Extracellular	2	0.999	nd	nd	nd	nd	7.1	1

Table S4-1: Predictions of Zg-VIPOs subcellular protein localization using 7 different generalist tools developed to discriminate the sorting between 4 or 5 compartments (membranes are not dissociated for ProtCompB whereas outer and inner membranes are separated in others). Resulting localization or probability scores are reported in the table. The best prediction of Zg-VIPOs are mentioned in bold in each line and in bold and underlined in the total predictions column. Potential secondary compartments are shown in bold in this latter column. Legend: not determined (nd).

Protein	Informations	Secretary Pathway tools					Lipoprotein tools			Both		total predictions
		PrediSi	Phobius	SOSU/signal	SecretomeP	Signal-3L	Signal-BLAST	LipoP	DOLOP	SPEPLip	SignalP	
Zg-IPO1	Signal peptide	no SP	SP	no SP	no SP	SP	SP	LPSP	no SP	no SP	LPSP	SP 7/12
	SP type							SPII			SPII	SPII
	Probability	0.4540	nd	nd	0.432871	0.984	100.0	6.3204	nd	nd	0.9935	
	Cleavage site	nd	nd	nd	nd	38/39 (17/18) (13/14)	S16/C17	S16/C17	nd	nd	S16/C17	S16/C17
	SP lenght (aa)	nd	17	nd	nd	38 (17) (13)	16	16	nd	nd	16	16
Zg-IPO2	Signal peptide	no SP	SP	no SP	no SP	SP	SP	LPSP	no SP	no SP	LPSP	SP 6/12
	SP type							SPII			SPII	SPII
	Probability	0.0927	nd	nd	0.146585	0.979	100.0	7.08603	nd	nd	0.9995	
	Cleavage site	nd	nd	nd	nd	18/19 (19/20) (38/39)	S17/C18	S17/C18	nd	nd	S17/C18	S17/C18
	SP lenght (aa)	nd	18	nd	nd	18	17	17	nd	nd	17	17
Zg-IPO3	Signal peptide	SP	SP	no SP	SP	SP	SP	SP	no SP	no SP	SP	SP 9/12
	SP type							SPI			SPI	SPI
	Probability	0.7426	nd	nd	0.934241	0.996	100.0	10.5526	nd	nd	0.9054	
	Cleavage site	A21/Q22	nd	nd	nd	21/22	A20/A21	A21/Q22	nd	nd	A21/Q22	A21/Q22
	SP lenght (aa)	21	21	nd	nd	21	20	21	nd	nd	21	21

Table S4-2: Predictions of the presence/absence of signal peptides (SP) and the type of these signals in Zg-IPOs protein sequences using 12 different specialized tools. Results are reported with the score probability, the location of cleavage site when found and the length of the signal peptide in amino acids. The best predictions are in bold in each line and are summarized in the total predictions column. Legend: type I signal peptide (SPI), type II signal peptide (SPII), not determined (nd).

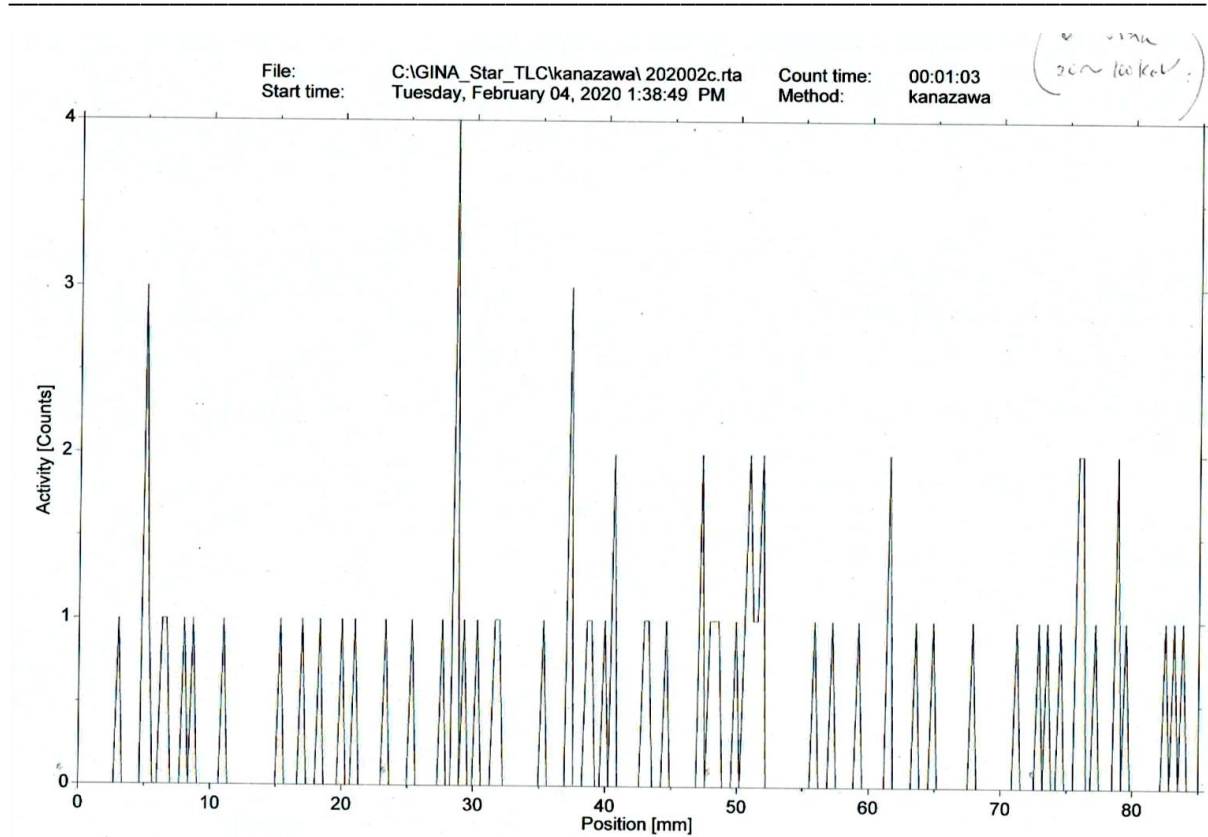


Figure S4-1: ^{125}I radioactivity measured on the mutant strain membrane fraction, migrated on a SDS-PAGE gel and placed on miniGita.

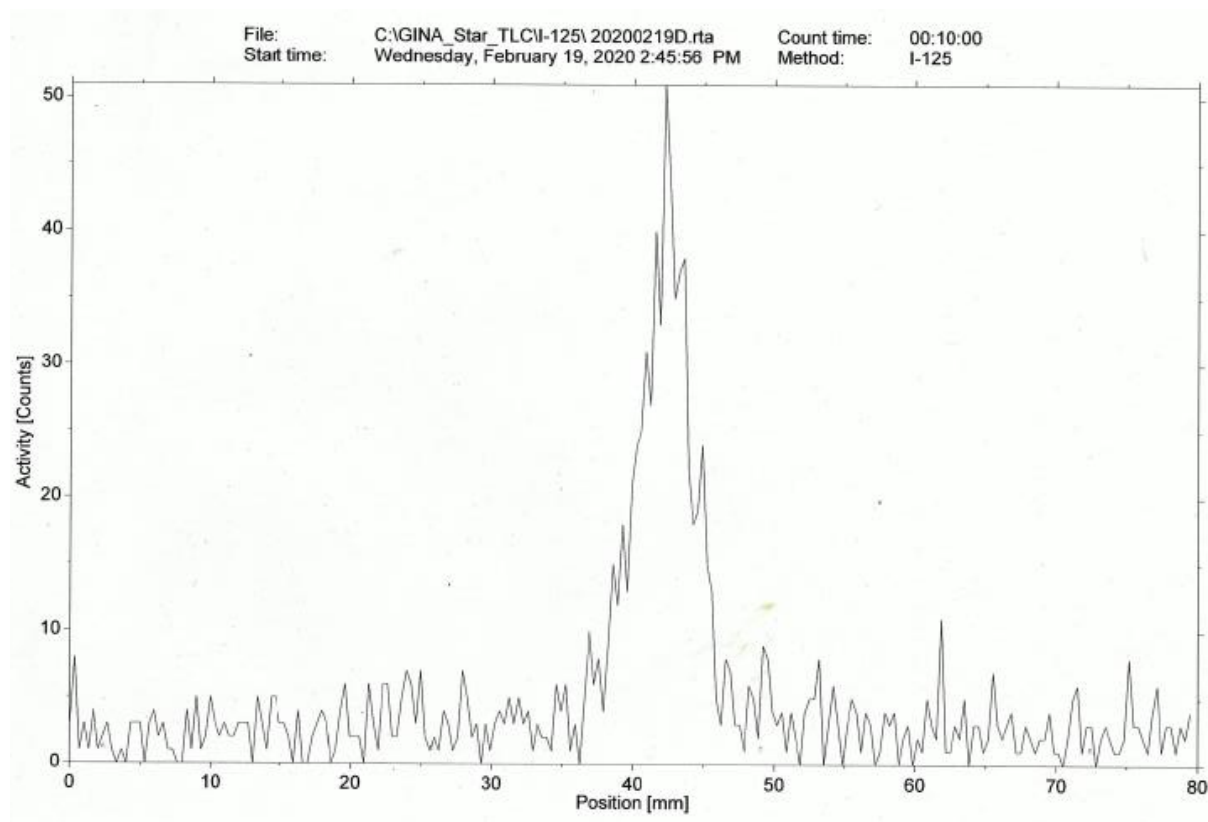


Figure S4-2: ^{125}I radioactivity measured on the wild-type strain membrane fraction, migrated on a SDS-PAGE gel and placed on miniGita.

Conclusion and Perspectives

The main goal of my thesis was to characterize at the biochemical, structural and functional levels some enzymes involved in the halogen-related metabolism in the bacterium *Zobellia galactanivorans*. The objective was to investigate the importance and the role of this specific metabolism in this model bacterium as marine bacteria may be significant actors in the global biogeochemical cycle of halogens, either as halogenated compounds producers, environmental detoxifiers or halogen accumulators. In this context, *Z. galactanivorans* possesses at least six enzymes identified as potentially interesting and my thesis was focused on two of them that might be involved in the VHOC production, iodide accumulation or detoxification.

First, I biochemically and structurally characterized the unique L-2-HAD protein, encoded on the genome of *Z. galactanivorans*. As expected from its belonging to this subfamily of HADs, this enzyme only transformed the short-chained halogenated compounds in S configuration, and was structurally similar to its closest homologues. Most structurally characterized homologues come from terrestrial bacteria, and are studied for their capacities to degrade toxic environmental halogenated compounds, and their potential in bioremediation. In order to determine if this enzyme gave a selective advantage to the bacterium, I decided to delete the *zghad* gene using a knock-out mutant approach. The implementation of this functional approach, still pioneer in *Zobellia*, was time-consuming, but worthwhile, as I obtained the first knock-out mutants at the end of 2019. Cultures of the wild-type and mutant strains with halogenated compounds illustrated a significant reduced growth for the mutant strain. This result brought forward that *Z. galactanivorans* might possess a selective advantage in the presence of toxic halogenated compounds, compared to other bacteria without a HAD enzyme. However, the ZgHAD enzyme could only catabolize a few ranges of substrates and *in vivo* tests need to be performed to explore the bioremediation capacities of *Z. galactanivorans*. Site-directed mutagenesis could be a complementary method to further investigate substrate specificity in the future and perhaps find a way to catabolize a greater variety of compounds.

Two closely-related VHPOs were biochemically and structurally characterized during a previous thesis work, as being VIPOs (Fournier et al., 2014). I studied the biochemistry of the recombinant enzyme obtained from the third VHPO encoded on the genome of *Z. galactanivorans*, and established that it was also specific to iodide oxidation: this is the third characterized VIPO in this bacterium. Its structural characterization however could not be completed due to difficulties in stabilizing the protein folding in solution. When the two other VIPOs were shown to be monomers, Zg-VIPO3 was purified as a mixture of monomers and dimers. This observation reminds the biochemical behavior of algal VBPOs that were shown to

be dimeric, but multimerizing in solution. Since the amino acid sequence of Zg-VIPO3 shares low similarities with its two closest crystallized homologues and is instead closer to a *Streptomyces* VCPO than the *Z. galactanivorans* VIPOs, the question of its biological role arises. Furthermore, steady-state kinetic analysis of this enzyme showed a very low activity towards iodide compared to Zg-VIPO1 and Zg-VIPO2. Consequently, the Zg-VIPO3 could have a different function in *Z. galactanivorans*. One hypothesis to be tested is a role in the biosynthesis of iodinated compounds, as found for the VCPO from *Streptomyces* sp. which is involved in the biosynthesis of halogenated antibiotics (McKinnie et al., 2018). In this case, producing a knockout mutant by deleting *zg-vipo3* and perform metabolic profiling of iodinated compounds could help identify the biological role of Zg-VIPO3.

One way to determine the biological role of a protein is to study its localization within the organism. A first *in silico* approach was not efficient to assertively predict protein localization, for none of the VIPOs. At the contrary, western-blot analyses of protein fractions gave some clues about the localization of VIPOs in *Z. galactanivorans* and once again the gene knockout was successful to compare phenotypes of wild-type and mutant strains, building some conclusions about the *in vivo* role of Zg-VIPO1. This was the first functional evidence that Zg-VIPO1 is involved in the iodide accumulation, associated to the membrane fraction of the bacterium. However, it is still unknown if this process is comparable to the one taking place in kelps, as the two marine organisms feature very different extracytoplasmic chemical compositions. Now, it will be necessary to further investigate the precise localization of Zg-VIPO1 in membranes by a more discriminating technique, as sucrose gradient, to efficiently separate outer and inner membranes. The iodide uptake and concentration in *Z. galactanivorans* seemed similar in terms of rapidity and efficiency to that of *Arenibacter* sp. strain C-21. Nonetheless, the enzymes involved in the uptake in this latter bacterium are unknown and may or may not be similar to those of *Z. galactanivorans*. Further comparisons of both bacterial genomes would be of interest.

Based on all results obtained during my thesis, the hypothetical model of halogen metabolism in *Z. galactanivorans* shown in figure 0-11, was updated in **figure 5-1**:

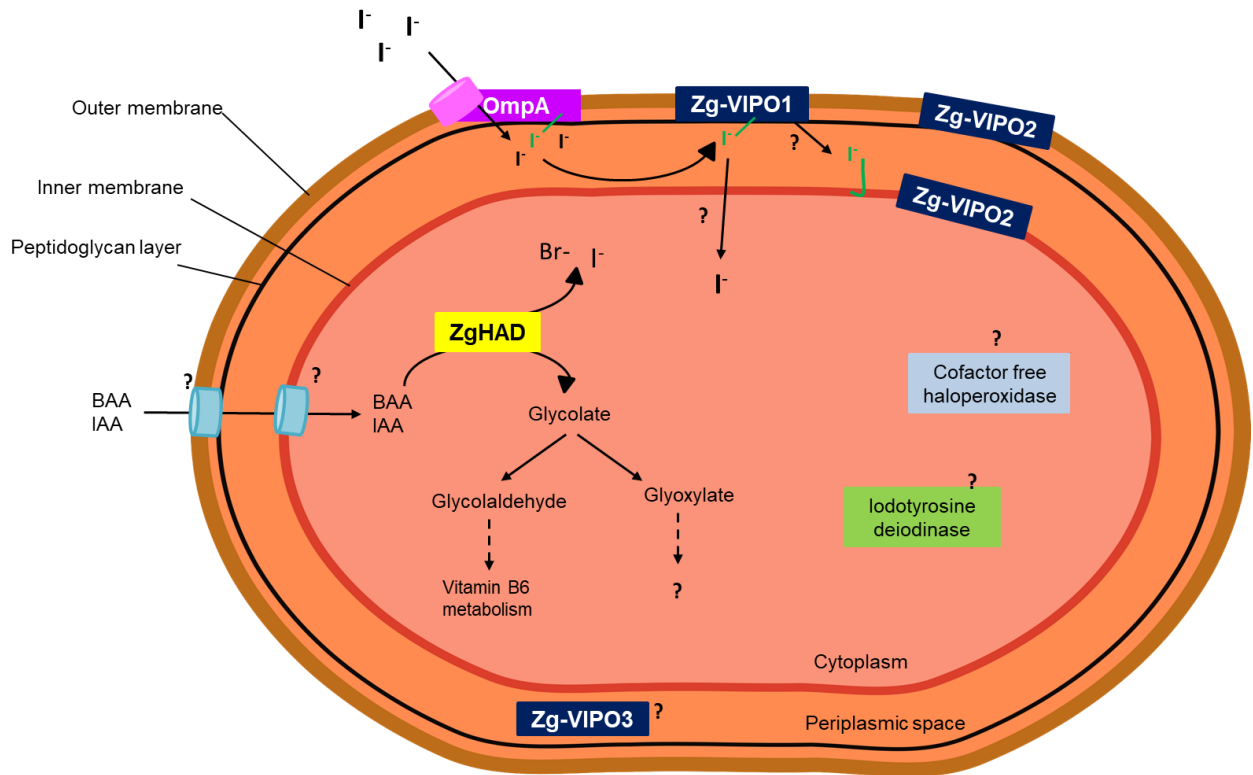


Figure 5-1: Hypothetical model of halogen-related metabolism within *Z. galactanivorans* (adapted from Fournier, 2014).

When the iodide uptake by the mutant strain of *Z. galactanivorans* was compared to the uptake in *C. fuscicola*, I noticed that the mutant strain was able to accumulate higher concentrations. It can be possible that one or the two other VIPOs is (are) also involved in this accumulation. However, the low catalytic turnover of Zg-VIPO3, in addition to a probable different subcellular localization, seems to indicate another biological function, as already mentioned above. This strengthens the idea that Zg-VIPO2 may participate, in a lesser manner, in iodide accumulation. To validate this hypothesis, a single knockout deletion of *zg-vipo2*, then production of a double mutant of *zg-vipo1* and *zg-vipo2* are needed.

The presence of iodinated proteins in the membranes of *Z. galactanivorans* was investigated, and an OmpA-like protein connecting the outer membrane and the periplasmic peptidoglycan layer was identified. The OmpA protein family is well-studied in bacteria and has multiple functions, such as maintaining the structural integrity of the outer membrane (Smith et al., 2017, Dai et al., 2017). Thus, this protein might be essential to incorporate iodide through the outer membrane. To further corroborate the hypothesis of a functional relationship between OmpA and Zg-VIPO1, deleting the OmpA-encoding gene in *Z. galactanivorans* and exploring if the bacterium is still able to accumulate iodine could be essential.

To analyze protein iodination in *Z. galactanivorans*, a more exhaustive LC-MS/MS analysis would be necessary, especially to target the C-term tyrosine of Zg-VIPOs. If more iodinated proteins are identified, it could validate their roles in iodide uptake.

Our results showed that iodine was associated with membrane protein fractions but the membranes have other components capable of reacting with oxidized iodine. Some electrophilic compounds with an aromatic core have been recently identified to be halogenated in some bacteria (He et al., 2020; Martins et al., 2019; Schöner et al., 2016) and it would be interesting to evaluate the presence of such iodinated phenolic compounds or analogues in *Z. galactanivorans* by metabolic profiling.

Important concentrations of I^- captured in the kelp apoplasm might be released in the environment of *Z. galactanivorans* when the biomass degradation of these brown algae occurs. The mechanisms of iodide concentration or detoxification could be important for bacteria in this case. However no involvement of Zg-VIPO1 has been correlated to the resistance of iodide high concentrations and the role of other enzymes like Zg-VIPO2 and Zg-VIPO3 in these processes would be interesting to study through gene deletion approaches.

Among the *Z. galactanivorans* halogenases, the putative cytoplasmic cofactor-free HPO is another interesting candidate to characterize: it should be first investigated further by biochemical exploration of its halogen specificity and substrates.

Thanks to the presence of three VIPOs and ZgHAD, with biochemical specificities towards iodine, it seems that the iodine-related metabolism is important in *Z. galactanivorans*, and by extension among other marine *Bacteroidetes*. The function of this specific metabolism in these bacteria is still unknown, as well as its importance during alga-bacteria interactions, or biofilm formation. Although we do not know which chemical compounds, excreted by algae, the bacteria are exposed to, the genome analysis has showed that this *Bacteroidetes* possesses genetic tools to keep up with oxidative stress. The surfaces of macroalgae provide a large interface with the bacterial microbiome and are also submitted to environment changes. Microbial communities form biofilms that differ depending on the seasons, their localization on the surface of the algae and the physiology of the algal hosts. During those interactions, many kinds of chemicals are secreted and can impact specific bacterial communities. Future experiments would consist of growing *Z. galactanivorans* WT and mutant strains with pieces of *L. digitata*, to analyze effects on growth/survival and genome regulation by transcriptomic approaches. To further explore compounds emitted by *Z. galactanivorans* in the presence of

macroalgae, and their impact on biofilm formation with other bacteria, metabolomic approaches could be a complementary well-adapted tool.

A last open question remains about the bacterial implication in the biogeochemical cycle of halogens. Since, *Z. galactanivorans* was shown to be a good bacterial model to study iodine metabolism, thanks to the numerous enzymes capable of iodination, it would be interesting to analyze the production of volatile halocarbons, and especially iodinated ones, by this bacteria in different physiological and environmental conditions. Moreover, the genome comparison of numerous microorganisms isolated from kelps, with the genome of *Z. galactanivorans*, would allow to question the occurrence and convergent evolution of iodine-specific enzymatic mechanisms in bacteria living on kelps surfaces and their potential importance in iodine biogenic cycling.

REFERENCES

- Adamu, A., Wahab, R.A., and Huyop, F. (2016) 1-2-Haloacid dehalogenase (DehL) from *Rhizobium* sp. RC1. *Springerplus* **5**: 695.
- Agarwal, V., Miles, Z.D., Winter, J.M., Eustáquio, A.S., El Gamal, A.A., and Moore, B.S. (2017) Enzymatic Halogenation and Dehalogenation Reactions: Pervasive and Mechanistically Diverse. *Chem Rev* **117**: 5619–5674.
- Agatsuma, Y., Endo, H., and Taniguchi, K. (2008) Inhibitory effect of 2,4-dibromophenol and 2,4,6-tribromophenol on larval survival and metamorphosis of the sea urchin *Strongylocentrotus nudus*. *Fish Sci* **74**: 837–841.
- Amachi, S., Kasahara, M., Fujii, T., Shinoyama, H., Hanada, S., Kamagata, Y., et al. (2004) Radiotracer experiments on biological volatilization of organic iodine from coastal seawaters. *Geomicrobiol J* **21**: 481–488.
- Amachi, S., Muramatsu, Y., Akiyama, Y., Miyazaki, K., Yoshiki, S., Hanada, S., et al. (2005a) Isolation of iodide-oxidizing bacteria from iodide-rich natural gas brines and seawaters. *Microb Ecol* **49**: 547–557.
- Amachi, S., Fujii, T., Shinoyama, H., and Muramatsu, Y. (2005b) Microbial Influences Environment on the Mobility and Transformation of Radioactive Iodine in the Environment. *J Nucl Radiochem Sci* **6**: 21–24.
- Amachi, S., Kawaguchi, N., Muramatsu, Y., Tsuchiya, S., Watanabe, Y., Shinoyama, H., and Fujii, T. (2007) Dissimilatory Iodate Reduction by Marine *Pseudomonas* sp. Strain SCT. *Appl Environ Microbiol* **73**: 5725–5730.
- Amachi, S. (2008) Microbial Contribution to Global Iodine Cycling: Volatilization, Accumulation, Reduction, Oxidation, and Sorption of Iodine. *Microbes Environ* **23**: 269–276.
- Ang, T.F., Maiangwa, J., Salleh, A.B., Normi, Y.M., and Leow, T.C. (2018) Dehalogenases: From improved performance to potential microbial dehalogenation applications. *Molecules* **23**: 1–40.
- Archer, S.D., Posman, K.M., DeStefano, J., Harrison, A.O., Ladina, A., Cheff, E.A., and Witt, D.P. (2019) Fluorescent detection of bromoperoxidase activity in microalgae and planktonic microbial communities using aminophenyl fluorescein. *Front Mar Sci* **6**: 1–11.
- Armenteros, J.J., Tsirigos, K.D., Sønderby, C.K., Petersen, T.N., Winther, O., Brunak, S., et al. (2019) SignalP 5.0 improves signal peptide predictions using deep neural networks. *Nat Biotechnol* **37**: 420–423.
- Arora, P.K. and Bae, H. (2014) Bacterial degradation of chlorophenols and their derivatives. *Microb Cell Fact* **13**: 1–17.

- Asplund, G., Grimvall, A., and Pettersson, C. (1989) Naturally produced adsorbable organic halogens (AOX) in humic substances from soil and water. *Sci Total Environ* **81–82**: 239–248.
- Atashgahi, S., Liebensteiner, M.G., Janssen, D.B., Smidt, H., Stams, A.J.M., and Sipkema, D. (2018) Microbial synthesis and transformation of inorganic and organic chlorine compounds. *Front Microbiol* **9**: 1–22.
- Babu, M.M. and Sankaran, K. (2002) DOLOP - Database of bacterial lipoproteins. *Bioinformatics* **18**: 641–643.
- Bachas-Daunert, P.G., Law, S.A., and Wei, Y. (2009) Characterization of a recombinant thermostable dehalogenase isolated from the hot spring thermophile *Sulfolobus tokodaii*. *Appl Biochem Biotechnol* **159**: 382–393.
- Baharum, H., Chu, W.C., Teo, S.S., Ng, K.Y., Rahim, R.A., and Ho, C.L. (2013) Molecular cloning, homology modeling and site-directed mutagenesis of vanadium-dependent bromoperoxidase (GcVBPO1) from *Gracilaria changii* (Rhodophyta). *Phytochemistry* **92**: 49–59.
- Ball, S.M., Hollingsworth, A.M., Humbles, J., Leblanc, C., Potina, P., and McFiggans, G. (2010) Spectroscopic studies of molecular iodine emitted into the gas phase by seaweed. *Atmos Chem Phys* **10**: 6237–6254.
- Ballschmiter, K. (2003) Pattern and sources of naturally produced organohalogens in the marine environment: Biogenic formation of organohalogens. *Chemosphere* **52**: 313–324.
- Barbeyron, T., L'Haridon, S., Corre, E., Kloareg, B., and Potin, P. (2001) *Zobellia galactanovorans* gen. nov., sp. nov., a marine species of *Flavobacteriaceae* isolated from a red alga, and classification of [*Cytophaga*] *uliginosa* (ZoBell and Upham 1944) Reichenbach 1989 as *Zobellia uliginosa* gen. nov., comb. nov. *Int J Syst Evol Microbiol* **51**: 985–997.
- Barbeyron, T., Thomas, F., Barbe, V., Teeling, H., Schenowitz, C., Dossat, C., et al. (2016) Habitat and taxon as driving forces of carbohydrate catabolism in marine heterotrophic bacteria: example of the model algae-associated bacterium *Zobellia galactanivorans* DsijT. *Environ Microbiol* **18**: 4610–4627.
- Barnett, P., Hemrika, W., Dekker, H.L., Muijsers, A.O., Renirie, R., and Wever, R. (1998) Isolation, characterization, and primary structure of the vanadium chloroperoxidase from the fungus *Embellisia didymospora*. *J Biol Chem* **273**: 23381–23387.
- Barth, P.T., Bolton, L. and Thomson, J.C. (1992) Cloning and partial sequencing of an operon encoding two *Pseudomonas putida* Haloalkanoate dehalogenases of opposite stereospecificity. *J Bacteriol.* **174**: 2612-2619.
- Belkin, S. (1992) Biodegradation of haloalkanes. *Biodegradation* **3**: 299–313.
- Bendtsen, J.D., Kierner, L., Fausbøll, A., and Brunak, S. (2005) Non-classical protein secretion in bacteria. *BMC Microbiol* **5**: 1–13.

- Bernhardt, P., Okino, T., Winter, J.M., Miyanaga, A., and Moore, B.S. (2011) A stereoselective vanadium-dependent chloroperoxidase in bacterial antibiotic biosynthesis. *J Am Chem Soc* **133**: 4268–4270.
- Bhasin, M., Garg, A., and Raghava, G.P.S. (2005) PSLpred: Prediction of subcellular localization of bacterial proteins. *Bioinformatics* **21**: 2522–2524.
- Bianco, A.C. and Kim, B.W. (2006) Deiodinases: Implications of the local control of thyroid hormone action. *J Clin Invest* **116**: 2571–2579.
- Björkstén, F. (1968) A Kinetic Study of the Horse-Radish Peroxidase-Catalyzed Oxidation of Iodide.pdf. *Eur J Biochem* **5**: 133–142.
- Blasiak, L. C.; Vaillancourt, F. H.; Walsh, C. T.; Drennan, C. L. (2006) Crystal structure of the non-haem iron halogenase SyrB2 in syringomycin biosynthesis. *Nature* **440**: 368–371.
- Brownell, D.K., Moore, R.M., and Cullen, J.J. (2010) Production of methyl halides by *Prochlorococcus* and *Synechococcus*. *Global Biogeochem Cycles* **24**: 1–7.
- Burroughs, A.M., Allen, K.N., Dunaway-Mariano, D., and Aravind, L. (2006) Evolutionary Genomics of the HAD Superfamily: Understanding the Structural Adaptations and Catalytic Diversity in a Superfamily of Phosphoesterases and Allied Enzymes. *J Mol Biol* **361**: 1003–1034.
- Cairns, S.S., Cornish, A., and Cooper, R.A. (1996). Cloning, sequencing and expression in *Escherichia coli* of two *Rhizobium sp.* genes encoding haloalkanoate dehalogenases of opposite stereospecificity. *European Journal of Biochemistry*. **235**: 744-749.
- Campanacci, V., Bishop, R.E., Blangy, S., Tegoni, M., and Cambillau, C. (2006) The membrane bound bacterial lipocalin Blc is a functional dimer with binding preference for lysophospholipids. *FEBS Lett* **580**: 4877–4883.
- Carpenter, L.J. and Liss, P.S. (2000) On temperate sources of bromoform and other reactive organic bromine gases. *J Geophys Res Atmos* **105**: 20539–20547.
- Carpenter, L.J. (2003) Iodine in the marine boundary layer. *Chem Rev* **103**: 4953–4962.
- Carpenter, L.J., MacDonald, S.M., Shaw, M.D., Kumar, R., Saunders, R.W., Parthipan, R., et al. (2013) Atmospheric iodine levels influenced by sea surface emissions of inorganic iodine. *Nat Geosci* **6**: 108–111.
- Carpenter, L.J., Reimann, S. (Lead A., Burkholder, J.B., Clerbaux, C., Hall, B.D., Hossaini, R., et al. (2014) Update on Ozone-Depleting Substances (ODSs) and Other Gases of Interest to the Montreal Protocol, Chapter 1 in *Scientific Assessment of Ozone Depletion: 2014*, Global Ozone Research and Monitoring Project-Report No. 55, World Meteorological Organization, Geneva, Switzerland.
- Carter, J.N., Beatty, K.E., Simpson, M.T., and Butler, A. (2002) Reactivity of recombinant and mutant vanadium bromoperoxidase from the red alga *Corallina officinalis*. *J Inorg Biochem* **91**: 59–69.

-
- Chan, W.Y., Wong, M., Guthrie, J., Savchenko, A., Yakunin, A., Pai, E., and Edwards, E.A. (2010) Sequence- and activity-based screening of microbial genomes for novel dehalogenases.pdf. *Microb Biotechnol* **3**: 107–120.
- Chance, R., Baker, A.R., Küpper, F.C., Hughes, C., Kloareg, B., and Malin, G. (2009) Release and transformations of inorganic iodine by marine macroalgae. *Estuar Coast Shelf Sci* **82**: 406–414.
- Choi, H., Mascuch, S., Villa, F., Byrum, T., Teasdale, M., Smith, J., et al. (2012) Honaucins A–C, Potent Inhibitors of Inflammation and Bacterial Quorum Sensing Synthetic Derivatives.pdf. *Chem Biol* **19**: 589–598.
- Colin, C., Leblanc, C., Wagner, E., Delage, L., Leize-Wagner, E., Van Dorsselaer, A., et al. (2003) The brown algal kelp *Laminaria digitata* features distinct bromoperoxidase and iodoperoxidase activities. *J Biol Chem* **278**: 23545–23552.
- Colin, C., Leblanc, C., Michel, G., Wagner, E., Leize-Wagner, E., Van Dorsselaer, A., and Potin, P. (2005) Vanadium-dependent iodoperoxidases in *Laminaria digitata*, a novel biochemical function diverging from brown algal bromoperoxidases. *J Biol Inorg Chem* **10**: 156–166.
- Cosse, A., Potin, P., and Leblanc, C. (2009) Patterns of gene expression induced by oligoguluronates reveal conserved and environment-specific molecular defense responses in the brown alga *Laminaria digitata*. *New Phytol* **182**: 239–250.
- Councell, T.B., Landa, E.R., and Lovley, D.R. (1997) Microbial reduction of iodate. *Water Air Soil Pollut* **100**: 99–106.
- Dai, S., Sun, C., Tan, K., Ye, S. and Zhang, R. (2017) Structure of thrombospondin type 3 repeats in bacterial outer membrane protein A reveals its intra-repeat disulfide bond-dependent calcium-binding capability. *Cell Calcium* **66**: 78-89.
- de Boer, E., Plat, H., Tromp, M.G.M., Wever, R., Franssen, M.C.R., van der Plas, H.C., et al. (1987) Vanadium containing bromoperoxidase: An example of an oxidoreductase with high operational stability in aqueous and organic media. *Biotechnol Bioeng* **30**: 607–610.
- de Boer, E. and Wever, R. (1988) The reaction mechanism of the novel vanadium-bromoperoxidase. A steady-state kinetic analysis. *J Biol Chem* **263**: 12326–12332.
- De Jong, R.M. and Dijkstra, B.W. (2003) Structure and mechanism of bacterial dehalogenases: Different ways to cleave a carbon-halogen bond. *Curr Opin Struct Biol* **13**: 722–730.
- Dong, C., Huang, F., Deng, H., Schaffrath, C., Spencer, J.B., O'Hagan, D., and Naismith, J.H. (2004) Crystal structure and mechanism of a bacterial fluorinating enzyme. *Nature* **427**: 561–565.
- Dong, C.; Flecks, S.; Unversucht, S.; Haupt, C.; van Pee, K. H.; Naismith, J. H. (2005) Tryptophan 7-halogenase (PrnA) structure suggests a mechanism for regioselective chlorination. *Science* **309**: 2216– 2219.

- Dudek, M., Dieudonné, A., Jouanneau, D., Rochat, T., Michel, G., Sarels, B., and Thomas, F. (2020) Regulation of alginate catabolism involves a GntR family repressor in the marine flavobacterium *Zobellia galactanivorans* DsijT. *Nucleic Acids Res* **48**: 7786–7800.
- Ehara, A., Suzuki, H., Kanesaki, Y., Yoshikawa, H., and Amachi, S. (2014) Draft genome sequence of strain Q-1, an iodide-oxidizing alphaproteobacterium isolated from natural gas brine water. *Genome Announc* **2**: 2013–2014.
- Eustaquio, A. S.; Pojer, F.; Noel, J. P.; Moore, B. S. (2008) Discovery and characterization of a marine bacterial SAM-dependent chlorinase. *Nat. Chem. Biol.* **4**: 69–74.
- Fariselli, P., Finocchiaro, G., and Casadio, R. (2003) SPEPlip: The detection of signal peptide and lipoprotein cleavage sites. *Bioinformatics* **19**: 2498–2499.
- Feiters, M.C., Leblanc, C., Küpper, F.C., Meyer-Klaucke, W., Michel, G., and Potin, P. (2005) Bromine is an endogenous component of a vanadium bromoperoxidase. *J Am Chem Soc* **127**: 15340–15341.
- Fenical, W. (1982) Natural Products Chemistry in the MARine Environment. *Science (80-)* **215**: 923–928.
- Ferrara, M., Perrone, G., Gambacorta, L., Epifani, F., Solfrizzo, M., and Gallo, A. (2016) Identification of a halogenase involved in the biosynthesis of ochratoxin A in *Aspergillus carbonarius*. *Appl Environ Microbiol* **82**: 5631–5641.
- Fetzner, S. (1998) Bacterial dehalogenation. *Appl Microbiol Biotechnol* **50**: 633–657.
- Ficko-Blean, E., Duffieux, D., Rebuffet, É., Larocque, R., Groisillier, A., Michel, G., and Czjzek, M. (2015) Biochemical and structural investigation of two paralogous glycoside hydrolases from *Zobellia galactanivorans*: Novel insights into the evolution, dimerization plasticity and catalytic mechanism of the GH117 family. *Acta Crystallogr Sect D Biol Crystallogr* **71**: 209–223.
- Ficko-Blean, E., Préchoux, A., Thomas, F., Rochat, T., Larocque, R., Zhu, Y., et al. (2017) Carrageenan catabolism is encoded by a complex regulon in marine heterotrophic bacteria. *Nat Commun* **8**:
- Fortin, P.D., Horsman, G.P., Yang, H.M., and Eltis, L.D. (2006) A glutathione S-transferase catalyzes the dehalogenation of inhibitory metabolites of polychlorinated biphenyls. *J Bacteriol* **188**: 4424–4430.
- Fournier, J. (2014) Evolution des mécanismes d'accumulation et de transport de l'iode dans les organismes marins : étude de la structure/fonction des protéines du métabolisme iodé chez la bactérie *Zobellia galactanivorans*.
- Fournier, J.B., Rebuffet, E., Delage, L., Grijol, R., Meslet-Cladière, L., Rzonca, J., et al. (2014) The vanadium iodoperoxidase from the marine *Flavobacteriaceae* species *Zobellia galactanivorans* reveals novel molecular and evolutionary features of halide specificity in the vanadium haloperoxidase enzyme family. *Appl Environ Microbiol* **80**: 7561–7573.

-
- Fournier, J.B. and Leblanc, C. (2014) Halogenation and Vanadium Haloperoxidases. *Outst Mar Mol Chem Biol Anal* **9783527334**: 225–242.
- Frank, K. and Sippl, M.J. (2008) High-performance signal peptide prediction based on sequence alignment techniques. *Bioinformatics* **24**: 2172–2176.
- Frank, A., Seel, C.J., Groll, M., and Gulder, T. (2016) Characterization of a Cyanobacterial Haloperoxidase and Evaluation of its Biocatalytic Halogenation Potential. *ChemBioChem* **17**: 2028–2032.
- Fujimori, T., Yoneyama, Y., Taniai, G., Kurihara, M., Tamegai, H., and Hashimoto, S. (2012) Methyl halide production by cultures of marine *Proteobacteria Erythrobacter* and *Pseudomonas* and isolated bacteria from brackish water. *Limnol Oceanogr* **57**: 154–162.
- Fuse, H., Inoue, H., Murakami, K., Takimura, O., and Yamaoka, Y. (2003) Production of free and organic iodine by *Roseovarius* spp. *FEMS Microbiol Lett* **229**: 189–194.
- Gall, E., Küpper, F.C., and Kloareg, B. (2004) A survey of iodine content in *Laminaria digitata*. *Bot Mar* **47**: 30–37.
- Garcia-Rodriguez, E., Ohshiro, T., Aibara, T., Izumi, Y., and Littlechild, J. (2005) Enhancing effect of calcium and vanadium ions on thermal stability of bromoperoxidase from *Corallina pilulifera*. *J Biol Inorg Chem* **10**: 275–282.
- Geigert, J., Lee, T.D., Dalietos, D.J., Hirano, D.S., and Neidleman, S.L. (1986) Epoxidation of alkenes by chloroperoxidase catalysis. *Biochem Biophys Res Commun* **136**: 778–782.
- Gereben, B., Zavacki, A.M., Ribich, S., Kim, B.W., Huang, S.A., Simonides, W.S., et al. (2008) Cellular and molecular basis of deiodinase-regulated thyroid hormone signaling. *Endocr Rev* **29**: 898–938.
- Gkotsi, D.S., Ludewig, H., Sharma, S. V., Connolly, J.A., Dhaliwal, J., Wang, Y., et al. (2019) A marine viral halogenase that iodinated diverse substrates. *Nat Chem* **11**: 1091–1097.
- Glasner, M.E., Gerlt, J.A., and Babbitt, P.C. (2006) Evolution of enzyme superfamilies. *Curr Opin Chem Biol* **10**: 492–497.
- Goldberg, T., Hecht, M., Hamp, T., Karl, T., Yachdav, G., Ahmed, N., et al. (2014) LocTree3 prediction of localization. *Nucleic Acids Res* **42**: 350–355.
- Gomi, M., Sonoyama, M., and Mitaku, S. (2004) High performance system for signal peptide prediction: SOSUISignal. *Chem-Bio Informatics J* **4**: 142–147.
- Goodwin, K.D., Schaefer, J.K., and Oremland, R.S. (1998) Bacterial oxidation of dibromomethane and methyl bromide in natural waters and enrichment cultures. *Appl Environ Microbiol* **64**: 4629–4636.

-
- Goudenège, D., Avner, S., Lucchetti-Miganeh, C., and Barloy-Hubler, F. (2010) CoBaltDB: Complete bacterial and archaeal orfeomes subcellular localization database and associated resources. *BMC Microbiol* **10**:
- Greenwood, N. and Earnshaw, A. (1997) *Chemistry of The Elements*, 2nd ed.; Butterworth-Heinemann.
- Greff, S., Zubia, M., Genta-Jouve, G., Massi, L., Perez, T., and Thomas, O.P. (2014) Mahorones, highly brominated cyclopentenones from the red alga *Asparagopsis taxiformis*. *J Nat Prod* **77**: 1150–1155.
- Gribble, G.W. (1998) Naturally Occurring Organohalogen Compounds. *Acc Chem Res* **31**: 141–152.
- Gribble, G.W. (1999) The diversity of naturally occurring organobromine compounds. *Chem Soc Rev* **28**: 335–346.
- Gribble, G.W. (2003) The diversity of naturally produced organohalogens. *Chemosphere* **52**: 289–297.
- Gribble, G.W. (2015) Biological activity of recently discovered halogenated marine natural products. *Mar Drugs* **13**: 4044–4136.
- Groisillier, A., Labourel, A., Michel, G., and Tonon, T. (2015) The mannitol utilization system of the marine bacterium *Zobellia galactanivorans*. *Appl Environ Microbiol* **81**: 1799–1812.
- Guillory, J.K. (2009) CRC Handbook of Chemistry and Physics. 90th Edition. *J Med Chem* **52**: 5560.
- Häggbloom, M.M. and Bossert, I.D. (2005) Halogenated Organic Compounds - A Global Perspective. *Dehalogenation* 3–29.
- Han, J., Zhang, J., Song, Z., Liu, M., Hu, J., Hou, C., et al. (2019) Genome- and MS-based mining of antibacterial chlorinated chromones and xanthenes from the phytopathogenic fungus *Bipolaris sorokiniana* strain 11134. *Appl Microbiol Biotechnol* **103**: 5167–5181.
- Harms, H., Poehlein, A., Thürmer, A., and König, G.M. (2017) Draft genome sequence of *Zobellia* sp. strain OII3, isolated from the coastal zone of the Baltic Sea. *Am Soc Microbiol* **5**: 5–6.
- Hay, M.E. and Fenical, W. (1988) Marine plant-herbivore interactions: the ecology of chemical defense. *Annu Rev Ecol Syst* **19**: 111–145.
- Hayashi, S. and Wu, C. (1990) Lipoproteins in Bacteria. *J Bioenerg Biomembr* **22**: 451–471.
- He, Y.W., Cao, X.Q., and Poplawsky, A.R. (2020) Chemical structure, biological roles, biosynthesis and regulation of the yellow xanthomonadin pigments in the phytopathogenic genus *Xanthomonas*. *Mol Plant-Microbe Interact* **33**: 705–714.

-
- Hehemann, J.H., Michel, G., Barbeyron, T., and Czjzek, M. (2010) Expression, purification and preliminary X-ray diffraction analysis of the catalytic module of a β - Agarase from the flavobacterium *Zobellia galactanivorans*. *Acta Crystallogr Sect F Struct Biol Cryst Commun* **66**: 413–417.
- Hehemann, J.H., Correc, G., Thomas, F., Bernard, T., Barbeyron, T., Jam, M., et al. (2012) Biochemical and structural characterization of the complex agarolytic enzyme system from the marine bacterium *Zobellia galactanivorans*. *J Biol Chem* **287**: 30571–30584.
- Hemrika, W., Renirie, R., Macedo-ribeiro, S., Messerschmidt, A., and Wever, R. (1999) Heterologous Expression of the the Vanadium-containing Chloroperoxidase from *Curvularia inaequalis* in *Saccharomyces cerevisiae* and Site-directed Mutagenesis of the Active Site Residues His496, Arg360, and Arg490. *J Biol Chem* **274**: 23820–23827.
- Hill, K.E., Marchesi, J.R., and Weightman, A.J. (1999) Investigation of two evolutionarily unrelated halocarboxylic acid dehalogenase gene families. *J Bacteriol* **181**: 2535–2547.
- Hill, V.L. and Manley, S.L. (2009) Release of reactive bromine and iodine from diatoms and its possible role in halogen transfer in polar and tropical oceans. *Limnol Oceanogr* **54**: 812–822.
- Hiller, K., Grote, A., Scheer, M., Münch, R., and Jahn, D. (2004) PrediSi: Prediction of signal peptides and their cleavage positions. *Nucleic Acids Res* **32**: 375–379.
- Hillwig, M.L. and Liu, X. (2014) A new family of iron-dependent halogenases acts on freestanding substrates. *Nat Chem Biol* **10**: 921–923.
- Hirata, M., Ikeda, M., Fukuda, F., Abe, M., Sawada, H., and Hashimoto, S. (2017) Effect of temperature on the production rates of methyl halides in cultures of marine Proteobacteria. *Mar Chem* **196**: 126–134.
- Hisano, T., Hata, Y., Fujii, T., Liu, J.Q., Kurihara, T., Esaki, N., and Soda, K. (1996) Crystallization and preliminary X-Ray crystallographic studies of L-2-haloacid dehalogenase from *Pseudomonas* sp. YL. *Proteins Struct Funct Genet* **24**: 520–522.
- Hofmann, B., Tölzer, S., Pelletier, I., Altenbuchner, J., Van Pée, K.H., and Hecht, H.J. (1998) Structural investigation of the cofactor-free chloroperoxidases. *J Mol Biol* **279**: 889–900.
- Hofrichter, M. and Ullrich, R. (2006) Heme-thiolate haloperoxidases: versatile biocatalysts with biotechnological and environmental significance. *Appl Microbiol Biotechnol* **71**: 276–288.
- Hollender, J., Hopp, J., and Dott, W. (1997) Degradation of 4-chlorophenol via the *meta* cleavage pathway by *Comamonas testosteroni* JH5. *Appl Environ Microbiol* **63**: 4567–4572.
- Horisaki, T., Yoshida, E., Sumiya, K., Takemura, T., Yamane, H., Nojiri, H. (2011) Isolation and characterization of monochloroacetic acid-degrading bacteria. *J Gen Appl Microbiol* **57**: 277–284.

-
- Huang, J., Xin, Y., and Zhang, W. (2011) Isolation, characterization and identification of a *Paracoccus* sp. 2-haloacid-degrading bacterium from the marine sponge *Hymeniacidon perlevis*. *J Basic Microbiol* **51**: 318–324.
- Huang, R.J., Thorenz, U.R., Kundel, M., Venables, D.S., Ceburnis, D., Ho, K.F., et al. (2013) The seaweeds *Fucus vesiculosus* and *Ascophyllum nodosum* are significant contributors to coastal iodine emissions. *Atmos Chem Phys* **13**: 5255–5264.
- Hug, L.A. and Edwards, E.A. (2013) Diversity of reductive dehalogenase genes from environmental samples and enrichment cultures identified with degenerate primer PCR screens. *Front Microbiol* **4**: 1–16.
- Imai, K., Asakawa, N., Tsuji, T., Akazawa, F., Ino, A., Sonoyama, M., and Mitaku, S. (2008) SOSUI-GramN: high performance prediction for sub-cellular localization of proteins in Gram-negative bacteria. *Bioinformatics* **2**: 417–421.
- Ingavat, N., Kavran, J.M., Sun, Z., and Rokita, S.E. (2017) Active Site Binding Is Not Sufficient for Reductive Deiodination by Iodotyrosine Deiodinase. *Biochemistry* **56**: 1130–1139.
- Isupov, M. N.; Dalby, A. R.; Brindley, A. A.; Izumi, Y.; Tanabe, T.; Murshudov, G. N.; Littlechild, J. A. (2000) Crystal structure of dodecameric vanadium-dependent bromoperoxidase from the red algae *Corallina officinalis*. *J. Mol. Biol.* **299**: 1035–1049.
- Ito, K., Nakajima, N., Yamamura, S., Tomita, M., Suzuki, H., and Amachi, S. (2016) Draft Genome Sequence of *Arenibacter* sp. Strain C-21, an Iodine- Accumulating Bacterium Isolated from Surface Marine Sediment. *Am Soc Microbiol* **4**: 863–864.
- Itoh, N., Izumi, Y., and Yamada, H. (1986) Characterization of nonheme type bromoperoxidase in *Corallina pilulifera*. *J Biol Chem* **261**: 5194–5200.
- Javier, L.H., Benzekri, H., Gut, M., Gonzalo Claros, M., van Bergeijk, S., Cañavate, J.P., and Machado, M. (2018) Characterization of Iodine-related molecular processes in the marine microalga *Tisochrysis lutea* (Haptophyta). *Front Mar Sci* **5**.
- Janssen, Dick B., Pries, F., Van der Ploeg, J. R. (1994). Genetics and Biochemistry of dehalogenating enzymes. *Annu. Rev. Microbiol.* **48**: 163–191.
- Janssen, D.B., Dinkla, I.J.T., Poelarends, G.J., and Terpstra, P. (2005) Bacterial degradation of xenobiotic compounds: Evolution and distribution of novel enzyme activities. *Environ Microbiol* **7**: 1868–1882.
- Jones, D.H.A., Barth, P.T., Byrom, D. and Thomas, C.M. (1992) Nucleotide sequence of the structural gene encoding a 2-haloalkanoic acid dehalogenase of *Pseudomonas putida* strain AJ1 and purification of the encoded protein. *Journal of General Microbiology.* **138**: 675-683.
- Johnson, T.L., Palenik, B., and Brahamsha, B. (2011) Characterization of a functional vanadium-dependent bromoperoxidase in the marine cyanobacterium *Synechococcus* sp. CC9311. *J Phycol* **47**: 792–801.

- Johnson, T.L., Brahamsha, B., Palenik, B., and Mühle, J. (2015) Halomethane production by vanadium-dependent bromoperoxidase in marine *Synechococcus*. *Limnol Oceanogr* **60**: 1823–1835.
- Jordan, P. and Vilter, H. (1991) Extraction of proteins from material rich in anionic mucilages: Partition and fractionation of vanadate-dependent bromoperoxidases from the brown algae *Laminaria digitata* and *L. saccharina* in aqueous polymer two-phase systems. *BBA - Gen Subj* **1073**: 98–106.
- Jordan, P., Kloareg, B., and Vilter, H. (1991) Detection of Vanadate-Dependent Bromoperoxidases in Protoplasts from the Brown Algae *Laminaria digitata* and *L. saccharina*. *J Plant Physiol* **137**: 520–524.
- Jordan, A., Harnisch, J., Borchers, R., Le Guern, F., and Shinohara, H. (2000) Volcanogenic halocarbons. *Environ Sci Technol* **34**: 1122–1124.
- Jugder, B.E., Ertan, H., Lee, M., Manfield, M., and Marquis, C.P. (2015) Reductive Dehalogenases Come of Age in Biological Destruction of Organohalides. *Trends Biotechnol* **33**: 595–610.
- Juncker, A.S., Willenbrock, H., von Heijne, G., Brunak, S., Nielsen, H., and Krogh, A. (2003) Prediction of lipoprotein signal peptides in Gram-negative bacteria. *Protein Sci* **12**: 1652–1662.
- Käll, L., Krogh, A., and Sonnhammer, E.L.L. (2004) A combined transmembrane topology and signal peptide prediction method. *J Mol Biol* **338**: 1027–1036.
- Kawasaki, H., Yahara, H., and Tonomura, K. (1981) Isolation and characterization of plasmid puol mediating dehalogenation of haloacetate and mercury resistance in *Moraxella* sp. B. *Agric Biol Chem* **45**: 1477–1481.
- Kaysser, L., Bernhardt, P., Nam, S.J., Loesgen, S., Ruby, J.G., Jensen, P.R., et al. (2012) Merochlorins A–D, cyclic meroterpenoid antibiotics biosynthesized in divergent pathways with vanadium-dependent chloroperoxidases. *J Am Chem Soc*, **134**: 11988–11991.
- Keppeler, F., Eiden, R., Niedan, V., Pracht, J., and Schöler, H.F. (2000) Halocarbons produced by natural Oxidation processes during degradation of organic matter. *Nature* **403**: 298–301.
- Köhler, R., Brokamp, A., Schwarze, R., Reiting, R.H., and Schmidt, F.R. (1998) Characteristics and DNA-sequence of a cryptic haloalkanoic acid dehalogenase from *Agrobacterium tumefaciens* RS5. *Curr Microbiol* **36**: 96-101.
- Koonin, E. V. and Tatusov, R.L. (1994) Computer analysis of bacterial haloacid dehalogenases defines a large superfamily of hydrolases with diverse specificity. *J Mol Biol* **244**: 125–132.
- Krenn, B.E., Plat, H., and Wever, R. (1988) Purification and some characteristics of a non-haem bromoperoxidase from *Streptomyces aureofaciens*. *Biochim Biophys Acta* **952**: 255–260.

- Kühnel, K., Blankenfeldt, W., Terner, J., and Schlichting, I. (2006) Crystal structures of chloroperoxidase with its bound substrates and complexed with formate, acetate, and nitrate. *J Biol Chem* **281**: 23990–23998.
- Kunka, A., Damborsky, J., and Prokop, Z. (2018) Haloalkane Dehalogenases From Marine Organisms. *Methods in Enzymology* **605**: 203-251.
- Küpper, F.C. and Vilter, H. (1998) Iodine uptake in *Laminariales* involves extracellular, haloperoxidase-mediated oxidation of iodide. *Planta* **207**: 163–171.
- Küpper, F.C., Kloareg, B., Guern, J., and Potin, P. (2001) Oligoguluronates elicit an oxidative burst in the brown algal kelp *Laminaria digitata*. *Plant Physiol* **125**: 278–291.
- Küpper, F.C., Carpenter, L.J., Woitsch, S., Weiller, M., Abela, R., Grolimund, D., et al. (2008) Iodide accumulation provides kelp with an inorganic antioxidant impacting atmospheric chemistry. *PNAS* **105**: 6954–6958.
- Kurata, A., Kurihara, T., Kamachi, H., and Esaki, N. (2005) 2-Haloacrylate reductase, a novel enzyme of the medium chain dehydrogenase/reductase superfamily that catalyzes the reduction of a carbon-carbon double bond of unsaturated organohalogen compounds. *J Biol Chem* **280**: 20286–20291.
- Kurihara, T., Liu, J.Q., Nardi-dei, V., Koshikawa, H., Esaki, N., and Soda, K. (1995) Comprehensive site-directed mutagenesis of L-2-halo acid dehalogenase to probe catalytic amino acid residues. *J Biochem* **117**: 1317–1322.
- Kurihara, T. and Esaki, N. (2008) Bacterial hydrolytic dehalogenases and related enzymes: Occurrences, reaction mechanisms, and applications. *Chem Rec* **8**: 67–74.
- Kwok, S.Y., Siu, A.F.M., Ngai, S.M., Che, C.M., and Tsang, J.S.H. (2007) Proteomic analysis of *Burkholderia cepacia* MBA4 in the degradation of monochloroacetate. *Proteomics* **7**: 1107–1116.
- La Barre, S., Potin, P., Leblanc, C., and Delage, L. (2010) The halogenated metabolism of brown algae (phaeophyta), its biological importance and its environmental significance. *Mar Drugs* **8**: 988–1010.
- Labourel, A., Jam, M., Jeudy, A., Hehemann, J.H., Czjzek, M., and Michel, G. (2014) The β -Glucanase ZgLamA from *Zobellia galactanivorans* Evolved a Bent Active Site Adapted for Efficient Degradation of Algal Laminarin. *J Biol Chem* **289**: 2027–2042.
- Labourel, A., Jam, M., Legentil, L., Sylla, B., Hehemann, J.H., Ferrières, V., et al. (2015) Structural and biochemical characterization of the laminarinase ZgLamCGH16 from *Zobellia galactanivorans* suggests preferred recognition of branched laminarin. *Acta Crystallogr Sect D Biol Crystallogr* **71**: 173–184.
- Lami, R., Grimaud, R., Sanchez-Brosseau, S., Six, C., Thomas, F., West, N.J., Joux, F., Urios, L. (2021) Marine bacterial models for experimental biology. *Established and emerging marine organisms in experimental biology*. In press

- Latham, H. (2008) Temperature stress-induced bleaching of the coralline alga *Corallina officinalis*: A role for the enzyme bromoperoxidase. *Biosci Horizons* **1**: 104–113.
- Laternus, F., Giese, B., Wiencke, C., and Adams, F.C. (2000) Low-molecular-weight organoiodine and organobromine compounds released by polar macroalgae - The influence of abiotic factors. *Fresenius J Anal Chem* **368**: 297–302.
- Laternus, F. (2001) Marine macroalgae in Polar Regions as natural sources for volatile organohalogens. *Environ Sci Pollut Res* **8**: 103–108.
- Laternus, F., Svensson, T., Wiencke, C., and Öberg, G. (2004) Ultraviolet radiation affects emission of ozone-depleting substances by marine macroalgae: Results from a laboratory incubation study. *Environ Sci Technol* **38**: 6605–6609.
- Laternus, F., Fahimi, I., Gryndel, M., Hartmann, A., Heal, M.R., Matucha, M., *et al.* (2005) Natural Formation and Degradation of Chloroacetic Acids and Volatile Organochlorines in Forest Soil. *Environ Sci & Pollut Res.* **12** : 233-244.
- Lazrus, A.L., Gandrud, B.W., and Woodard, R.N. (1975) Stratospheric halogen measurements. *Geophys Res Lett* **2**: 439–441.
- Leblanc, C., Colin, C., Cosse, A., Delage, L., La Barre, S., Morin, P., *et al.* (2006) Iodine transfers in the coastal marine environment: the key role of brown algae and of their vanadium-dependent haloperoxidases. *Biochimie* **88**: 1773–1785.
- Leblanc, C., Vilter, H., Fournier, J.B., Delage, L., Potin, P., Rebuffet, E., *et al.* (2015) Vanadium haloperoxidases: From the discovery 30 years ago to X-ray crystallographic and V K-edge absorption spectroscopic studies. *Coord Chem Rev* **301–302**: 134–146.
- Leedham, E.C., Hughes, C., Keng, F.S.L., Phang, S.M., Malin, G., and Sturges, W.T. (2013) Emission of atmospherically significant halocarbons by naturally occurring and farmed tropical macroalgae. *Biogeosciences* **10**: 3615–3633.
- Lemesheva, V., Birkemeyer, C., Garbary, D., and Tarakhovskaya, E. (2020) Vanadium-dependent haloperoxidase activity and phlorotannin incorporation into the cell wall during early embryogenesis of *Fucus vesiculosus* (Phaeophyceae). *Eur J Phycol* **55**: 275–284.
- Lertampaiporn, S., Nuannimnoi, S., Vorapreeda, T., Chokesajjawatee, N., Visessanguan, W., and Thammarongtham, C. (2019) PSO-LocBact: A Consensus Method for Optimizing Multiple Classifier Results for Predicting the Subcellular Localization of Bacterial Proteins. *Biomed Res Int* **2019**..
- Liu, J.Q., Kurihara, T., Hasan, A.K., Nardi-Dei, V., Koshikawa, H., Esaki, N., and Soda, K. (1994) Purification and characterization of thermostable and nonthermostable 2-haloacid dehalogenases with different stereospecificities from *Pseudomonas* sp. strain YL. *Appl Environ Microbiol* **60**: 2389–93.
- Ludewig, H., Molyneux, S., Ferrinho, S., Guo, K., Lynch, R., Gkotsi, D.S., and Goss, R.J. (2020) Halogenases: structures and functions. *Curr Opin Struct Biol* **65**: 51–60.

- Martins, T.P., Rouger, C., Glasser, N.R., Freitas, S., De Fraissinette, N.B., Balskus, E.P., et al. (2019) Chemistry, bioactivity and biosynthesis of cyanobacterial alkylresorcinols. *Nat Prod Rep* **36**: 1437–1461.
- Mata, L., Gaspar, H., and Santos, R. (2012) Carbon/nutrient balance in relation to biomass production and halogenated compound content in the red alga *Asparagopsis taxiformis* (bonnemaisoniaceae). *J Phycol* **48**: 248–253.
- Matucha, M., Gryndler, M., Forczek, S.T., Uhlirova, H., Fuksova, K. and Schröder, P. (2003) Chloroacetic acids in environmental processes. *Environ Chem Lett.* **1**: 127-130.
- McCarthy, D.L., Louie, D.F., and Copley, S.D. (1997) Identification of a covalent intermediate between glutathione and cysteine13 formed during catalysis by tetrachlorohydroquinone dehalogenase. *J Am Chem Soc* **119**: 11337–11338.
- McKinnie, S.M.K., Miles, Z.D., and Moore, B.S. (2018) Characterization and Biochemical Assays of *Streptomyces* Vanadium-Dependent Chloroperoxidases. *Methods in Enzymology* **604**: 405-424.
- McTamney, P.M. and Rokita, S.E. (2009) A mammalian reductive deiodinase has broad power to dehalogenate chlorinated and brominated substrates. *J Am Chem Soc* **131**: 14212–14213.
- Mena-Benitez, G.L., Gandia-Herrero, F., Graham, S., Larson, T.R., McQueen-Mason, S.J., French, C.E., et al. (2008) Engineering a Catabolic Pathway in Plants for the Degradation of 1,2-Dichloroethane. *Plant Physiol* **147**: 1192–1198.
- Messerschmidt, A. and Wever, R. (1996) X-ray structure of a vanadium-containing enzyme: chloroperoxidase from the fungus *Curvularia inaequalis*. *Proc Natl Acad Sci U S A* **93**: 392–396.
- Moore, R.M., Webb, M., Tokarczyk, R., and Wever, R. (1996) Bromoperoxidase and iodoperoxidase enzymes and production of halogenated methanes in marine diatom cultures. *J Geophys Res C Ocean* **101**: 20899–20908.
- Moore, R.M. and Groszko, W. (1999) Methyl iodide distribution in the ocean and fluxes to the atmosphere. *J Geophys Res* **104**: 11163–11171.
- Murdiyatmo, U., Asmara, W., Tsang, J.S., Baines, A.J., Bull, A.T. and Hardman, D.J. (1992) Molecular biology of the 2-haloacid halidohydrolase IVa from *Pseudomonas cepacia* MBA4. *Biochem J.* **284**:87-93.
- Nakamura, T., Yamaguchi, A., Kondo, H., Watanabe, H., Kurihara, T., Esaki, N., et al. (2009) Roles of K151 and D180 in L-2-Haloacid Dehalogenase from *Pseudomonas* sp. YL: Analysis by Molecular Dynamics and Ab Initio Fragment Molecular Orbital Calculations. *J Comput Chem* **30**: 2625–2634.
- Nardi-Dei, V., Kurihara, T., Okamura, T., Liu, J.Q., Koshikawa, H., Ozaki, H., et al. (1994) Comparative studies of genes encoding thermostable L-2-halo acid dehalogenase from

- Pseudomonas* sp. strain YL, other dehalogenases, and two related hypothetical proteins from *Escherichia coli*. *Appl Environ Microbiol* **60**: 3375–3380.
- Naretto, A., Fanuel, M., Ropartz, D., Rogniaux, H., Larocque, R., Czjzek, M., et al. (2019) The agar-specific hydrolase ZgAgaC from the marine bacterium *Zobellia galactanivorans* defines a new GH16 protein subfamily. *J Biol Chem* **294**: 6923–6939.
- Nedashkovskaya, O.I., Suzuki, M., Vancanneyt, M., Cleenwerck, I., Lysenko, A.M., Mikhailov, V. V., and Swings, J. (2004) *Zobellia amurskyensis* sp. nov., *Zobellia laminariae* sp. nov. and *Zobellia russellii* sp. nov., novel marine bacteria of the family *Flavobacteriaceae*. *Int J Syst Evol Microbiol* **54**: 1643–1648.
- Novak, H.R., Sayer, C., Isupov, M.N., Paszkiewicz, K., Gotz, D., Spragg, A.M., and Littlechild, J.A. (2013a) Marine *Rhodobacteraceae* L -haloacid dehalogenase contains a novel His / Glu dyad that could activate the catalytic water. *FEBS J* **280**: 1664–1680.
- Novak, H. R., Sayer, C., Panning, J., and Littlechild, J. A. (2013b). Characterisation of an l-Haloacid Dehalogenase from the Marine Psychrophile *Psychromonas ingrahamii* with Potential Industrial Application. *Mar. Biotechnol.* **15**: 695–705.
- O’Dowd, C.D., Jimenez, J.L., Bahreini, R., Flagan, R.C., Seinfeld, J.H., Hämerl, K., et al. (2002) Marine aerosol formation from biogenic iodine emissions. *Nature* **417**: 632–636.
- O’Hagan, D. and Harper, D.B. (1999) Fluorine-containing natural products. *J Fluor Chem* **100**: 127–133.
- Orser, C. S., Dutton, J., Lange, C., Jablonski, P., Xun, L., and Hargis, M. (1993). Characterization of a *Flavobacterium* glutathione S-transferase gene involved in reductive dechlorination. *J. Bacteriol.* **175**: 2640–2644.
- Palmer, C.J., Anders, T.L., Carpenter, L.J., Küpper, F.C., and McFiggans, G.B. (2005) Iodine and halocarbon response of *Laminaria digitata* to oxidative stress and links to atmospheric new particle production. *Environ Chem* **2**: 282–290.
- Pang, B.C.M. and Tsang, J.S.H. (2001) Mutagenic analysis of the conserved residues in dehalogenase IVa of *Burkholderia cepacia* MBA4. *FEMS Microbiol Lett* **204**: 135–140.
- Paradis-Bleau, C., Markovski, M., Uehara, T., Lupoli, T.J., Walker, S., Kahne, D.E., and Bernhardt, T.G. (2010) Lipoprotein cofactors located in the outer membrane activate bacterial cell wall polymerases. *Cell* **143**: 1110–1120.
- Park, J.S., Lee, W.C., Yeo, K.J., Ryu, K., Kumarasiri, M., Heseck, D., et al. (2012) Mechanism of anchoring of OmpA protein to the cell wall peptidoglycan of the gram-negative bacterial outer membrane. *FASEB J* **26**: 219–228.
- Paul, C. and Pohnert, G. (2011) Production and role of volatile halogenated compounds from marine algae. *Nat Prod Rep* **28**: 186–195.

-
- Paul, N.A., De Nys, R., and Steinberg, P.D. (2006) Chemical defence against bacteria in the red alga *Asparagopsis armata*: Linking structure with function. *Mar Ecol Prog Ser* **306**: 87–101.
- Peng, C. and Gao, F. (2014) Protein localization analysis of essential genes in prokaryotes. *Sci Rep* **4**: 1–7.
- Persoon, I.F., Hoogenkamp, M.A., Bury, A., Wesselink, P.R., Hartog, A.F., Wever, R., Crielaard, W. (2012) Effect of vanadium chloroperoxidase on *Enterococcus faecalis* biofilms. *J. Endod.* **38**: 72–74
- Phintha, A., Prakinee, K., Jaruvat, A., Lawan, N., Visitsatthawong, S., Kantiwiriyanitch, C., et al. (2020) Dissecting the low catalytic capability of flavin-dependent halogenases. *J Biol Chem* **296**: 100068.
- Potin P, Sanseau A, Le Gall Y, Rochas C, Kloareg B. (1991) Purification and characterization of a new kappa-carrageenase from a marine *Cytophaga*-like bacterium. The Federation of European Biochemical Societies Journal **201**: 241–247.
- Radlow, M., Czjzek, M., Jeudy, A., Dabin, J., Delage, L., Leblanc, C., and Hartung, J. (2018) X-ray Diffraction and Density Functional Theory Provide Insight into Vanadate Binding to Homohexameric Bromoperoxidase II and the Mechanism of Bromide Oxidation. *ACS Chem Biol* **13**: 1243–1259.
- Ridder, I.S., Rozeboom, H.J., Kalk, K.H., Janssen, D.B., and Dijkstra, B.W. (1997) Three-dimensional structure of L-2-haloacid dehalogenase from *Xanthobacter autotrophicus* GJ10 complexed with the substrate-analogue formate. *J Biol Chem* **272**: 33015–33022.
- Rousset, B., Dupuy, C., Miot, F., & Dumont, J. (2015). Thyroid hormone synthesis and secretion. *Endotext* (ed. L. J. De Groot, G. Chrousos, K. Dungan, K. R. Feingold, A. Grossman, J. M. Hershman, C. Koch, M. Korbonits, R. McLachlan, M. New et al.). South Dartmouth, MA, USA: MDText.com.
- Ruecker, A., Weigold, P., Behrens, S., Jochmann, M., Laaks, J., and Kappler, A. (2014) Predominance of biotic over abiotic formation of halogenated hydrocarbons in hypersaline sediments in Western Australia. *Environ Sci Technol* **48**: 9170–9178.
- Rye, C.A., Isupov, M.N., Lebedev, A.A., and Littlechild, J.A. (2009) Biochemical and structural studies of a l-haloacid dehalogenase from the thermophilic archaeon *Sulfolobus tokodaii*. *Extremophiles* **13**: 179–190.
- Saiz-Lopez, A., Mahajan, A.S., Salmon, R.A., Bauguitte, S.J.B., Jones, A.E., Roscoe, H.K., and Plane, J.M.C. (2007) Boundary layer halogens in coastal Antarctica. *Science (80-)* **317**: 348–351.
- Salaün, S., la Barre, S., Santos-Goncalvez, M. Dos, Potin, P., Haras, D., and Bazire, A. (2012) Influence of Exudates of the Kelp *Laminaria Digitata* on Biofilm Formation of Associated and Exogenous Bacterial Epiphytes. *Microb Ecol* **64**: 359–369.

- Salaün, S. (2015). Interactions entre la macroalgue brune *Laminaria digitata* et ses épibiontes bactériens : études moléculaire et spectroscopiques : capacité d'adhésion et de formation de biofilm.
- Sato, N., Hamamoto, K., Kurihara, M., Abe, M., and Hashimoto, S. (2019) Methyl halide production by cultures of marine thraustochytrids, *Aurantiochytrium* sp., *Botryochytrium radiatum*, and *Schizochytrium* sp. *Mar Chem* **208**: 95–102.
- Sayed, R.Z. and Patel, P.R. (2011) Soil microorganisms and environmental health. *Int J Biotechnol Biosci* **1**: 41–66.
- Schmidberger, J.W., Wilce, J.A., Tsang, J.S.H., and Wilce, M.C.J. (2007) Crystal Structures of the Substrate Free-enzyme, and Reaction Intermediate of the HAD Superfamily Member, Haloacid Dehalogenase DehIVa from *Burkholderia cepacia* MBA4. *J Mol Biol* **368**: 706–717.
- Schneider, B., Muller, R., Frank, R., and Lingens, F. (1991) Complete nucleotide sequences and comparison of the structural genes of two 2-haloalkanoic acid dehalogenases from *Pseudomonas* sp. strain CBS3. *J Bacteriol* **173**: 1530–1535.
- Schneider, B., Müller, R., Frank, R., and Lingens, F. (1993) Site-Directed Mutagenesis of the 2-Haloalkanoic Acid Dehalogenase I Gene from *Pseudomonas* sp. Strain CBS3 and its Effect on Catalytic Activity. *Biol Chem Hoppe Seyler* **374**: 489–496.
- Schöner, T.A., Gassel, S., Osawa, A., Tobias, N.J., Okuno, Y., Sakakibara, Y., et al. (2016) Aryl Polyenes, a Highly Abundant Class of Bacterial Natural Products, Are Functionally Related to Antioxidative Carotenoids. *ChemBioChem* **17**: 247–253.
- Schwehr, K.A. and Santschi, P.H. (2003) Sensitive determination of iodine species, including organo-iodine, for freshwater and seawater samples using high performance liquid chromatography and spectrophotometric detection. *Anal Chim Acta* **482**: 59–71.
- Senn, H.M. (2014) Insights into enzymatic halogenation from computational studies. *Front Chem* **2**: 1–15.
- Seydel, A., Gounon, P., and Pugsley, A.P. (1999) Testing the “+2 rule” for lipoprotein sorting in the *Escherichia coli* cell envelope with a new genetic selection. *Mol Microbiol* **34**: 810–821.
- Sheffield, D.J., Harry, T., Smith, A.J., and Rogers, L.J. (1992) Purification and characterization of the vanadium bromoperoxidase from the macroalga *Corallina officinalis*. *Phytochemistry* **32**: 21–26.
- Simons, B.H., Barnett, P., Vollenbroek, E.G.M., Dekker, H.L., Muijsers, A.O., Messerschmidt, A., and Wever, R. (1995) Primary Structure and Characterization of the Vanadium Chloroperoxidase from the Fungus *Curvularia inaequalis*. *Eur J Biochem* **229**: 566–574.
- Siuda JF & DeBerbardi JF (1973) Naturally occurring halogenated organic compounds. *Lloydia* **36**:107-143

-
- Smith, S.G.J., Mahon, V., Lambert, M.A., and Fagan, R.P. (2007) A molecular Swiss army knife: OmpA structure, function and expression. *FEMS Microbiol Lett* **273**: 1–11.
- Strittmatter, M., Grenville-Briggs, L.J., Breithut, L., Van West, P., Gachon, C.M.M., and Küpper, F.C. (2016) Infection of the brown alga *Ectocarpus siliculosus* by the oomycete *Eurychasma dicksonii* induces oxidative stress and halogen metabolism. *Plant Cell Environ* **39**: 259–271.
- Sun, Z. and Rokita, S.E. (2018) Toward a Halophenol Dehalogenase from Iodotyrosine Deiodinase via Computational Design. *ACS Catal* **8**: 11783–11793.
- Sundaramoorthy, M.; Turner, J.; Poulos, T. L. (1995) The crystal structure of chloroperoxidase: a heme peroxidase–cytochrome P450 functional hybrid. *Structure* **3**: 1367–1377.
- Suzuki, M., Eda, Y., Ohsawa, S., Kanasaki, Y., Yoshikawa, H., Tanaka, K., et al. (2012) Iodide oxidation by a novel multicopper oxidase from the *Alphaproteobacterium* strain Q-1. *Appl Environ Microbiol* **78**: 3941–3949.
- Taguchi, T., Ebihara, K., Yanagisaki, C., Yoshikawa, J., Horiguchi, H., and Amachi, S. (2018) Decolorization of recalcitrant dyes by a multicopper oxidase produced by *Iodidimonas* sp. Q-1 with iodide as a novel inorganic natural redox mediator. *Sci Rep* **8**: 2–9.
- Thomas, S.R., McTamney, P.M., Adler, J.M., LeRonde-LeBlanc, N., and Rokita, S.E. (2009) Crystal structure of iodotyrosine deiodinase, a novel flavoprotein responsible for iodide salvage in thyroid glands. *J Biol Chem* **284**: 19659–19667.
- Thomas, F. (2011) Identification et caractérisation du système alginolytique de la bactérie marine *Zobellia galactanivorans*.
- Thomas, F., Barbeyron, T., Tonon, T., Génicot, S., Czjzek, M., and Michel, G. (2012) Characterization of the first alginolytic operons in a marine bacterium: From their emergence in marine *Flavobacteria* to their independent transfers to marine *Proteobacteria* and human gut *Bacteroides*. *Environ Microbiol* **14**: 2379–2394.
- Thomas, F., Lundqvist, L.C.E., Jam, M., Jeudy, A., Barbeyron, T., Sandström, C., et al. (2013) Comparative characterization of two marine alginate lyases from *Zobellia galactanivorans* reveals distinct modes of action and exquisite adaptation to their natural substrate. *J Biol Chem* **288**: 23021–23037.
- Thomas, F., Bordron, P., Eveillard, D., and Michel, G. (2017) Gene expression analysis of *Zobellia galactanivorans* during the degradation of algal polysaccharides reveals both substrate-specific and shared transcriptome-wide responses. *Front Microbiol* **8**: 1–14.
- Timmins, A. and De Visser, S.P. (2018) A comparative review on the catalytic mechanism of nonheme iron hydroxylases and halogenases. *Catalysts* **8**:
- Torz, M. and Beschkov, V. (2005) Biodegradation of monochloroacetic acid used as a sole carbon and energy source by *Xanthobacter autotrophicus* GJ10 strain in batch and continuous culture. *Biodegradation* **16**: 423–33.

- Truesdale, V.W. (2008) The biogeochemical effect of seaweeds upon close-to natural concentrations of dissolved iodate and iodide in seawater - Preliminary study with *Laminaria digitata* and *Fucus serratus*. *Estuar Coast Shelf Sci* **78**: 155–165.
- Tsang, J.S.H. and Pang, B.C.M. (2000) Identification of the dimerization domain of dehalogenase IVa of *Burkholderia cepacia* MBA4. *Appl Environ Microbiol* **66**: 3180–3186.
- Vaillancourt, F.H., Yeh, E., Vosburg, D.A., O'Connor, S.E., and Walsh, C.T. (2005) Cryptic chlorination by a non-haem iron enzyme during cyclopropyl amino acid biosynthesis. *Nature* **436**: 1191–1194.
- Van der Ploeg, J., Van Hall, G., and Janssen, D.B. (1991) Characterization of the haloacid dehalogenase from *Xanthobacter autotrophicus* GJ10 and sequencing of the dhIB gene. *J Bacteriol* **173**: 7925–7933.
- Van Pée, K.H. (1996) Biosynthesis of Halogenated. *Biotechnology* **50**: 375–99.
- Verhaeghe, E., Buisson, D., Zekri, E., Leblanc, C., Potin, P., and Ambroise, Y. (2008a) A colorimetric assay for steady-state analyses of iodo- and bromoperoxidase activities. *Anal Biochem* **379**: 60–65.
- Verhaeghe, E.F., Fraysse, A., Guerquin-Kern, J.L., Wu, T. Di, Devès, G., Mioskowski, C., et al. (2008b) Microchemical imaging of iodine distribution in the brown alga *Laminaria digitata* suggests a new mechanism for its accumulation. *J Biol Inorg Chem* **13**: 257–269.
- Voss, M., Honda Malca, S., and Buller, R. (2020) Exploring the Biocatalytic Potential of Fe/ α -Ketoglutarate-Dependent Halogenases. *Chem - A Eur J* **26**: 7336–7345.
- Wang, Y., Feng, Y., Cao, X., Liu, Y., and Xue, S. (2018) Insights into the molecular mechanism of dehalogenation catalyzed by D-2-haloacid dehalogenase from crystal structures. *Sci Rep* **8**: 1–9.
- Weissflog, L., Lange, C.A., Pfennigsdorff, A., Kotte, K., Elansky, N., Lisitzyna, L., et al. (2005) Sediments of salt lakes as a new source of volatile highly chlorinated C1/C2 hydrocarbons. *Geophys Res Lett* **32**: 1–4.
- Weyand, M., Hecht, H.J., Kiesz, M., Liaud, M.F., Vilter, H., and Schomburg, D. (1999) X-ray structure determination of a vanadium-dependent haloperoxidase from *Ascophyllum nodosum* at 2.0 Å resolution. *J Mol Biol* **293**: 595–611.
- Winter, J.M. and Moore, B.S. (2009) Exploring the chemistry and biology of vanadium-dependent haloperoxidases. *J Biol Chem* **284**: 18577–18581.
- Wischang, D. and Hartung, J. (2011) Parameters for bromination of pyrroles in bromoperoxidase-catalyzed oxidations. *Tetrahedron* **67**: 4048–4054.
- Wischang, D., Radlow, M., Schulz, H., Vilter, H., Viehweger, L., Altmeyer, M.O., et al. (2012) Molecular cloning, structure, and reactivity of the second bromoperoxidase from *Ascophyllum nodosum*. *Bioorg Chem* **44**: 25–34.

-
- Wolfframm, C., Lingens, F., Mutzel, R., and Pée, K.H. van (1993) Chloroperoxidase-encoding gene from *Pseudomonas pyrrocinia*: sequence, expression in heterologous hosts, and purification of the enzyme. *Gene* **130**: 131–135.
- Wong, G.T.F. and Zhang, L.S. (2003) Seasonal variations in the speciation of dissolved iodine in the Chesapeake Bay. *Estuar Coast Shelf Sci* **56**: 1093–1106.
- Woolard, F.X., Moore, R.E., and Roller, P.P. (1979) Halogenated acetic and acrylic acids from the red alga *Asparagopsis taxiformis*. *Phytochemistry* **18**: 617–620.
- Xiao, X., Wu, Z.C., and Chou, K.C. (2011) A multi-label classifier for predicting the subcellular localization of gram-negative bacterial proteins with both single and multiple sites. *PLoS One* **6**:
- Xu, G. and Wang, B.G. (2016) Independent evolution of six families of halogenating enzymes. *PLoS One* **11**: 1–13.
- Yeager, C.M., Amachi, S., Grandbois, R., Kaplan, D.I., Xu, C., Schwehr, K.A., and Santschi, P.H. (2017) Microbial Transformation of Iodine: From Radioisotopes to Iodine Deficiency. *Adv Appl Microbiol* **101**: 83–136.
- Ye, N., Zhang, X., Miao, M., Fan, X., Zheng, Y., Xu, D., et al. (2015) Saccharina genomes provide novel insight into kelp biology. *Nat Commun* **6**:
- Yeh, E., Cole, L.J., Barr, E.W., Bollinger, J.M., Ballou, D.P., and Walsh, C.T. (2006) Flavin redox chemistry precedes substrate chlorination during the reaction of the flavin-dependent halogenase RebH. *Biochemistry* **45**: 7904–7912.
- Yu, M., Faan, Y.W., Chung, W.Y.K., and Tsang, J.S.H. (2007) Isolation and characterization of a novel haloacid permease from *Burkholderia cepacia* MBA4. *Appl Environ Microbiol* **73**: 4874–4880.
- Yu, N.Y., Wagner, J.R., Laird, M.R., Melli, G., Rey, S., Lo, R., et al. (2010) PSORTb 3.0: Improved protein subcellular localization prediction with refined localization subcategories and predictive capabilities for all prokaryotes. *Bioinformatics* **26**: 1608–1615.
- Yu, C.S., Cheng, C.W., Su, W.C., Chang, K.C., Huang, S.W., Hwang, J.K., and Lu, C.H. (2014) CELLO2GO: A web server for protein subCELLular lOcalization prediction with functional gene ontology annotation. *PLoS One* **9**:
- Yuliana, T., Nakajima, N., Yamamura, S., Tomita, M., Suzuki, H., and Amachi, S. (2017) Draft Genome Sequence of *Roseovarius* sp. A-2, an Iodide-Oxidizing Bacterium Isolated from Natural Gas Brine Water, Chiba, Japan. *J Genomics* **5**: 51–53.
- Zhang, W.X., Pan, X., and Shen, H. Bin (2020) Signal-3L 3.0: Improving Signal Peptide Prediction through Combining Attention Deep Learning with Window-Based Scoring. *J Chem Inf Model* **60**: 3679–3686.

References

- Zhu, X., Robinson, D.A., McEwan, A.R., O'Hagan, D., and Naismith, J.H. (2007) Mechanism of enzymatic fluorination in *Streptomyces cattleya*. *J Am Chem Soc* **129**: 14597–14604.
- Zhu, Y., Thomas, F., Larocque, R., Li, N., Duffieux, D., Cladière, L., et al. (2017) Genetic analyses unravel the crucial role of a horizontally acquired alginate lyase for brown algal biomass degradation by *Zobellia galactanivorans*. *Environ Microbiol* **19**: 2164–2181.

Résumé

Dans l'environnement marin, de nombreux organismes participent au cycle biogéochimique des halogènes en émettant des composés organiques volatils halogénés. Cependant les mécanismes enzymatiques responsables de la biosynthèse, de la captation et du stockage de ces métabolites particuliers sont souvent mal connus, notamment chez les bactéries marines. L'annotation du génome de *Zobellia galactanivorans*, une flavobactérie marine vivant à la surface des macroalgues, a permis d'identifier plusieurs gènes potentiellement impliqués dans ce métabolisme halogéné. Au cours de cette thèse, j'ai entrepris des analyses de biochimie et de biologie structurale, et développé des approches fonctionnelles à partir des gènes codant pour des iodoperoxydases à vanadium (VIPO), et pour une haloacide déhalogénase (HAD). J'ai déterminé les substrats préférentiels de l'enzyme ZgHAD et analysé sa stabilité enzymatique et ses paramètres cinétiques. J'ai également résolu la structure 3D de ZgHAD. La délétion du gène *had* chez un mutant a révélé que ce gène conférerait un avantage sélectif à la bactérie en présence de BAA et IAA, des haloacides potentiellement toxiques et présent dans l'environnement marin. Par des analyses biochimiques, j'ai aussi caractérisé la troisième VIPO, spécifique à l'oxydation de l'iodure chez *Z. galactanivorans* (Zg-VIPO3). Grâce à la production d'un mutant knock-out pour *zg-vipol*, j'ai montré l'implication directe de ce gène dans la captation d'iode par la bactérie, localisé par immunomarquage les activités VIPO dans des fractions membranaires et identifié, via des analyses LC-MS/MS, un autre acteur potentiel, une protéine membranaire, homologue de OmpA. Les résultats de ces travaux apportent une meilleure compréhension des rôles biologiques de ces enzymes et ont permis de proposer un modèle hypothétique du métabolisme halogéné de *Z. galactanivorans*, dans le contexte des interactions de cette bactérie marine avec son environnement.

Abstract

In the marine environment, numerous organisms participate in the biogeochemical cycle of halogens by emitting halogenated volatile organic compounds. However, the enzymatic mechanisms involved in the biosynthesis, uptake and storage of those particular compounds are often poorly known, especially in marine bacteria. The annotation of the genome of *Zobellia galactanivorans*, a marine flavobacterium living on the surface of macroalgae, allowed to identify several genes potentially involved in this halogen-related metabolism. During this PhD project, I have performed biochemical and structural analyses, and developed functional approaches on genes, coding for vanadium-dependent iodoperoxidases (VIPO) and for a haloacid dehalogenase (HAD). I have determined the specific substrates of the ZgHAD enzyme and analyzed its enzymatic stability, and steady-state parameters. The gene knockout approach revealed that the expression of *had* gene could provide a selective advantage to this bacterium in the presence of BAA and IAA, haloacids potentially toxic and present in the marine environment. I have also solved the 3D structure of ZgHAD. Through biochemical analyses, I have characterized the third VIPO, specific to iodide oxidation, in *Z. galactanivorans* (Zg-VIPO3). Thanks to the obtention of a *zg-vipol* gene knockout mutant, I have shown the direct involvement of this gene in iodine uptake in the bacteria, localized by immunolabelling the VIPO activities in membrane fractions and identified, through LC-MS/MS analyses, another potential actor, a membrane OmpA-like protein. The results of this work provide a better understanding of the biological roles of these enzymes and allow to propose a hypothetical model of the halogen metabolism of *Z. galactanivorans*, in a context of the interactions of this marine bacterium with its environment.